Evidence-based development and evaluation of haptic interfaces for manual control

Fu, Wei

DOI
10.4233/uuid:b5953a17-322d-49e6-87ba-e299673e8b84

Publication date
2019

Document Version
Final published version

Citation (APA)
Fu, W. (2019). *Evidence-based development and evaluation of haptic interfaces for manual control*. [Dissertation (TU Delft), Delft University of Technology]. https://doi.org/10.4233/uuid:b5953a17-322d-49e6-87ba-e299673e8b84

Important note
To cite this publication, please use the final published version (if applicable).
Please check the document version above.

EVIDENCE-BASED DEVELOPMENT AND EVALUATION OF HAPTIC INTERFACES FOR MANUAL CONTROL

EVIDENCE-BASED DEVELOPMENT AND EVALUATION OF HAPTIC INTERFACES FOR MANUAL CONTROL

Dissertation

for the purpose of obtaining the degree of doctor
at Delft University of Technology,
by the authority of the Rector Magnificus prof. dr. ir. T.H.J.J. van der Hagen,
chair of the Board for Doctorates,
to be defended publicly on
Thursday 20 June 2019 at 15:00 o'clock

by

Wei FU

Master of Science in Control Theory and Control Engineering,
Northwestern Polytechnical University, China,
born in Xi'an, China.

This dissertation has been approved by the promotors:

dr. ir. M. M. van Paassen and prof. dr. ir. M. Mulder

Composition of the doctoral committee:

Rector Magnificus,	chairperson
Dr. ir. M. M. van Paassen,	Delft University of Technology, promotor
Prof. dr. ir. M. Mulder,	Delft University of Technology, promotor
Independent members:	
Prof. dr. A. M. L. Kappers	Eindhoven University of Technology
Prof. dr. ir. P. Breedveld	Delft University of Technology
Prof. dr. D. G. Simons	Delft University of Technology
Dr. J. Hartcher-O'Brien	Delft University of Technology
Other member:	
Prof. dr. ir. D. A. Abbink	Delft University of Technology

Keywords: Haptic interface, haptic perception, manual control behavior, neuromuscular system, mechanical properties, mass-spring-damper systems, haptic display transparency

Printed by: Off Page

Cover by: Gehua Wen

ISBN 978-94-6366-177-5

An electronic version of this dissertation is available at
`http://repository.tudelft.nl/`.

To my beloved wife, Gehua

CONTENTS

SUMMARY

EVIDENCE-BASED DEVELOPMENT AND EVALUATION OF HAPTIC INTERFACES FOR MANUAL CONTROL

Wei FU

At present, the rapid development of automation technologies allows robots remarkable precision and endurance, as well as the strength in accomplishing repetitive tasks. Despite this, manual control is still indispensable in many domains where robots and humans play complementary roles, as humans demonstrate superior competence in improvisation and flexibility, as well as the excellent ability to take on tasks where things cannot be fully specified. *Haptic interfaces* provide a prime example which combines the strengths of these two elements, allowing them to interact and merge into a highly integrated control loop. A haptic interface is usually created by providing force feedback related to the task on a control device. The haptic feedback makes performing manual control more intuitive, allowing the operator to physically act upon what (s)he feels, rather than generating the control activity through only interpreting other sensory inputs, such as visual and auditory cues. Over the last few decades, haptic interfaces have gained popularity as being powerful tools to facilitate manual control.

By analogy with a visual interface, one can interpret a haptic interface as the *display* that presents information to and accepts commands from a human operator. While giving input through the interface, the neuromuscular system of the operator also acts as the *eye* that perceives the information being presented by a display. This highly interactive nature underlines the importance of orienting the development of all haptic systems towards humans, particularly towards what humans feel and how they need to act. To facilitate future development of haptic interfaces, this thesis focuses on two of the main challenges that have not been adequately addressed from such a human-centric perspective: (i) among various possibilities, how can we select the one that works more effectively with humans, i.e., using understanding of *human control behavior* (how humans act) to guide the development of the philosophy of the design?, and (ii) how can we know whether a device ensures a transparent haptic interaction, i.e., incorporating the characteristics of *human haptic perception* (what humans feel) into the evaluation of the quality of the display?

This thesis consists of three parts. The first challenge is addressed in the first part, which focuses on the design philosophy of applications in aircraft and presents a haptic interface that more effectively exploits the potential of human controllers. The second challenge is addressed in the second and third parts, which establish the understanding of human haptic perception and demonstrate how such knowledge can be used to evaluate the quality of the haptic display, respectively.

The design philosophy determines to what extent a haptic system can improve pilots' flight control performance. It is important to configure the haptic feedback such that the pilot is efficiently integrated into the flight control loop. In general, existing haptic applications work as support systems that provide additional forces on the control device, to inform a pilot about the current flight condition, the task, and constraints. The control device itself, however, is still a *passive* system (usually a passive displacement device, the displacement of which is used as the pilot's control input, as in most modern fly-by-wire aircraft) with dynamics independent of and decoupled from those of the aircraft being controlled. It hampers the establishment of a full haptic connection between the pilot and the aircraft. A pilot cannot be sufficiently integrated into the control loop, which has become a major limiting factor for the performance of manual flight control.

How might this be improved? Haptic feedback should be configured to create a *direct connection*, which allows for more effectively exploiting the potential of human controllers. This thesis explores the possibilities of involving the pilot's *neuromuscular system* in regulating the aircraft states, as it has a much faster response and greater robustness than cognitive activities. To this end, the states of the control device should directly reflect the states of the aircraft. We first revisit and evaluate the active manipulator, an established concept that is different from, but can be complementary to, existing haptic interfaces. Different to a passive displacement control device, the active manipulator moves by tracking a particular aircraft state (in our case: aircraft attitude rate) while deriving the manual control input from the pilot's force.

This thesis investigates the effect of such a control device on pilots' control behavior, and in particular, what role the neuromuscular system plays in the control loop. First, experimental participants are asked to perform compensatory tracking tasks, in which the manual flight control is simplified into compensating for the visually presented tracking error. Results show that the active manipulator significantly facilitates manual control by integrating a large portion of the aircraft dynamics into the manipulator/neuromuscular system. This reduces the order of the effective vehicle dynamics, and couples the control of the integrated dynamics, as well as the disturbance rejection, to the control of the arm position. Furthermore, with two uncorrelated forcing functions, we are able to estimate the impedance of the neuromuscular system, which provides clear evidence of the involvement of the muscle co-contraction in disturbance rejection. Second, results show that the control task is only facilitated by the feedback about a low-frequency segment of the aircraft attitude rate. Disturbances with substantial energy beyond this range can not be rejected by the neuromuscular system, and cause the arm to move involuntarily. To alleviate this without affecting the flight control performance, a lag-lead filter is designed to selectively decouple the dynamics of the active manipulator from the aircraft.

The second part of the thesis presents a study on the characteristics of human hap-

tic perception, which are particularly relevant to the evaluation of the fidelity of haptic displays. The term "fidelity" refers to the degree of similarity between the system dynamics that a haptic interface depicts and the system dynamics one intends to present. Correctly portraying the desired system dynamics is important to ensure that professionals can rely on their skills to accomplish tasks efficiently and proficiently. However, limitations of a haptic device, due to the limited bandwidth of the electronics and the digital controller, as well as the inherent dynamics of the actuator, can cause changes in the force feedback and thereby distortions of the information it conveys. It is important to understand how a distortion alters what the operator feels, and when this starts to occur.

Optimizing the haptic presentation requires one to know how the difference between the presented and intended system dynamics is characterized by humans. As depicting *mass*, *stiffness*, and *damping* is most relevant to the majority of practical applications, this thesis investigates how dynamic distortions affect the human perception of these three mechanical properties. Our study is initiated with the investigation into the effects of time delays in force feedback. Through psychophysical experiments, this thesis reveals that human perception of a system's mass, stiffness, and damping can be derived from the *real* and *imaginary* parts of that system's frequency response. The perception changes associated with delayed force feedback can be accounted for by changes in the two complex components. On this basis, the thesis proposes a framework that allows a unified view of the effects of all changes in the magnitude and phase characteristics of a system's frequency response.

Another key parameter reflecting the performance of a haptic device is whether and when it leads the human operator to an experience that is different from what is intended. A distortion is not discernible if it is beyond the resolution of human haptic perception. Certainly, the human threshold for perceiving changes is a more reasonable standard for determining when a device performs in a satisfactory way. In view of this, knowledge about the human *just-noticeable difference* (JND) in system dynamics is crucial. Over the past decades, most researchers have focused on the JNDs in *stiffness*, *mass*, and *damping*. Because possible interactions in the way humans estimate these mechanical properties are typically overlooked, previous findings do not adequately describe the corresponding JNDs, and can not be generalized to the threshold for perceptual changes in the dynamics of the system that these mechanical properties belong to.

This thesis extends our understanding by building a mathematical model of the JNDs in the three mechanical properties. This model can describe the interaction between the perceptions of the three properties, for example, the effects of a system's stiffness and mass on the JND in the system's damping. More importantly, it establishes a link between JNDs in a system's mechanical properties and the human difference threshold for the system's dynamics. The model integrates JNDs in a system's stiffness, mass, and damping into the JNDs in the *real* and *imaginary* parts of the system's frequency response. Experimental results demonstrate that the JNDs in the two complex components are both *proportional* to the magnitude of the system's frequency response. In addition, it is shown that this model applies to systems with arbitrary dynamic orders. This leads to a unified model that describes the threshold for changes in human perception of any system dynamics with two dimensions: the real and imagi-

nary axes in the complex plane.

The third part of the thesis demonstrates how the established understanding of human haptic perception can be applied in practice. First, a two-step approach to a perception-oriented evaluation of the fidelity of haptic displays is proposed. These two steps, respectively, show when and how a particular haptic device alters what the operator perceives. Second, to provide more insights into the active manipulator presented in this thesis, we evaluate the control feel associated with the aircraft dynamics conveyed by the feedback of the aircraft rotational velocity. Findings from the second part allow us to reveal the characteristics of the perceived manipulator dynamics and quantify the perception with three basic mechanical properties.

Future research and innovations can be facilitated by the findings from this thesis. The first part presents a new design philosophy for future aircraft control devices. The active manipulator can be seamlessly combined with existing haptic support systems, such as flight envelope protection systems and haptic shared control systems. The studies presented in the second and third parts provide clear guidelines for future design and evaluation of haptic displays. Detailed insights are now available for creating an effective balance between stability and transparency.

SAMENVATTING

EVIDENCE-BASED DEVELOPMENT AND EVALUATION OF HAPTIC INTERFACES FOR MANUAL CONTROL

Wei FU

De huidige snelle voortgang van automatisering stelt robots in staat tot het automatisch en precies uitvoeren van repetitieve werkzaamheden. Niettegenstaande deze ontwikkeling is het handmatig uitvoeren van taken nog steeds nodig in vele domeinen. Daar kunnen robots en mensen complementair werken, waarbij mensen improvisatie en flexibiliteit inbrengen, en hun vaardigheid om taken te volbrengen die slecht of deels gespecificeerd zijn. *Haptische interfaces* zijn bij uitstek geschikt om de krachten van deze twee spelers te verenigen, zodat mens en automatisering kunnen samenwerken in een in verre mate geïntegreerde regellus. Een haptische interface wordt gewoonlijk gerealiseerd door een taakgerelateerde krachtterugkoppeling op de interface. De haptische terugkoppeling maakt de handmatige besturing meer intuïtief, en stelt de bestuurder in staat om fysiek te reageren op het gevoel van de interface, in plaats van de stuuractie te genereren alleen op basis van de interpretatie van andere sensorische signalen, zoals visuele en auditieve cues. In de laatste jaren zijn haptische interfaces een grotere rol gaan spelen als middelen om handmatige besturing te vergemakkelijken.

Analoog aan een visuele interface kan men een haptische interface beschouwen als een *display* dat informatie toont, en in dit geval ook instructies van de bestuurder accepteert. Het neuromusculaire systeem van de bestuurder geeft de instructies door aan de interface, en functioneert ook als *oog*, dat informatie van het display waarneemt. Dit interactieve aspect van haptische displays maakt het van belang om de menselijk aspecten bij de ontwikkeling van haptische systemen mee te nemen, specifiek gericht op eigenschappen menselijke waarneming en actie. Om het ontwerp van haptische interfaces te ondersteunen richt dit proefschrift zich op twee vragen die nog onvoldoende belicht zijn vanuit een mensgericht perspectief: (i) hoe kunnen we, uit vele ontwerpmogelijkheden, het ontwerp kiezen dat de beste samenwerking voortbrengt, hierbij gebruik makend van de kennis over menselijk stuurgedrag bij de ontwikkeling van de ontwerpfilosofie? en (ii) hoe kunnen we de kwaliteit van de haptische interactie

waarborgen, daarbij gebruik makend van de eigenschappen van de menselijke haptische perceptie (dus van wat mensen voelen) voor het beoordelen van de kwaliteit van een display?

Dit proefschrift is uit drie delen opgebouwd. Het eerste deel bespreekt de eerste van de hierboven vermelde vragen, richt zich op de ontwerpfilosofie in de context van toepassing voor vliegtuigen, en presenteert een haptische interface die de kracht van de menselijke bestuurder beter benut. De tweede vraag wordt behandeld in het tweede en derde deel, die respectievelijk ingaan op de theorie van menselijke haptische waarneming en aantonen hoe die theorie gebruikt kan worden om de kwaliteit van haptische displays te evalueren.

De ontwerpfilosofie bepaalt hoe een haptisch systeem de besturingsprestaties van de vlieger kan ondersteunen. Het is van belang om de haptische terugkoppeling zo te configureren dat de vlieger een efficiënt onderdeel wordt van de regellus. In het algemeen werkt bestaande haptische ondersteuning door het geven van additionele krachten op het stuurorgaan, waarmee de vlieger geïnformeerd wordt over de huidige vliegtoestand, de taak en de beperkingen. Het stuurorgaan zelf is echter nog steeds een passief apparaat (in het algemeen wordt daarbij de verplaatsing gebruikt as stuursignaal naar het vliegtuig), en de dynamica daarvan zijn niet gekoppeld aan die van het bestuurde vliegtuig. Dit staat het realiseren van een complete haptische koppeling tussen het vliegtuig en de vlieger in de weg, en verhindert daarmee verdere verbetering van handmatige besturing.

Hoe kan dit verbeterd worden? Haptische terugkoppeling zou een directe verbinding moeten vormen, waarmee het potentieel van menselijke bestuurders nog veel effectiever ingezet kan worden. Dit proefschrift verkent de mogelijkheden om het neuromusculair systeem van de vlieger bij de controle van de vliegtuigtoestand, omdat dit een snellere response en grotere betrouwbaarheid heeft dan cognitieve activiteiten. Hiertoe moet de toestand van het stuurorgaan een directe reflectie zijn van de toestand van het bestuurde systeem. We beginnen met een hernieuwde evaluatie van actieve stuurorganen, een bestaand concept dat verschilt van de huidige haptische interfaces, maar een complementaire rol kan spelen. Anders dan een passief stuurorgaan gebaseerd op verplaatsing, beweegt een actief stuurorgaan volgens een specifieke toestand van het vliegtuig (in ons geval: de rolsnelheid), terwijl het stuursignaal afgeleid wordt uit de kracht uitgeoefend door de vlieger.

Dit proefschrift onderzoekt het effect van een dergelijk stuurorgaan op het stuurgedrag van de vlieger, en in het bijzonder welke rol het neuromusculair systeem heeft in de regellus. Deelnemers in een experiment zijn gevraagd om compenserende stuurtaken uit te voeren, waarin de handmatige besturing is vereenvoudigd tot het wegregelen van een visueel gepresenteerde afwijking. Resultaten tonen aan dat een actief stuurorgaan in belangrijke mate de handmatige besturing vereenvoudigt, door een gedeelte van de vliegtuigdynamica te absorberen in de regellus gerealiseerd door het actieve stuurorgaan en het neuromusculair systeem. Dit reduceert effectief de orde van de voertuigdynamica en koppelt de besturing van de geabsorbeerde dynamica, alsmede de onderdrukking van verstoringen, aan de besturing van de arm positie. Daarnaast was het mogelijk om, met twee ongecorreleerde testsignalen, de impedantie van het neuromusculair systeem te schatten, hetgeen duidelijk bewijs geeft van de rol van spier co-contractie in de onderdrukking van de verstoring. Daarnaast laten de resul-

taten zien dat de stuurtaak slechts geholpen wordt door terugkoppeling in de lagere frequenties van de rolsnelheid. Verstoringen met significante energie in hogere frequenties kunnen niet effectief onderdrukt worden door het neuromusculair systeem en veroorzaken ongecontroleerde armbewegingen. Om dit probleem te onderdrukken zonder een nadelig effect op de stuurprestaties, is een na-ijlend en voorijlend filter toegepast, om selectief de dynamica van de actieve manipulator van die van het vliegtuig te ontkoppelen.

Het tweede deel van dit proefschrift bevat een studie naar de karakteristieken van menselijk haptische waarneming, wat vooral van belang is voor de bepaling van de getrouwheid van haptische displays. De term getrouwheid duidt op de mate van gelijkheid tussen de systeemdynamica die door het haptische display wordt getoond en de beoogde dynamica. Correcte weergave van manipulator dynamica is van belang voor het ontwikkelen van vaardigheden door professionals. Echter, beperkingen van een haptisch apparaat, door beperkte bandbreedte van de elektronica en de digitale regelaar, en door de inherente dynamische eigenschappen van de actuator, kunnen de krachtterugkoppeling wijzigen en daardoor vervromingen aanbrengen in de overgebrachte informatie. Begrip van de effecten van een vervorming op het gevoel van de menselijke bestuurder, en de condities waaronder dit optreedt is belangrijk.

Het optimaliseren van de haptische presentatie vereist kennis over hoe het verschil tussen gepresenteerde en beoogde systeemdynamica wordt geïnterpreteerd door mensen. Omdat de representatie van massa, stijfheid en demping de meest relevante aspecten zijn voor het overgrote deel van de toepassingen, onderzoekt dit proefschrift hoe afwijkingen van dynamica de menselijke waarneming van deze eigenschappen beïnvloedt. Het onderzoek start met de effecten van tijdvertraging op krachtterugkoppeling. Met psychofysische experimenten wordt aangetoond dat menselijke waarneming van de massa, stijfheid en demping van een systeem afgeleid kan worden uit de reële en imaginaire delen van de frequentieresponsie van het systeem. De veranderingen in waarneming gerelateerd aan de vertraagde krachtterugkoppeling kunnen verklaard worden uit de veranderingen in deze twee complexe componenten. Hierop gebaseerd stelt het proefschrift een raamwerk voor dat de effecten van alle veranderingen in grootte en fase van de frequentieresponsie van een systeem beschrijft.

Een ander belangrijk aspect van de kwaliteit van een haptisch apparaat is of, en wanneer, de mens een andere dynamica ervaart dan die bedoeld is. Een afwijking is niet waarneembaar als die onder de waarnemingsdrempel is. Uiteraard is de waarnemingsdrempel voor veranderingen in apparaatdynamica een meer geschikte standaard voor kwaliteit dan technische criteria zonder een dergelijk fundament. Hiertoe is kennis over de just waarneembare verschillen (Just Notable Difference, JND) essentieel. In afgelopen decennia hebben onderzoekers zich gericht op het bepalen van JND's voor stijfheid, massa en demping. Omdat interacties tussen deze mechanische eigenschappen gewoonlijk niet in aanmerking genomen werden, zijn deze bevindingen niet compleet in het beschrijven van de JND's, en kunnen ze niet algemeen toegepast worden om de drempels voor verandering in perceptie van de gecombineerde systeemdynamica te beschrijven.

Dit proefschrift breidt het begrip op dit terrein uit door een mathematisch model te creëren voor de JND's in de drie mechanische eigenschappen. Dit model kan de interactie tussen de waarneming van deze drie eigenschappen, een voorbeeld hiervan

zijn de effecten van de stijfheid en massa van een systeem op de JND voor de demping. Bovendien verbindt het de JND's in de mechanische eigenschappen en de waarnemingsdrempel voor systeemdynamica. Het model integreert JND's voor de stijfheid, massa en demping met de JND's in de reële en imaginaire delen van de frequentieresponsie van een systeem. Experimentele resultaten tonen aan dat de JND's in de beide complexe delen in verhouding staan tot de amplitude van de frequentieresponsie. Daarnaast is aangetoond dat dit toegepast kan worden op systemen met arbitraire orde voor de dynamica. Dit resulteert in een enkel model dat de drempel beschrijft voor veranderingen in menselijke waarneming voor ieder mechanisch systeem door slechts twee dimensies; de reële en imaginaire componenten van de responsie in het complexe vlak.

Het derde deel van dit proefschrift laat zien het ontwikkelde begrip van menselijke waarneming van dynamische eigenschappen in de praktijk kan worden toegepast. Ten eerste wordt een benadering in twee stappen voor de evaluatie van de getrouwheid van haptische displays op basis van de kennis van haptische perceptie voorgesteld. Deze twee stappen tonen wanneer en hoe een haptisch apparaat de waarneming beïnvloedt. Ten tweede, om verder inzicht te geven in de actieve manipulator besproken in dit proefschrift, wordt het besturingsgevoel geëvalueerd dat gecreëerd wordt door de vliegtuigdynamica en de terugkoppeling van de vliegtuig rolsnelheid. De resultaten van het tweede deel van het proefschrift stellen ons in staat om de karakteristieken van de waargenomen manipulator dynamica te duiden en de perceptie kwantitatief te maken door middle van de drie basis mechanische eigenschappen.

De resultaten in dit proefschrift staan hopelijk aan het begin van toekomstig onderzoek en toekomstige innovaties. Het eerste deel presenteert een nieuwe ontwerpfilosofie voor toekomstige stuurorganen in vliegtuigen. De actieve manipulator kan naadloos worden gecombineerd met bestaande haptisch ondersteuning, beschermingssystemen voor de vlucht envelop en systemen voor haptisch gedeelde besturing. De studies in het tweede en derde deel voorzien in richtlijnen voor ontwerp en evaluatie van haptische displays. Gedetailleerd inzicht is nu beschikbaar voor het scheppen van een effectieve balans tussen stabiliteit en transparantie van haptische apparaten.

1

INTRODUCTION

The secret of getting ahead is getting started.

Mark Twain

1.1. EMERGENCE OF HAPTIC INTERFACES

The rapid development of digital technology allows humans to create new automated tools and accomplish tasks that are more complicated and challenging than ever before. With high endurance and the ability to survive in adverse situations, robots can often effectively complement humans by extending their capabilities. Examples are remote operations without physical human presence in extreme environments, where placing professionals on site would be dangerous or prohibitively expensive, such as deep-water or space exploration [1, 2], and nuclear-plant inspection [3]. Additionally, advanced servomotors equipped with vibration suppression technology can help surgeons perform less invasive and more accurate operations that involve minimal incisions [4].

Due to this, manual control tends to rely on, and is increasingly supported by digital systems; however, this often comes at the expense of losing the *haptic sense* of the task, which is present in conventional control tasks. The lack of this haptic sense makes it more difficult to optimize the performance of human controllers. For example, the control device in many modern fly-by-wire aircraft is decoupled from the surface actuators. It does not feed back aerodynamic forces, a useful piece of information that is often available with mechanical transmission means. Pilots have to rely on other sources, such as visual, auditory, and motion cues. The loss of the coupling of *perception* and *execution* in the haptic channel further confines pilots to a supervisory role, reducing their engagement in the control loop and increasing the risk of overloading the visual channel.

The advent of *haptic interfaces* offers the possibility of re-establishing the perception-action coupling through the haptic channel. Despite the many forms they take, which range from a wearable arm exoskeleton [5] (see Fig. 1.1a) to a Phantom haptic manipulator [6] (see Fig. 1.1b) to a flight-simulator side stick (see Fig. 1.1c), haptic communication in most applications is created by providing *force feedback* to a human operator through the control device. Haptic feedback can relieve the (visual) workload and make a task much more intuitive, allowing operators to *physically act upon what they feel.* Over the last few decades, haptic interfaces have gained popularity as powerful tools to facilitate and improve manual control [7–15].

Although digital control systems often cut apart the conventional physical connec-

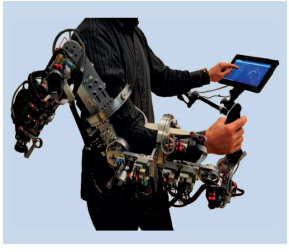

(a)

(b)

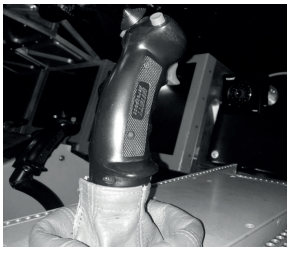

(c)

Figure 1.1: Examples of some existing haptic devices: (a) A wearable arm exoskeleton [5]; (b) A Phantom Premium haptic device [6]; (c) A MOOG side stick in SIMONA research simulator at TU Delft.

tion, they provide numerous possibilities for generating *artificial* haptic feedback. Depending on what is needed, haptic interfaces are configured to present different aspects of tasks: for example, the dynamics of the controlled element (such as a vehicle [9, 16] or a slave robot [17]) or the dynamics of the environment in which the task is being operated [18–22]. In addition, haptic feedback can be used as an instruction aid to trainees in manual control tasks, such as in the case of pilots learning to perform the flare maneuver [23]. Recent advances in haptic technology also enable an automation system to communicate its intentions through the control device, allowing its actions to be better understood, corrected, or even overridden by an operator, a design philosophy known as haptic shared control [11, 12, 24].

This remarkable design freedom in turn also complicates the development of haptic interfaces. Devising effective equipment requires expertise across many fields, from human perception and psychophysics to control systems engineering, introducing various challenges for designers and engineers. The main goal of this thesis is to provide some novel and clear guidelines that may help designers of haptic interfaces in evaluating and improving their designs. Without doubt, it is important to develop and assess applications from a human-centric perspective, particularly one that is focused on what humans feel and how they need to act. The thesis will focus on such human factors in the context of two aspects that are crucial for the success of any haptic device: *haptic design philosophy*, which determines the degree of usefulness of a particular setting of haptic feedback, and *haptic display quality*, which concerns to what extent the feedback is presented as intended and how the feedback is interpreted by the operator. To this end, the study of the thesis is based on evidence regarding human *control behavior* and *haptic perception*. The following two sections will identify the challenges associated with these two factors, set the objectives of this thesis, and frame the key research questions that will need to be addressed to achieve our goal.

1.2. EXPLOITING THE POTENTIAL OF HUMAN CONTROLLERS

The first element that is crucial for a successful haptic design, is the design philosophy (i.e., the selection of what a device feeds back to the human operator). It determines to what extent a haptic interface can support the operator, and especially to what extent a particular setting of haptic feedback can exploit the potential of human controllers. As the best design philosophy varies with applications, we focus solely on the case of haptic interfaces in the manual control of aircraft. As in the previous section, here the gap to be filled in this field helps to define our second objective, and the corresponding key research question that will be addressed in this thesis.

When flying a fly-by-wire aircraft, a pilot controls its attitude by means of the deflection angle of a control device, usually a *passive* system (a passive manipulator) which does not provide any feedback about aircraft states. Fig. 1.2 gives an example: the control of the aircraft roll attitude. The pilot only receives the attitude feedback through vision (cockpit displays, outside view) and physical motion, whereas the control device moves passively, with its own dynamics that are *decoupled* from those of the aircraft.

Existing haptic interfaces developed for aircraft control work as support systems that inform the pilot about the current flight condition, the task, and constraints (e.g.,

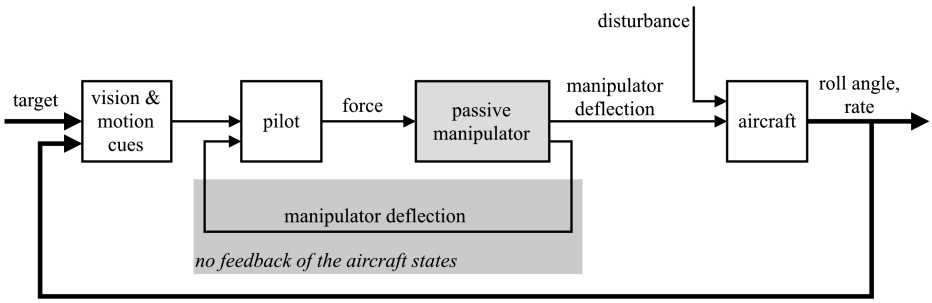

Figure 1.2: Schematic diagram of the control of the aircraft roll attitude with a passive control device.

boundaries or dangers) in the environment [10, 13, 14, 25–27]. The common approach taken is to provide additional forces that are independent of the inherent control-device dynamics. Although such haptic systems can lead to considerable improvements in pilots' performance [10, 25], they are still augmenting manual flight control *on the basis of a passive instrument.* The control device itself fails to establish a haptic connection between a pilot and the aircraft being controlled. The pilot's neuromuscular system is merely acting as an execution unit, an inner loop that follows a given cognitive instruction generated in the brain based on visual and motion feedback [28].

Although human brains are extremely versatile controllers that can easily adapt to various systems, the outer loop that they form with visual and motion feedback is much slower than the neuromuscular system loop [29]. For example, reflexive responses have time delays of less than 50 ms, which are much shorter than those in responses to visual stimuli (200-500 ms) [29, 30]. The control performance can be markedly improved when the element being controlled is integrated into the inner loop (i.e., when the controlled element is directly connected to, rather than decoupled from, our limbs). For instance, we can accurately move a ball that is held in our hands, and reject disturbances acting on it, even with our eyes closed; in contrast, it requires much more effort when one must control the ball's movement only through a string.

This is because when the controlled element is directly connected to the limb, its motion is obtained through proprioception, the sense though which humans perceive their body movements. This results in a local feedback loop, integrating the external dynamics into the control of the limb position. Compared to those established with other sensory feedback, this local loop has substantially higher bandwidth and stability margin. Furthermore, spinal reflexes and muscle co-contraction can increase the instantaneous resistance to perturbations, allowing one to stabilize and regulate the movement of the controlled element without cognitive activities [29, 30].

1.2.1. RESEARCH OBJECTIVE AND KEY QUESTION

RESEARCH OBJECTIVE

A passive control device limits the potential capability of a pilot, leaving much room for possible improvements in control performance and stability. To take advantage of the aforementioned human attribute, the neuromuscular system should be more

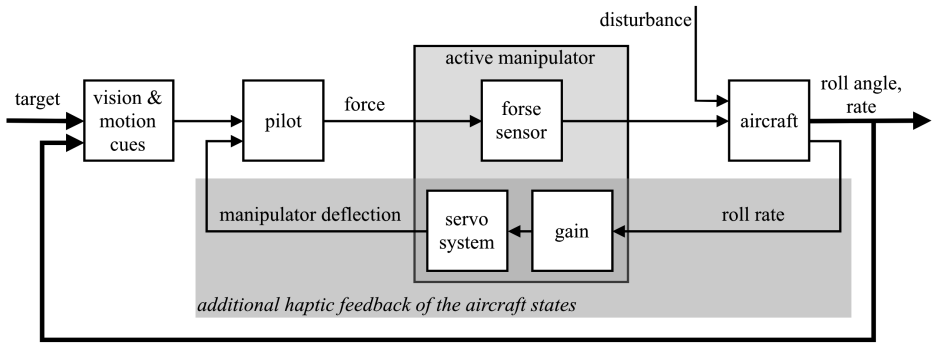

Figure 1.3: Schematic diagram of the control of the aircraft roll attitude with an active manipulator.

1

effectively involved in manual aircraft control. Haptic feedback should be provided to create a projection of the vehicle on the control device, allowing the neuromuscular system to *share* the regulation of the aircraft attitude with the brain. This leads to our first research objective:

Research objective I

Explore a haptic interface that establishes a full haptic connection, particularly one that more effectively exploits the potential of human controllers.

KEY RESEARCH QUESTION

To attain the first objective, this thesis draws primarily on an established concept, the active manipulator [9, 31], that *synchronizes* a control device with the aircraft. Fig. 1.3 illustrates flight control with such an instrument. The aircraft control surfaces are fed with the force that the pilot exerts on the manipulator (the control device), in which a force sensor is mounted. The manipulator is attached to a position servo system, which can track one of the aircraft states, for instance the aircraft angular velocity.

Bilateral information transmission is therefore achieved in the haptic channel. Previous studies show that the active manipulator can greatly facilitate manual aircraft control [9, 31]. However, the rationale behind such facilitation is not fully understood. What role the neuromuscular system plays in the control loop, and what dynamics are still processed in the brain, remain unexplored. The lack of theoretical background significantly impedes any further development of the active manipulator. Furthermore, the existing prototype suffers from low operational quality, as will be seen in Chapter 2. The current throughput of high-frequency components of aerodynamic disturbances, mainly turbulence which is inevitably present in the control-device movement when feeding back the angular velocity, cause involuntary arm movements.

This leads us to refine our objective, and thus to ask the first key research question that will be addressed in this thesis:

Key Question I-1

How does the active manipulator improve the flight control performance, and can we use this knowledge to further develop this concept?

1.3. CHARACTERISTICS OF HUMAN HAPTIC PERCEPTION

In addition to determining the most effective haptic feedback, the second element that is crucial for a successful haptic design, is the quality of the haptic presentation. The term "fidelity" (or "transparency") refers to the degree of similarity between the system dynamics that a haptic interface depicts and the system dynamics one intends to present. The display fidelity is crucial for a successful application of haptic interfaces, since it indicates the extent of the correctness of the information the operator is acting upon. Ideally, the dynamics portrayed by a haptic device should appear to be the same as the dynamics that one intends to communicate [32]. Such perfect transparency is indeed considered by most researchers to be the benchmark for the performance of their devices [33–37].

Yet, inevitable limitations of haptic devices, such as the inherent actuator dynamics, the limited bandwidth of the control systems, and the transmission time delays in tele-operation, can impair this communication. Transparency sometimes has to be further sacrificed to avoid stability issues caused by these limiting factors [33, 38, 39]. For example, excessively reducing the apparent mass of an admittance display causes instability [40]. Furthermore, control schemes that aim to compensate for the reduced stability margin, such as virtual coupling [19, 41], real-time passivity conservation [42, 43], and scattering/wave-variable transformation [44, 45], may further undermine the interface effectiveness.

It is usually possible to determine the degree by which a haptic display deviates from its intended dynamics, and to express that deviation in technical terms [46, 47]. However, it is not always known whether these deviations can be felt by a human, and, if so, how they then affect the perception of the display. Clearly, there is a need to assess and evaluate the quality of haptic feedback from a perceptual perspective. Optimizing haptic presentation, e.g., by adjusting the intended mechanical characteristics to counteract the distortion, entails understanding effects of the aforementioned factors on how humans *characterize* the system. Furthermore, a human-centric treatment would allow for a more efficient trade-off between transparency and stability. A distortion is *not discernible* if it is beyond the resolution of human haptic perception. Working towards a perfect transparency can place excessive and (because small changes are no longer perceived) even unnecessary demands on a haptic device. Hence, it is crucial to better understand when a haptic interface starts to alter what the operator feels.

1.3.1. RESEARCH OBJECTIVE AND KEY QUESTIONS

RESEARCH OBJECTIVE

Surprisingly, many studies in haptics do not consider the human perception of the haptic device in sufficient detail. This most likely stems from the fact that our understanding of the properties of human haptic perception is rather limited. This leads to

the second objective of this thesis:

Research objective II

Identify, model and understand the characteristics of human haptic perception, to facilitate the development and evaluation of haptic devices, as well as to guide the optimization of haptic presentation according to what humans perceive.

KEY RESEARCH QUESTIONS

To make the problem more tractable, some restrictions have to be placed on the scope of this thesis. First, to utilize powerful analytic tools, our study is restricted to *linear* systems. Second, this thesis focuses predominantly on haptic interaction with *mass-spring-damper* systems. Nevertheless, as will be seen in Chapters 3-5, our findings also apply to systems with higher orders. Third, this thesis is restricted to *continuous* haptic interactions with *soft* objects. This means that systems with infinite mechanical impedance (such as a stiff wall), and the effects of transient responses (such as the moment of contact), are excluded from consideration.

To clarify our objective, imagine that a human operator is interacting with an arbitrary system, as shown in Fig. 1.4. We define the effect of a haptic device as an independent block (the one in dark gray), which can change the system dynamics that appear on the human side.

First, we should know how the dynamics which the operator experiences can differ from those of the original system. As the majority of environments that humans come across in daily life resemble mechanical systems in general, we are particularly interested in the perception of the system's mass, damping, and stiffness. However, conventional means, such as examining changes in the dynamics' magnitude and phase through a bode plot, fail to explain the effect on how humans actually perceive these mechanical properties. Of all the aforementioned causes of the display distortion, our understanding of the perception change associated with *delayed feedback* is the most

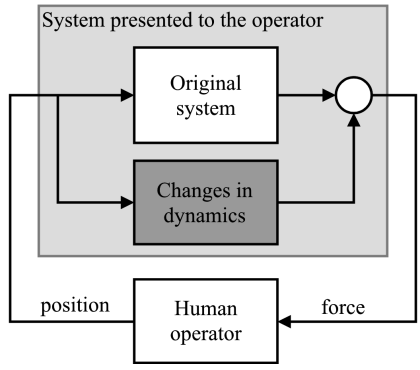

Figure 1.4: Haptic interaction between a human operator and an arbitrary system.

limited. The infinite number of poles introduced by a time delay into the system dynamics complicates any prediction of its effect.

Previous studies show that humans, instead of correcting their perception for the time delay, are inclined to interpret delayed feedback as changes in mass, damping, and stiffness of the system [48–53]. For example, they *underestimate* the stiffness of an elastic force field when the sensed force lags behind the displacement [49, 52]. The reported effects of different time-delay magnitudes are, however, in fact very inconsistent [49, 51]. To date, a systematic approach to *quantitatively* assess and predict is still not available, mainly because the underlying principle of how delays affect the perceived mechanical properties has yet to be identified.

This leads to the second key question of this thesis, which needs to be answered to attain the research objective:

Key Question II-1

How does delayed haptic feedback affect humans as they estimate the mass, damping, and stiffness characteristics of the original system?

Secondly, we should know when a perception change occurs, that is, when does a haptic device starts to alter what the operator feels. The *threshold* for affecting perception is usually called the *just-noticeable difference* (JND) – the minimum amount of change that a human can detect in a stimulus [54–56]. However, attempts to directly measure the JND in system dynamics are scarce. This is primarily due to the difficulty of selecting representative control variables and because the lack of a systematic approach prevents generalization from a limited number of studies. Nevertheless, this problem can be circumvented by focusing on the JNDs in mechanical properties.

Over the last two decades, numerous studies have indeed investigated the JNDs in mass, stiffness, and damping [57–63]. Previous findings, however, are based on the assumption that each mechanical property is sensed in isolation (e.g., the interaction with a spring that possesses negligible mass and damping). They fail to account for the observed *interactions* among perceptions of the three properties [64]. For example, the JND in a system's damping is affected by the system's mass and stiffness [64]. Due to this, existing results are limited in their applicability, and it is difficult to generalize from them to the JND in system dynamics. We must therefore extend the existing threshold models, leading to the third key question of this thesis:

Key Question II-2

How can we build a threshold model that adequately describes the perceptual interactions among mechanical properties and would allow for a generalization from JNDs in a system's mechanical properties to the JND in the dynamics of the system?

1.4. RESEARCH APPROACH

1.4.1. EXPLORING HUMAN CONTROL BEHAVIOR

To address the Key Question I-1, we first need to investigate how pilots adapt their control behavior for the active manipulator. To this end, we ask our participants to perform *compensatory tracking* [65, 66], a task that is relevant to manual flight control, and that at the same time makes the human control behavior easier to understand. Furthermore, we consider humans, in the context of such a tracking task, to be approximately linear time-invariant systems. This allows us to use the estimated frequency responses to quantitatively investigate the human control behavior perturbed by the devised task input, a methodology known as the *cybernetic approach* [65, 67, 68].

MANUAL CONTROL CYBERNETICS IN COMPENSATORY TRACKING

Compensatory tracking is one of the major approaches to understand how humans engage in closed-loop control [28, 65, 67–71]. This task restricts a pilot to respond solely to a single, visually presented error signal, which represents a deviation from some desired reference. It significantly reduces the complexity of the human controller into a single-input single-output system, while preserving key characteristics such as the ability to adapt to various controlled elements [65].

Fig. 1.5 illustrates the process of such a control task, showing how the pilot becomes a serial element that acts on the error signal to generate the control activity. To investigate the possibly different effects of the haptic feedback on target following and disturbance rejection, we design two forcing functions for independent evaluation of the corresponding manual control behavior. The error signal is the difference between the first forcing function, which represents the desired pitch or roll angle, and the current aircraft attitude. The aircraft model is fed with the pilot control input and the second forcing function, which represents turbulence acting on the aircraft.

Rather than collecting subjective feedback about the task, we evaluate the performance of human controllers on the basis of objective measurements of the task variables, such as the error signal and the pilot's control activity. This allows for estimation of the frequency response function of the pilot dynamics. With quasi-random multisine forcing functions, the human controller resembles a linear time-invariant system [65, 68]. More importantly, humans systematically adapt to various controlled elements by adopting sufficient lag-lead equalization, such that the open-loop response

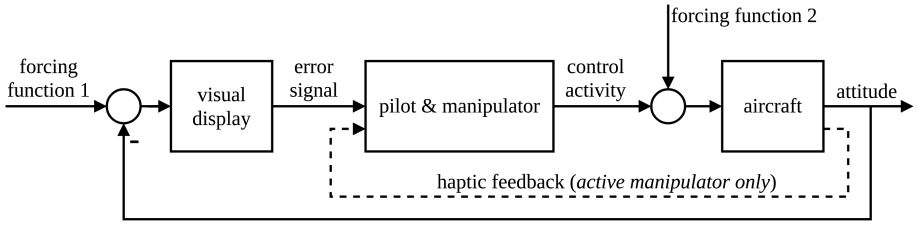

Figure 1.5: A schematic diagram of the target-following and disturbance-rejection compensatory control task performed in this thesis. For clarity, the haptic feedback provided by the active manipulator is also shown. In this thesis, the active manipulator provides the feedback about the aircraft angular velocity.

of the entire system (the closed-loop system shown in Fig. 1.5) possesses the characteristics of a *single integrator* in the crossover region (i.e., the crossover model) [65].

Such a remarkable feature allows us to understand how pilots adapt their behavior for the active manipulator by examining the changes caused by this control device in the *crossover frequency* and the *phase margin* of the open-loop response. With two uncorrelated forcing functions, investigations can be conducted independently into the crossover characteristics for target following and disturbance rejection. More importantly, the two forcing functions allow for identification of both the pilot's response to the visual presentation (i.e., the dynamics processed by the brain) and his or her response to the haptic feedback about aircraft states (i.e., the role of the neuromuscular system) [28]. The analysis associated with this approach is presented in Chapter 2.

1.4.2. INVESTIGATING PERCEPTION CHARACTERISTICS

Addressing the Key Questions II-1 and II-2 requires us to investigate the perception changes associated with delayed force feedback, and measure the human perception thresholds under conditions which defines different degrees of mutual effects between the three mechanical properties. To this end, *psychophysical experiments* are conducted in this thesis. Experimental results are analyzed in the *frequency domain*, in an attempt to explain observed phenomena in a more systematic fashion. This subsection gives a brief overview of the approaches we use.

PSYCHOPHYSICAL METHODS

The term "psychophysics", as stated in [72] on page 462, refers to "*The analysis of perceptual processes by studying the effect on a subject's experience or behaviour of systematically varying the properties of a stimulus along one or more physical dimensions*". Over the past century, many sophisticated methods have been developed and used for research into all sensory systems, i.e., vision, hearing, touch, taste, and smell [73]. In this thesis, the first two key research questions are addressed using two different psychophysical approaches.

The most straightforward way to understand how humans characterize changes in system dynamics as changes in the three mechanical properties, is to quantitatively measure their perception. In this thesis, we adopt the *method of adjustment* [73], in which each of the participants is asked to make a number of comparisons between two mass-spring-damper systems: a reference system and a control system. The difference between these two applied systems is only a time delay in the force feedback that the participant receives from the reference system. The participant is allowed to freely adjust the mass, damping, and stiffness of the control system until he or she reaches the point of subjective equality, the point where one feels the two systems to be the same. Thus, the parameters of the control system are the objective measurements that demonstrate the effects of delayed force feedback on the perceived mechanical properties. In the experiment, different time delays are tested to explore the effects of the delay magnitude. Chapter 3 will describe this procedure in greater detail, and discuss the experimental results.

In this thesis, the perception threshold is obtained using the *adaptive staircase procedure* [73], a method that allows for efficient measurement of the JND. Like the method described above, the staircase procedure also requires a participant to make

a number of comparisons between a reference system and a control system. The difference between the two mass-spring-damper systems lies in the mechanical property in which we measure the JND. The staircase procedure, as the name implies, adjusts the tested mechanical property of the control system after each comparison in order to reveal when the participant is just able to detect a change. To understand the interaction between mass, damping, and stiffness, the JND in each property is measured under conditions that differ in the other two properties. Readers are referred to Chapters 4 and 5 for more details about this approach.

EXPLAINING PSYCHOPHYSICAL FINDINGS USING FREQUENCY-RESPONSE FORMULATION

Humans are unable to directly sense mechanical properties due to the lack of dedicated sensors. Unlike directly sensed signals that can be received passively, the perception of mechanical properties must involve active interaction. We *estimate* mass, damping, and stiffness based on the relation between movement and force, signals that are mainly measured by receptors in muscles, skin, and joints [57, 58, 74, 75].

For linear systems, such a relation is determined by the *frequency response function* (FRF). This indicates that we can link human perception to the FRF and can conduct our investigation in the freqency domain. The maturity of linear system theory allows us to formulate various candidate models for the model identification of the perception threshold. It also helps to clarify the principle of how time delays affect the perceived mechanical properties, since the FRF provides detailed insights into the changes in the relation between movement and force.

As a time domain variable is a function of time, a frequency domain variable is a function of frequency. To accurately represent the perception characteristics in the frequency domain, we need to collect the psychophysical results at different frequencies. A convenient approach is to *confine* haptic interactions to *each individual frequency*, a method that resembles the frequency-sweep technique adopted in model identification of mechanical systems. In our study, this is achieved by asking participants to track *sinusoidal* movements, defined at different frequencies, while performing the psychophysical tasks mentioned earlier. Detailed discussions follow in Chapters 3, 4, and 5.

1.5. THESIS OUTLINE

This thesis consists of seven chapters and two appendices. Except for the Introduction and Conclusion chapters, all are based on peer-reviewed articles that are either published or currently under review. Details about these articles appear at the beginning of each chapter. The text is in general identical to the published work, with slight adjustments made to obtain smooth transitions and a consistent terminology. Therefore, each chapter can be read independently.

This main body of this thesis has three parts, see Fig. 1.6 for an illustration of the structure. The first two parts correspond to the two main research objectives. The first part develops a design philosophy different from that behind the conventional passive control device. It presents a means of creating haptic feedback that more effectively exploits the potential of human controllers. The second part establishes the understanding of the characteristics of human haptic perception, which is necessary

for a human-centric evaluation of the quality of haptic displays. To facilitate the understanding of the practical application of the advances made in the second part, the third part then gives examples of how a perception-oriented evaluation of haptic presentation can be performed, such as the evaluation of display fidelity of haptic devices and the control feel of the active manipulator developed in the first part. In addition, the two appendices, Appendix A and Appendix B, present results from psychophysical studies carried out alongside the main line of the thesis.

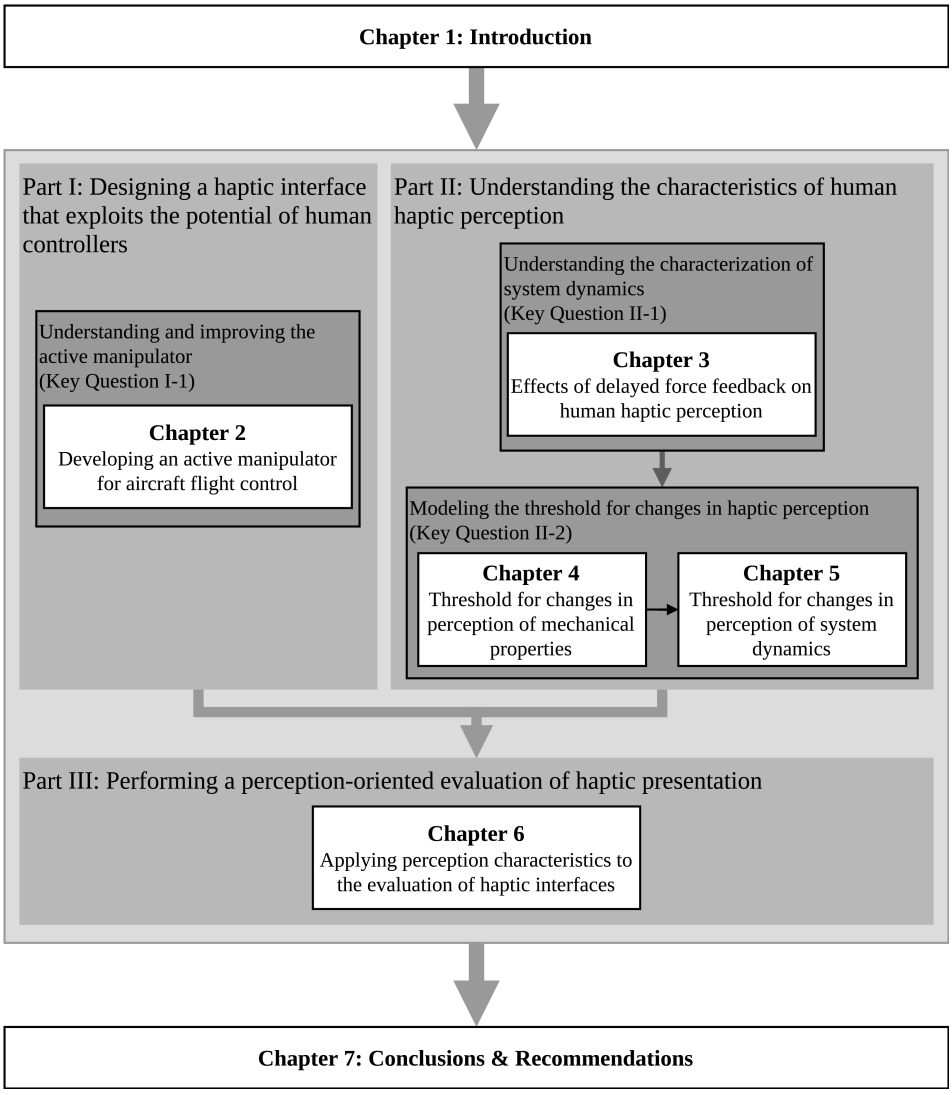

Figure 1.6: The outline of the thesis

1.5.1. PART I: DESIGNING A HAPTIC INTERFACE THAT EXPLOITS THE POTENTIAL OF HUMAN CONTROLLERS

Part I includes Chapter 2, which takes on the challenge posed by the Key Question I-1 that corresponds to our first objective.

Chapter 2 explores the rationale behind how the active manipulator improves pilots' flight control performance, and further develops this concept. First, The human control behavior associated with this particular control device is evaluated using cybernetic approach. We observed a positive correlation between the performance improvement brought by the active manipulator and the bandwidth of the forcing functions. This is accounted for by the fact that the feedback about the aircraft's rotational velocity makes the majority of the aircraft dynamics be absorbed by the control device and thereby controlled by the neuromuscular system. What is left (i.e., the effective controlled element) is an *integrator*, allowing pilots to act as simple, proportional controllers. Furthermore, the haptic feedback allows pilots to feel the disturbance acting on the aircraft through the motion of the manipulator. The two independent forcing functions enable us to estimate the impedance of the neuromuscular system, which provides clear evidence of the involvement of the muscle co-contraction in disturbance rejection.

Second, we further improve the operational quality of the active manipulator without impeding its effectiveness. The involuntary arm movements, caused by the feedback about aerodynamic disturbance, are considerably attenuated. This is achieved by selectively *decoupling* the control device from the aircraft using a lag-lead filter, the design of which is based on passivity theory, and adjusted according to subjects' crossover characteristics observed in compensatory tasks.

1.5.2. PART II: UNDERSTANDING CHARACTERISTICS OF HUMAN HAPTIC PERCEPTION

Part II, which is comprised of Chapters 3, 4, and 5, describes the approach to address our second research objective. Key Question II-1 is addressed in Chapter 3, and Key Question II-2 is addressed in Chapters 4 and 5.

Chapter 3 first demonstrates the underlying principles of how dynamic distortions are characterized by humans as changes in the mechanical properties. We initiate our investigation with psychophysical experiments on the effect of time delays. Based on the experimental findings, we explain how time delays affect human perception and how this is correlated with the delay magnitude. Furthermore, using a frequency response model of system dynamics formulated as an impedance, we propose a framework that relates the perception of mass, damping, and stiffness to the real and imaginary parts of the system dynamics' frequency response. This framework can explain the effects of all changes in the magnitude and phase characteristics, allowing a unified view on human perception changes associated with all other causes (such as the actuator dynamics).

Chapters 4 and 5 extend our understanding of the perception threshold by establishing a mathematical model of the JND in system dynamics. The model is obtained by mapping frequency-domain formulations to the observations from a number of psychophysical experiments. The model is first proposed in Chapter 4, then extended

in Chapter 5. It successfully captures the interactions between the perceptions of mechanical properties. More importantly, it links the JNDs in mass, damping, and stiffness to the JNDs in the system's frequency response. This allows us to generalize all previous findings, and represent the threshold for perceiving changes in the dynamics of a system with two dimensions: the real and imaginary axes in the complex plane.

1.5.3. PART III: PERFORMING A PERCEPTION-ORIENTED EVALUATION OF HAPTIC PRESENTATION

Part III includes Chapter 6, which demonstrates how the understanding of human haptic perception can be applied in practice. First, a two-step approach to a perception-oriented evaluation of the fidelity of haptic displays is proposed. A numerical example is given to facilitate the understanding of how the threshold model, and the perception framework, proposed in Part II can be applied. These two steps, respectively, show when and how a particular haptic device alters what the operator perceives. Second, to provide more insights into the active manipulator developed in Chapter 2, Chapter 6 evaluates the control feel associated with the aircraft dynamics conveyed by the feedback of the aircraft rotational velocity. Findings from the previous chapters allow us to reveal the characteristics of the perceived manipulator dynamics and quantify the perception in terms of three basic mechanical properties.

REFERENCES

[1] D. Yoerger and J. J. Slotine, "Supervisory control architecture for underwater teleoperation," in *IEEE Int. Conf. on Robotics and Automation*, vol. 4, Raleigh, USA, Mar 1987, pp. 2068–2073.

[2] G. Schmidt, G. Landis, and S. Oleson, "HERRO missions to mars and venus using telerobotic surface exploration from orbit," in *AIAA SPACE 2011 Conf. & Expo.*, no. AIAA-2011-7343, Long Beach, USA, Sept 2011.

[3] G. Clement, J. Vertut, R. Fournier, B. Espiau, and G. Andre, "An overview of CAT control in nuclear services," in *IEEE Int. Conf. on Robotics and Automation*, vol. 2, St. Louis, USA, Mar 1985, pp. 713–718.

[4] A. R. Lanfranco, A. E. Castellanos, J. P. Desai, and W. C. Meyers, "Robotic surgery: A current perspective," *Annals of Surgery*, vol. 239, no. 1, pp. 14–21, 2004.

[5] J. Rebelo, T. Sednaoui, E. B. den Exter, T. Krueger, and A. Schiele, "Bilateral robot teleoperation: A wearable arm exoskeleton featuring an intuitive user interface," *IEEE Robotics Automation Magazine*, vol. 21, no. 4, pp. 62–69, 2014.

[6] 3D systems phantom premium. 3D Systems. [Online]. Available: https://www.3dsystems.com/haptics-devices/3d-systems-phantom-premium

[7] A. M. Okamura, "Haptic feedback in robot-assisted minimally invasive surgery," *Current Opinion in Urology*, vol. 19, no. 1, pp. 102–7, 2009.

[8] R. J. Stone, "Haptic feedback: A brief history from telepresence to virtual reality," in *Int. Workshop on Haptic Human-Computer Interaction*, Glasgow, United Kingdom, Aug 2001, pp. 1–16.

[9] R. J. A. W. Hosman, B. Benard, and H. Fourquet, "Active and passive side stick controllers in manual aircraft control," in *IEEE Int. Conf. on Systems, Man and Cybernetics (SMC)*, Los Angeles, USA, Nov 1990, pp. 527–529.

[10] S. de Stigter, M. Mulder, and M. M. van Paassen, "Design and evaluation of a haptic flight director," *J. of Guidance, Control, and Dynamics*, vol. 30, no. 1, pp. 35–46, 2007.

[11] D. A. Abbink, M. Mulder, and E. R. Boer, "Haptic shared control: Smoothly shifting control authority?" *Cognition, Tech. & Work*, vol. 14, no. 1, pp. 19–28, 2012.

[12] M. Mulder, D. A. Abbink, and E. R. Boer, "Sharing control with haptics: Seamless driver support from manual to automatic control," *Human Factors*, vol. 54, no. 5, pp. 786–798, 2012.

[13] J. Smisek, E. Sunil, M. M. van Paassen, D. A. Abbink, and M. Mulder, "Neuromuscular-system-based tuning of a haptic shared control interface for UAV teleoperation," *IEEE Trans. on Human-Machine Systems*, vol. 47, no. 4, pp. 449–461, 2017.

[14] T. M. Lam, M. Mulder, and M. M. van Paassen, "Haptic feedback in uninhabited aerial vehicle teleoperation with time delay," *J. of Guidance, Control, and Dynamics*, vol. 31, no. 6, pp. 1728–1739, 2008.

[15] T. M. Lam, H. W. Boschloo, M. Mulder, and M. M. van Paassen, "Artificial force field for haptic feedback in UAV teleoperation," *IEEE Trans. on Systems, Man, and Cybernetics - Part A: Systems and Humans*, vol. 39, no. 6, pp. 1316–1330, 2009.

[16] X. Hou, R. Mahony, and F. Schill, "Comparative study of haptic interfaces for bilateral teleoperation of VTOL aerial robots," *IEEE Trans. on Systems, Man, and Cybernetics: Systems*, vol. 46, no. 10, pp. 1352–1363, 2016.

[17] J. G. W. Wildenbeest, R. J. Kuiper, F. C. T. van der Helm, and D. A. Abbink, "Position control for slow dynamic systems: Haptic feedback makes system constraints tangible," in *IEEE Int. Conf. on Systems, Man, and Cybernetics (SMC)*, San Diego, USA, Oct 2014, pp. 3990–3995.

[18] I. Nisky, A. Pressman, C. M. Pugh, F. A. M. Ivaldi, and A. Karniel, "Perception and action in teleoperated needle insertion," *IEEE Trans. on Haptics*, vol. 4, no. 3, pp. 155–166, 2011.

[19] R. J. Adams and B. Hannaford, "Stable haptic interaction with virtual environments," *IEEE Trans. Robotics and Automation*, vol. 15, no. 3, pp. 465–474, 1999.

[20] J. K. Salisbury and M. A. Srinivasan, "Phantom-based haptic interaction with virtual objects," *IEEE Computer Graphics and Applications*, vol. 17, no. 5, pp. 6–10, 1997.

[21] M. C. Cavusoglu, F. Tendick, M. Cohn, and S. S. Sastry, "A laparoscopic telesurgical workstation," *IEEE Trans. on Robotics and Automation*, vol. 15, no. 4, pp. 728–739, 1999.

[22] Y. Yokokohji and T. Yoshikawa, "Bilateral control of master-slave manipulators for ideal kinesthetic coupling-formulation and experiment," *IEEE Trans. on Robotics and Automation*, vol. 10, no. 5, pp. 605–620, 1994.

[23] P. J. Deldycke, D. Van Baelen, D. M. Pool, M. van Paassen, and M. Mulder, "Design and evaluation of a haptic aid for training of the manual flare manoeuvre," in *AIAA Modeling and Simulation Technologies Conf.*, no. AIAA-2018-0113, Kissimmee, USA, Jan 2018.

[24] S. M. Petermeijer, D. A. Abbink, M. Mulder, and J. C. F. de Winter, "The effect of haptic support systems on driver performance: A literature survey," *IEEE Trans. on Haptics*, vol. 8, no. 4, pp. 467–479, 2015.

[25] D. Van Baelen, J. Ellerbroek, M. M. van Paassen, and M. Mulder, "Design of a haptic feedback system for flight envelope protection," in *AIAA Modeling and Simulation Tech. Conf.*, no. AIAA-2018-0117, Kissimmee, USA, Jan 2018.

[26] M. Olivari, F. M. Nieuwenhuizen, H. H. Bülthoff, and L. Pollini, "Pilot adaptation to different classes of haptic aids in tracking tasks," *J. of Guidance, Control, and Dynamics*, vol. 37, no. 6, pp. 1741–1753, 2014.

[27] F. Flemisch, Y. Canpolat, E. Altendorf, G. Weßel, M. Itoh, F. Flemisch, M. Baltzer, M. P. Lemoine, D. A. Abbink, and P. Schutte, "Shared and cooperative control of ground and air vehicles: Introduction and general overview," in *IEEE Int. Conf. on Systems, Man, and Cybernetics (SMC)*, Banff, Canada, Oct 2017, pp. 858–863.

[28] M. M. van Paassen, J. C. van der Vaart, and J. A. Mulder, "Model of the neuromuscular dynamics of the human pilot's arm," *J. of Aircraft*, vol. 41, no. 6, pp. 1482–1490, 2004.

[29] M. M. van Paassen, "Biophysics in aircraft control: A model of the neuromuscular system of the pilot's arm," Ph.D. dissertation, TU Delft, Delft University of Technology, 1994.

[30] D. A. Abbink, "Neuromuscular analysis of haptic gas pedal feedback during car following," Ph.D. dissertation, TU Delft, Delft University of Technology, 2006.

[31] R. J. A. W. Hosman and J. C. van der Vaart, "Active and passive side stick controllers: Tracking task performance and pilot control behavior," in *AGARD Conf. on the Man-Machine Interface in Tactical Aircraft Design and Combat Automation*, no. 425, Stuttgart, Germany, Sept 1988.

[32] B. Hannaford, "A design framework for teleoperators with kinesthetic feedback," *IEEE Trans. on Robotics and Automation*, vol. 5, no. 4, pp. 426–434, 1989.

[33] D. A. Lawrence, "Stability and transparency in bilateral teleoperation," *IEEE Trans. on Robotics and Automation*, vol. 9, no. 5, pp. 624–637, 1993.

[34] K. H. Zaad and S. E. Salcudean, "Adaptive transparent impedance reflecting teleoperation," in *IEEE Int. Conf. on Robotics and Automation*, vol. 2, Minneapolis, USA, Apr 1996, pp. 1369–1374.

[35] J. Kim, P. H. Chang, and H. Park, "Two-channel transparency-optimized control architectures in bilateral teleoperation with time delay," *IEEE Trans. on Control Systems Technology*, vol. 21, no. 1, pp. 40–51, 2013.

[36] P. F. Hokayem and M. W. Spong, "Bilateral teleoperation: An historical survey," *Automatica*, vol. 42, no. 12, pp. 2035–2057, 2006.

[37] P. Mitra and G. Niemeyer, "Model-mediated telemanipulation," *The Int. J. of Robotics Research*, vol. 27, no. 2, pp. 253–262, 2008.

[38] B. Hannaford, "Stability and performance tradeoffs in bi-lateral telemanipulation," in *Int. Conf. on Robotics and Automation*, vol. 3, Scottsdale, USA, May 1989, pp. 1764–1767.

[39] R. Daniel and P. McAree, "Fundamental limits of performance for force reflecting teleoperation," *The Int. J. of Robotics Research*, vol. 17, no. 8, pp. 811–830, 1998.

[40] N. Colonnese and A. M. Okamura, "M-width: Stability, noise characterization, and accuracy of rendering virtual mass," *The Int. J. of Robotics Research*, vol. 34, no. 6, pp. 781–798, 2015.

[41] R. J. Adams and B. Hannaford, "Control law design for haptic interfaces to virtual reality," *IEEE Trans. on Control Systems Technology*, vol. 10, no. 1, pp. 3–13, 2002.

[42] B. Hannaford and J. H. Ryu, "Time-domain passivity control of haptic interfaces," *IEEE Trans. on Robotics and Automation*, vol. 18, no. 1, pp. 1–10, 2002.

[43] J. H. Ryu, D. S. Kwon, and B. Hannaford, "Stability guaranteed control: Time domain passivity approach," *IEEE Trans. on Control Systems Technology*, vol. 12, no. 6, pp. 860–868, 2004.

[44] R. J. Anderson and M. W. Spong, "Bilateral control of teleoperators with time delay," *IEEE Trans. on Automatic Control*, vol. 34, no. 5, pp. 494–501, 1989.

[45] G. Niemeyer and J. J. E. Slotine, "Stable adaptive teleoperation," *IEEE J. of Oceanic Engineering*, vol. 16, no. 1, pp. 152–162, 1991.

[46] P. H. Chang and J. Kim, "Telepresence index for bilateral teleoperations," *IEEE Trans. on Systems, Man, and Cybernetics, Part B (Cybernetics)*, vol. 42, no. 1, pp. 81–92, 2012.

[47] W. Iida and K. Ohnishi, "Reproducibility and operationality in bilateral teleoperation," in *The 8th IEEE International Workshop on Advanced Motion Control*, Kawasaki, Japan, Mar 2004, pp. 217–222.

[48] A. Pressman, L. J. Welty, A. Karniel, and F. A. Mussa Ivaldi, "Perception of delayed stiffness," *The Int. J. of Robotics Research*, vol. 26, no. 11-12, pp. 1191–1203, 2007.

[49] I. Nisky, F. A. Mussa Ivaldi, and A. Karniel, "A regression and boundary-crossing-based model for the perception of delayed stiffness," *IEEE Trans. on Haptics*, vol. 1, no. 2, pp. 73–82, 2008.

[50] I. Nisky, P. Baraduc, and A. Karniel, "Proximodistal gradient in the perception of delayed stiffness," *J. of Neurophysiology*, vol. 103, no. 6, pp. 3017–3026, 2010.

[51] N. Colonnese, A. F. Siu, C. M. Abbott, and A. M. Okamura, "Rendered and characterized closed-loop accuracy of impedance-type haptic displays," *IEEE Trans. on Haptics*, vol. 8, no. 4, pp. 434–446, 2015.

[52] R. Leib, A. Karniel, and I. Nisky, "The effect of force feedback delay on stiffness perception and grip force modulation during tool-mediated interaction with elastic force fields," *J. of Neurophysiology*, vol. 113, no. 9, pp. 3076–3089, 2015.

[53] S. Hirche, A. Bauer, and M. Buss, "Transparency of haptic telepresence systems with constant time delay," in *IEEE Conf. on Control Applications*, Toronto, Canada, Aug 2005, pp. 328–333.

[54] X. D. Pang, H. Z. Tan, and N. I. Durlach, "Manual discrimination of force using active finger motion," *Perception & Psychophysics*, vol. 49, no. 6, pp. 531–540, 1991.

[55] S. Feyzabadi, S. Straube, M. Folgheraiter, E. A. Kirchner, S. K. Kim, and J. C. Albiez, "Human force discrimination during active arm motion for force feedback design," *IEEE Trans. on Haptics*, vol. 6, no. 3, pp. 309–319, 2013.

[56] D. A. Abbink and F. C. T. van der Helm, "Force perception measurements at the foot," in *IEEE Int. Conf. on Systems, Man and Cybernetics (SMC)*, vol. 3, The Hague, Netherlands, Oct 2004, pp. 2525–2529.

[57] L. A. Jones, "Kinesthetic sensing," in *Workshop on Human and Machine Haptics*, Pacific Grove, USA, Dec 1997, pp. 1–10.

[58] H. Z. Tan, N. I. Durlach, G. L. Beauregard, and M. A. Srinivasan, "Manual discrimination of compliance using active pinch grasp: The roles of force and work cues," *Perception & Psychophysics*, vol. 57, no. 4, pp. 495–510, 1995.

[59] L. A. Jones and I. W. Hunter, "A perceptual analysis of stiffness," *Experimental Brain Research*, vol. 79, no. 1, pp. 150–156, 1990.

[60] ——, "A perceptual analysis of viscosity," *Experimental Brain Research*, vol. 94, no. 2, pp. 343–351, 1993.

[61] G. L. Beauregard, M. A. Srinivasan, and N. I. Durlach, "The manual resolution of viscosity and mass," in *ASME Dynamic Systems and Control Division*, vol. 1, 1995, pp. 657–662.

[62] M. Kühner, J. Wild, H. Bubb, K. Bengler, and J. Schneider, "Haptic perception of viscous friction of rotary switches," in *IEEE World Haptics Conf.*, Istanbul, Turkey, Jun 2011, pp. 587–591.

[63] J. Schmidtler and M. Körber, "Human perception of inertial mass for joint human-robot object manipulation," *ACM Trans. on Applied Perception (TAP)*, vol. 15, no. 3, 2018.

[64] M. Rank, T. Schauß, A. Peer, S. Hirche, and R. L. Klatzky, "Masking effects for damping JND," in *Int. Conf. on Human Haptic Sensing and Touch Enabled Computer Applications*, Tampere, Finland, Jun 2012, pp. 145–150.

[65] D. T. McRuer and H. R. Jex, "A review of quasi-linear pilot models," *IEEE Trans. on Human Factors in Electronics*, vol. HFE-8, no. 3, pp. 231–249, 1967.

[66] D. T. McRuer, "Human pilot dynamics in compensatory systems," Systems Technology Inc., Hawthorne, USA, Tech. Rep., 1965.

[67] H. J. Damveld, G. C. Beerens, M. M. van Paassen, and M. Mulder, "Design of forcing functions for the identification of human control behavior," *J. of Guidance, Control, and Dynamics*, vol. 33, no. 4, pp. 1064–1081, 2010.

[68] M. Mulder, D. M. Pool, D. A. Abbink, E. R. Boer, P. M. T. Zaal, F. M. Drop, K. van der El, and M. M. van Paassen, "Manual control cybernetics: State-of-the-art and current trends," *IEEE Trans. on Human-Machine Systems*, vol. 48, no. 5, pp. 468–485, 2018.

[69] D. M. Pool, M. Mulder, M. M. van Paassen, and J. C. van der Vaart, "Effects of peripheral visual and physical motion cues in roll-axis tracking tasks," *J. of Guidance, Control, and Dynamics*, vol. 31, no. 6, pp. 1608–1622, 2008.

[70] P. M. T. Zaal, D. M. Pool, J. de Bruin, M. Mulder, and M. M. van Paassen, "Use of pitch and heave motion cues in a pitch control task," *J. of Guidance, Control, and Dynamics*, vol. 32, no. 2, pp. 366–377, 2009.

[71] G. C. Beerens, H. J. Damveld, M. Mulder, M. M. van Paassen, and J. C. van der Vaart, "Investigation into crossover regression in compensatory manual tracking tasks," *J. of Guidance, Control, and Dynamics*, vol. 32, no. 5, pp. 1429–1445, 2009.

[72] V. Bruce, P. R. Green, and M. A. Georgeson, *Visual Perception: Physiology, Psychology, & Ecology*. Psychology Press, 2003.

[73] F. A. A. Kingdom and N. Prins, *Psychophysics: a Practical Introduction*. Academic Press, 2016.

[74] W. Fu, M. M. van Paassen, and M. Mulder, "The influence of discrimination strategy on the JND in human haptic perception of manipulator stiffness," in *AIAA Modeling and Simulation Technologies Conf.*, no. AIAA-2017-3668, Denver, USA, Jun 2017.

[75] ——, "On the relationship between the force JND and the stiffness JND in haptic perception," in *ACM Symp. on Applied Perception*, no. 11, Cottbus, Germany, Sept 2017.

PART I

DESIGNING A HAPTIC INTERFACE THAT EXPLOITS THE POTENTIAL OF HUMAN CONTROLLERS

2

DEVELOPING AN ACTIVE MANIPULATOR IN AIRCRAFT FLIGHT CONTROL

As discussed in the Introduction, the active manipulator represents one way to more effectively exploit the potential of human controllers. The objectives of this chapter are to explore the benefit of the active manipulator, to investigate the associated manual control behavior using a cybernetic approach, and most importantly, to use such knowledge to further improve the effectiveness of such a control device. We find that the active manipulator facilitates manual aircraft control by transforming the effective controlled element into a single integrator, and at the same time integrating disturbance rejection into the neuromuscular system. Based on the passivity theory and subjects' crossover characteristics observed during compensatory tasks, we selectively decoupled the active manipulator from the aircraft in the frequency spectrum. This considerably improves the operational quality of the control device by attenuating the high-frequency aerodynamic disturbance present in the feedback of the aircraft rotational rate.

This chapter has been published as: W. Fu, M. M. van Paassen and M. Mulder, "Developing Active Manipulators in Aircraft Flight Control," *Journal of Guidance, Control, and Dynamics*, published online, pp. 1-13, 2019.

2.1. INTRODUCTION

In recent years, haptic interfaces have received increased interest and facilitated manual control task innovations in many fields, such as surgical robots, terrestrial and space operations, as well as nuclear plant operations [1–7]. In general, a haptic interface is established with a control manipulator, through which a human operator exerts control while haptically receiving information about the controlled system.

In contrast to the conventional aircraft control, where the pilot controls the aircraft through a passive manipulator and only receives information about the aircraft states through the vision and motion sensory systems, a haptic interface can introduce additional ways to inform the pilot. The fly-by-wire system of modern aircraft offers the possibility to design the control manipulator as a haptic interface, thereby establishing bilateral transmission of information and facilitating manual aircraft control. In general, existing haptic interfaces developed for aircraft control work as support systems which inform the pilot about one or more aspects, such as the current flight condition, the task, or constraints (e.g., boundaries, dangers) in the environment. The common approach taken is by providing additional forces commanded by a haptic support system [7, 8]. However, the manipulator itself is still a passive device with its own dynamics, decoupled from those of the aircraft. Due to this, a direct connection between the pilot and the aircraft is not fully established.

Apart from the haptic support systems, there is still much room for improvement on the manipulator itself. To this end, in this study we fundamentally change the nature of the manipulator. The current work draws primarily on the foundation laid by previous attempts by Hosman et al. [9, 10] in which the active manipulator was developed. The active manipulator is based on the admittance display architecture [11], in which a particular state of the controlled aircraft (in our case: attitude rate) is displayed through the movement of the control manipulator. The pilot's control input to the aircraft, in this case, is derived from the force applied to the manipulator (see Section 2.2 for more details). In this way, the manipulator is completely coupled to the aircraft.

It was demonstrated that the prototype of the active manipulator led to considerable improvements in the flight-control performance [9, 10]. However, knowledge about the guiding principle that accounts for such improvements is still lacking, largely impeding attempts at further development of the active manipulator. In this study an investigation was conducted firstly, to allow for corroboration of the previous findings, and to gather theoretical evidence that supports those findings. To this end, an experiment in which participants performed compensatory tasks with various forcing-function bandwidths was carried out. Secondly, we found that the control task was facilitated by only the feedback of a certain low-frequency segment of the power spectrum of the aircraft state. Due to the disturbance (e.g., turbulence) acting on the aircraft, the feedback beyond this frequency range actually *reduced* the operational quality of the active manipulator. A lag-lead filter was designed to selectively decouple the dynamics of the active manipulator from those of the aircraft. The viability of the filter was then proven by the control task in a second experiment.

This chapter is organized as follows: Section 2.2 elaborates on the design principle behind the active manipulator. The set-up of the first experiment that compares the active and passive manipulators, and the analysis of the results are given in Sections

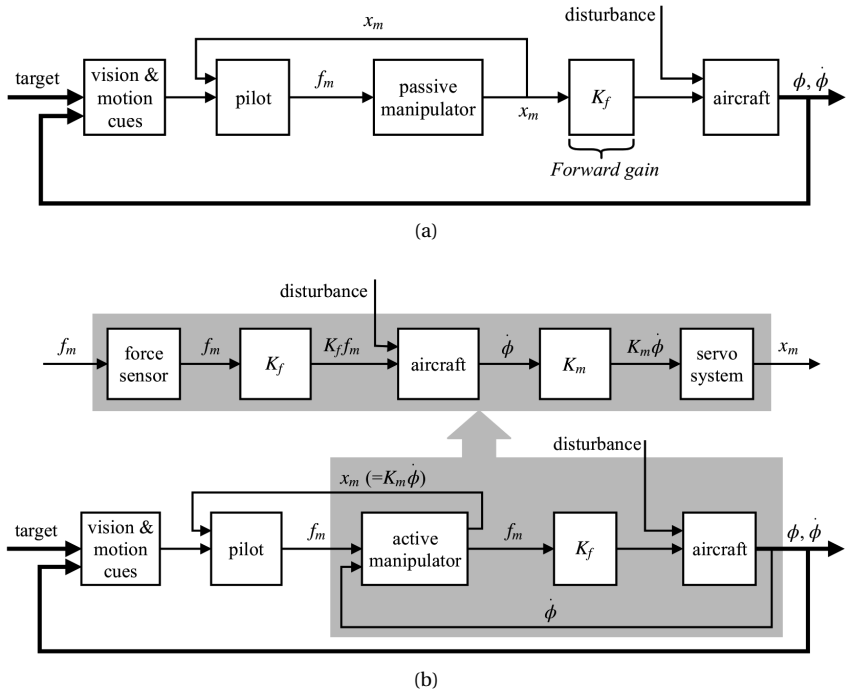

Figure 2.1: Schematic diagrams of the control of the aircraft roll attitude with: (a) the passive manipulator; (b) the active manipulator. Here, f_m, x_m, and ϕ denote the torque that the pilot applies to the manipulator, the deflection angle of the manipulator, and the roll angle of the aircraft, respectively.

2.3 and 2.4, respectively. The principle behind the pilot's performance improvement associated with the active manipulator is revealed in Section 2.5. Section 2.6 presents the design of a lag-lead filter to improve performance, the tuning of which was tested experimentally as discussed in Section 2.7. The contributions of this study are discussed and summarized in Sections 2.8 and 2.9.

2.2. ACTIVE MANIPULATOR

In conventional aircraft control, the pilot controls the aircraft by means of the deflection angle of a passive manipulator. For instance, consider the control of the aircraft roll angle, as can be seen in Fig. 2.1a. The passive manipulator usually resembles a mass-spring-damper system. Changing the manipulator deflection angle (x_m) resembles moving a mass that is connected with a spring and a damper to an infinitely stiff basis. However, due to the aircraft dynamics the manipulator movement is different than the aircraft's and does not reflect any of the true aircraft states. The pilot can only perceive the information about the aircraft states through vision and motion.

In addition to other sensory channels, the active manipulator involves the haptic channel in perceiving the aircraft's state information. It allows the pilot to directly perceive an aircraft output – typically the aircraft rotational velocity – through the ma-

Figure 2.2: Devices used for the experiment.

nipulator. Figure 2.1b shows an example of the control of the aircraft roll angle. As can be seen, the force that the pilot applies to the manipulator (f_m) is measured and fed to the aircraft. At the same time, the manipulator deflection is driven by a position servo system which tracks the angular velocity of the aircraft ($\dot{\phi}$). If we ignore the dynamics of the force sensor and servo system, the deflection of the active manipulator, x_m, is proportional to $\dot{\phi}$: $x_m = K_m\dot{\phi}$.

As compared to the passive manipulator, the active manipulator leads to significant improvements in flight control performance [9, 10]. However, as mentioned earlier, these findings lack a theoretical basis. Hence, to obtain more insights, and provide a comparison with previous results, we conducted an experiment, discussed in the next section.

2.3. EXPERIMENT ONE: EFFECTS OF THE ACTIVE MANIPULATOR ON HUMAN CONTROL BEHAVIOR

A roll-axis compensatory task, which involves both target following and disturbance rejection, is performed. The two manipulator types, namely the active and passive manipulator, are compared in terms of the task performance. The target and disturbance signals are designed with three different bandwidths to evaluate the active manipulator in cases of different task difficulties. A factorial combination of the two manipulator types and the three forcing-function bandwidths yields six experimental conditions. Twelve subjects participated in the experiment. To ensure stable performance, extensive training was performed before the measurements were collected. The remainder of this section gives details about the experiment.

2.3.1. APPARATUS

The visual display (an LCD screen) and the manipulator used for the experiment are marked by white boxes in Fig. 2.2. The manipulator is a control loading device which is equipped with a force sensor and driven by an electro-hydraulic position servo system with a bandwidth around 40 Hz. Such a device allows for the realization of both passive and active manipulators. The manipulator is supplied with a handle, diame-

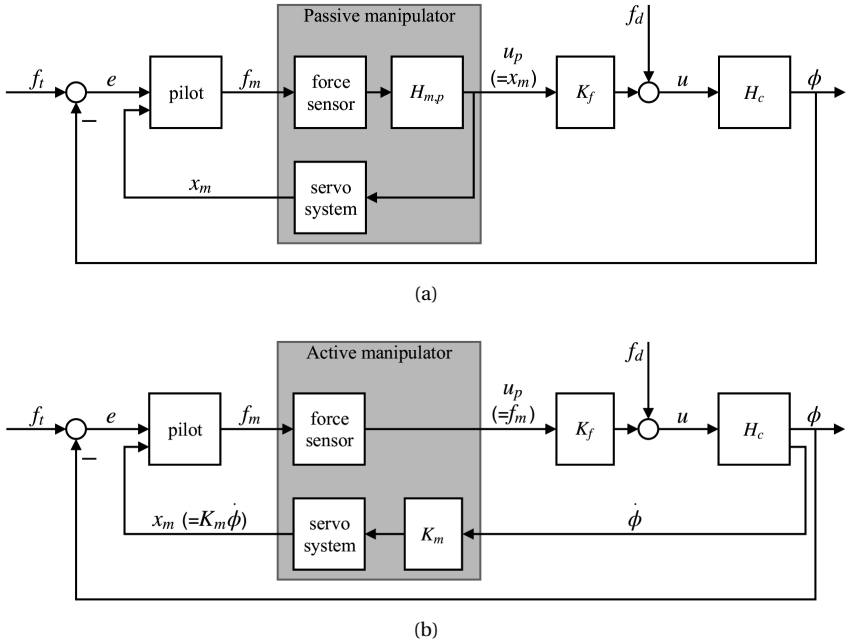

Figure 2.3: Schematic diagrams of the compensatory task: (a) with the passive manipulator; (b) with the active manipulator.

ter 35 mm, with grooves for placement of the fingers. When a hand is correctly placed on the handle, the center of the hand lies 90 mm above the manipulator rotation axis. During the experiment, the manipulator movement around the pitch axis (fore/aft) is fixed at the neutral position. The range of travel with respect to the roll axis is limited to ±0.47 rad.

2.3.2. SETUP OF THE COMPENSATORY TASK

Figures 2.3a and 2.3b respectively illustrate the compensatory tasks with the two manipulator types. Please note that except for the manipulator setup and the variable u_p (the pilot's control input to the aircraft), the tasks with the two manipulator types are exactly the same. The task requires the pilot to minimize tracking error e, the difference between the target forcing function f_t and the controlled-element output ϕ: $e = f_t - \phi$. In the experiment, e is presented on the visual display with a simplified artificial horizon indicator, as can be seen from Fig. 2.4.

The pilot generates the control signal u_p using the manipulator, on the basis of the visually perceived e. Here, u_p is different between the two manipulator types. For the passive manipulator, u_p is the manipulator deflection angle: $u_p = x_m$. The shaded area in Fig. 2.3a gives a simplified diagram of how the passive manipulator is realized using our control loading device.

In this study the dynamics of a linear mass-spring-damper system are used as the

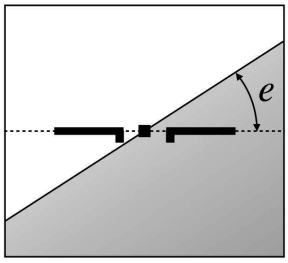

Figure 2.4: Simplified artificial horizon.

Table 2.1: Dynamic properties of the passive manipulator

$m_{m,p}$ [kgm^2]	$b_{m,p}$ [Nms/rad]	$k_{m,p}$ [Nm/rad]
0.012	0.2	2.0

desired dynamics of the passive manipulator:

$$H_{m,p}(s) = \frac{X_m(s)}{F_m(s)} = \frac{1}{m_{m,p}s^2 + b_{m,p}s + k_{m,p}} \tag{2.1}$$

In this study we ignore the effect of the force sensor and the servo system, therefore the realized manipulator dynamics are considered to be the same as the desired dynamics $H_{m,p}$. Table 2.1 lists the mass, damping and stiffness properties of the passive manipulator. Please note that all the mechanical properties are expressed in the rotational coordinate system, the corresponding linear values can be derived using the distance from the effective grip point to the axis of rotation (90 mm, see Section 2.3.1).

In the case of the active manipulator, the control signal u_p equals the force f_m that the pilot exerts on the manipulator: $u_p = f_m$. The shaded area in Fig. 2.3b shows how the active manipulator is implemented. As mentioned earlier, the manipulator deflection x_m is proportional to the aircraft rotational velocity ($x_m = K_m\dot{\phi}$). However, the maximum $\dot{\phi}$ is limited by the maximum excursion of the manipulator. In order to ensure that the tasks corresponding to the two manipulator types have the same static gain of the controlled element, the servo-system gain K_m is set to the inverse of the static gain of the controlled element:

$$x_m = K_m \cdot \dot{\phi} = \frac{1}{K_c} \cdot \dot{\phi} \tag{2.2}$$

The forward gain K_f is set to 1 for both manipulator types. The controlled-element input u is the combination of the control signal u_p and the disturbance forcing function f_d.

CONTROLLED ELEMENT

The roll dynamics of a typical wide-body jet aircraft [12] are used as the dynamics of the controlled element in the experiment. The spiral mode is simplified to a single

integrator. The roll subsidence and the open-loop gain are deliberately adjusted in order to make the aircraft not too difficult to control.

$$H_c(s) = \frac{\Phi(s)}{U(s)} = \underbrace{\frac{1}{0.083s+1}}_{\text{actuator dynamics}} \cdot \underbrace{K_c \cdot \frac{2.259s^2+0.821s+1}{s(0.4s+1)(1.647s^2+0.336s+1)}}_{\text{aileron-to-roll-angle dynamics}} \tag{2.3}$$

Here the open-loop gain (i.e., the static gain) is $K_c = 3.5$.

DATA COLLECTION

An experimental run lasts 90 seconds, during which the subject performs the compensatory task and the data are recorded. The first 8.08 seconds are used as the run-in time, to allow the subject to adjust to the task. The remaining 81.92 seconds yield the measurement data. The measurements are collected with a sampling frequency of 200 Hz. In the experiment, each subject repeated the experimental run of each condition for a number of times. The number of repetitions varied from 8 to 10, depending on how rapidly the performance converged to a stable level. The last five repetitions were used for the final analysis.

FORCING FUNCTIONS

The two forcing functions f_t and f_d are both defined as the sum of ten different sinusoids [13]:

$$f_t(t) = \sum_{k=1}^{10} A_t(k) \cdot \sin(\omega_t(k)\, t + \theta_t(k)) \tag{2.4}$$

$$f_d(t) = \sum_{k=1}^{10} A_d(k) \cdot \sin(\omega_d(k)\, t + \theta_d(k)) \tag{2.5}$$

Using the two forcing functions, both the pilot's reaction to the visual presentation and the response to the manipulator movement, and thus the neuromuscular impedance during the task, can be estimated [14]. To prevent participants from recognizing the signal pattern, the starting phases of the sine components are chosen randomly [15].

A lag-lead low-pass filter is selected to define the amplitudes of the forcing functions:

$$H_{ff} = K_{ff} \cdot \frac{\frac{1}{\omega_{ff,L}^2} s^2 + \frac{2 \cdot \zeta_{ff}}{\omega_{ff,L}} s + 1}{\frac{1}{\omega_{ff,l}^2} s^2 + \frac{2 \cdot \zeta_{ff}}{\omega_{ff,l}} s + 1}, \tag{2.6}$$

Table 2.2: The corner frequencies of the magnitudes of the forcing functions

Bandwidth	$\omega_{ff,l}$ [rad/s]	$\omega_{ff,L}$ [rad/s]
BW1	0.60	4.80
BW2	1.00	8.00
BW2	1.65	13.2

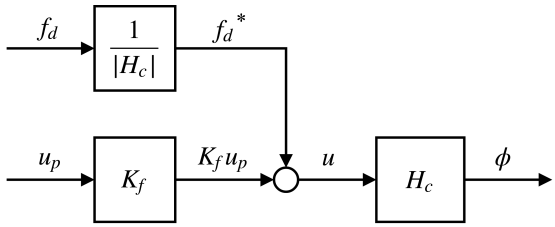

Figure 2.5: The pre-filtering of the disturbance forcing function.

where the gain K_{ff} and the damping ratio ζ_{ff} are 0.2 and 0.7, respectively. The amplitude of each sinusoidal component of the forcing functions is given by the magnitude of the filter at the corresponding frequency. To obtain three different forcing-function bandwidths, the two corner frequencies are adjusted, as listed in Table 2.2.

To keep the target-following task and the disturbance-rejection task equal in difficulty, the disturbance forcing function is adapted by scaling its magnitude with the inverse of $|H_c|$, as illustrated by Fig. 2.5. Details about the definition of the two forcing functions are given in Tables 2.3 and 2.4, respectively. Figure 2.6 gives an example of the two forcing functions with the second bandwidth (BW2). Please note that the disturbance forcing function shown in this figure is that before the adaptation.

2.4. RESULTS, ANALYSIS AND DISCUSSION

The measurements of the last five repetitions performed by each subject are averaged for the analysis. Comparisons between the two manipulator types are made in terms of the tracking error and the control effort, as well as the estimated open- and closed-loop frequency response functions. Two-way repeated measures analysis of variance

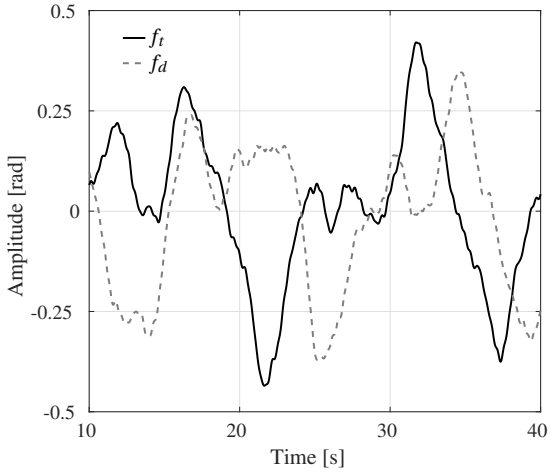

Figure 2.6: Segments of the target and disturbance forcing functions, BW2.

Table 2.3: Target forcing function f_t

k	period	ω_t [rad/s]	A_t, [rad]			ϕ_t, [rad]		
			BW1	BW2	BW3	BW1	BW2	BW3
1	5	0.3835	0.1864	0.1984	0.1999	1.7411	2.3319	4.9089
2	11	0.8437	0.0910	0.1645	0.1944	5.4434	5.5352	0.9319
3	21	1.6107	0.0277	0.0724	0.1462	3.3194	0.6807	5.0653
4	37	2.8379	0.0094	0.0248	0.0645	3.8945	5.8910	0.4305
5	51	3.9117	0.0056	0.0134	0.0352	1.2212	3.2216	1.8187
6	71	5.4456	0.0039	0.0074	0.0185	4.3954	0.9325	5.9087
7	101	7.7466	0.0033	0.0045	0.0095	3.0397	5.6708	4.8104
8	137	10.5078	0.0032	0.0036	0.0058	0.0160	1.1480	1.8858
9	191	14.6495	0.0031	0.0032	0.0040	5.4767	4.4054	2.0951
10	224	17.1806	0.0031	0.0032	0.0036	3.4525	4.0862	1.6544

Table 2.4: Pre-filtered disturbance forcing function f_d^*

k	period	ω_t [rad/s]	A_d, [rad]			ϕ_d, [rad]		
			BW1	BW2	BW3	BW1	BW2	BW3
1	6	0.4602	0.0242	0.0273	0.0278	1.2829	5.1081	0.4333
2	13	0.9971	0.0102	0.0213	0.0281	0.9194	4.1567	3.1062
3	23	1.7641	0.0097	0.0258	0.0557	1.8334	3.8964	0.1702
4	38	2.9146	0.0084	0.0220	0.0574	2.5865	1.1398	3.9334
5	53	4.0650	0.0090	0.0209	0.0551	1.5750	3.2806	1.2733
6	73	5.5990	0.0120	0.0221	0.0550	3.7298	3.5648	3.7481
7	103	7.9000	0.0215	0.0289	0.0599	1.5056	1.8805	3.0091
8	139	10.6612	0.0413	0.0462	0.0736	3.1201	1.6206	1.5561
9	194	14.8796	0.0934	0.0964	0.1173	1.0491	2.2507	1.9728
10	227	17.4107	0.1407	0.1430	0.1606	4.8887	4.3722	5.5454

Table 2.5: Results of ANOVA tests for tracking errors and control activities

	RMS of e			RMS of f_m		
	MT	BW	MT*BW	MT	BW	MT*BW
F value	$F(1,11)$	$F(1.16,12.73)^a$	$F(2,22)$	$F(1,11)$	$F(2,22)$	$F(2,22)$
	655.2	867.9	215.9	27.72	103.4	0.405
Sig.	$p<0.05$	$p<0.05$	$p<0.05$	$p<0.05$	$p<0.05$	$p>0.05$

[a] This F value is reported after a Greenhouse-Geisser correction

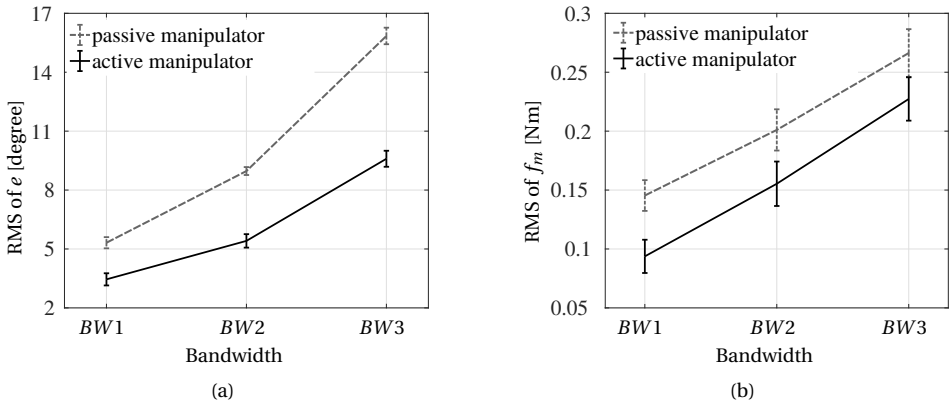

Figure 2.7: RMS of the error and force signals for different conditions.

(ANOVA) tests are performed to reveal the effects of the two independent factors. Tables 2.5 and 2.6 show the corresponding statistical results. Please note that in the tables MT and BW represent manipulator type and bandwidth, respectively.

2.4.1. TRACKING ERROR AND CONTROL ACTIVITY

TRACKING ERROR

The left plot of Fig. 2.7 shows the root mean square (RMS) of the error variable e (mean ± 95% confidence interval corrected for between-subject variability). As can be seen, the active manipulator leads to remarkably better performance. A two-way repeated measures ANOVA reveals significant effects of both the manipulator type and the forcing-function bandwidth on e, see Table 2.5. In addition, a significant interaction between these two independent factors is found. It can be readily seen from the figure that a larger improvement in performance is associated with a higher forcing-function bandwidth.

CONTROL ACTIVITY

The control signals corresponding to the two manipulator types are f_m (active manipulator) and x_m (passive manipulator), respectively. Direct comparison between these two different variables may be misleading. Therefore, the control activities are evaluated on the basis of the force signals f_m, as can be seen from the right plot of Fig. 2.7. Compared to the passive manipulator, the active manipulator leads to significant reduction in the exerted forces. The forces for both manipulator types increase significantly as a result of the extended forcing-function bandwidth. This effect is independent of the manipulator type, as no interactions are found, see Table 2.5.

2.4.2. FREQUENCY-DOMAIN ANALYSIS

In compensatory tasks with quasi-random multi-sine forcing functions, a human controller resembles a linear time-invariant system [16]. This allows us to estimate the fre-

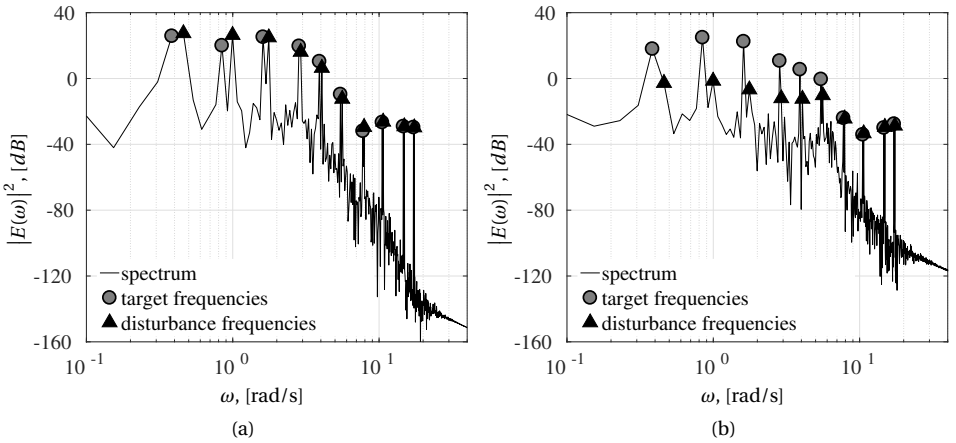

Figure 2.8: Power spectra of the error $e(t)$ (one subject, BW2): (a) the passive manipulator; (b) the active manipulator.

quency responses of the control loops, and to generalize from the findings of our study. The following subsections provides details about the frequency-domain analysis.

POWER SPECTRUM OF THE TRACKING ERROR

The power spectrum of the error e, corresponding to the forcing function BW2, produced by one subject is shown in Fig. 2.8. Similar characteristics are observed for all other bandwidths and subjects. In the case of the passive manipulator, the magnitudes of e at the frequencies of the target and the disturbance are similar. For the active manipulator, the magnitudes that correspond to the frequencies of the target remain at roughly the same level as the passive manipulator. However, in the low-frequency region, those related to the disturbance are considerably attenuated. This demonstrates an apparent advantage of the active manipulator in rejecting the lower-frequency disturbances. Moreover, the different extents to which the error is attenuated with the active manipulator also indicates that the two tasks are accomplished with different mechanisms.

OPEN- AND CLOSED-LOOP RESPONSES

The open- and closed-loop responses are investigated. Due to the fact that the active manipulator causes different power spectra of e at the frequencies of the target and the disturbance, the frequency responses for the two tasks are estimated separately. The open-loop frequency response of target following is obtained from the relation between e and ϕ at the frequencies of f_t:

$$H_{OL,t}(\omega j) = \frac{\Phi_t(\omega j)}{E_t(\omega j)}\,, \tag{2.7}$$

The target-following closed-loop response is obtained by:

$$H_{CL,t}(\omega j) = \frac{\Phi_t(\omega j)}{F_t(\omega j)} \tag{2.8}$$

Table 2.6: Results of ANOVA tests for crossover characteristics

crossover frequency ω_c			phase margin ϕ_m		
MT	BW	MT*BW	MT	BW	MT*BW
target following					
$F(1,11)$ 13.63	$F(2,22)$ 66.43	$F(1.35,14.90)^a$ 3.187	$F(1,11)$ 44.27	$F(2,22)$ 152.9	$F(1.37,15.03)^a$ 2.993
$p<0.05$	$p<0.05$	$p>0.05$	$p<0.05$	$p<0.05$	$p>0.05$
disturbance rejection					
$F(1,11)$ 298.6	$F(2,22)$ 4.987	$F(2,22)$ 43.76	$F(1,11)$ 14.49	$F(2,22)$ 17.38	$F(2,22)$ 2.406
$p<0.05$	$p<0.05$	$p<0.05$	$p<0.05$	$p<0.05$	$p>0.05$

[a] These F values are reported after Greenhouse-Geisser corrections

Figure 2.9 shows the average of the open- and closed-loop responses generated by subjects for the forcing function BW2. Similar characteristics of the responses can be observed for the other two bandwidths. In the crossover region the magnitudes of the open-loop responses for the two manipulator types are similar and resemble those of a single integrator, as expected by McRuer's crossover model [16]. The active manipulator leads to a smaller phase lag and a greater phase margin. This leads to a larger bandwidth, less overshoots, and smaller phase lags in the closed-loop response, as compared to the passive manipulator.

Fig. 2.10 shows the crossover frequencies ω_c and the phase margins ϕ_m of the open-loop responses averaged over all subjects (mean ± 95% confidence interval corrected for between-subject variability). Results from a two-way repeated measures ANOVA suggest that the effect of the manipulator type on ω_c is significant, see Table 2.6. Except for the lowest forcing-function bandwidth, the active manipulator leads to a higher ω_c than the passive manipulator. The effect of the forcing-function bandwidth is also significant. For the active manipulator, ω_c remains at roughly the same level for the fist two forcing-function bandwidths, and then regresses for the highest bandwidth. For the passive manipulator, a regressing trend can be easily seen.

Effects of both independent variables on ϕ_m are found to be significant. The active manipulator leads to a significantly higher ϕ_m than the passive manipulator for all three bandwidths. Also, for the active manipulator, ϕ_m remains roughly the same for the first two forcing function bandwidths. For the highest bandwidth, subjects regressed their ω_c to increase their ϕ_m and maintain stability of the closed-loop system. The ϕ_m corresponding to the passive manipulator increases as the forcing-function bandwidth increases, as a result of crossover regression.

The open-loop frequency response of disturbance rejection is derived through:

$$H_{OL,d}(\omega j) = \frac{U_{p,d}(\omega j)}{U_d(\omega j)}\,, \tag{2.9}$$

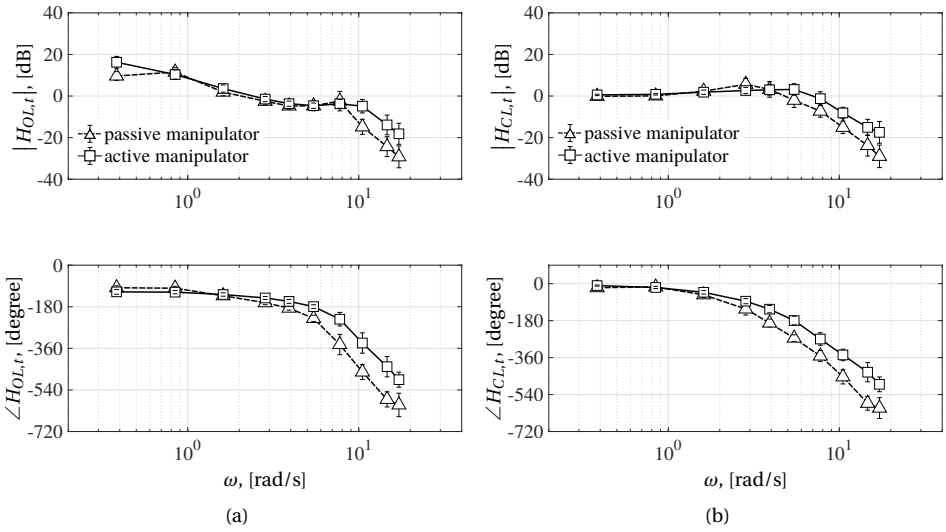

Figure 2.9: Target following frequency responses of subjects (mean ± std), BW2: (a) open-loop response; (b) closed-loop response

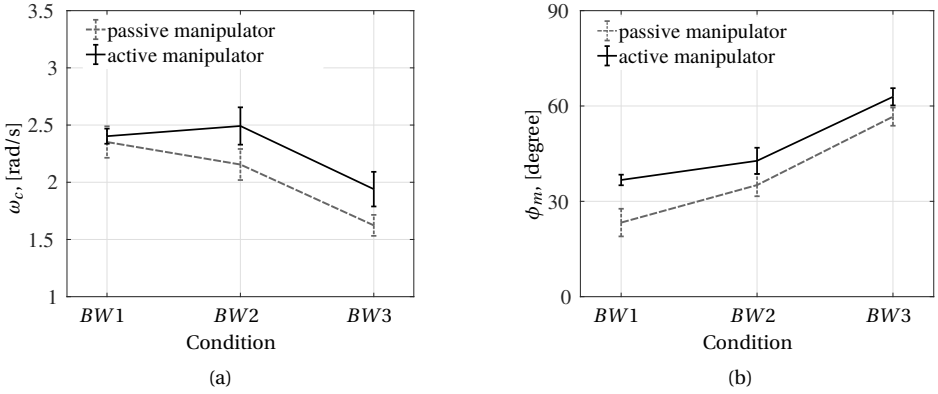

Figure 2.10: Crossover characteristics of target-following open-loop responses of subjects (mean ± 95%CI).

where $U_p = F_m$ in the case of the active manipulator and $U_p = X_m$ in the case of the passive manipulator. Since the disturbance is fed into the system before the controlled element (see Fig. 2.5), selecting f_d^* as the input to the closed-loop system will include the aircraft dynamics in the numerator. This will make the information provided by the

closed-loop response not straightforward. Therefore, the following correction is made:

$$\begin{aligned} \left|H_{CL,d}(\omega j)\right| &= \left|\frac{\Phi_d(\omega j)}{F_d^*(\omega j)} / H_c(\omega j)\right| = \left|\frac{\Phi_d(\omega j)}{F_d(\omega j)}\right| \\ \angle H_{CL,d}(\omega j) &= \angle\frac{\Phi_d(\omega j)}{F_d^*(\omega j)} - \angle H_c(\omega j) \end{aligned} \tag{2.10}$$

This results in the frequency response of a closed-loop system into which the disturbance is fed directly at the output of the controlled element.

Figure 2.11 shows the average of the open- and closed-loop frequency response estimates for all subjects, for the BW2 condition. The characteristics of the frequency responses estimated for the other two bandwidths are similar. As can be seen, different manipulator types lead to notable differences in the frequency responses, the differences are much larger than those observed in target following. This is in line with that observed from the power spectrum of the error signal (see Fig. 2.8). The active manipulator leads to a larger open-loop gain in the crossover region. Moreover, the open-loop phase lag corresponding to the active manipulator is much smaller and remains at approximately -90 degrees over the whole tested range of frequency. Therefore, the closed-loop system demonstrates significant improvements in the rejection bandwidth and produces smaller overshoots.

The crossover frequencies ω_c and phase margins ϕ_m of the open-loop responses generated by all subjects are shown in Fig. 2.12 (mean ± 95% confidence interval corrected for between-subject variability). As can be seen from Table 2.6, the effects of the manipulator type and the forcing-functions bandwidth on ω_c are significant. The interaction between these two factors is also significant, which can be expected since the two manipulator types cause the forcing-function bandwidth to have opposite effects on ω_c. For the passive manipulator, apparent crossover regression occurs. This is similar to target following where a declining trend of ω_c is also observed, see Fig. 2.10. In contrast, ω_c for the active manipulator demonstrates a notable increasing trend as forcing function bandwidth increases.

As a result of crossover regression, the ϕ_m corresponding to the passive manipulator increases as the bandwidth increases. Due to this, a significant effect of the forcing-function bandwidth is found. The active manipulator allows for significantly higher phase margins. In contrast to the passive manipulator, the ϕ_m with regard to the active manipulator remains roughly independent of the forcing-function bandwidth.

2.4.3. DISCUSSION

With the passive manipulator, subjects generated very similar open-loop responses for the target-following and disturbance-rejection tasks. The crossover frequencies ω_c and the phase margins ϕ_m corresponding to these two tasks, as well as the the effects of the forcing-function bandwidth, are similar. This is expected, as our subjects received the information of both the target and the disturbance *only* through the error presented visually. Consequently, their actions for these two tasks must be similar.

In general, the active manipulator leads to a pronounced performance improvement. It seems that a greater improvement is associated with higher task difficulty

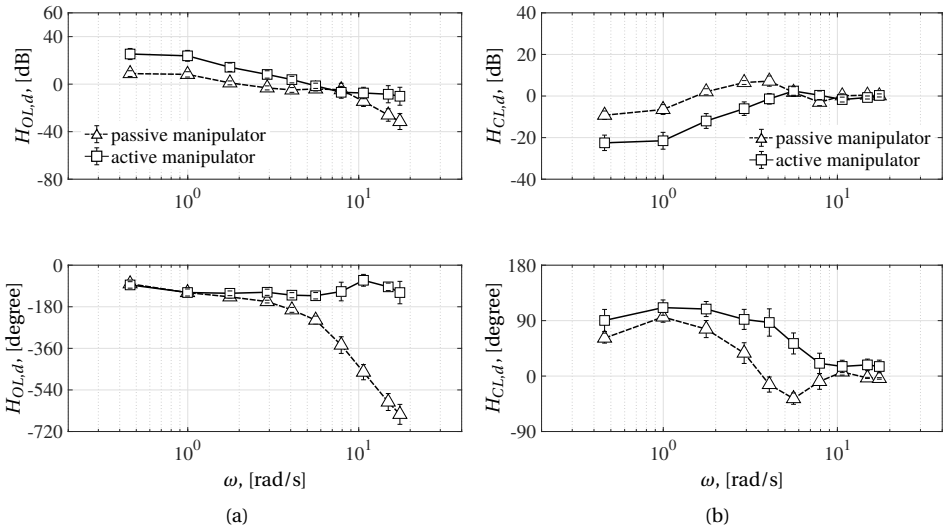

Figure 2.11: Disturbance rejection frequency responses of subjects (mean ± std), BW2: (a) open-loop response; (b) closed-loop response

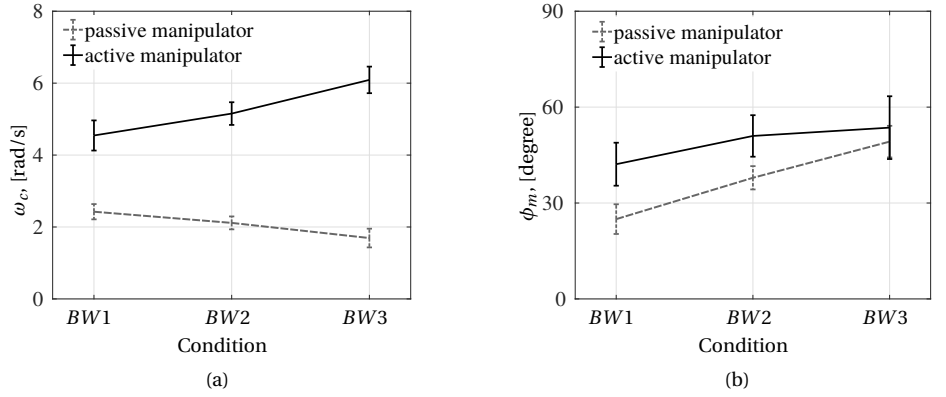

Figure 2.12: Crossover characteristics of disturbance-rejection open-loop responses of subjects (mean ± 95%CI).

(the higher forcing-function bandwidths). An interesting fact associated with the active manipulator is that a clear distinction exists in the open-loop frequency response between target following and disturbance rejection, as well as in the characteristics of ω_c and ϕ_m. Disturbance rejection possesses higher open-loop gains and smaller phase lags than target following. Moreover, crossover regression occurs in target following in the case of the highest forcing-function bandwidth. However, the crossover frequency of the disturbance rejection loop does not regress, instead, it *increases* when

the forcing-function bandwidth increases.

This remarkable difference indicates that with the active manipulator, following the target and rejecting the disturbance are accomplished independently, although these two tasks are performed simultaneously. This is likely caused by the fact that subjects can benefit from the haptic feedback of the aircraft rotational velocity. The neuromuscular system which controls the movement of the manipulator may play a more important role in controlling the aircraft state. This hypothesis will be further explored in the following section.

2.5. THE MECHANISM OF AIRCRAFT CONTROL WITH THE ACTIVE MANIPULATOR

The mechanism of controlling the aircraft with the active manipulator can be presented more intuitively by means of a two-port network representation [17, 18], as can be seen in Fig. 2.13. Please note that the disturbance f_d and the forward gain K_f are omitted here for the reason of simplicity. In addition, the arrow under $K_m\dot{\phi}$ indicates the direction of the energy flow, which is not necessarily the direction of the transmission of $\dot{\phi}$ [18].

We assume that the sampling and the servo system have negligible effects on the overall dynamics in the frequency range of interest. In this case, the force sensor and the servo system act as transparent mediums that directly connect the pilot to the aircraft. When the pilot applies a force on the manipulator, a change occurs in the aircraft rotational velocity. The manipulator moves at the same moment, as if it is moved by the pilot directly. In other words, when the pilot moves the manipulator, the rotational velocity of the aircraft exhibits exactly the same changes. One can imagine that the pilot still controls the aircraft attitude by means of the manipulator deflection, as he/she does with the passive manipulator. The dynamics of the manipulator *become* the dynamics that correspond to the aircraft rotational velocity in response to the aircraft

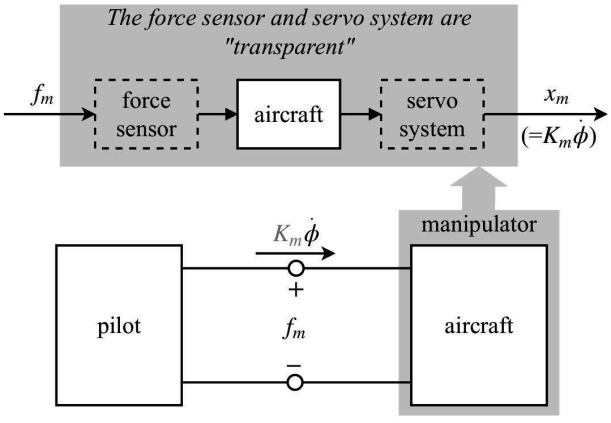

Figure 2.13: Two-port representation [17, 18] of the pilot-manipulator system.

input:

$$H_{m,a} = \frac{X_m(s)}{F_m(s)} = K_m \cdot s \cdot \frac{\Phi(s)}{U(s)} = K_m \cdot sH_c(s) \tag{2.11}$$

Then, independent of the aircraft dynamics, the dynamics of the *effective* controlled element always *become* a single integrator:

$$H_{c,eff} = \frac{\Phi(s)}{X_m(s)} = \frac{1}{K_m} \cdot \frac{1}{s} \tag{2.12}$$

The observed improvement in target following can therefore be explained by the simplification of the controlled element, as expected by McRuer's crossover model [16]. Moreover, it is readily appreciable that the disturbance acting on the aircraft becomes the disturbance to the manipulator. Rejection of the disturbance can then be easily achieved by stabilizing the manipulator *position*. With the active manipulator, this task is *integrated* into the neuromuscular system, and becomes largely independent of the elimination of the visual error e. This explains the distinction in the response between target following and disturbance rejection.

To understand the effects of the forcing-function bandwidth on disturbance rejection, the impedance of the neuromuscular system of our subjects is estimated. Here, the term 'impedance' is defined as a measure of how much the human arm 'resists' a disturbance motion. To this end, the pilot dynamics are first represented by three components, as shown by Fig. 2.14.

The pilot force f_m is divided into three components, i.e., f_x, f_e and N. The first two variables are the outputs of two internal systems H_x and H_e, and the last one accounts for any nonlinearity of the pilot dynamics. Assume for the moment that this remnant N is small as compared to f_e and f_x, then the dynamics of the pilot can be accurately described by the two internal systems. The system H_x generates the force component in response to the movement of the manipulator, and indicates the mechanical impedance of the neuromuscular system [14]. Due to the fact that the energy of the error signal e can be considered to be small at the frequencies of the disturbance (see Fig. 2.8b), disturbance rejection is mainly accomplished by the loop that is shaded in

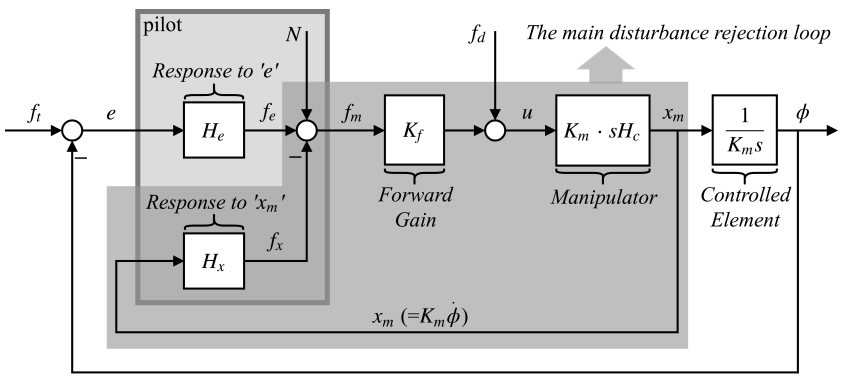

Figure 2.14: The schematic diagram where the pilot is represented by two subsystems.

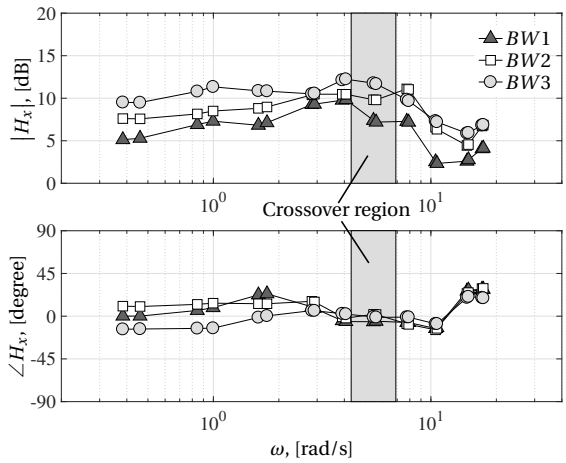

Figure 2.15: Subjects' average neuromuscular impedance corresponding to the three forcing-function bandwidths.

Fig. 2.14. In this case, the neuromuscular impedance H_x becomes the dynamic gain of the feedback path. This indicates that a greater magnitude of H_x (a higher impedance, i.e., more resistance to changing stick deflections) will lead to better rejection of the disturbance.

The remainder of the pilot dynamics, including the pilot adaptation behavior, the internal representation, the neural filters and so forth [14], is accounted for by H_e. This system, which generates the force in response to the *visually* presented error signal, is used in this study as an intermediate variable for separating H_x from the dynamics of the pilot. Readers are referred to the work by van Paassen et al. [14, 19] for greater detail about these two internal systems.

Figure 2.15 shows the bode plot of the estimated H_x, for the three bandwidths considered. The characteristics of H_x are consistent with the findings shown earlier (see Fig. 2.12). In general, higher forcing-function bandwidths lead to higher magnitudes of the impedance ($|H_x|$). In the crossover region, the increase in $|H_x|$ increases the open-loop gain. As a result, the crossover frequency ω_c increases as the forcing-function bandwidth increases. The increase in magnitude indicates that our subjects stiffened their arms when the disturbance on the manipulator became stronger. This is indeed confirmed by an interview carried out after the experiment with our subjects.

The phase characteristics corresponding to the three bandwidths are similar. In the crossover region, the phase lags ($\angle H_x$) under the three conditions are approximately the same. This explains why no significant changes in the phase margin ϕ_m were found.

2.6. IMPROVING THE ACTIVE MANIPULATOR

The current configuration of the active manipulator feeds back the aircraft rotational rate with its full spectrum. As a result, the effects of the high-frequency components of the disturbance acting on the aircraft are also presented to the pilot. As can be seen

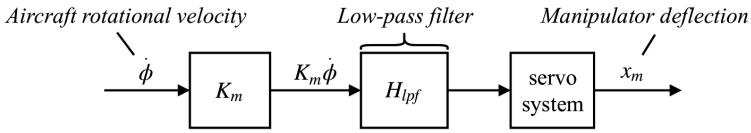

Figure 2.16: The configuration of the active manipulator with a low-pass filter.

from Figs. 2.8 and 2.11, humans only have limited bandwidth for disturbance rejection. The components of the disturbance beyond the bandwidth are still present in the movement of the manipulator, leading the pilot's arm to involuntarily move with the manipulator. During the experiment, many subjects indicated that this involuntary movement was intrusive and reduced the operational relevance of the active manipulator.

To provide better operational quality, we designed a low-pass filter, placed before the servo system, illustrated in Fig. 2.16.

When the low-pass filter $H_{lpf}(s)$ is implemented, the manipulator deflection can be expressed as:

$$X_m(s) = K_m \cdot s \cdot \Phi(s) \cdot H_{lpf}(s) \tag{2.13}$$

In this case, the manipulator dynamics become:

$$H_{m,af} = \frac{X_m(s)}{U(s)} = K_m \cdot sH_c(s) \cdot H_{lpf}(s) \tag{2.14}$$

The pilot still directly perceives the aircraft rotational velocity through the manipulator, but now within the passband of H_{lpf}. The aircraft rotational motion which lies within the stopband of the filter is no longer present in the movement of the manipulator. On the one hand, the filter H_{lpf} should sufficiently filter out the high-frequency disturbance that is beyond human capability. On the other hand, the filter should not deteriorate the dynamics of the effective controlled element. A properly designed filter should attenuate the energy of the disturbance that lies beyond the crossover region of the disturbance-rejection response, while maintaining the dynamics of the controlled element as a single integrator in the crossover region of the target-following response, see Eq. (2.12).

In addition, the original passivity properties of the manipulator should be preserved to maintain the stable interaction between the pilot and the aircraft [18, 20–22]. In our case, this is equivalent to avoiding causing the phase lag of the manipulator dynamics to exceed -180°. Due to the dynamics of the aircraft (see Eq. (2.3)), any additional phase lag at high frequencies will cause the manipulator to lose the passivity (see Fig. 2.17) and may lead to an unstable haptic interaction [21]. Therefore, a lag-lead filter with the following dynamics is designed:

$$H_{lpf} = \frac{\omega_{lpf,l}^2}{\omega_{lpf,L}^2} \cdot \frac{s^2 + 2\zeta_{lpf} \cdot \omega_{lpf,L} + \omega_{lpf,L}^2}{s^2 + 2\zeta_{lpf} \cdot \omega_{lpf,l} + \omega_{lpf,l}^2}, \tag{2.15}$$

where $\omega_{lpf,l} < \omega_{lpf,L}$, and $\zeta_{lpf} = 0.7$.

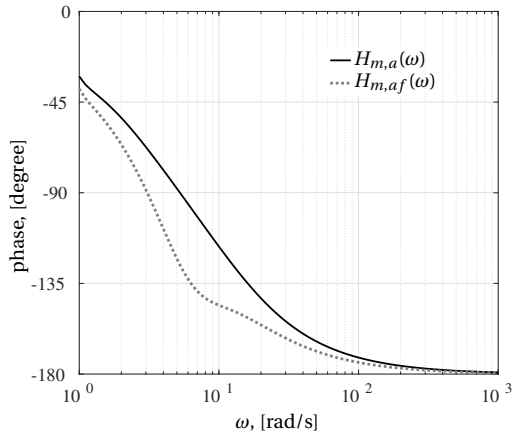

Figure 2.17: The phase characteristics of the active manipulator with/without the lag-lead filter.

The first corner frequency can be selected based on the findings from the experiment. As can be seen from Fig. 2.12, the crossover frequency ω_c for disturbance rejection lies in the range of 4.5 to 6.1 rad/s. The higher end of this range corresponds to a high level of the neuromuscular impedance which, according to our experimental participants, caused considerable muscle fatigue. The impedance levels that correspond to the two lower values of ω_c were considered by our participants to be satisfactory. Therefore, in this study we set $\omega_{lpf,l} = 5$ rad/s, a value that is also sufficiently higher than the crossover frequency of the target-following response. With this setting we expect the target-following performance to remain the same [16].

In order to preserve the passivity of the manipulator, we set $\omega_{lpf,L} = 8$ rad/s. Figure 2.17 shows the phase characteristics of the manipulator with this filter. As can be seen, the passivity of the manipulator is maintained at high frequencies. Thus the stability of the interaction between the pilot and the aircraft is guaranteed. More importantly, the information of the aircraft state is well preserved within the target-following bandwidth, while that beyond the disturbance-rejection bandwidth is largely attenuated by 60%, as shown by Fig. 2.18.

2.7. EXPERIMENT TWO: TESTING THE LAG-LEAD FILTER

2.7.1. EXPERIMENT DESIGN

In order to evaluate the new configuration of the active manipulator, we carried out a second experiment with four participants. The experimental task is again target-follow-ing and disturbance-rejection compensatory tracking. The setups of the two forcing functions, f_t and f_d, are the same as the BW2 condition used in the first experiment, as shown in Tables 2.3 and 2.4. All remaining setups of the experiment, including the controlled-element dynamics, duration of each experimental run, the data collection, the experimental devices and so forth are the same as the first experiment.

The new configuration of the active manipulator will be compared with the original one (used in the first experiment). To reduce the increase caused by the filter in the

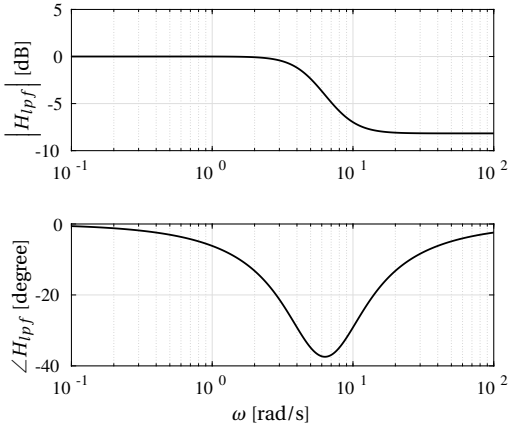

Figure 2.18: Bode plot of the lag-lead filter.

mechanical impedance of the manipulator, the forward gain K_f (see Figs. 2.1b and 2.3b) is set to 2.5. This gain of the original setup is set to the same value for a fair comparison.

2.7.2. RESULTS

As mentioned earlier, the selected filter is able to reduce the high-frequency components of the disturbance by approximately 60%. Due to this, during the experiment our subjects barely noticed any involuntary arm movements. Furthermore, the lag-lead filter did not affect the task performance, as can be seen in Fig. 2.19 which presents the RMS of the error signal e (average and the 95% confidence interval corrected for between-subject variability). The result from a dependent t-test suggests that the tracking errors corresponding to the two manipulator setups are comparable ($t(3) = -0.745, p > 0.05$).

Figure 2.20 presents the open- and closed-loop frequency responses of target following, generated by our subjects. As can be seen, the two configurations lead to approximately the same frequency responses. Figure 2.21 shows the crossover frequency ω_c and the phase margin ϕ_m (mean ± 95% confidence interval corrected for between-subject variability).

Dependent t-tests reveal that the ω_c and ϕ_m corresponding to the two configurations are approximately the same ($t(3) = -2.643, p > 0.05$ for ω_c and $t(3) = 1.962, p > 0.05$ for ϕ_m). This confirms that the lag-lead filter does not affect the target-following performance of our subjects, and that the equivalent controlled element dynamics still approximate to a single integrator.

Figure 2.22 shows the open- and closed-loop frequency responses of disturbance rejection. In general, the two configurations result in similar responses. The open-loop gain is not affected by the lag-lead filter, and still possesses the characteristics of a single integrator. As a result, the closed-loop bandwidths for the two manipulator configurations are approximately the same. However, the lag-lead filter leads to a larger open-loop phase lag at the crossover region.

The ω_c and ϕ_m of the disturbance-rejection responses that correspond to the two manipulator configurations are presented in Fig. 2.23, (average and the 95% confidence interval corrected for between-subject variability). As expected, the two configurations lead to similar ω_c, as suggested by the result of a dependent t-test: $t(3) = 2.206, p > 0.05$. However, the lag-lead filter caused a significant reduction of about 40 degrees in ϕ_m ($t(3) = -7.981, p < 0.05$).

This reduction in the phase margin is due to the phase lag introduced by the lag-lead filter. As can be seen from Fig. 2.18, the filter introduces roughly the same amount of the phase lag at the crossover region, approximately 40 degrees. Nevertheless, this reduction in ϕ_m does not affect the performance of our subjects. The remaining phase margin of around 30 degrees still guarantees a good closed-loop response.

2.8. DISCUSSION

In this study, we first revisited the active manipulator proposed in previous work [9, 10]. The observed improvement in the task performance is similar to the previous findings, except that in the previous work the effect of the manipulator type on the disturbance-rejection phase margin was not significant. However, this is probably due to the fact that the forcing functions used in our current work are different. As discussed in Section 2.4, the difference in ϕ_m between the two manipulator types may vary with different forcing-function bandwidths (see Fig. 2.12). Another possible reason lies in the number of subjects. In the previous work, only two subjects participated in the experiment, which may not be sufficient for the elimination of individual variations. In our current work, 12 subjects were invited, which would lead to a more generalized and reliable conclusion.

The control input to the aircraft in the case of the active manipulator is the pilot's force, instead of the manipulator deflection as in the case of the passive manipulator. Despite the different control inputs, controlling the aircraft attitude with the two manipulator types are in fact similar, a process achieved by means of the manipulator

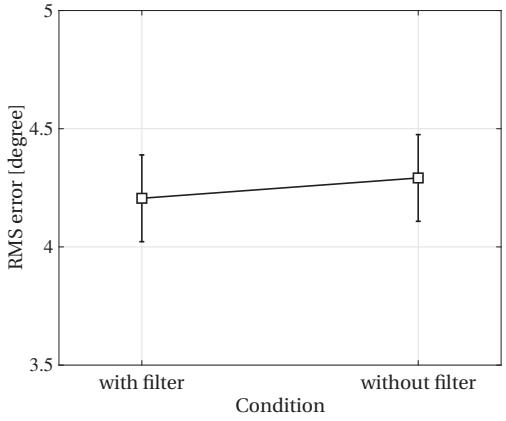

Figure 2.19: The root mean square of the error signals produced by subjects (mean ± 95%CI).

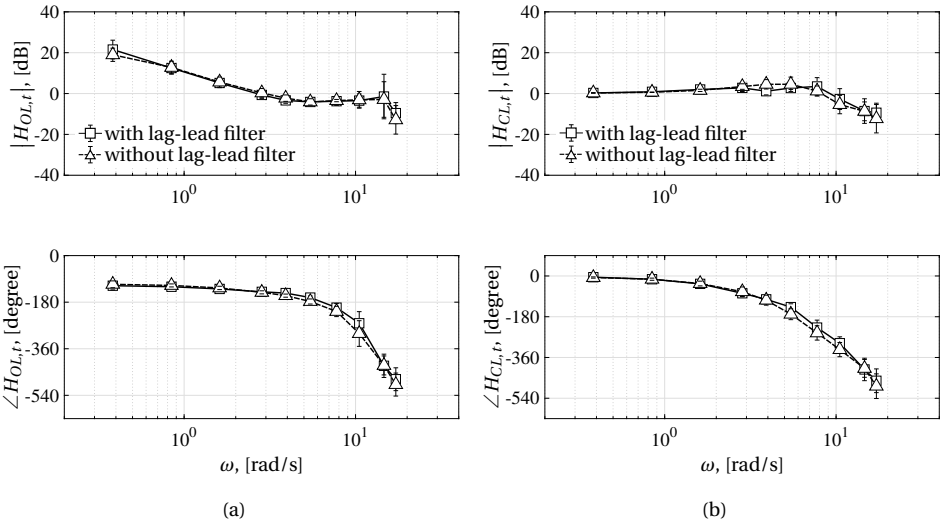

Figure 2.20: Target following frequency responses of subjects (mean ± std): (a) open-loop response; (b) closed-loop response

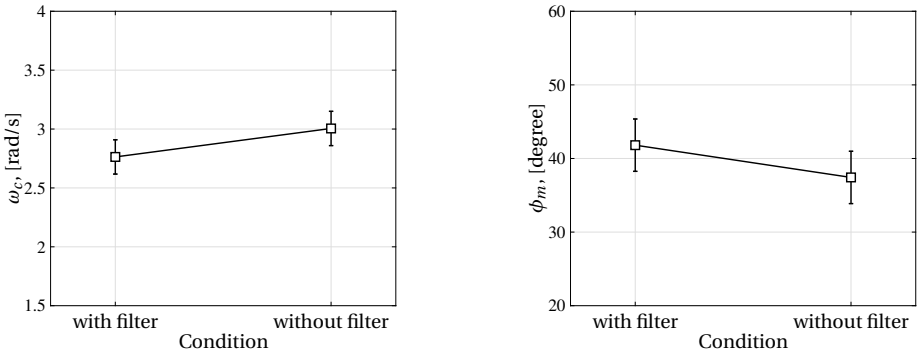

Figure 2.21: Crossover frequencies and phase margins of target-following responses (mean ± 95%CI).

deflection. As shown by the analysis in Section 2.5, the control input to the effective controlled element in the case of the active manipulator is still the manipulator deflection. In addition, our previous study shows that pilots can perform control tasks much better with an active manipulator than an isometric (force) control device [10]. One can imagine that the performance improvement associated with the active manipulator is due to the haptic feedback instead of the change in the control input.

With the feedback about the rotational velocity, the active manipulator leads to a more pronounced improvement as the difficulty of the task increases. This is due to the fact that the active manipulator *simplifies* the dynamics of the controlled element into a single integrator, independently of the aircraft dynamics. Furthermore, the rejection

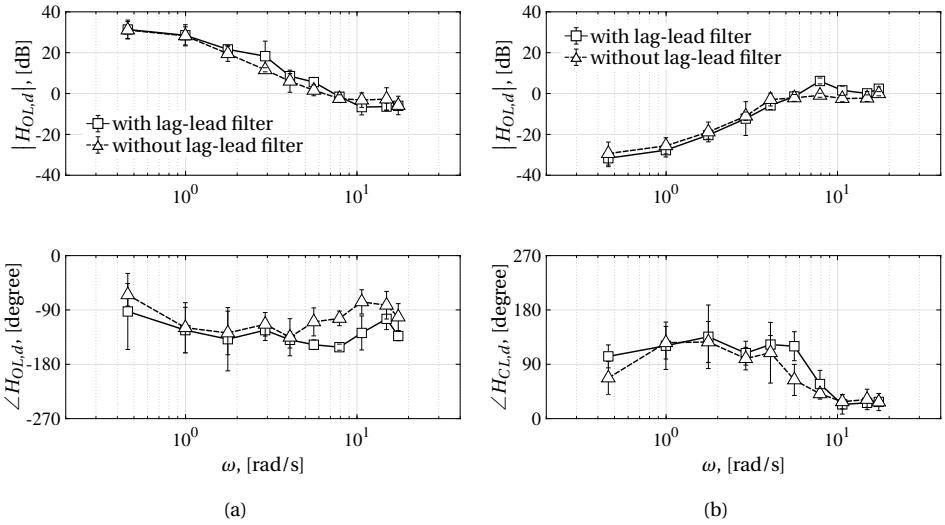

Figure 2.22: Disturbance rejection frequency responses of subjects (mean ± std): (a) open-loop response; (b) closed-loop response

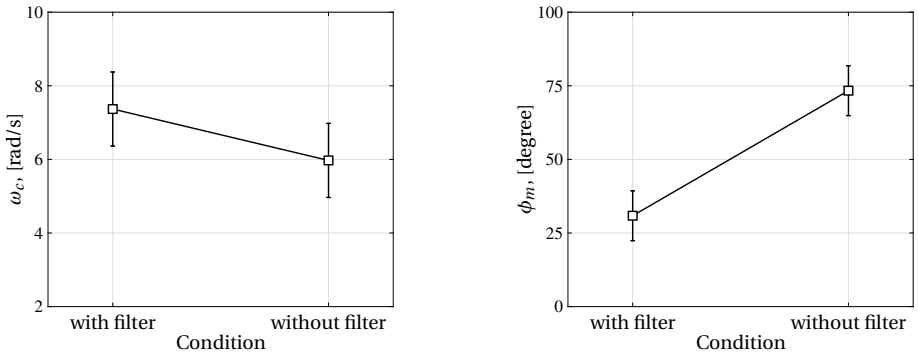

Figure 2.23: Crossover frequencies and phase margins of the disturbance rejection responses (mean ± 95%CI).

of the disturbance is integrated into the *coupled* neuromuscular-manipulator system. This allows one to *haptically* perform the disturbance-rejection task *separately* from the (predominantly *visual*) target-following task. With an active manipulator, regulating the aircraft states is largely allocated to the cerebellum which is responsible for the control of limb movements [23, 24]. The workload of the cerebrum, which is responsible for the equalization of visual presentation, is therefore reduced. In addition, the haptic feedback more effectively involves spinal reflexes and muscle co-contraction in rejecting the disturbance acting on the aircraft, allowing for much faster and more robust responses [25].

According to our subjects, the high-frequency components of the disturbance act-

ing on the aircraft reduced the operational quality of the active manipulator. We successfully mitigated this effect by means of a lag-lead filter, tested in the second experiment. Note that in practice the dynamics of the aircraft may be (slowly) time-varying, depending on the current flight condition, like altitude and speed. This entails adjusting the lead coefficient of the filter according to different equilibrium conditions. The passband of the filter should also be adjusted using the data collected from pilots and the power spectrum of the actual disturbance, as well as the highest neuromuscular impedance which does not lead to considerable physical fatigue.

This study, in line with previous studies into active manipulators, used unaugmented aircraft dynamics. However, there is no reason why an active manipulator cannot be combined with an aircraft equipped with a stability or control augmentation system, given that one evaluates the effective dynamics of the manipulator to be compatible with control by the neuromuscular system. An additional advantage of such a set-up would be that pilots could also feel – through the manipulator – the effect of any flight envelope protection systems [26], or the actions of the autopilot. The current study only evaluated the feedback of aircraft attitude rate on the stick. Rate feedback is a sensible choice, since it makes the dynamics controlled effectively those of a single integrator, which is known to result in high performance and low workload. Furthermore, the second experiment demonstrates that a filtered feedback system is also appropriate. This creates further possibilities for optimizing the effective manipulator dynamics according to the mechanical characteristics perceived by the pilot (see Part III).

2.9. CONCLUSION

This study presents a new evaluation of a haptic interface for aircraft control. The proposed haptic interface, termed the active manipulator, feeds back the aircraft rotational rate through the manipulator defection angle. Results from a first target tracking and disturbance rejection experiment indicate that the active manipulator leads to a significant improvement in task performance, as compared to the passive manipulator. Theoretical analysis shows that the active manipulator simplifies the dynamics of the controlled element into a single integrator, *independent* of the actual aircraft dynamics. It is also shown that the disturbance rejection part of the task is effectively *integrated* into the neuromuscular system, and becomes largely independent of the target following part of the task.

High-frequency components of the disturbance signal results in involuntary arm movements which reduce the operational effectiveness of the active manipulator. A lag-lead filter is developed and tested in a second experiment. Results show that the implementation of the low-pass filter leads to comparable task performance, and considerably improves the operational quality of the active manipulator.

REFERENCES

[1] W. R. Ferrell, "Delayed force feedback," *Human Factors*, vol. 8, no. 5, pp. 449–455, 1966.

[2] R. J. Anderson and M. W. Spong, "Bilateral control of teleoperators with time delay," *IEEE Trans. on Automatic Control*, vol. 34, no. 5, pp. 494–501, 1989.

[3] G. Niemeyer and J. J. E. Slotine, "Stable adaptive teleoperation," *IEEE J. of Oceanic Engineering*, vol. 16, no. 1, pp. 152–162, 1991.

[4] J. H. Ryu, D. S. Kwon, and B. Hannaford, "Stable teleoperation with time-domain passivity control," *IEEE Trans. on Robotics and Automation*, vol. 20, no. 2, pp. 365–373, 2004.

[5] T. M. Lam, M. Mulder, and M. M. van Paassen, "Haptic feedback in uninhabited aerial vehicle teleoperation with time delay," *J. of Guidance, Control, and Dynamics*, vol. 31, no. 6, pp. 1728–1739, 2008.

[6] S. Hirche, T. Matiakis, and M. Buss, "A distributed controller approach for delay-independent stability of networked control systems," *Automatica*, vol. 45, no. 8, pp. 1828–1836, 2009.

[7] M. Mulder, D. A. Abbink, M. M. van Paassen, and M. Mulder, "Design of a haptic gas pedal for active car-following support," *IEEE Trans. on Intelligent Transportation Systems*, vol. 12, no. 1, pp. 268–279, 2011.

[8] S. de Stigter, M. Mulder, and M. M. van Paassen, "Design and evaluation of a haptic flight director," *J. of Guidance, Control, and Dynamics*, vol. 30, no. 1, pp. 35–46, 2007.

[9] R. J. A. W. Hosman, B. Benard, and H. Fourquet, "Active and passive side stick controllers in manual aircraft control," in *IEEE Int. Conf. on Systems, Man and Cybernetics (SMC)*, Los Angeles, USA, Nov 1990, pp. 527–529.

[10] R. J. A. W. Hosman and J. C. van der Vaart, "Active and passive side stick controllers: Tracking task performance and pilot control behavior," in *AGARD Conf. on the Man-Machine Interface in Tactical Aircraft Design and Combat Automation*, no. 425, Stuttgart, Germany, Sept 1988.

[11] R. J. Adams and B. Hannaford, "Stable haptic interaction with virtual environments," *IEEE Trans. Robotics and Automation*, vol. 15, no. 3, pp. 465–474, 1999.

[12] R. K. Heffley and W. F. Jewell, "Aircraft handling qualities data," NASA, Tech. Rep., Dec 1972.

[13] M. M. van Paassen and M. Mulder, "Identification of human control behavior," in *Int. Encyclopedia of Ergonomics and Human Factors (2nd Edition)*, W. Karwowski, Ed. London, UK: Taylor & Francis, 2006, pp. 400–407.

[14] M. M. van Paassen, J. C. van der Vaart, and J. A. Mulder, "Model of the neuromuscular dynamics of the human pilot's arm," *J. of Aircraft*, vol. 41, no. 6, pp. 1482–1490, 2004.

[15] H. J. Damveld, G. C. Beerens, M. Mulder, and M. M. Van Paassen, "Design of forcing functions for the identification of human control behavior," *J. of Guidance, Control, and Dynamics*, vol. 33, no. 4, pp. 1064–1081, 2010.

[16] D. T. McRuer and H. R. Jex, "A review of quasi-linear pilot models," *IEEE Trans. on Human Factors in Electronics*, vol. HFE-8, no. 3, pp. 231–249, 1967.

[17] B. Hannaford, "A design framework for teleoperators with kinesthetic feedback," *IEEE Trans. on Robotics and Automation*, vol. 5, no. 4, pp. 426–434, 1989.

[18] S. S. Haykin, *Active Network Theory*. Addison-Wesley, 1970, vol. 2680.

[19] M. M. van Paassen, "Biophysics in aircraft control: A model of the neuromuscular system of the pilot's arm," Ph.D. dissertation, TU Delft, Delft University of Technology, 1994.

[20] E. Colgate and N. Hogan, "The interaction of robots with passive environments: Application to force feedback control," in *Advanced Robotics: 1989*. Springer, 1989, pp. 465–474.

[21] J. E. Colgate, "Coupled stability of multiport systems — theory and experiments," *J. of Dynamic Systems, Measurement, and Control*, vol. 116, no. 3, pp. 419–428, 1994.

[22] B. Hannaford and J. H. Ryu, "Time-domain passivity control of haptic interfaces," *IEEE Trans. on Robotics and Automation*, vol. 18, no. 1, pp. 1–10, 2002.

[23] D. M. Wolpert and Z. Ghahramani, "Computational principles of movement neuroscience," *Nature Neuroscience*, vol. 3, pp. 1212–1217, 2000.

[24] M. Kawato, "Internal models for motor control and trajectory planning," *Current Opinion in Neurobiology*, vol. 9, no. 6, pp. 718–727, 1999.

[25] D. A. Abbink, "Neuromuscular analysis of haptic gas pedal feedback during car following," Ph.D. dissertation, TU Delft, Delft University of Technology, 2006.

[26] D. Van Baelen, J. Ellerbroek, M. M. van Paassen, and M. Mulder, "Design of a haptic feedback system for flight envelope protection," in *AIAA Modeling and Simulation Tech. Conf.*, no. AIAA-2018-0117, Kissimmee, USA, Jan 2018.

Part II

Understanding the characteristics of human haptic perception

3

EFFECTS OF DELAYED FORCE FEEDBACK ON HUMAN HAPTIC PERCEPTION

As stated in the Introduction, time delays in haptic communication affect the human ability to assess the mechanical properties (damping, mass, and stiffness) of the system being operated; our understanding of this effect is very limited. This chapter describes two psychophysical experiments, both of which employ the method of adjustment presented in the Introduction, to reveal the underlying principle of how our perception changes with delayed force feedback. We find that the altered perceptions are due to the fact that humans cannot distinguish the phase shift caused by a delay in the movement-force relation from changes in the three mechanical properties. This key finding produces the main contribution of this chapter: a unified framework – based on a visualization of the frequency response function of the lumped (original system and delay) dynamics – that can accurately predict all effects due to time delays.

This chapter has been published as: W. Fu, M. M. van Paassen, D. A. Abbink and M. Mulder, "Framework for Human Haptic Perception with Delayed Force Feedback," *IEEE Transactions on Human-Machine Systems*, vol. 49, no. 2, pp. 171-182, 2019.

3.1. INTRODUCTION

Tele-operation systems allow the human operator to accomplish tasks on a remote or hazardous site without the need for physical presence. This field has prompted the continuous development since the mid of last century [1–4]. Providing haptic force feedback that directly reflects the environment properties is essential for maximizing the potential of tele-operation systems. It enables the human operator to sense mechanical properties – damping, mass and stiffness – of the environment.

A system with poor transparency may adversely affect the operator's perception of the properties of the environment, limiting the performance on the task [5]. Designing high-transparency tele-operation systems is therefore of primary importance [6]. However, the information of damping, mass and stiffness is inevitably distorted as the force feedback passes though different mediums (slave, communication channel, master device) before reaching the operator. Effective mitigation of these distortions, in particular those caused by time delays, requires us to first understand *how* these mediums affect the perception of the mechanical properties.

Many studies attempted to understand the effect of time delays [7–12]. It seems that humans cannot separate the delays from the perception of the mechanical properties. Instead, the delay in the force leads to improper estimations of the environment properties [7, 8]. During continuous contact with an elastic force field, humans underestimate the spring stiffness when the delay exists [8, 11, 13]. However, such an underestimation disappears in the case of small delays (up to 30 ms) [10]. Apparently, the reported effects related to different time-delay magnitudes on the haptic perception of spring stiffness are inconsistent. Moreover, a detailed exploration of the effect of delays on perceived damping and mass properties is still lacking.

To this end, we aim to establish a clear understanding of the effect of the delayed force feedback on human perception of *damping, mass and stiffness* properties of linear dynamic environments. This study consists of two user studies. In a first experiment, we investigate the variation associated with the time-delay magnitude in the perception. Attempts are also made to explore the correlation between the delay-caused perception changes and the frequency at which the interaction between the human operator and the environment occurs. The experiment allows us to reveal the fundamental principle that governs the perception change associated with delayed force feedback. On the basis of the principle revealed, we establish a framework that unifies the effect of delays on the perception of all three mechanical properties. It also provides a straightforward visualization which allows for a prediction of the perception change associated with delayed force feedback. With a second experiment, we tested its predictions, and showed that knowledge of both the time delay and the interaction frequency is sufficient to describe the assessment of the mechanical properties perceived with delayed force feedback.

The remainder of the chapter is organized as follows: Section 3.2 provides details about the first experiment. Section 3.3 gives the results of the experiment and the analysis of the results. In Section 3.4 we reveal the principle behind the change caused by delays in the mechanical properties perceived. A unifying framework is proposed in Section 3.5. Section 3.6 elaborates on the second experiment which corroborates the proposed framework. Section 3.7 discusses findings of this study, the limitation of

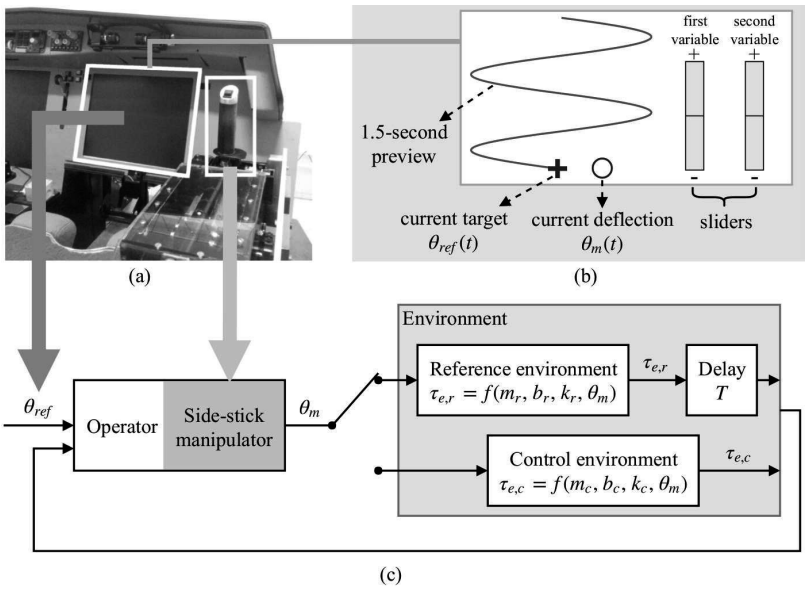

Figure 3.1: (a): The devices used for the experiment. The LCD screen and the side-stick manipulator are marked by white boxes. (b): Contents shown on the LCD screen. The left part is the visual display for the tracking task. The preview curve moves downward as time progresses, and the two symbols '+' and '∘' only move horizontally (see Section 3.2.3). The two bars on the right are used for the adjustment of the parameters of the control environment (see Section 3.2.4). (c): The schematic diagram of the experimental procedure.

the present work, and the future work. Section 3.8 concludes the contributions of this study.

3.2. EXPERIMENTAL METHODS

An experiment was conducted to measure human haptic perception of damping, mass and stiffness properties when force feedback was delayed. It was performed by 12 participants (10 male, 2 female), ranged in age from 24 to 55 years with a mean of 33.7, all right-handed and without a history of impairments in moving the arm or hand. Participants were graduate students and academic staff members of TU Delft. All had sufficient knowledge about how each of these three mechanical properties feels, but were naive about the effect of the time delay on the perception of mechanical properties. The study was approved by the Human Research Ethics Committee of TU Delft, and informed consent was obtained from participants before the experiment.

In this experiment, the effect of the magnitude of the delay time was studied. We also studied the frequency-dependence of the effect of delays, by asking subjects to apply sinusoidal excitation movements at different frequencies.

3.2.1. PROCEDURE

Fig. 3.1c shows a schematic diagram of the experiment. The subject (the operator) haptically perceives one of two environments through a side-stick manipulator. One

environment is a *reference* environment, and the other is a *control* environment. Both environments consist of a mass, damper or spring load simulated with one degree of freedom in the lateral direction. Their forces in response to the manipulator movement can be expressed as:

$$\begin{aligned}\tau_{e,j}(t) &= f(m_j, b_j, k_j, \theta_m) \\ &= m_j \cdot \ddot{\theta}_m(t) + b_j \cdot \dot{\theta}_m(t) + k_j \cdot \theta_m(t)\end{aligned} \tag{3.1}$$

Here, the subscript $j \in \{r, c\}$, where r and c refers to reference and control, respectively. m, b and k are the mass, damping and spring coefficients. τ_e and θ_m denote the environment torque and the manipulator deflection angle. The force of the reference environment $\tau_{e,r}$ is delayed, while that of the control environment $\tau_{e,c}$ is not delayed.

The experiment has a 'perceive & adjust' procedure. The subject initiates an experimental run by selecting one of the two environments. During each experimental run, the subject interacts with the selected environment using a prescribed sinusoidal manipulator movement. Such a manipulator movement will be realized by performing a tracking task. Each experimental run lasts for a fixed length of time. Details about the tracking task and the duration of the experimental run will be given later. After each run, the manipulator automatically moves back to the center, and the subject can adjust the mechanical properties of the control environment before he/she initiates another experimental run (see Section 3.2.4 for the tuning procedure). The subject is asked to repeat this procedure until the two environments are the same in the perceived damping, mass, and stiffness properties.

The dynamics of the side-stick manipulator are the same for the two environments. Therefore, although the subject perceives the lumped dynamics of the manipulator and the environment, the dynamics of the manipulator will not affect the comparison between the two environments. Section 3.2.5 gives the manipulator dynamics and the information about the hardware in greater detail.

Section 3.2.2 gives the settings of the reference environment. The initial settings of m_c, b_c, and k_c of the control environment are taken to be identical to those of the reference environment. Their final values adjusted by subjects will be taken as the measurements, they will indicate the mechanical properties subjects perceived from the delayed reference environment.

Subjects were not informed that the force feedback from the reference environment was delayed. If our subjects are able to perceive the time delay and isolate it from the correct information of the mechanical properties, the three parameters of the control environment should remain at their initial settings. However, if the delay can not be assessed separately, it will affect subjects' perception of the mechanical properties, and the three parameters will change.

3.2.2. CONDITIONS

Three different reference environments were tested. To reduce complexity, each reference environment only possessed a single mechanical characteristic, i.e., damper, mass or spring. Table 3.1 lists the settings of the three reference environments. All these settings chosen here are within the typical manipulator setting range for manual control tasks [14]. Please note that in this chapter all the mechanical properties are

Table 3.1: Settings of the three reference environments

Environment	Damping b_r [Nm·s/rad]	Mass m_r [kgm^2]	Stiffness k_r [Nm/rad]
Damper	0.3	0	0
Mass	0	0.035	0
Spring	0	0	2.0

expressed in a rotational coordinate system, the corresponding linear quantity can be derived using the distance from the effective grip point on the manipulator to the axis of rotation of the manipulator (90 mm, see the Section 3.2.5).

Two time delays $t_{d,i,(i\in\{1,2\})}$ ($t_{d,1}$= 100 ms, $t_{d,2}$= 170 ms) were studied. To investigate the frequency dependency of the effects of delays, we selected two frequencies for the prescribed sinusoidal manipulator deflection $\omega_{i,(i\in\{1,2\})}$ (ω_1= 6 rad/s, ω_2= 8 rad/s). A factorial combination of these two independent variables results in four conditions for each of the three reference environments. The duration of an experimental run was set to 7.35s in the case of ω_i= 6 rad/s and 5.5s in the case of ω_i= 8 rad/s.

3.2.3. PRESCRIBED MANIPULATOR MOVEMENT

To ensure that our subjects moved the manipulator at the desired frequency ω_i (and with that excited the environments at that frequency), they performed a preview tracking task [15] in each experimental run. The visual display of the tracking task was shown by an LCD screen in front of the subject, as can be seen from Fig. 3.1a. Fig. 3.1b illustrates the tracking display in greater detail. The reference manipulator deflection is calculated according to:

$$\theta_{ref}(t) = 0.37 \cdot \sin(\omega_i t) \tag{3.2}$$

In this chapter, the manipulator deflection is given in [rad]. In the experiment, the first and last full cycle of this prescribed movement are used as fade-in and -out phases. The movement amplitude gradually increases from 0 to 0.37 during the fade-in phase, and decreases from 0.37 to 0 during the fade-out phase. To perform the tracking task, the subject needs to reduce the distance between the *current* manipulator deflection $\theta_m(t)$ (shown by "∘" in Fig. 3.1b) and the current reference deflection $\theta_{ref}(t)$ (shown by "+"). The two symbols only move horizontally. The visual preview, shown as a winding curve, contains 1.5-second future information of the reference deflection. It moves downwards as time progresses.

3.2.4. TUNING OF THE CONTROL ENVIRONMENT

Rather than asking our subjects to adjust all three coefficients (b_c, m_c and k_c) of the control environment, we reduce the complexity of the procedure through coupling the adjustments of m_c and k_c. This can be motivated from the frequency response func-

tion (FRF) of the control environment:

$$\begin{aligned} H_c(\omega j) = \frac{F_{e,c}(\omega j)}{\Theta_m(\omega j)} &= m_c \cdot (\omega j)^2 + b_c \cdot \omega j + k_c \\ &= \underbrace{k_c - m_c \cdot \omega^2}_{\Re H_c(\omega j)} + \underbrace{b_c \cdot \omega j}_{\Im H_c(\omega j)} \end{aligned} \tag{3.3}$$

Here, $F_{e,c}(\omega)$ and $\Theta_m(\omega)$ are the Fourier transforms of $\tau_{e,c}$ and θ_m. $\Re H_c$ and $\Im H_c$ are the real and imaginary parts of the complex-valued FRF.

Due to the tracking task, subjects will only excite the environment at a single frequency of ω_i. The force of the environment is determined by the FRF at this particular frequency. Firstly, the real part of this complex number is determined by k_c and m_c combined, see Eq. (3.3). It generates a spring or inertia force in response to the movement, depending on its current sign [16]. When $\Re H_c(\omega_i j)$ is positive, it generates a spring force of which the ratio to the displacement is $\Re H_c(\omega_i j)$. The combination of k_c and m_c that yields a particular harmonic spring force is not unique. However, the harmonic spring forces generated by all combinations are equal to that generated by a pure spring with zero mass and a spring constant of $\Re H_c(\omega_i j)$. A negative $\Re H_c(\omega_i j)$ generates an inertia force which is directly proportional to the acceleration. Similarly, all combinations of k_c and m_c that generate a particular harmonic inertia force can be represented by a pure mass of $-\Re H_c(\omega_i j)/\omega_i^2$. Due to this characteristic and the fact that a system generates only one of the two forces (the spring and the inertia forces) at a single frequency, the adjustment of the mass and stiffness can be combined by means of the real part $\Re H_c$. Secondly, the damping is adjusted with the imaginary part $\Im H_c$, independent of the other two parameters. In the experiment, the computer calculates the three mechanical properties according to the following rule:

$$\begin{aligned} b_c &= \frac{\Im H_c(\omega_i j)}{\omega_i j} \\ k_c &= \begin{cases} \Re H_c(\omega_i j) & \text{, if } \Re H_c(\omega_i j) \geq 0 \\ 0 & \text{, if } \Re H_c(\omega_i j) < 0 \end{cases} \\ m_c &= \begin{cases} 0 & \text{, if } \Re H_c(\omega_i j) \geq 0 \\ \dfrac{-\Re H_c(\omega_i j)}{\omega_i^2} & \text{, if } \Re H_c(\omega_i j) < 0 \end{cases} \end{aligned} \tag{3.4}$$

In the experiment, $\Re H_c$ and $\Im H_c$ were labeled as the 'first variable' and 'second variable', respectively. Subjects could individually adjust these two variables, using two vertical sliders shown on the screen (see Fig. 3.1b). Before the experiment, the relation between the two variables and the three mechanical properties was explained to subjects. All subjects received sufficient training for the adjustment of the mechanical properties.

3.2.5. MANIPULATOR DYNAMICS

The manipulator, an admittance haptic device, is driven by an electro-hydraulic servo motor. Position of the manipulator and moment on the manipulator are led through

presample filters (bandwidth = 200 Hz) before being digitized at 2500 Hz and read into the laboratory computer. The manipulator's control system is executed at 2500 Hz, and effective position following bandwidth is around 40 Hz. The manipulator is supplied with a handle, diameter 35 mm, with grooves for placement of the fingers. When a hand is correctly placed on the handle, the center of the hand lies 90 mm above the manipulator rotation axis. The equivalent (simulated) dynamics of the manipulator can be expressed as:

$$H_m(s) = \frac{\Theta_m(s)}{F_m(s)} = \frac{1}{m_m \cdot s^2 + b_m \cdot s + k_m} \tag{3.5}$$

Here F_m denotes the force that the subject applies to the manipulator.

The manipulator dynamics were configured to guarantee the stability of the overall system. In the experiment, m_m was set to 0.01 kgm^2 for the delayed-spring experiment (the experiment in which the reference environment was a spring), and 0.06 kgm^2 for both delayed-mass and -damper experiments. b_m was 0.3 Nms/rad for the delayed-spring experiment, and 0.05 Nms/rad for both delayed-mass and -damper experiments. The effort to move the manipulator was minimized by setting stiffness k_m to be $m_m \cdot \omega_i^2$. With such settings, the prescribed excitation frequency ω_i becomes the eigenfrequency of the manipulator. Thus the manipulator itself only generates a damping force during the experiment, since the responses of the stiffness and mass are counteracted by each other. Note that the dynamics of the manipulator were identical for each reference environment and its corresponding control environment, although different settings were used for different reference environments. Please note that in the experiment, the manipulator could only move laterally (left and right). The movement in the longitudinal direction (forward and backward) is fixed at the center.

3.3. RESULTS

In the experiment, our subjects performed the tracking task with considerable accuracy. The frequencies of the actual manipulator movement with regard to the two desired frequencies were 6.011±0.032 rad/s and 8.019±0.040 rad/s (mean±std.), respectively. This indicates that the measurements accurately reflect the effects of the condition tested.

Each subject spent a similar amount of time on the adjustment of mechanical properties under all conditions. All finished the experiment with confidence that the two environments were perceived to be the same. The original mechanical properties of all the three reference environments were *under*estimated. In addition, the delay in the force feedback led our subjects to perceive each of the reference environments as having *one more* mechanical property. Additional spring stiffness was perceived from the delayed damper environment; an additional damping property was perceived from the delayed mass environment; an additional property related to negative damping was perceived from the delayed spring. Different experimental conditions led to different extents of these changes in the perception. Table 3.2 lists the measurements of the mechanical properties perceived from each reference environment, i.e., the final values of b_c, m_c, and k_c of the control environment. Table 3.3 shows the results from two-way repeated measures ANOVAs which indicate the effect of the independent factors. Please note that in the tables the term 95%CI denotes the 95% confidence interval

Table 3.2: The mechanical properties perceived by subjects from the delayed reference environments

Delayed Environment		Perceived mechanical properties, mean ± 95%CI			
		t_d: 100 [ms] ω: 6 [rad/s]	t_d: 170 [ms] ω: 6 [rad/s]	t_d: 100 [ms] ω: 8 [rad/s]	t_d: 170 [ms] ω: 8 [rad/s]
damper	b_c [Nms/rad]	.2499±.0089	.1475±.0075	.2126±.0116	.0437±.0124
	k_c [Nm/rad]	0.931±.0357	1.547±.1044	1.586±.1455	2.253±.1071
mass	m_c [kgm^2]	.0275±.0015	.0176±.0013	.0236±.0008	.0070±.0013
	b_c [Nms/rad]	.1205±.0066	.1814±.0060	.2073±.0070	.2811±.0084
spring	k_c [Nm/rad]	1.690±.0586	1.011±.1030	1.423±.0939	0.435±.0825
	b_c [Nms/rad]	-.195±.0087	-.285±.0119	-.180±.0106	-.233±.0055

Table 3.3: The mechanical properties perceived by subjects and the results of statistical tests

Delayed Environment	Perceived mechaincal properties	Factor Impact, DOF: (1, 11)					
		$t_d * \omega$		t_d		ω	
		F	Sig.	F	Sig.	F	Sig.
damper	b_c	106	.000	299	.000	210	.000
	k_c	.241	.633	84.5	.000	197	.000
mass	m_c	17.7	.001	504	.000	111	.000
	b_c	2.13	.172	441	.000	598	.000
spring	k_c	23.9	.000	235	.000	64.9	.000
	b_c	32.6	.000	103	.000	51.8	.000

corrected for between-subject variability, and that a significance value of .000 means p <0.0005.

3.3.1. PERCEPTION OF DELAYED DAMPER

The perceived damping, b_c, under all the four conditions is smaller than the reference damping of 0.3 Nms/rad. The effects of both the delay time t_d and the excitation frequency ω are significant: an increase in either t_d or ω causes more *under*estimation. This can be seen more straightforwardly from the left plot of Fig. 3.2a. In addition, the red line drops faster than the blue line due to a significant interaction. This indicates that the change caused by t_d in the perception is more pronounced when ω increases.

The additional spring stiffness perceived by our subjects varies significantly with

t_d and ω. As can be seen from the right plot of Fig. 3.2a, higher t_d or ω significantly increase the level of the spring stiffness perceived.

3.3.2. PERCEPTION OF DELAYED MASS

The delayed mass was *under*estimated under all conditions. Greater underestimations occurred when either of t_d or ω increased, as can be seen from the left plot of Fig. 3.2b. In addition, a significant interaction leads to the faster drop of the red line, indicating that the effects of the time delay is amplified when the frequency increases.

Under different conditions, different amounts of *additional* damping were perceived from the delayed mass. The increase in b_c due to a larger t_d or ω as shown in the right plot of Fig. 3.2b, was significant.

3.3.3. PERCEPTION OF DELAYED SPRING

The delay in the force feedback led our subjects to *under*estimate the spring stiffness of the reference spring environment. Moreover, subjects related a part of the environment response to negative damping. These two mechanical properties perceived varied significantly with both t_d and ω, as can be seen from Fig. 3.2c. Moreover, a strong interaction was revealed: the slopes of the two lines in both plots are different. Again, this indicates that the effect of t_d depends on ω.

3.3.4. DISCUSSION

The results clearly demonstrate that the time delay affects the human perception of all the three mechanical properties. It appears as if the delay 'shifts' a part of the perception of the original property towards the perception of another. This shift in perception depends on both the time delay and the excitation frequency. In conclusion of the impacts of these two factors: different time delay magnitudes have different effects on the dynamics perceived, and changes in perception are more pronounced with larger delays. In addition, the effect of the time delay varies with the frequency at which the environment is excited, demonstrating a clear frequency-dependence.

3.4. BLACK-BOX MODELING PRINCIPLE AND EVALUATION

In this section, we will investigate how the mechanical properties were estimated by our subjects, and reveal the principle behind the perceptual changes caused by the experimental variations. We will first carry out an analysis in the time domain, then visualize it in the frequency domain. The findings will then be verified by the experiment results.

3.4.1. PRINCIPLE BEHIND THE PERCEPTION CHANGE

INVESTIGATION INTO THE SUBJECTS' STRATEGY

After the experiment, we asked our subjects to explain their strategy for adjusting the mechanical properties. We found that all subjects were unaware of the delay in the force feedback from the reference environment. In order to match the damping of the two environments, subjects compared the forces that they perceived at around the center of the manipulator movement (i.e., the point where the deflection angle is zero,

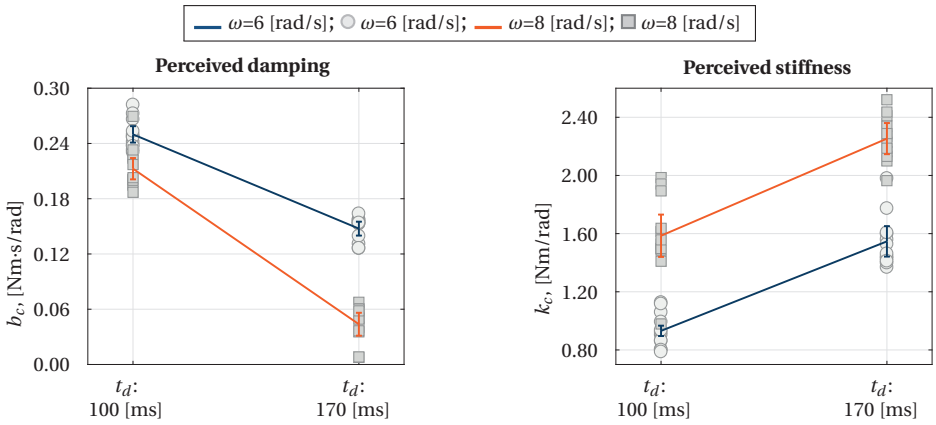

(a) Delayed damper environment

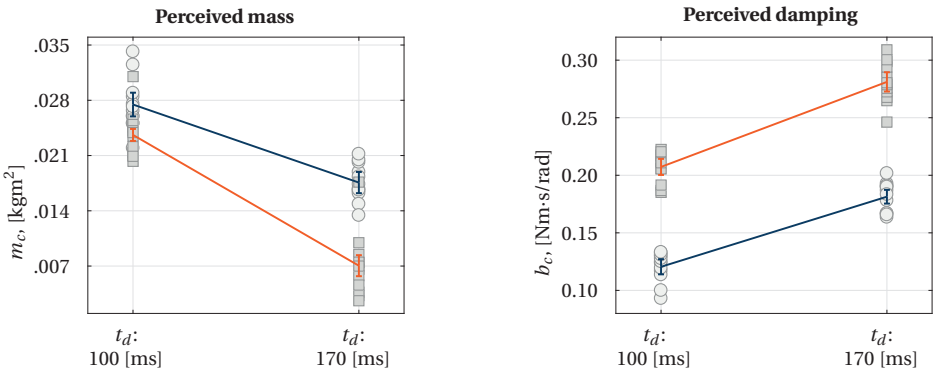

(b) Delayed mass environment

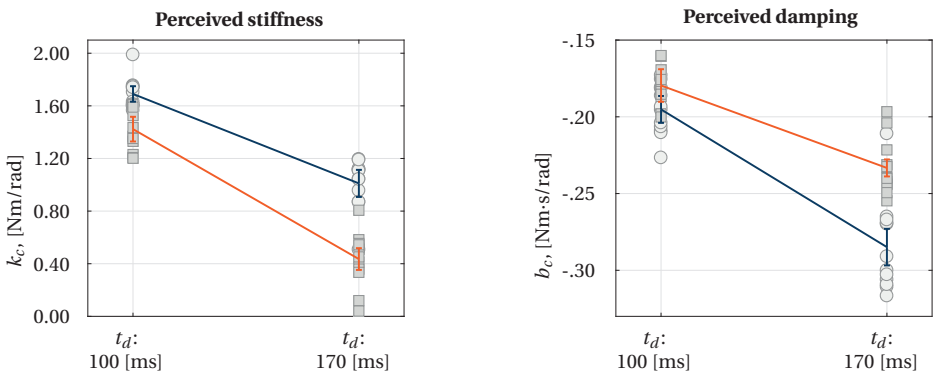

(c) Delayed spring environment

Figure 3.2: Mechanical properties subjects perceived from the delayed reference environments. The data is shown with mean and 95% confidence interval corrected for between-subject variability (represented by the bars). The symbols (square and circle) represent the measurements from individual subjects.

$\theta_m \approx 0$). They related the amount of this force to the damping level. Both the mass and stiffness levels were estimated at the extremes of the manipulator movement (the peaks of the deflection). At the extremes, the force pulling the manipulator back to the center (elastic force) was related to the stiffness level, while the force needed to change the direction of the manipulator velocity (inertia force) was related to the mass level. This indicates that our subjects estimated the mechanical properties on the basis of the correlation between the movement and force, in line with the findings reported in [7, 17, 18].

TIME-DOMAIN ANALYSIS

For an undelayed environment, the forces that one would experience at the deflection angles mentioned above indeed reflect the true levels of the corresponding properties. For example, consider a pure damper environment which possesses a damping of b and zero mass and zero stiffness. Here we use b instead of an explicit numerical number for the damping, as the example shown in the figure is not limited to any particular value of damping.

When the human operator moves the manipulator with a sinusoidal profile, as prescribed during the experiment, the velocity profile of the manipulator is a cosine which reaches the peak when the deflection angle is zero, see Fig. 3.3. When relating the force perceived at this point to the damping, one is actually estimating the ratio of this force to the velocity maximum. Because the force caused by the damping is proportional to the velocity, if the force feedback is not delayed, it will indeed be perfectly 'in phase' with the manipulator velocity, as can be seen from the force profile shown as the gray curve in Fig. 3.3. Therefore, the damping estimation on this basis approximates the true level of damping.

However, due to the time delay, the force feedback from the damper environment *does not align* – is not 'in phase' – with the manipulator velocity. As can be seen from the force profile shown as the red curve, the force at the center is smaller, so does its ratio to the maximum velocity. This reduced ratio results in an *underestimation* of the environment damping. In addition, the delay causes resistant forces at the two extremes of the manipulator deflection, leading subjects to perceive a *non-zero* environment stiffness. This explains the 'shifts' in the perception observed earlier.

FREQUENCY-DOMAIN ANALYSIS

From the above we conclude that our subjects based their estimation of the environment properties on the phase characteristics between their actions on the manipulator (the manipulator movement) and the force feedback they received. A time delay in the force feedback causes this phase characteristic to change, leading our subjects to perceive different mechanical properties. With regard to the example shown in Fig. 3.3, an undelayed environment that possesses a lower damping and a non-zero stiffness can generate exactly the same phase change. Hence, the perception changes observed in the experiment are due to the fact that subjects *cannot distinguish* between the phase changes caused by the delays and the phase changes resulting from changes in damping, spring or mass properties. This principle can be interpreted as a 'black-box estimation problem', where the candidate model is always a single mechanical system no

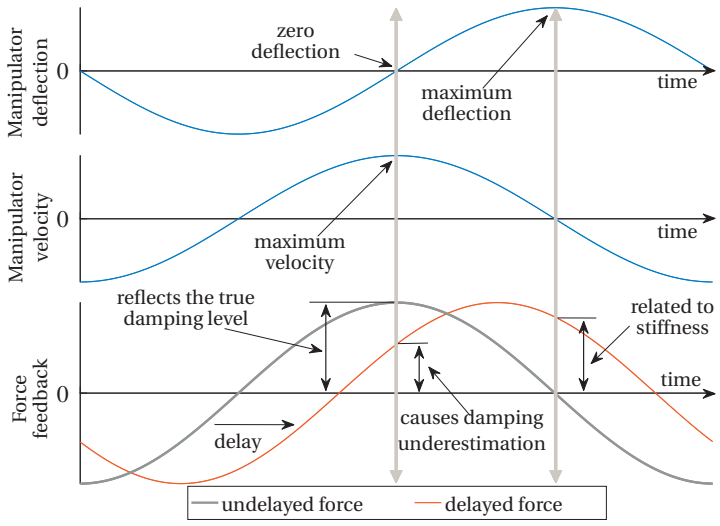

Figure 3.3: An illustration of the relation between the manipulator deflection (top), manipulator velocity (middle) and the force feedback (bottom), for a pure damper environment. For a clear comparison, only one cycle is shown.

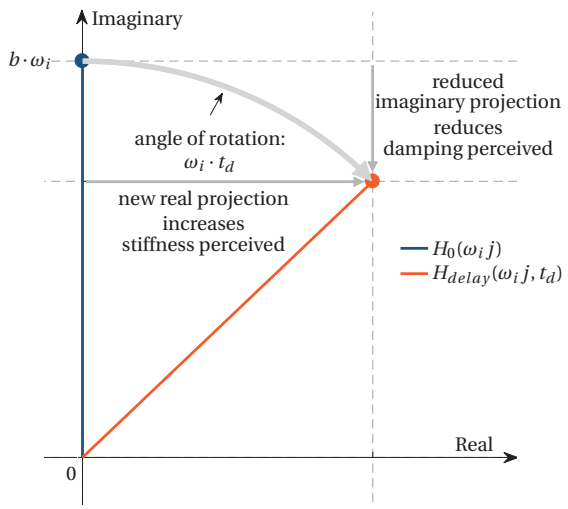

Figure 3.4: The single-frequency Nyquist plots of a pure damper environment with undelayed force feedback (blue vector) and t_d-second delayed force feedback (red vector).

matter what the actual structure of the system is. That is, humans are inclined to always interpret what they feel as a mass, spring, damper system, no matter whether the force feedback they obtain is delayed or not.

To better understand this, we describe the correlation between the position and force of a delayed mass-spring-damper system with the frequency response function

(FRF):

$$H_{delay}(\omega j, t_d) = \frac{F(\omega j)}{\Theta(\omega j)} = \underbrace{e^{-\omega j \cdot t_d}}_{delay} \cdot \underbrace{(m \cdot (\omega j)^2 + b \cdot \omega j + k)}_{H_0} \tag{3.6}$$

where t_d is the delay constant. In order not to cause confusion, note that we express the system dynamics with a *position*-force form, instead of the perhaps more commonly-used impedance Z that describes the *velocity*-force relation.

When considered at a single frequency, the complex-valued FRF is a vector in the complex plane. Excited at this frequency, the system behaves like a single mechanical impedance, i.e., the characteristics of its force response are described by the FRF's projections on the two axes [16]:

- The force response at the velocity maximum – the force that our subjects used to estimate *damping* – is determined by the projection on the imaginary axis.
- The force response at motion extremes – the force that our subjects used to estimate the *stiffness or mass* – is determined by the projection on the real axis. A positive real projection results in an elastic (spring) force; a negative one results in an inertia force.
- The magnitudes of the aforementioned forces relate linearly to the size of the corresponding projections.

Now consider a pure damper environment ($b \neq 0$, $m = k = 0$), and draw the corresponding H_{delay} and H_0 at a single frequency ω_i on the complex plane – a single-frequency Nyquist plot – as shown in Fig. 3.4. As can be seen, the FRF of the undelayed environment (H_0, the blue vector) is located on the imaginary axis. So this system only generates a force in phase with the manipulator velocity, while at the extremes the force is zero; it has a force profile similar to the gray curve in Fig. 3.3. The FRF of the delayed environment ($H_{delay}(\omega_i j, t_d)$, the red vector) has a same magnitude, but is *rotated* by $\omega_i \cdot t_d$ radians in clockwise direction, because of the time delay. Due to this, $H_{delay}(\omega_i j, t_d)$ has a *smaller* projection on the imaginary axis and a *new* projection on the real axis.

The findings of the experiment show that our subjects did not separate the delay from the perception of the mechanical properties. This means the time-delayed dynamics H_{delay} rather than the original dynamics H_0, was used as the basis of the estimation of the environment properties. A reduction in the imaginary projection reduces the force at the velocity maximum, causing humans to perceive a lower damping. The additional projection on the positive real axis leads our subjects to feel an elastic force. As a result, the environment feels 'more elastic', causing a perception of additional spring stiffness.

Similarly, all the dependencies on the time delay magnitude t_d and excitation frequency ω, and their interactions, can also be explained. In the experiment, the variation in t_d or ω led to different phase shifts, causing different changes in the perception of the environment dynamics. Because the phase shift is the *product* of these two variables, the effect of each of these two factors is bound to increase when the other factor increases. Also due to the trigonometric relation between the FRF vector and its projections on the two axes, the effects of these two factors are nonlinear.

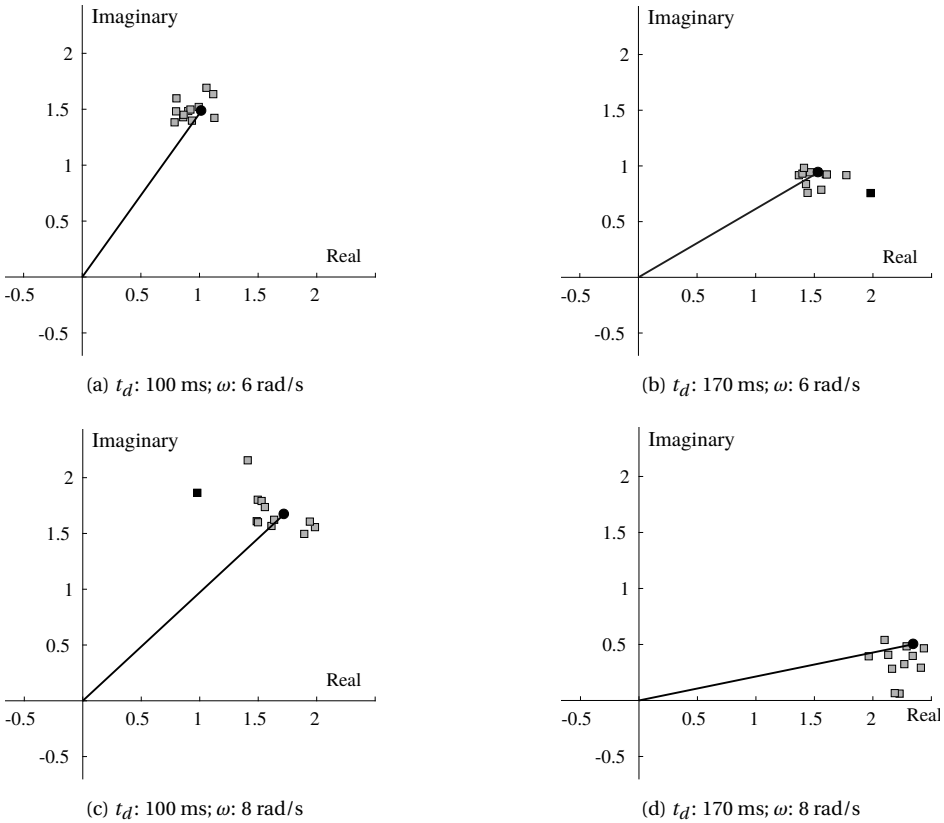

(a) t_d: 100 ms; ω: 6 rad/s

(b) t_d: 170 ms; ω: 6 rad/s

(c) t_d: 100 ms; ω: 8 rad/s

(d) t_d: 170 ms; ω: 8 rad/s

Figure 3.5: The Nyquist-plot predictions of the perceptions of the delayed reference damper environment, $H_{delay}(\omega_i j, t_{d,i})$ (shown by the black vector), and the measurements of subjects' perceptions, $H_c(\omega_i j)$ (shown by gray squares). Outliers are marked by black squares.

3.4.2. VERIFICATION

The aforementioned principle can be verified using the measurements of the experiment. First, take the parameters listed in Table 3.1 and the settings of $t_{d,i}$ and ω_i into Eq. (3.6), $H_{delay}(\omega_i j, t_{d,i})$ of the reference damper environment under different conditions can be obtained. This complex number yields the prediction of how the delayed damper will be perceived. Secondly, the FRFs of the control environments $H_c(\omega_i j)$ yield the frequency-domain measurements of the perception of the delayed damper. Fig. 3.5 shows the comparisons between the predictions and measurements in the complex plane. As can be seen, the measurements from all subjects are close to the predictions.

The perceptual changes associated with the delayed mass and spring environments can similarly be explained, and the measurements also matched the predictions very well, as shown in Figs. 3.6 and 3.7. The experiment measurements provide clear evidence of the "black-box modeling" principle, indicating that, while matching the per-

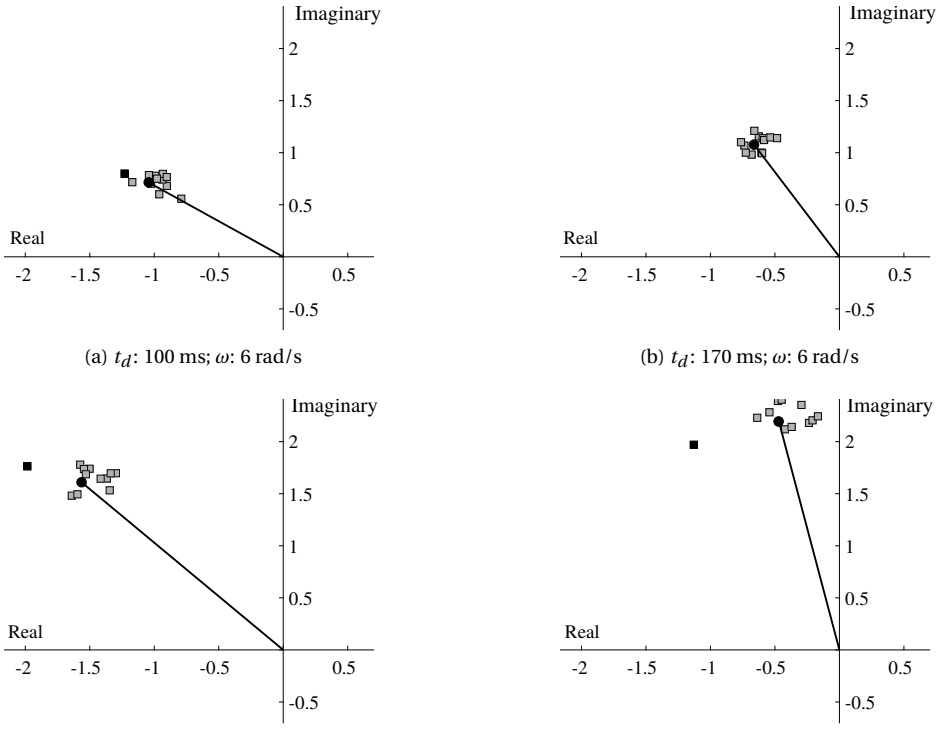

(a) t_d: 100 ms; ω: 6 rad/s

(b) t_d: 170 ms; ω: 6 rad/s

(c) t_d: 100 ms; ω: 8 rad/s

(d) t_d: 170 ms; ω: 8 rad/s

Figure 3.6: The Nyquist-plot predictions of the perceptions of the delayed reference mass environment, $H_{delay}(\omega_i j, t_{d,i})$ (shown by the black vector), and the measurements of subjects' perceptions, $H_c(\omega_i j)$ (shown by gray squares). Outliers are marked by black squares.

ceptions of two environments, our subjects were actually matching the frequency responses of the two environments at the prescribed frequency ω_i.

3.5. FRAMEWORK

In this section we take a combined mass-damper environment as an example, to illustrate how the principle discussed in the previous section can be extended to more general cases, e.g., cases where the environment consists of multiple mechanical properties. We start from a single excitation frequency, and then proceed to multiple frequencies. The extended principle provides a unified framework describing the effects of time delays on the perception of linear dynamic environments.

3.5.1. SINGLE FREQUENCY

Consider a combined mass-damper environment at a single frequency of ω_a. This environment possesses a damping of b and mass of m and zero stiffness. Again, values of the variables used for this example are not limited to particular numbers. Fig. 3.8

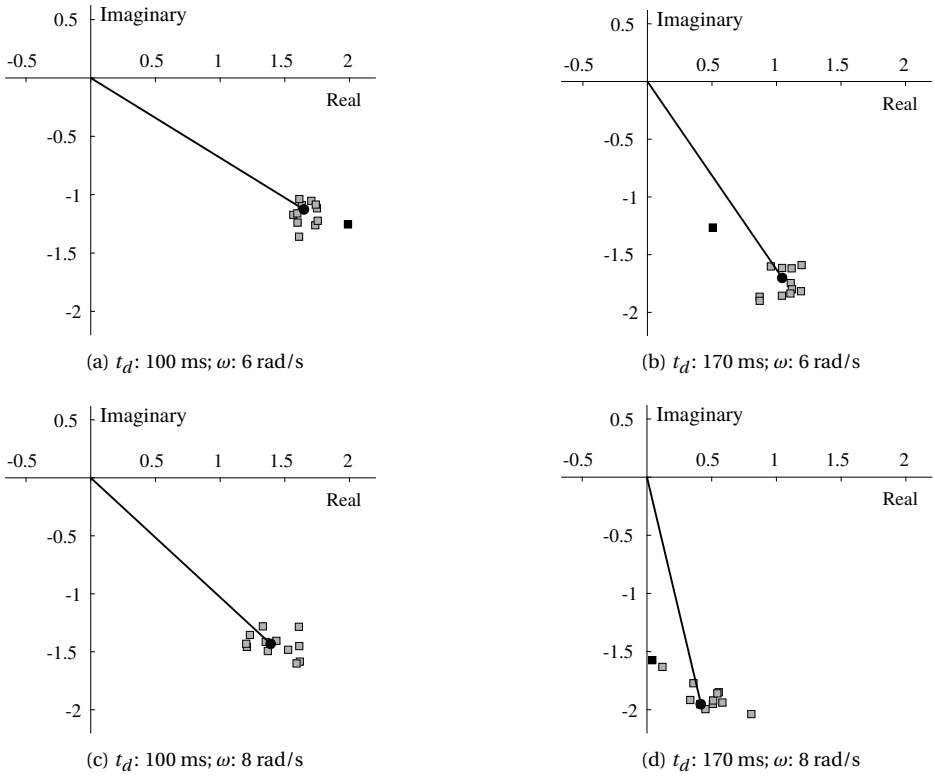

(a) t_d: 100 ms; ω: 6 rad/s

(b) t_d: 170 ms; ω: 6 rad/s

(c) t_d: 100 ms; ω: 8 rad/s

(d) t_d: 170 ms; ω: 8 rad/s

Figure 3.7: The Nyquist-plot predictions of the perceptions of the delayed reference spring environment, $H_{delay}(\omega_i j, t_{d,i})$ (shown by the black vector), and the measurements of subjects' perceptions, $H_c(\omega_i j)$ (shown by gray squares). Outliers are marked by black squares.

shows the single-frequency Nyquist plots of the undelayed dynamics of this environment ($H_0(\omega_a j)$) and the time-delayed dynamics with a time delay T_a ($H_{delay}(\omega_a j, T_a)$).

The FRF of the undelayed system (H_0) has projections on the negative real axis and positive imaginary axis. These two projections respectively determine the inertia force felt at the extremes of the manipulator deflection, and the damping force felt around the zero deflections. From the changed projections on the two axes, one can see that the delay causes this environment to be perceived as having a lower mass and higher damping, as compared to the reference. However, the change in the perception is not consistent over the entire frequency range. If the product $\omega_a \cdot T_a$ is further increased, for instance when increasing the excitation frequency ω_a, $H_{delay}(\omega_a j)$ may move to the first quadrant of the complex plane. In this case, the projection on the real axis becomes *positive*, the original inertia behavior disappears completely, and an elastic force is exhibited instead. The original mass-damper environment will then be perceived as a *spring*-damper environment. With an even larger value of $\omega_a \cdot T_a$, the environment can exhibit an inertia behavior again. Such 'switching' between different perceived mechanical properties occurs with increasing rotation angle $\omega_a \cdot T_a$, with a

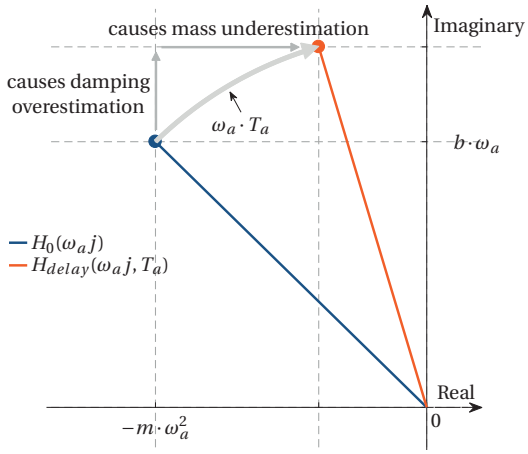

Figure 3.8: Single-frequency Nyquist plots of a combined mass-damper system with undelayed force feedback (blue vector) and T_a-second delayed force feedback (red vector).

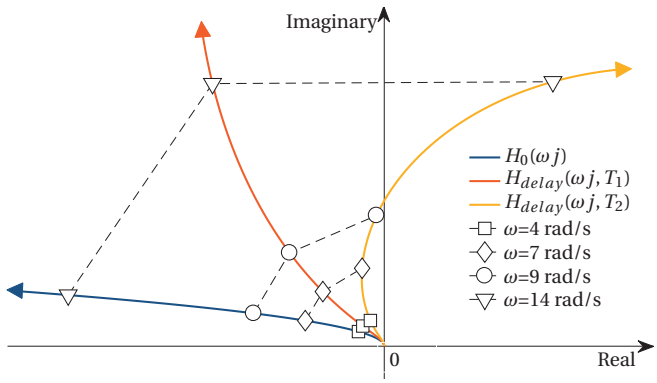

Figure 3.9: The Nyquist plots of a typical mass-damper system with undelayed (blue) and delayed force feedback (red and yellow). The delay times are T_1=60 ms and T_2=140 ms, respectively. The frequency range shown is 0-15 rad/s. The arrows of the curves indicate the increase of frequency. At frequencies of 4, 7, 9, 14 rad/s, respective responses are marked and connected to facilitate comparison.

period of 2π rad.

3.5.2. MULTIPLE FREQUENCIES

Now we proceed to a wider frequency range of 0 to 15 rad/s. The higher end of this range is slightly beyond the approximate (open-loop) natural frequency of human arm neuromuscular system [14]. Consider two different time delays: T_1=60 ms and T_2=140 ms. Fig. 3.9 shows the Nyquist plots of the corresponding $H_0(\omega j)$ and $H_{delay}(\omega j)$ of the mass-damper environment used earlier for this frequency range.

As can be seen, the time delays move the FRF of the original environment clockwise. We first analyze the effect of T_1: the red curve. At all the frequencies in the selected range, the projection on the real axis decreases in size, while the imaginary pro-

jection increases. As a result, the mass will be always *under*estimated and the damping will be always *over*estimated, no matter how the operator interacts with the environment.

However, the extents of the under- and over-estimation vary with the frequency. This is due to the fact that the delay-caused phase shift becomes larger as the frequency increases, shifting a larger proportion of mass into the damping. The perception will in fact depend on how the human operator interacts with the environment. Slow interaction movements will result in less distortion of the mechanical properties perceived, whereas fast movements cause more pronounced changes.

The trend of changes in the perception also depends on the delay time, as demonstrated by the larger time delay T_2. The corresponding FRF is shown as the yellow curve in Fig. 3.9. This curve intersects the imaginary axis at around 9 rad/s. When the interaction occurs below this frequency, the changes in the perceived mass and damping still follow the tendency discussed above while being more pronounced. However, the system begins to exhibit a spring behavior at higher frequencies, as the real-axis projection becomes positive. If the operator interacts with the environment with only fast movements, the inertia force is hardly presented. The elastic force makes the environment perceived to be similar to a spring. Moreover, with larger delays this spring behavior will appear earlier, because the FRF enters the first quadrant at lower frequencies. One can also imagine that the imaginary projection starts decreasing at higher frequencies or in the case of a larger delay time. Due to this, the viscous damping behavior exhibited by the delayed environment becomes weaker.

Similar analyses can be carried out to assess the effect of delays on the perception of damping, mass and stiffness properties of all linear environments. The black-box modeling principle, in combination with the Nyquist-plot visualization, forms a framework that intuitively provides information of all delay-caused changes in the perception. In conclusion, the effect of delayed force feedback on human perception of environment mechanical properties is not consistent. Knowledge of the frequency range of excitation and the delay time is necessary to assess the full effect. But even when such knowledge exists, using fixed values to approximate the mechanical properties perceived by a human operator is still difficult, especially when the delay is large. Nevertheless, the *general trend* of how the delay affects the perception can be predicted. In order to corroborate the proposed framework, a second user study is carried out in the next section.

3.6. FRAMEWORK VERIFICATION

A second experiment was conducted to evaluate the proposed framework. The experiment followed a same 'perceive & adjust' procedure. Subjects interacted with the two environments with the same side-stick manipulator. The reference environment was a typical mass-damper environment, of which the mass property would be perceived to be more dominating than the damping property. The force feedback from this environment was delayed by 80 ms. Table 3.4 gives details about this environment.

The control environment was a mass-spring-damper system from which the force feedback was not delayed. The initial settings of the mass, spring, and damper coefficients (m_c, b_c, and k_c) of this environment were the same as the reference environ-

Table 3.4: Parameters of the reference environment

Damping b_r [Nms/rad]	Mass m_r [kgm^2]	Stiffness k_r [Nm/rad]	Delay T [ms]
0.07	0.03	0	80

ment. Subjects were asked to adjust the dynamics of the control environment until its three mechanical properties approximate to those of the delayed reference environment. In this experiment, instead of the two complex components, subjects directly adjusted the mass, spring, and damper coefficients using three vertical sliders shown on the screen. Moreover, unlike the first experiment in which the interaction was fixed at a particular frequency, in the second experiment subjects were allowed to freely move the manipulator to explore the environments, but were asked to avoid hitting the manipulator's end stops and not make violent movements. The duration of each individual interaction with an environment was not limited. No feedback of the manipulator movement was given on the display.

The dynamics of the manipulator were set to m_m=0.035 kgm^2, b_m=0.05 Nms/rad and k_m=0 Nm/rad, respectively. Again, the dynamics of the manipulator were identical for the reference environment and the control environment. Please note that in the experiment, the manipulator could only move laterally (left and right). The movement in the longitudinal direction (forward and backward) is fixed at the center.

Fig. 3.10 shows the Nyquist plot of the delayed reference environment, along with the dynamics without the time delay. The frequency range shown here is 0 to 15 rad/s. We believe this frequency range is sufficient for the assessment of the effect of time

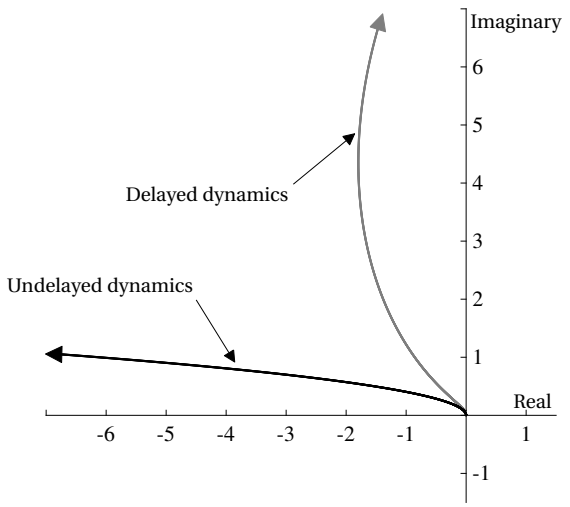

Figure 3.10: The dynamics of the delayed reference environment, and the dynamics without the delay.

delay, since humans can not generate movement beyond the bandwidth of their neuromuscular systems [14]. As can be seen from the figure, we expect subjects to perceive the delayed reference environment as having less mass but higher damping, as compared to the original undelayed dynamics. In addition, no stiffness would be perceived since the delayed environment does not exhibit any spring behavior within this frequency range.

The final values of m_c, b_c, and k_c of the control environment will indicate the mechanical properties perceived from the reference environment. As discussed earlier, the behavior exhibited by a delayed environment depend on the frequencies at which the excitation mainly occurs. Since the manipulator movements applied by different subjects may differ, we expect the perception differs between individual subjects.

Six subjects (5 male and 1 female, between the age of 26 to 56 years with a mean age of 32.2), graduate students and academic staff members of TU Delft, participated in the experiment. They were all right-handed and did not have any history of impairment in moving the arm or hand. All subjects had sufficient knowledge about how each of the three mechanical properties feels, but were naive about the effect of the time delay on the perception of mechanical properties. In addition, subjects did not know the force feedback from the reference environment was delayed. This user study was approved by the Human Research Ethics Committee of TU Delft. Informed consent was obtained from all subjects before the experiment.

3.6.1. RESULT

Table 3.5 lists the the final values of m_c, b_c, and k_c of the control environment adjusted by subjects. Except for the stiffness property, the mass and damping properties perceived by different subjects of the delayed reference environment are considerably different. As expected, all subjects *under*estimated the mass and *over*estimated the damping. Moreover, no spring behaviors were perceived.

The differences in the mechanical properties perceived can be accounted for by the differences in the frequency of excitation between subjects. Although subjects were encouraged to use whatever movements they would like to interact with the environments, the manipulator movements applied by all subjects were still dominated by clear sinusoidal profiles. Fig. 3.11 gives an example which shows the manipulator movement generated by one subject during a single interaction with the reference environment.

A similar human behavior was also mentioned by Nisky et al. in [19]. It seems that

Table 3.5: The mechanical properties perceived by subjects.

	Subject					
	1	2	3	4	5	6
b_c [Nms/rad]	0.271	0.165	0.206	0.106	0.135	0.150
m_c [kgm^2]	0.014	0.019	0.017	0.023	0.021	0.020
k_c [Nm/rad]	0.000	0.000	0.000	0.000	0.000	0.000

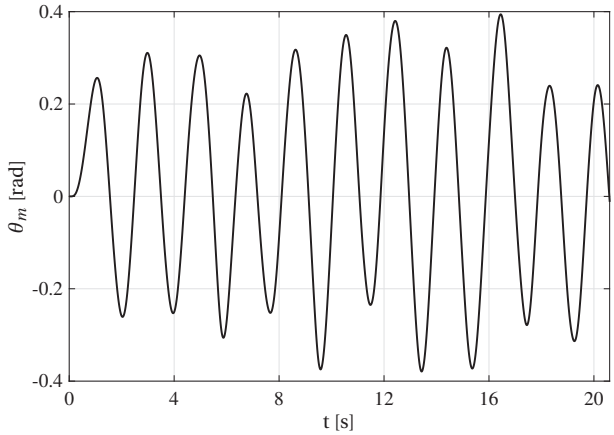

Figure 3.11: The manipulator deflection angle θ_m generated by a subject during a single interaction.

humans are inclined to use a sinusoidal profile to establish their impressions about a mechanical property. According to an interview carried out after the experiment, subjects attempted to interact with the control environment with similar manipulator movements to what they generated for the reference environment. The two environments were then compared in terms of the correlation between the movement and the force.

Due to this, we hypothesize that the frequency responses of the two environments would be the closest at the frequencies at which the environments were excited the most. Fig. 3.12 shows the power spectrum of the manipulator deflection angle generated by a subject during the entire experiment. The peak of the power spectrum occurs close to 4 rad/s. This is the frequency at which the majority of the interaction took place, i.e., the approximate frequency of the sinusoidal profile. Noticeable energy can also be seen at frequencies below 0.1 rad/s which account for nearly static manipulator deflections. According to our subjects, such slow movements were applied at the beginning of the experiment to obtain the static spring force which was used to determine the spring stiffness of the environments.

Our hypothesis can be verified by plotting the difference in the frequency response between the two environments on top of the power spectrum of the manipulator deflection angle. The absolute value of the frequency-response difference can be obtained from:

$$\left|\Delta H(\omega)\right| = \left|H_{ref}(\omega, T) - H_{con}(\omega)\right| \tag{3.7}$$

Here H_{ref} and H_{con} denote the FRFs of the delayed reference environment and the control environment, respectively.

Now, consider the frequency range of 0 to 15 rad/s. For a better illustration, the power spectrum is scaled up and shown with its average over each frequency bin of 1.0 rad/s, as can be seen from Fig. 3.13.

In general, the characteristics of $\left|\Delta H(\omega)\right|$ for all subjects are similar. $\left|\Delta H(\omega)\right|$ starts from zero as both environments do not generate any static spring force. It then increases as the energy of the excitation reduces. As expected, the minimum value of

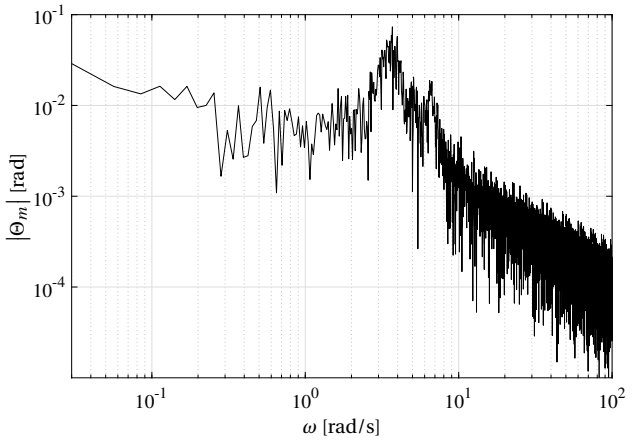

Figure 3.12: The magnitude of the Fourier transform of the manipulator deflection angle generated by a subject during the entire experiment

$|\Delta H(\omega)|$ occurs at roughly the same frequency at which the power spectrum of the manipulator movement reaches the peak. The quick increase in the dynamic difference at higher frequencies is due to the fact that the noticeable difference in the mechanical properties increases as the system magnitude increases (see Chapters 4 and 5). To take this into account, the ratio of the dynamic difference to the system magnitude ($\left|\frac{\Delta H(\omega)}{H_{ref}(\omega,T)}\right|$) is also shown in Fig. 3.13.

To avoid numerical singularity, the lower end of the frequency range used to calculate the ratio is set to 0.1 rad/s. As can be seen, the slope at higher frequencies becomes lower and corresponds better to the characteristics of the power spectrum. The minimum of this difference ratio occurs at the same frequency as the absolute difference, coinciding with the peak of the power spectrum.

3.6.2. DISCUSSION

The experimental findings confirm our hypothesis, and demonstrate the validity of the framework proposed in Section 3.5. Clearly, the mechanical properties of an environment will be perceived differently when the human operator excites the environment at different frequencies. Although the exact change in the perception varies with the frequency of excitation, in this experiment we have demonstrated that the *general trend* of how the perception will change is readily appreciable using our framework.

We also found that humans may assess different mechanical properties at different frequencies. In the experiment, subjects assessed the stiffness of the environments with nearly static manipulator movements. According to subjects, this is due to the fact that in this case the spring force was less 'polluted' by the forces generated by the damping and mass properties. Since the damping and inertia forces are stronger at higher frequencies, at lower frequencies subjects can estimate the stiffness with higher accuracy. This can be accounted for by the perception threshold which increases as the magnitude of the system dynamics increases (see Chapters 4 and 5). However, in cases where the damping and mass are negligible compared to the spring stiffness, accurate

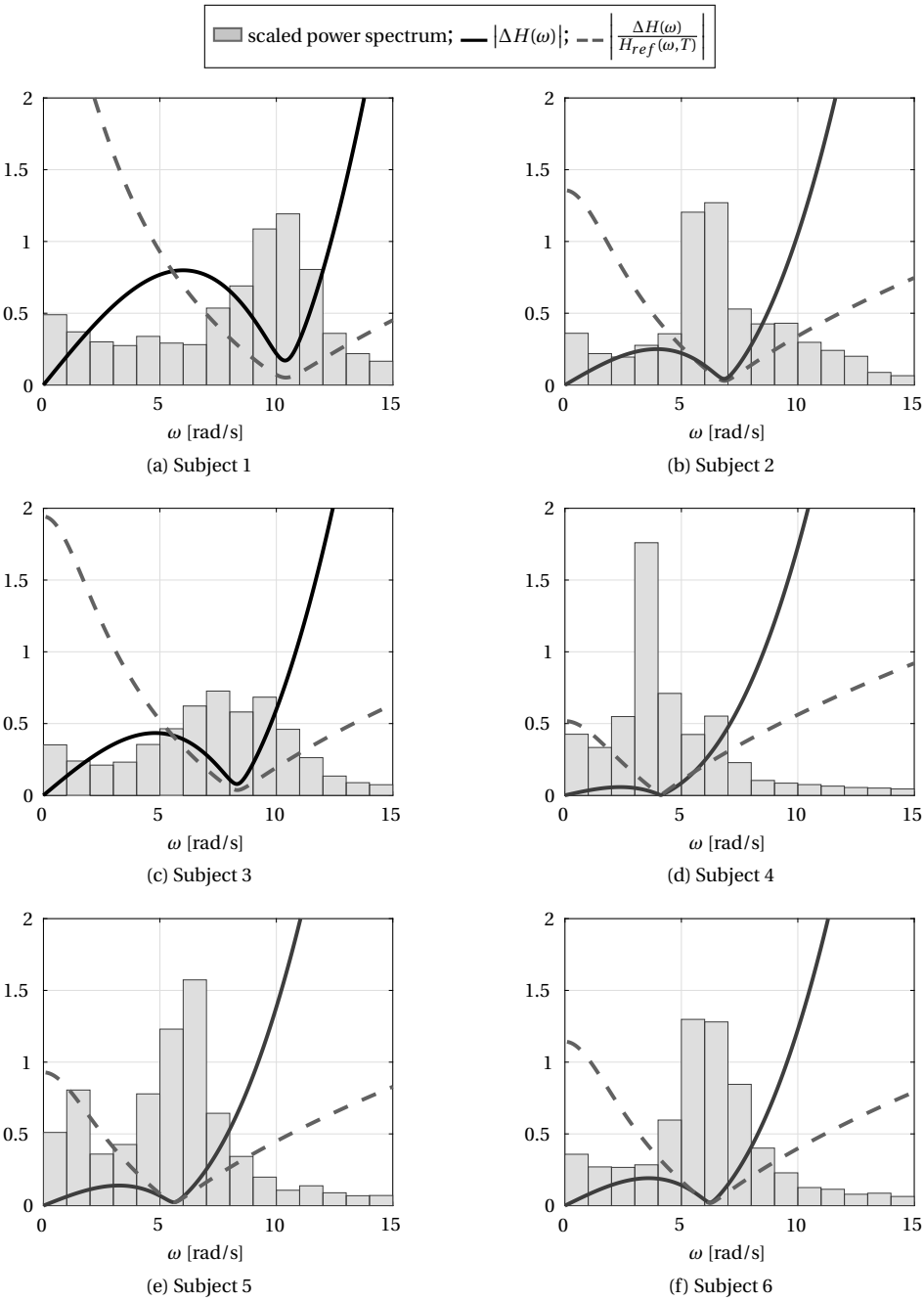

Figure 3.13: The difference in the frequency response between the delayed reference and control environments, plotted on top of the scaled power spectrum of the manipulator movement.

estimation of stiffness can also be obtained using faster movements. It remains unclear whether in such cases subjects will still select static movements for the assessment of the stiffness or be different in the movement frequency as they did to assess the mass and damping properties. A possible correlation may exist between the excitation movement and the dynamics of the environment. This question needs to be answered in future research.

It is of interest to note that the manipulator movement our subjects employed to explore the properties of the environments resembles a sinusoid. This was also reported in [7, 19] during the interaction with spring-like environments. The reason for such behaviors is beyond the scope of this study, but certainly needs to be addressed in further research.

3.7. GENERAL DISCUSSION

Our framework is based on examining the frequency response function of the lumped dynamics of the environment and the time delay. This uses the fact that humans do not separate the time delay from the perception of the mechanical properties. Instead, the dynamics of the time delay and the mechanical properties are lumped together and perceived as a single mechanical system. This is consistent with the findings of previous research [7, 8, 10, 12]. A similar phenomenon also exists in the motor control in tracking tasks [20]. It is suggested that the central nervous system compensates for delays in a sensory channel by means of a representation that resembles a mechanical system.

Our findings related to the perception of stiffness are in line with previous work [8, 13, 21], in which the underestimation is also observed during continuous interaction with the environment. In addition, we find that changes in the perception of all three mechanical properties respect the *same* principle. However, as a result of the threshold for perceiving a difference in the mechanical properties, not all delays can cause a change in the perception. For a noticeable change in the stiffness, a minimum delay of 36 ms is reported [22]. Delays below this noticeable level, as tested in [10], are therefore unlikely to cause significant effects.

In the present study, our subjects interacted with the environments using a side-stick manipulator. Such a setup of the manipulator led the lower arm to be the body part that was mainly involved in the interaction. We found that subjects were inclined to consider the movement to be the cause and the force to be the result, as also suggested by Nisky et al. in [9]. However, if the estimation would be on resulting movement in response to an applied force, as is hypothesized in [9] to match the control strategy for the shoulder joint, a different elaboration of the black-box estimation framework might be needed.

Clearly, due care should be taken when trying to evaluate the mechanical properties of a remote environment when force feedback is delayed. The effect of a time delay can be easily assessed using our framework. With knowledge of the frequency of excitation applied by the human operator, the mechanical properties perceived can be approximated by means of fitting the dynamics of the delayed environment with a mass-spring-damper system at the frequencies where the excitation mainly occurs.

Such an approximation can be fairly accurate in the case of self-exploration tasks,

as humans are inclined to employ a sinusoidal profile to interact with the environment. In tasks which involve tracking, the mechanical properties perceived by the human operator is determined by the reference signal of the tracking task. If the reference signal possesses considerable energy over a relatively wide frequency range, the accuracy of the approximation depends on the magnitude of the time delay. The approximation can still be accurate when the delay is small, as demonstrated by [10]. However, when time delay increases, quantifying its effect using a model with a limited order is not possible any more. As shown by both experiments carried out in this study, there need not be a consistent change in the perception of each mechanical property in the presence of a delay. The change depends on the *product* of the delay time and the excitation frequency. Nevertheless, our framework still provides clear insights into the general changing trend in the perception of the mechanical properties.

As discussed earlier, the FRF of the time-delayed dynamics switches over the four quadrants with a frequency 'period' of $\omega = 2\pi / T_{delay}$ rad/s. One can imagine that the FRF of the time-delayed dynamics can even spiral across all the four quadrants when the delay time is sufficiently large. In this case, a slight change in the excitation frequency will lead the environment to exhibit completely different behavior. Due to this, assessing the mechanical properties of the environment becomes very difficult for a human operator. As a result, the human operator will probably stop perceiving the environment as a mechanical system. It is therefore of interest for future research to understand the delay magnitude from which this situation starts to occur.

Furthermore, the framework proposed in this study is based on the assumption of the continuous interaction between the human operator and the environment. However, discontinuous interaction, during which the boundary of the force field is frequently crossed, can have different effects on the perception of mechanical properties [7, 8]. Extension of the framework, which takes this effect into account, should be made to include this effect.

3.8. CONCLUSION

In this chapter we investigated the effects of delayed forced feedback on the haptic perception of damping, mass, stiffness properties of dynamic environments. In a first experiment, we observed that all mechanical properties were underestimated with time delays, and subjects perceived different mechanical properties than simulated. These changes in perception were accounted for by the fact that our subjects could not separate phase differences due to delayed force feedback from phase differences due to different environment mechanical properties. This key finding led us to define a unified framework – based on a visualization of the frequency response function of the lumped (environment and delay) dynamics – which can accurately predict all effects due to time delays. Our framework is verified by a second experiment, in which participants could explore a mass-damper environment with freely-selected movement patterns. The experimental findings showed that the delayed force caused an underestimation of the mass but an overestimation of the damping, as predicted by the framework. The framework also explains how perception of these two mechanical properties varied between individual subjects, depending on the frequency content of the movement pattern.

REFERENCES

[1] W. R. Ferrell, "Delayed force feedback," *Human Factors*, vol. 8, no. 5, pp. 449–455, 1966.

[2] R. J. Anderson and M. W. Spong, "Bilateral control of teleoperators with time delay," *IEEE Trans. on Automatic Control*, vol. 34, no. 5, pp. 494–501, 1989.

[3] G. Niemeyer and J. J. E. Slotine, "Stable adaptive teleoperation," *IEEE J. of Oceanic Engineering*, vol. 16, no. 1, pp. 152–162, 1991.

[4] S. Hirche, T. Matiakis, and M. Buss, "A distributed controller approach for delay-independent stability of networked control systems," *Automatica*, vol. 45, no. 8, pp. 1828–1836, 2009.

[5] J. G. W. Wildenbeest, R. J. Kuiper, F. C. T. van der Helm, and D. A. Abbink, "Position control for slow dynamic systems: Haptic feedback makes system constraints tangible," in *IEEE Int. Conf. on Systems, Man, and Cybernetics (SMC)*, San Diego, USA, Oct 2014, pp. 3990–3995.

[6] D. A. Lawrence, "Stability and transparency in bilateral teleoperation," *IEEE Trans. on Robotics and Automation*, vol. 9, no. 5, pp. 624–637, 1993.

[7] A. Pressman, L. J. Welty, A. Karniel, and F. A. Mussa Ivaldi, "Perception of delayed stiffness," *The Int. J. of Robotics Research*, vol. 26, no. 11-12, pp. 1191–1203, 2007.

[8] I. Nisky, F. A. Mussa Ivaldi, and A. Karniel, "A regression and boundary-crossing-based model for the perception of delayed stiffness," *IEEE Trans. on Haptics*, vol. 1, no. 2, pp. 73–82, 2008.

[9] I. Nisky, P. Baraduc, and A. Karniel, "Proximodistal gradient in the perception of delayed stiffness," *J. of Neurophysiology*, vol. 103, no. 6, pp. 3017–3026, 2010.

[10] N. Colonnese, A. F. Siu, C. M. Abbott, and A. M. Okamura, "Rendered and characterized closed-loop accuracy of impedance-type haptic displays," *IEEE Trans. on Haptics*, vol. 8, no. 4, pp. 434–446, 2015.

[11] R. Leib, A. Karniel, and I. Nisky, "The effect of force feedback delay on stiffness perception and grip force modulation during tool-mediated interaction with elastic force fields," *J. of Neurophysiology*, vol. 113, no. 9, pp. 3076–3089, 2015.

[12] S. Hirche, A. Bauer, and M. Buss, "Transparency of haptic telepresence systems with constant time delay," in *IEEE Conf. on Control Applications*, Toronto, Canada, Aug 2005, pp. 328–333.

[13] M. Di Luca, B. Knörlein, M. O. Ernst, and M. Harders, "Effects of visual-haptic asynchronies and loading-unloading movements on compliance perception," *Brain Research Bulletin*, vol. 85, no. 5, pp. 245–259, 2011.

[14] M. M. van Paassen, J. C. van der Vaart, and J. A. Mulder, "Model of the neuromuscular dynamics of the human pilot's arm," *J. of Aircraft*, vol. 41, no. 6, pp. 1482–1490, 2004.

[15] K. van der El, D. M. Pool, H. J. Damveld, M. M. van Paassen, and M. Mulder, "An empirical human controller model for preview tracking tasks," *IEEE Trans. on Cybernetics*, vol. 46, no. 11, pp. 2609–2621, 2016.

[16] D. Findeisen, *System Dynamics and Mechanical Vibrations: An Introduction*. Springer Science & Business Media, 2013.

[17] W. Fu, M. M. van Paassen, and M. Mulder, "On the relationship between the force JND and the stiffness JND in haptic perception," in *ACM Symp. on Applied Perception*, no. 11, Cottbus, Germany, Sept 2017.

[18] R. Leib, F. Mawase, A. Karniel, O. Donchin, J. Rothwell, I. Nisky, and M. Davare, "Stimulation of PPC affects the mapping between motion and force signals for stiffness perception but not motion control," *J. of Neuroscience*, vol. 36, no. 41, pp. 10 545–10 559, 2016.

[19] I. Nisky, F. A. Mussa Ivaldi, and A. Karniel, "Analytical study of perceptual and motor transparency in bilateral teleoperation," *IEEE Trans. on Human-Machine Systems*, vol. 43, no. 6, pp. 570–582, 2013.

[20] R. Leib, A. Karniel, and F. A. Mussa Ivaldi, "The mechanical representation of temporal delays," *Sci. reports*, vol. 7, no. 2017-7669, 2017.

[21] B. Knorlein, M. D. Luca, and M. Harders, "Influence of visual and haptic delays on stiffness perception in augmented reality," in *2009 8th IEEE Int. Symp. on Mixed and Augmented Reality*, Oct 2009, pp. 49–52.

[22] M. Rank, Z. Shi, H. J. Müller, and S. Hirche, "The influence of different haptic environments on time delay discrimination in force feedback," in *Int. Conf. on Human Haptic Sensing and Touch Enabled Computer Applications*. Springer, 2010, pp. 205–212.

4

THRESHOLD FOR CHANGES IN PERCEPTION OF MECHANICAL PROPERTIES

As discussed in the Introduction, a distortion is not discernible if it is beyond the resolution of human haptic perception. It is important to know when a perception change occurs. As underlined in the Introduction, the JNDs in mass, stiffness, and damping, as well as the interaction among them, have not been fully explored. To this end, this chapter proposes an extension of the conventional JND law. Two particular cases are studied: 1) the JND in perceiving the stiffness of systems with various mass properties; 2) the JND in perceiving the damping of systems with different stiffness and mass. On the basis of weighting the frequency response magnitude of mechanical properties, we extend the corresponding JND laws by performing model identification to fit the observations from two psychophysical experiments.

This chapter has been published as: W. Fu, A. Landman, M. M. van Paassen and M. Mulder, "Modeling Human Difference Threshold in Perceiving Mechanical Properties From Force," *IEEE Transactions on Human-Machine Systems*, vol. 48, no. 4, pp. 359-368, 2018.

4.1. INTRODUCTION

In many manual control tasks, a control manipulator serves as the haptic interface between humans and machines. In bilateral tele-operation, the human operator uses the manipulator to command the motion of the slave robot in the remote environment, while estimating the mechanical properties of the environment – stiffness, mass and damping – through the force feedback. In flight, the pilot controls the attitude of the aircraft by steering, and changes in the aerodynamic force acting on the control surface, when fed back to the pilot, result in changes in the mechanical properties of the manipulator.

Rendering the proper dynamic information of tasks through the force feedback is of primary importance to a haptic interface. However, the desired information of stiffness, mass and damping conveyed by the force feedback is inevitably distorted. Probable causes are limitations from the digital control systems and actuators, and transmission time delays that occur in many tele-operation systems. Similar to perception limitations in other human modalities, a change in a haptic stimulus must also exceed a certain level to become perceivable. This level, the minimal perceivable change, is referred to as the Just Noticeable Difference (JND).

Knowledge on how large a difference in the force feedback must be to result in different human perception of mechanical properties, i.e., the JND in perceiving manipulator stiffness, damping and mass, is important to the design of haptic interfaces. This can be used to balance the trade-off between transparency and stability of bilateral tele-operation systems [1–4], to assess the fidelity of control loading devices of flight training simulators [5, 6], and is also relevant for the design of haptic support systems in vehicle control [7–9].

In the last few decades, many investigations have been carried out on this topic. The majority of work is based on the assumption that each mechanical property – stiffness, mass or damping – is rendered in isolation. Under this assumption, the human JND can be expressed with Weber's law [10–14], which states that the JND is a fixed proportion of the reference stimulus level. However, in most manual control tasks, the system dynamics presented by manipulators are usually defined by more than one mechanical property. In that case, Weber's law does not apply to the corresponding JNDs, largely limiting the applicability of the present research. For example, the JND in the damping of a system increases when the system possesses higher mass or stiffness [15]. It seems that the perceptions of different properties are *coupled*, and that a change in one property can be "masked" by variations in the other two properties.

To take better advantage of this perceptual characteristic for the design of haptic interfaces, an extension of the JND law is necessary for cases when multiple mechanical properties define the appeared manipulator dynamics. In this chapter, we address the following two research questions:

1. When stiffness and mass properties exist simultaneously, how do changes in the mass affect the JND in the stiffness that humans perceive from the force feedback?

2. When a combined mass-spring-damper system is presented, how do the system's mass and stiffness affect human JND in the system's damping?

In Section 4.2 we will argue why these two cases, among many other potential variations, are the most important to address. In this chapter we will build mathematical models to extend the JND laws for these two cases. We apply psychophysical findings to formulate the JND using the control-theoretic frequency response function (FRF). In addition, we will decompose the characterization of the JND into investigations with individual manipulator excitation frequencies, and select a representative frequency, 6 rad/s, for the investigation in this study.

The contributions of this chapter are twofold:

1. An extension of the stiffness JND law: Eq. (4.16).
   - From a psychophysical experiment, we find that the JND in a system's stiffness violates Weber's law when the system's mass varies. The Weber fraction for stiffness decreases with increasing mass.
   - We successfully model the stiffness JND by weighting the frequency responses of stiffness and mass. In the frequency domain, the stiffness JND is proportional to the combined response of the system's stiffness and mass.
2. An extension of the damping JND law: Eq. (4.17).
   - We find that the JND in the damping of a system violates Weber's law when the system's mass and stiffness varies. The Weber fraction for damping increases when the joint frequency response of the system's stiffness and mass is higher.
   - The damping JND law is extended using the most accurate model from three candidate models. In the frequency domain, the response of the damping JND is a fixed proportion of the response of the combined mass-spring-damper system.

The remainder of this chapter is organized as follows: In the next section, we elaborate the two research questions of this study. In Section 4.3, we design conditions for the human factor experiment, and propose candidate models for the corresponding JNDs. The experimental setup is given in Section 4.4. The experiment results are given in Section 4.5. We extend the JND laws for the two considered cases and validate the extension in Section 4.6. Our work is further discussed in Section 4.7 and concluded in Section 4.8.

4.2. RESEARCH QUESTIONS AND OBJECTIVES

In many cases, the dynamics of a control manipulator can be adequately described as a mass-spring-damper system. Changing a manipulator's displacement (or deflection angle) resembles moving a mass that is connected with a spring and a damper to an infinitely stiff basis. The frequency response function (FRF) of the system dynamics describes the effect of stiffness (k), mass (m), and damping (b) on the system's harmonic force (or torque) response to a given displacement (or deflection):

$$\begin{aligned} H(\omega j) = \frac{F(\omega j)}{X(\omega j)} &= G_k(\omega j) + G_m(\omega j) + G_b(\omega j) \\ &= \underbrace{k - m\cdot\omega^2}_{\Re H(\omega j)=G_k(\omega j)+G_m(\omega j)} + \underbrace{b\cdot\omega\cdot j}_{\Im H(\omega j)=G_b(\omega j)} \end{aligned} \tag{4.1}$$

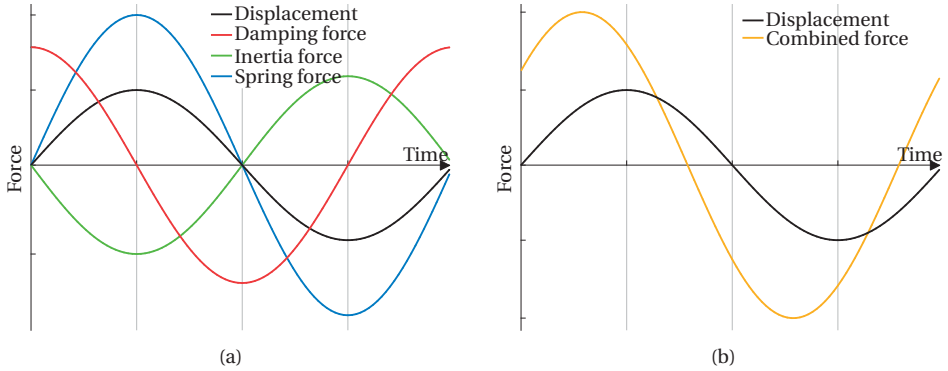

Figure 4.1: An illustration of the stationary force responses of different mechanical properties, excited by a sinusoidal displacement. (a): Isolated force responses of the three mechanical properties. (b): The force response of a combined mass-spring-damper system.

Here $F(\omega j)$ and $X(\omega j)$ denote the force (or torque) and displacement (or deflection), respectively. It follows that $F(\omega j)$ is a combination of three force (or torque) components, which are determined by the frequency responses of stiffness, mass and damping: G_k, G_m and G_b. Without loss of generality, in this section we refer to the terms "deflection" and "torque" as "displacement" and "force" for the sake of clarity.

The majority of past research investigates the JND when each property is rendered in isolation. In such cases only one term in Eq. (4.1) is active (i.e., G_k, G_m, or G_b). A system possessing such dynamics has a fixed phase difference between its movement and force response. For example, as illustrated by Fig. 4.1a, a system behaving like a spring or mass, when being moved with a sinusoidal displacement, yields a force *synchronous* to its displacement. The forces generated by these two properties have opposite directions, however. The force generated by a pure damper system is proportional to the system's *velocity*, with a ratio of b (the damping level). Thus in response to a sinusoidal input the force has a 90-degrees phase difference to the displacement. A change in an isolated mechanical property only changes the amplitude of the system's force response but never changes the phase characteristic. Hence, a human operator can identify the property's type from the phase characteristics. Changes in the amplitude (strength) of the force give him/her accurate indication of changes in this property. In this case, the JND in the three mechanical properties can be described with Weber's law:

$$\frac{\Delta I_{jnd}}{I} = \text{constant}, \tag{4.2}$$

where I and ΔI_{jnd} denote the reference property (stimulus) and the corresponding JND, respectively.

However, in more general and relevant cases where a manipulator behaves as a *combined* system, the force response is affected by multiple mechanical properties *simultaneously*. Fig. 4.1b illustrates the force of a combined mass-spring-damper system: the sum of the forces resulting from stiffness, mass and damping. The magnitude or the phase characteristics of this combined force no longer reflects the characteris-

tics of individual properties that are discussed above. And a change in any of the three mechanical properties changes both the magnitude and phase of this combined force. In this case, identifying a change in one mechanical property requires one to distinguish the force caused by this property from the forces caused by the other two. The accuracy of this identification depends on the accuracy of extracting information of individual properties from the combined force.

As can be seen in Eq. (4.1), we distinguish the real and imaginary components in a manipulator's FRF (i.e., $\Re H$ and $\Im H$). Our two research questions directly follow from this equation:

1. The responses of stiffness and mass are linearly coupled, constituting a joint response (i.e., the real part $\Re H$). This causes us to wonder whether humans can still separate the response (the force) of either property from the joint response. In order to investigate this possible coupling, the JND in the stiffness of systems with various mass will be studied, for the zero damping case.

2. Damping determines the imaginary part $\Im H$, and it responds asynchronously to $\Re H$ (the joint response of stiffness and mass). Humans should be able to extract the damping force from the combined total force, but the accuracy may be affected. To quantify the possible joint effect of stiffness and mass on the accuracy of perceiving the damping, the JND in the damping of combined mass-spring-damper systems with various $\Re H$ will be studied.

In order to extend the JND laws for these two cases, we will perform system identification to estimate the weights of frequency-response contributions of the three mechanical properties. As can be seen from Eq. (4.1), the frequency of excitation ω also plays an important role. This suggests that the characterization of the corresponding JNDs could be performed by investigation at individual frequencies using individual sinusoidal manipulator movements. We start our investigation at a single frequency of excitation, representative of frequencies utilized by participants when a manipulator motion profile can be freely chosen, in this case 6 rad/s (about 1 Hz). Details of the realized manipulator movement is given in Section 4.4.3.

4.3. CANDIDATE MODELS AND EXPERIMENT DESIGN

This section designs the conditions for two human-factor experiments where the two research questions are addressed. Here we define Δk_{jnd} and Δb_{jnd} as the JNDs in stiffness and damping, their FRFs are:

$$\begin{aligned} \Delta G_k(\omega j)_{jnd} &= \Delta k_{jnd} \\ \Delta G_b(\omega j)_{jnd} &= \Delta b_{jnd} \cdot (\omega j) \end{aligned} \tag{4.3}$$

In the next two subsections we propose candidate models of $\Delta G_{k,jnd}$ and $\Delta G_{b,jnd}$, for the system identification purpose.

Table 4.1: Conditions of the two experiments

Experiment	Conditions	Stiffness k [Nm/rad]	Mass m [kgm^2]	Damping b [Nms/rad]	Ratio r_i $\left\lvert\frac{\Re H(\omega j)}{\Im H(\omega j)}\right\rvert$
Stiffness JND	C_k1	2.50	0.0100	0	-
	C_k2	3.75	0.0447	0	-
	C_k3	5.00	0.0794	0	-
Damping JND	C_b1	0.36	0.01	0.25	0.00
	C_b2	1.11	0.01	0.25	0.50
	C_b3	1.86	0.01	0.25	1.00
	C_b4	2.61	0.01	0.25	1.50
	C_b5	3.36	0.01	0.25	2.00

4.3.1. CASE 1: STIFFNESS JND

EXPERIMENTAL CONDITIONS

Three conditions will be tested to study the effect of mass on the stiffness JND. The experiment measures the JND in the stiffness of systems with different stiffness and mass. The systems' damping was kept at zero in all testing conditions to solely focus on the effect of mass. Throughout this chapter, the three conditions are labeled as $C_k i$ ($i = 1,2,3$), and Table 4.1 gives their detailed configurations. The settings of stiffness and mass are chosen from the typical manipulator setting range for vehicle simulators [16]. Note that all mechanical properties are defined in a rotational coordinate system, since the manipulator used in the experiments generates torque in response to its deflection (see details of the device in Section 4.4.1).

MODEL

If humans can accurately extract the force caused by stiffness, the stiffness JND will follow Weber's law, i.e., $\Delta G_{k,jnd}$ will increase in proportion to G_k. If mass affects the perception of stiffness, $\Delta G_{k,jnd}$ will be determined by both G_k and G_m.

The following model of $\Delta G_{k,jnd}$ will be used to estimate the effect of mass:

$$\Delta \hat{G}_{k,jnd} = p_{s,1} \cdot G_k + p_{s,2} \cdot G_m \tag{4.4}$$

Here, $p_{s,1}$ and $p_{s,2}$ denote the weights of the two factors. The Weber fraction for stiffness can be expressed as follows:

$$\hat{W}_k = \left| \frac{\Delta \hat{k}_{jnd}}{k} \right| = \left| \frac{\Delta \hat{G}_{k,jnd}}{G_k} \right| = \frac{p_{s,1} \cdot k - p_{s,2} \cdot m\omega^2}{k} \tag{4.5}$$

The two weights can be determined using the measurements of the stiffness JND. The value of $p_{s,2}$ will indicate the exact relation between the stiffness JND and mass.

4.3.2. CASE 2: DAMPING JND

EXPERIMENTAL CONDITIONS

As already discussed above, the response of damping is asynchronous to those of stiffness and mass. In the complex plane its frequency response is perpendicular to the other two mechanical properties, so formulating the damping JND may require a more complex model than the linear model used for the stiffness JND. We will therefore propose three candidate models in the next subsection. To obtain sufficient measurements for an accurate parameter estimation and a fair model comparison, we measure the damping JND under five conditions. These conditions have the same reference damping level but five different levels of $\Re H$. Since the damping JND follows Weber's law in the case where humans perceive damping in isolation, one level of damping is sufficient to show whether this law is violated or not when varying the other two properties. The chosen damping level is commonly used in manual control research setups [16]. We label the conditions as $C_b i$ $(i = 1,\ldots,5)$ throughout this chapter, they define different ratios (r_i) between $|\Re H|$ and $|G_b|$ (or $|\Im H|$) at the desired excitation frequency of 6 rad/s, as shown in Table 4.1.

As a change in $\Re H$ can account for changes in either or both stiffness and mass (see Eq. (4.1)), the five conditions will allow us to determine the joint effect of stiffness and mass on the damping JND. When considered at a single frequency, any change in $\Re H$ can be always obtained by only adjusting the stiffness, we thus used different manipulator stiffness settings to obtain the desired variations in $\Re H$.

CANDIDATE MODELS

The Weber fraction for damping (W_b) can be derived from the frequency response of the damping JND ($\Delta G_{b,jnd}$):

$$W_b = \left| \frac{\Delta b_{jnd}}{b} \right| = \left| \frac{\Delta G_{b,jnd}}{G_b} \right| \tag{4.6}$$

The first condition marks a zero effect of $\Re H$, and is used as the baseline. If no effects of $\Re H$ exist, W_b will remain invariant over the five conditions. If $\Re H$ affects the damping JND, differences in measurements will be found between the baseline and other conditions. By observing how W_b changes with r, the exact effect can be studied. To quantify the possible effects, we propose three candidate models.

An intuitive way would be to estimate the weights of the two factors separately. Thus we define N_1 and N_2 as the weighted effects of G_b (determined by damping) and $\Re H$ (determined by stiffness and mass), respectively:

$$N_1 = p_{b,1} \cdot \left|G_b\right| \quad , \quad N_2 = p_{b,2} \cdot \left|\Re H\right| \tag{4.7}$$

Here, $p_{b,1}$ and $p_{b,2}$ denote the weights of the two factors.

THE FIRST MODEL

We assume a simple relation, namely that the two factors determine ΔG_b through a linear addition:

$$\left|\Delta \hat{G}_{b,jnd}\right| = N_1 + N_2 = \left|G_b\right| \cdot (p_{b,1} + p_{b,2} \cdot r) \quad , \tag{4.8}$$

with r the ratio of $|\Re H|/|G_b|$. Substituting the above equation into Eq. (4.6), we get the estimated Weber fraction for damping:

$$\hat{W}_b = \left| \frac{\Delta \hat{G}_{b,jnd}}{G_b} \right| = p_{b,1} + p_{b,2} \cdot r \tag{4.9}$$

THE SECOND MODEL

As can be seen from Eq. (4.1), the two factors, G_b (imaginary part) and $\Re H$ (real part), are perpendicular to each other in the complex plane. Considering this characteristic, one could assume that these factors affect the JND threshold through a weighted power addition:

$$\left| \Delta \hat{G}_{b,jnd} \right| = \sqrt{N_1^2 + N_2^2} = \left| G_b \right| \cdot \sqrt{p_{b,1}^2 + p_{b,2}^2 \cdot r^2} \tag{4.10}$$

Here N_1 and N_2 are defined by Eq. (4.7)). Substituting the above equation into Eq. (4.6)), results in:

$$\hat{W}_b = \left| \frac{\Delta \hat{G}_{b,jnd}}{G_b} \right| = \sqrt{p_{b,1}^2 + p_{b,2}^2 \cdot r^2} \tag{4.11}$$

THE THIRD MODEL

In practice, the estimation of the damping JND using two different factors can be tedious. It will be more efficient if the damping JND can be described with a single factor, in a way similar to Weber's law. We therefore formulate the damping JND using the FRF of the combined system ($H(\omega j)$) to include the effects of both G_b and $\Re H$:

$$\begin{aligned} \left| \Delta \hat{G}_{b,jnd} \right| &= p_b \cdot |H| \\ &= p_b \cdot \left| G_b \right| \cdot \sqrt{r^2 + 1} \end{aligned} \tag{4.12}$$

This model considers the frequency response of the damping JND to be a constant fraction of the combined system's frequency response. Taking the equation above into Eq. (4.6), we get:

$$\hat{W}_b = \left| \frac{\Delta \hat{G}_{b,jnd}}{G_b} \right| = p_b \cdot \sqrt{r^2 + 1} \tag{4.13}$$

4.4. EXPERIMENTAL SETUP AND METHOD

4.4.1. APPARATUS AND PARTICIPANTS

The experiments were performed in the Human-Machine Interaction Laboratory at the faculty of Aerospace Engineering, TU Delft. An illustration of the devices is given in Fig. 4.2. An admittance-type side-stick manipulator driven by an electro-hydraulic motor was used in the experiment. The manipulator is supplied with a handle, diameter 35 mm, with grooves for placement of the fingers. It could move in the left/right

Figure 4.2: The apparatus used in the JND experiment. The side-stick manipulator and the LCD screen are marked by white rectangles. The manipulator could be deflected laterally (left/right) like a joystick. The LCD screen only displays the visual presentation of the tracking task.

direction (lateral) like a joystick. When a hand is correctly placed on the handle, the center of the hand lies 90 mm above the manipulator rotation axis. The manipulator can be configured to present different mass-spring-damper dynamics to a human operator. Position of the manipulator and moment on the manipulator are led through presample filters (bandwidth = 200 HZ) before being digitized at 2500 HZ and read into the laboratory computer. The manipulator's control system is executed at 2500 HZ, and effective position following bandwidth is around 40 HZ. Therefore the dynamics defined in Table 4.1 can be accurately realized at the desired frequency of excitation (6 rad/s, approximately 1 Hz).

An LCD screen, placed in front of the seat, was used to help subjects follow the prescribed sinusoidal manipulator movement (detailed description of the visual presentation is given in Section 4.4.3). Subjects were asked to wear an active noise suppression headphone (David Clark H10-66XL), to cancel possible auditory cues.

Eight human subjects participated in both experiments. All participants were right-handed and reported no hand/arm impairment history. Informed consent was obtained from all subjects before the experiments. This study was approved by the Human Research Ethics Committee of Delft University of Technology.

4.4.2. PROCEDURE

In this study, only the upper JNDs were investigated. The JNDs were measured by a one-up/two-down adaptive staircase procedure [17]. The ratio of the down stepsize to the up stepsize was 0.5488. The measured JND was in accordance with 80.35% correct performance [18]. An example of the staircase procedure is shown in Fig. 4.3.

For each condition, a complete staircase procedure was performed by the subject. It generally consisted of 20 to 30 trials. Each trial consisted of two 6.3-second simulations. In one of the two simulations in each trial, the side-stick manipulator was configured to present the dynamics of a reference system, and in the other simulation it presented a controlled system. The dynamics of the reference system, which were the same over all trials, were defined by the condition being tested (see Table 4.1). The

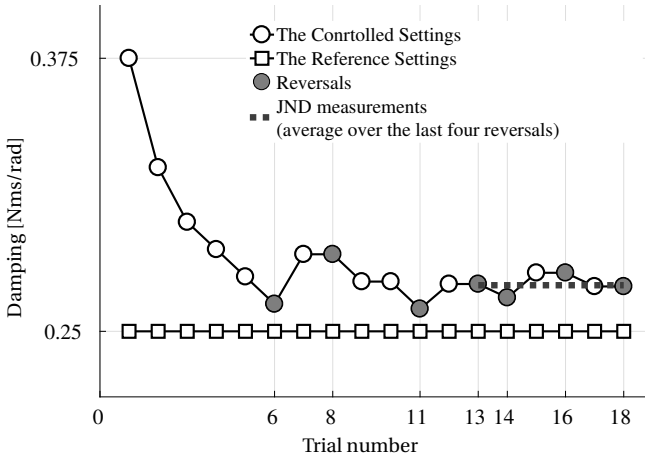

Figure 4.3: An example of the staircase procedure obtained in the damping JND experiment. One up/one down procedure was used before the first reversal for a quick convergence. The reference damping setting was fixed during the entire procedure, and the controlled damping setting was adjusted by the subject's responses.

controlled system only differed from the reference system in the mechanical property being tested (stiffness or damping) by an adjusted *increment*. The sequence in which the two simulations of each trial were presented to the subject was random, based on a prior probability of 0.5.

In each simulation, the subject was asked to move the manipulator by following a prescribed sinusoidal deflection while perceiving the manipulator dynamics (the prescribed manipulator deflection will be elaborated in Section 4.4.3). After each trial, the subject was asked to report in which of the two simulations he or she experienced the higher manipulator stiffness (in the stiffness JND experiment) or the higher damping (in the damping JND experiment). The increment for the next trial was increased when a subject gave a wrong answer (e.g., the 6th, 11th, 14th and 18th trial in Fig. 4.3), and was reduced when the subject gave correct answers in two consecutive trials. Here we define a reversal as the trial where the staircase curve changes direction (see solid markers in Fig. 4.3). The procedure ended when the 7th reversal occurred, or when the total number of trials reached 40. The JND was defined as the average of the last four reversals (trial 13, 14, 16 and 18 in the figure), as illustrated by the dashed line in Fig. 4.3.

Each subject performed the two experiments on two separate days in a random order. Sufficient training preceding the experiment was performed to improve the tracking performance (described in Section 4.4.3) and to familiarize subjects with the comparison task.

4.4.3. PRESCRIBED MANIPULATOR MOVEMENT

In order to ensure that the discrimination task would be conducted with the desired single-frequency sinusoidal manipulator movement, subjects were required to perform a preview tracking task. The visual presentation of the tracking task is illustrated

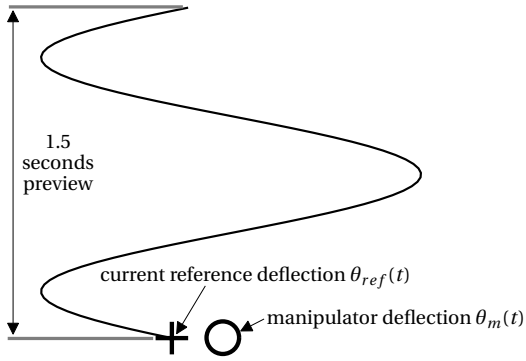

Figure 4.4: The visual presentation of the preview tracking task shown on the LCD screen. To reduce the tracking error (i.e., the difference between "+" and "∘") exampled here, the subject has to push the manipulator towards the left.

in Fig. 4.4. Note that only the sinusoidal curve and the two symbols ("+" and "∘") in this figure were actually shown to the subject. This display was provided on an LCD screen placed in front of the subject (marked by white rectangle in Fig. 4.2). The reference manipulator deflection $\theta_{ref}(t)$ (shown as "+" on the display) was calculated using:

$$\theta_{ref}(t) = \begin{cases} \alpha \cdot \theta_0(t), \text{ if } t < 1.0 \\ \beta \cdot \theta_0(t), \text{ if } t > 5.3 \\ \theta_0(t), \text{ else} \end{cases} \tag{4.14}$$

$$\text{where, } \theta_0(t) = 0.37 \cdot \sin(6t),\ \alpha = t,\ \beta = 6.3 - t.$$

The first and last seconds were used as fade-in/out phases, during which the amplitude of the reference movement gradually in/decreases. The current manipulator deflection $\theta_m(t)$ applied by the subject was measured and shown as "∘" on the display. To perform the tracking task, the subject was instructed to minimize the error between "∘" (the current manipulator deflection $\theta_m(t)$) and "+" (the current reference deflection $\theta_{ref}(t)$). These two symbols can only move horizontally. The visual preview, shown as a winding curve (blue line), contains 1.5-second future information of the reference deflection. It moves downwards as time progresses.

4.4.4. MODEL PARAMETER ESTIMATION AND VALIDATION

Parameters of the models proposed in Section 4.3 can be estimated using the JND measurements. The estimation involves the minimization of a weighted, output-error based criterion J:

$$J = \sum_{i=1}^{N} f(\varepsilon_i^2, \sigma_{\bar{x},i}) \tag{4.15}$$

$$\text{where} \quad \varepsilon_i = \lambda_i - \tilde{W}_i(\hat{p}, \tilde{\omega}_i).$$

Here, N denotes the total number of conditions (N=3 for the stiffness JND experiment and N=5 for the damping JND experiment). The subscript i of all variables denotes

the condition number. $\hat{p}$ is the parameter set that needs to be estimated. λ denotes the sample mean of the measured Weber fraction. $\sigma_{\overline{x}}$ denotes the corresponding standard error (the standard deviation of the sample mean) corrected for between-subjects variability. This variable is used to generate the weighting factor for the parameter estimation process. $\hat{W}$ is the estimate of the Weber fraction given by the candidate models. $\tilde{\omega}$ denotes the actual manipulator movement frequency that subjects generated during the experiment. A 'leave-one-out' cross validation procedure is employed to select the best candidate model for the damping JND.

4.5. RESULTS AND ANALYSIS

Subjects performed the tracking task with considerable accuracy. The manipulator was excited at the desired frequency, as can be seen from the actual frequency of excitation ($\tilde{\omega}$) determined from the measured data, listed in Table 4.4. Thereby the JND measurements accurately reflect the effects of the testing factors under the desired testing condition. In the following two sub-sections, we discuss the results of the two experiments.

4.5.1. EXPERIMENT 1: STIFFNESS JND

The JND measurements are shown as Weber fractions (the normalized JND: $\Delta k_{jnd}/k$) with the sample mean and ±95% confidence intervals corrected for between subjects variability, in Table 4.2. The result of a one-way repeated measures ANOVA shows that the effect of different condition settings on this fraction is significant ($F(2,14) = 10.9, p < 0.05$). Post-hoc pairwise comparisons (after Holm-Bonferroni correction) reveal that each condition is significantly different from the other two, see Table 4.2. However, the *absolute* values of the stiffness JND: Δk_{jnd}, of the three conditions are approximately the same (see Table 4.2), and seem unaffected by the different settings (one-way repeated measures ANOVA: $F(2,14) = 0.54, p = 0.95$).

This result shows that our subjects were able to detect a *fixed absolute amount* but

Table 4.2: Stiffness JND measurements and post-hoc results

Conditions $m \mid k$	Normalized JND: $\frac{\Delta k_{jnd}}{k}$ [%]	Normalized JND: Post-Hoc Sig. (p value)	Absolute JND: Δk_{jnd} [Nm/rad]
C_k1: 0.0100 | 2.50	10.9 ± 2.1	C_k1 vs. C_k2: .033*	$0.27 \pm .068$
C_k2: 0.0447 | 3.75	6.9 ± 0.9	C_k2 vs. C_k3: .018*	$0.26 \pm .029$
C_k3: 0.0794 | 5.00	5.2 ± 1.6	C_k3 vs. C_k1: .009*	$0.26 \pm .059$

Units of variables m and k are given in Table 4.1. Symbol * indicates that the result of the post-hoc T-test is significant (after a Holm-Bonferroni correction).

smaller proportion of stiffness change from the force when the reference stiffness level increases. This violates Weber's law that is given in Eq. (4.2). Such a violation is caused by the variation in the mass: apparently a higher mass level leads to a lower *normalized* stiffness JND.

4.5.2. EXPERIMENT 2: DAMPING JND

Table 4.3 shows the measurements of the damping JND with sample means and ±95% confidence intervals corrected for between-subject variability. The obtained damping JND shows a clear increasing trend as $\Re H$ increases. This means that the least detectable damping change becomes *a larger proportion* of the reference damping when the joint response of stiffness and mass increases. This violates Weber's law.

A one-way repeated-measures ANOVA shows that the effect of r on the damping JND is significant: $F(4,28) = 7.75, p < 0.05$. Contrast tests (with Holm-Bonferroni correction), comparing conditions C_b2:5 to the baseline condition C_b1, reveal the effect of r to be significant when r is larger than 1.5, see Table 4.3. These results confirm that the *joint* response of stiffness and mass affects the damping JND, although this effect is signiifcant only for higher values of r.

4.6. EXTENSION OF THE JND LAWS

This section extends the JND laws for the two tested cases: 1) human JND in the stiffness of linear systems with various mass and negligible damping; 2) human JND in the damping of combined systems with various stiffness and mass. The model parameters are estimated from the experimental results shown by Tables 4.2 - 4.4 with the procedure explained in Section 4.4.4. The corresponding JND laws for the two cases will be extended accordingly. We also investigate our subjects' strategies used for the discrimination task, to explain the underlying principle of the experimental observations, and also to backup the proposed extensions of the JND law.

Table 4.3: Damping JND measurements and contest test results

Conditions damping b | ratio r	Normalized JND: $\frac{\Delta b_{jnd}}{b}$ (%)	Contrast test Baseline C_b1 Sig. (p value)
C_b1: 0.25 | 0.0	9.8 ± 2.0	-
C_b2: 0.25 | 0.5	10.6 ± 2.3	.573
C_b3: 0.25 | 1.0	12.6 ± 4.4	.304
C_b4: 0.25 | 1.5	16.3 ± 2.9	.011*
C_b5: 0.25 | 2.0	20.8 ± 3.9	.000*

The unit of damping b is given in Table 4.1. The first condition C_b1 was used as the baseline condition in the contrast test. Symbol * indicates that the result of the contrast test remains significant after Holm-Bonferroni correction.

Table 4.4: Actual frequency of excitation and the resultant ratio r

	Exp 1			Exp 2				
	C_k1	C_k2	C_k3	C_b1	C_b2	C_b3	C_b4	C_b5
$\tilde{\omega}$	5.98	6.00	6.02	5.96	5.97	5.98	5.97	5.98
$\tilde{r}$	-	-	-	.003	.505	1.00	1.51	2.00

4.6.1. EXTENSION OF THE STIFFNESS JND LAW

MODEL IDENTIFICATION

The estimated parameters of the model Eq. (4.5) are given in Table 4.5. With these two parameters, the model provides accurate estimates of the observed stiffness JNDs, as shown by the diamonds in Fig. 4.5. The weights of G_k and G_m (0.126 and 0.130) are approximately identical, indicating that the stiffness and mass affect the stiffness JND in the same manner. Hence, our model can be simplified to become:

$$\frac{\Delta G_k(\omega j)_{jnd}}{G_{k+m}(\omega j)} = \frac{\Delta G_k(\omega j)_{jnd}}{\Re H(\omega j)} = \frac{\Delta k_{jnd}}{(k - m\omega^2)} = p_s, \tag{4.16}$$

with a single ratio constant p_s of 0.124. Here we use G_{k+m} to represent the combined frequency response of stiffness and mass: $G_k + G_m$ (which is also the real part of the system's frequency response, $\Re H$). As can been seen, this simplified model replaces the reference property in the denominator of Eq. (4.2) with this combined response.

The stiffness JND can still be described with Weber's law in the frequency domain, if the reference stimulus is defined from a different perceptive. If we define the reference stimulus as the *combined* frequency response of stiffness and mass, the stiffness JND is

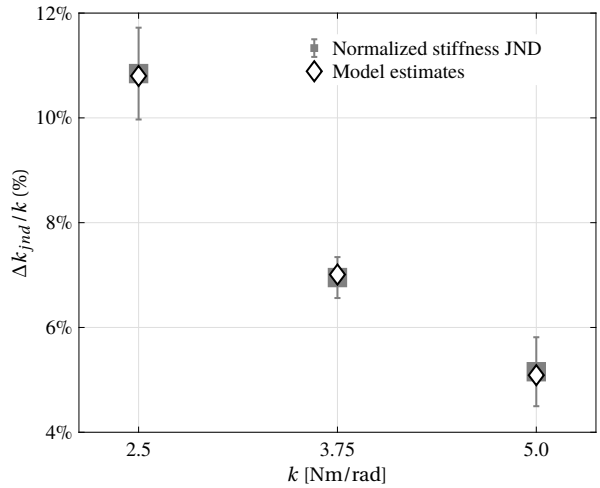

Figure 4.5: Normalized stiffness JND measurements and model estimates. The measurements are shown with sample means (gray square) and standard errors corrected for between subject variability (error bars).

Table 4.5: Model parameter estimates

Stiffness JND		Damping JND				
		Model 1		Model 2		Model 3
$p_{s,1}$	$p_{s,2}$	$p_{b,1}$	$p_{b,2}$	$p_{b,1}$	$p_{b,2}$	p_b
.126	.130	.086	.053	.095	.090	.092

proportional to this stimulus. This can be validated by the experimental data. Fig. 4.6 shows the stiffness JND that is normalized to the newly defined stimulus: G_{k+m}. When the JND is expressed in this way, no statistical differences can be observed (one-way repeated measures ANOVA: $F(2,14) = 0.04$, $p = 0.96$).

Eq. (4.16) enables us to extend the JND law for the first case: the JND in the stiffness of systems with various mass and negligible damping. In addition, this extension does not conflict with the original law given in Eq. (4.2). When the movement frequency ω approaches zero, or the manipulator mass m is negligible, the two laws become identical.

PRINCIPLE INVESTIGATION

From the experiment we found that a variation in manipulator mass affects the least detectable *proportion* of difference in stiffness, however, not the *absolute value*. With a closer examination of the condition settings given in Table 4.1, it can be found that the newly defined reference stimulus, G_{k+m} in Eq. (4.16), is identical for all three conditions at the prescribed excitation frequency (6 rad/s). Since the extended JND law indicates that the stiffness JND is a fixed proportion of G_{k+m}, the invariant absolute value is therefore a consequence of our experiment settings.

The principle governing how our subjects estimate a stiffness change can help us

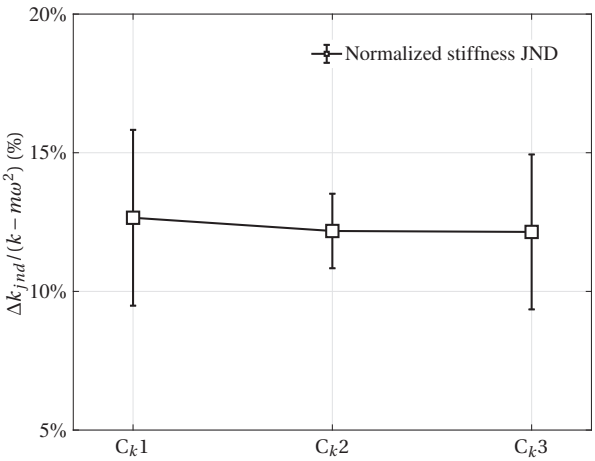

Figure 4.6: The stiffness JND Δk_{jnd} normalized to the combined frequency response of stiffness and mass. Error bars represent the 95% confidence intervals corrected for between subject variability.

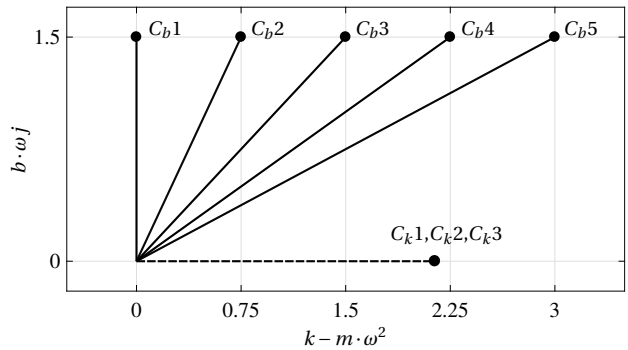

Figure 4.7: Frequency responses at 6 rad/s, of different condition settings of the two experiments, plotted in the complex plane.

to explain the extended law of the stiffness JND. After the experiment, we asked our subjects to reflect on their strategies for the discrimination task. All of them indicated that, to identify the stiffness difference between the two simulations, they compared the forces they perceived at the *extremes* of the manipulator deflection (max($|\theta_{ref}|$): when $\theta_{ref}(t) = \pm 0.37$ rad). As discussed in Section 4.2, it is at this deflection where both the spring and inertia forces become maximal. The force that subjects use to estimate the stiffness is actually the maximum of a *combined* force, which is determined by stiffness and mass together. Apparently, our subjects could not separate the spring force and the inertia force when these two force components are combined. Due to this, the perceived change is a change in the combined response of these two mechanical properties.

This manifests that our subjects only perceive the "effective stiffness" [19] rather than the true stiffness. The "effective stiffness" equals the real part of the system's FRF, therefore it is the newly defined stimulus: G_{k+m}. To better illustrate this, we plot G_{k+m} at the prescribed frequency in the complex plane, as shown by the dashed vector in Fig. 4.7.

This vector describes how the system responds to a sinusoidal excitation signal [20]. Its magnitude and phase angle define, respectively, the amplitude difference and the phase difference between the movement and force. With our experimental settings, the three conditions have identical vectors, all located on the positive real axis. This horizontal vector generates an "effective spring force" proportional to the deflection angle of the manipulator. Thus, our subjects' strategy is equivalent to comparing the positive real projection of the system: the effective stiffness. Since the force difference threshold follows Weber's law, perceiving the change in the maximum of the "effective spring force" leads the stiffness JND to be proportional to the effective stiffness G_{k+m}.

4.6.2. EXTENSION OF THE DAMPING JND LAW

MODEL IDENTIFICATION AND SELECTION

The estimated parameters of the three candidate models are shown in Table 4.5. Model predictions using these parameter estimates are shown in Fig. 4.8 together with the JND measurements. The first model, based on a linear structure, does not accurately

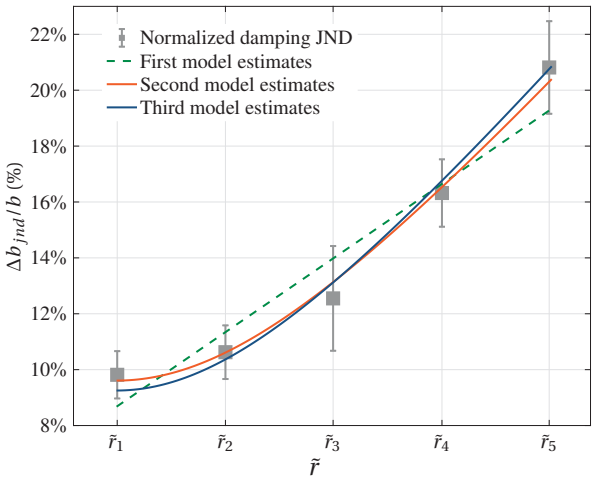

Figure 4.8: The normalized damping JND measurements, and estimates from the three candidate models. The measurements are shown with sample means (gray square) and standard errors (error bars) corrected for between subject variability.

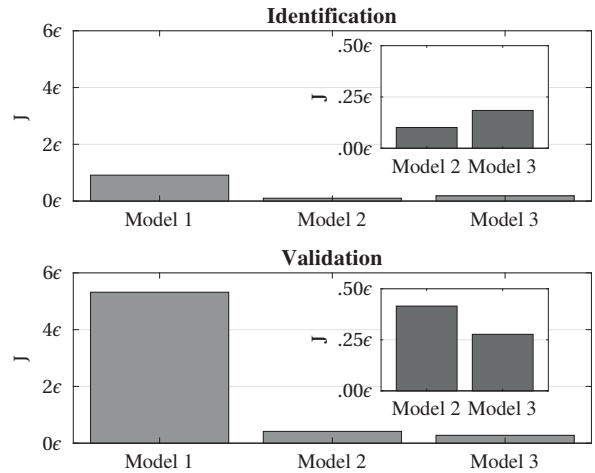

Figure 4.9: Scaled fitting errors (outputs of cost functions in Eq. (4.15)) of the three candidate models, given by the identification and validation processes of the "leave-one-out" method. ϵ denotes the scaling factor. The small plots are zoom-in comparisons between the second and third model.

fit the measurements. Its estimation error is acceptable, but the validation error is high (see Fig. 4.9). The second and third models, based on nonlinear structures, both provided good predictions with similar low errors for both identification and validation. In addition, the values of the two parameters of the second model are almost identical. In this case, Eq. (4.11) resembles Eq. (4.13), equalizing the second and third models.

The third model considers the damping JND to be proportional to the combined system in the frequency domain. This can be further evaluated by normalizing the

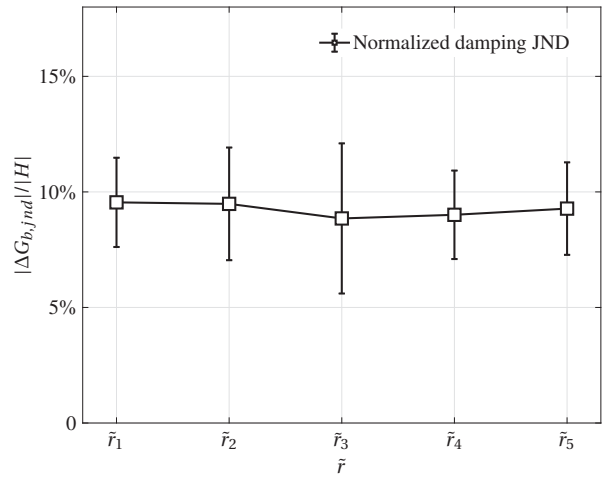

Figure 4.10: The damping JND frequency-response magnitude normalized to the combined system magnitude. Error bars represent the 95% confidence intervals corrected for between subject variability.

measured $|\Delta G_{b,jnd}|$ to the frequency response of the combined system $|H|$, as shown by Fig. 4.10. No significant difference can be found among the five conditions (one-way repeated measures ANOVA: $F(4,28) = 0.07$, $p = 0.99$).

With the third model, the damping JND can be expressed with Weber's law in the frequency domain if we consider the combined system to be the reference stimulus, that is, the least amount of a damping change that makes the system feel differently, is proportional to the system's magnitude:

$$\left|\frac{\Delta G_b(\omega j)_{jnd}}{H(\omega j)}\right| = \left|\frac{\Delta\Im H(\omega j)_{jnd}}{H(\omega j)}\right| = \left|\frac{\Delta b_{jnd}\cdot\omega j}{m\cdot(\omega j)^2 + b\cdot\omega j + k}\right| = p_b \tag{4.17}$$

The above formula enables us to extend the JND law for the second case: the JND in the damping of systems with various stiffness and mass. This extension does not conflict with the original JND law given in Eq. (4.2). When the stiffness and mass of a system are negligible, this extended law is identical to the original one.

PRINCIPLE INVESTIGATION

From the experiment we found that the damping JND becomes higher when a higher joint response of stiffness and mass is rendered. Similar to the first experiment we asked our subjects about their discrimination strategy. Subjects reported that, when comparing different levels of damping, they concentrated on the forces they perceived at around the center of the manipulator movement, regardless of the variation in condition settings (the center means the point where the manipulator deflection angle is zero). Because of the prescribed sinusoidal movement, this force equals the maximum damping force, as discussed in Section 4.2, see Fig. 4.1. When discerning changes in the force at this point, one is actually estimating the changes in the *ratio* of this force to the maximum velocity, which is the level of damping.

This strategy indicates that subjects are able to extract the damping force from the combined force (for example extracting the damping force from the yellow line in Fig. 4.1). But the experimental observation also indicates that the perception of this force is disturbed by the responses of stiffness and mass. This is reasonable, because for a fixed level of damping, increasing mass or stiffness yields a larger magnitude of the real part $\Re H$, which in turn increases the magnitude of the system overall frequency response function, see Fig. 4.7. As a result, the effort (the force) to apply the prescribed manipulator movement also increases. This may cause more uncertainty (a higher noise level) in the force sensory channel, leading to a higher force difference threshold. The increase in the damping JND is likely a consequence of this.

4.7. DISCUSSION

In this study, we extend the basic JND laws using the frequency response of JNDs for the two studied cases. In doing so, we provide a novel perspective on describing human haptic JND in their perception of mechanical properties, which may facilitate the application of such sensory characteristics to engineering design. In this section, we summarize our main findings and discuss their practical relevance, we analyze the impact of our experiment design, and discuss possible future extensions of our work.

4.7.1. SUMMARY OF RESULTS AND PRACTICAL RELEVANCE

CASE 1: STIFFNESS JND

Our extended JND law indicates that the stiffness JND is a fixed proportion of the combined response of stiffness and mass: the "effective stiffness". In case of a mass-spring system, the effective stiffness is lower than the true stiffness level when the system is excited at a non-zero frequency, see Eq. (4.16). Evaluating the fidelity of a haptic interface using the traditional JND law is apparently conservative when the mass is not negligible.

CASE 2: DAMPING JND

The extended JND law expresses the response of the damping JND as a fixed proportion of the system magnitude in the frequency domain. On this basis, the fidelity of the rendered damping of a haptic interface can be evaluated at individual frequencies. In most cases an increase in the manipulator damping improves the stability of the haptic interface. Our model specifies a less stringent requirement than the original law, see Eq. (4.17), allowing more room to balance the tradeoff between fidelity and stability.

4.7.2. LIMITATIONS OF THE EXPERIMENTAL DESIGN

The results of this study were obtained from a fixed amplitude and frequency of excitation, with a side-stick manipulator. Changes in the excitation signal or the manipulator type may have different implications.

EXCITATION AMPLITUDE

In this study, the amplitude of the prescribed manipulator movement was fixed at 0.37 rad. Our proposed models still apply to other movement amplitudes that lead to moderate manipulator forces (not too high or too low), since changing this variable does

not affect human capability of perceiving a force difference [10, 21–23]. Whereas in the case of amplitudes that produce manipulator forces around the perception boundary, the ratio constant p should be adjusted.

EXCITATION FREQUENCY

The impact of the frequency needs further investigation. The model structure should not be affected by a different excitation frequency, as the principle of how humans perceive a dynamic difference from the force should be unaffected. However, the proportion of the perceivable changes – the ratio constant p in the models – may be affected. Thus, the proposed models need to be tested at different frequencies, which will be done in the next chapter.

TYPE OF MANIPULATOR

Although the experiment is conducted with a side-stick manipulator, we believe that the proposed models also apply to other control manipulators. Again, perceiving dynamic differences from the force should be independent of the shape and size of a manipulator. However, different muscle groups may be involved when controlling a different manipulator, and this may cause a different level of force threshold [23]. Therefore measuring the ratio constant p would still be needed when applying our models to other manipulators.

4.7.3. GENERAL DISCUSSION

We find that the stiffness JND is affected by the mass, because the inertia force and spring force are coupled. This in turn, indicates that the spring stiffness affect the mass JND in the same manner. Moreover, it can be readily appreciated that the JNDs in mass and stiffness are coupled in exactly the same way as the coupled responses of these two mechanical properties, and that this joint JND is determined by the combined response of stiffness and mass. This allows for representing the JNDs in a system's stiffness and mass using the JND in the real part of the system's frequency response. In addition, the JND in a system's damping can be represented by the JND in the imaginary part of the system's frequency response. Eq. (4.17) shows the effect of the real-part dynamics on the JND in the imaginary part. One can imagine that the JND in the real part can be also affected by the imaginary part (i.e., the joint JND in a system's stiffness and mass can be affected by the system's damping). We expect to use the damping JND model to describe this joint JND for cases where the system's damping varies. This will be studied in the following chapter.

4.8. CONCLUSION

This chapter proposes models to extend the laws for JND in manipulator dynamics. Two typical cases are considered: 1) the JND in manipulator stiffness under effects of manipulator mass; 2) the JND in manipulator damping under effects of stiffness and mass. The JND models are obtained based on a combination of frequency response functions and validated by results from psychophysical experiments. The experimental observations show that increases in mass reduce the normalized stiffness JND (the Weber fraction for stiffness), and that increases in the combined response of stiffness

and mass increases the damping JND. With the extended JND laws, all these effects can be explained. The extended JND laws indicate that the stiffness JND is proportional to the combined frequency response of stiffness and mass, i.e., the "effective stiffness", instead of the true stiffness; and that the damping JND can be expressed with Weber's law using the frequency response of the combined system as the reference stimulus.

REFERENCES

[1] D. A. Lawrence, "Stability and transparency in bilateral teleoperation," *IEEE Trans. on Robotics and Automation*, vol. 9, no. 5, pp. 624–637, 1993.

[2] P. H. Chang and J. Kim, "Telepresence index for bilateral teleoperations," *IEEE Trans. on Systems, Man, and Cybernetics, Part B (Cybernetics)*, vol. 42, no. 1, pp. 81–92, 2012.

[3] P. F. Hokayem and M. W. Spong, "Bilateral teleoperation: An historical survey," *Automatica*, vol. 42, no. 12, pp. 2035–2057, 2006.

[4] S. Hirche and M. Buss, "Human-oriented control for haptic teleoperation," *Proc. of the IEEE*, vol. 100, no. 3, pp. 623–647, 2012.

[5] A. Gerretsen, M. Mulder, and M. M. van Paassen, "Comparison of position-loop, velocity-loop and force-loop based control loading architectures," in *AIAA Modeling and Simulation Technologies Conf. and Exhibit, San Francisco, CA*, San Francisco, USA, Aug 2005, pp. 1–18.

[6] W. Fu, M. M. van Paassen, and M. Mulder, "On the relationship between the force JND and the stiffness JND in haptic perception," in *ACM Symp. on Applied Perception*, no. 11, Cottbus, Germany, Sept 2017.

[7] D. A. Abbink and M. Mulder, "Exploring the dimensions of haptic feedback support in manual control," *J. of Computing and Information Science in Engineering*, vol. 9, no. 1, pp. 011 006–011 006(9), 2009.

[8] M. D. Penna, M. M. van Paassen, D. A. Abbink, M. Mulder, and M. Mulder, "Reducing steering wheel stiffness is beneficial in supporting evasive maneuvers," in *IEEE Int. Conf. on Systems, Man and Cybernetics (SMC)*, Oct 2010, pp. 1628–1635.

[9] J. Smisek, E. Sunil, M. M. van Paassen, D. A. Abbink, and M. Mulder, "Neuromuscular-system-based tuning of a haptic shared control interface for UAV teleoperation," *IEEE Trans. on Human-Machine Systems*, vol. 47, no. 4, pp. 449–461, 2017.

[10] L. A. Jones, "Kinesthetic sensing," in *Workshop on Human and Machine Haptics*, Pacific Grove, USA, Dec 1997, pp. 1–10.

[11] H. Z. Tan, N. I. Durlach, G. L. Beauregard, and M. A. Srinivasan, "Manual discrimination of compliance using active pinch grasp: The roles of force and work cues," *Perception & Psychophysics*, vol. 57, no. 4, pp. 495–510, 1995.

[12] L. A. Jones and I. W. Hunter, "A perceptual analysis of stiffness," *Experimental Brain Research*, vol. 79, no. 1, pp. 150–156, 1990.

[13] ——, "A perceptual analysis of viscosity," *Experimental Brain Research*, vol. 94, no. 2, pp. 343–351, 1993.

[14] G. L. Beauregard, M. A. Srinivasan, and N. I. Durlach, "The manual resolution of viscosity and mass," in *ASME Dynamic Systems and Control Division*, vol. 1, 1995, pp. 657–662.

[15] M. Rank, T. Schauß, A. Peer, S. Hirche, and R. L. Klatzky, "Masking effects for damping JND," in *Int. Conf. on Human Haptic Sensing and Touch Enabled Computer Applications*, Tampere, Finland, Jun 2012, pp. 145–150.

[16] M. M. van Paassen, J. C. van der Vaart, and J. A. Mulder, "Model of the neuromuscular dynamics of the human pilot's arm," *J. of Aircraft*, vol. 41, no. 6, pp. 1482–1490, 2004.

[17] F. A. A. Kingdom and N. Prins, *Psychophysics: a Practical Introduction*. Academic Press, 2016.

[18] M. A. García-Pérez, "Forced-choice staircases with fixed step sizes: Asymptotic and small-sample properties," *Vision Research*, vol. 38, no. 12, pp. 1861–1881, 1998.

[19] N. Colonnese, A. F. Siu, C. M. Abbott, and A. M. Okamura, "Rendered and characterized closed-loop accuracy of impedance-type haptic displays," *IEEE Trans. on Haptics*, vol. 8, no. 4, pp. 434–446, 2015.

[20] D. Findeisen, *System Dynamics and Mechanical Vibrations: An Introduction*. Springer Science & Business Media, 2013.

[21] L. A. Jones, "Matching forces: Constant errors and differential thresholds," *Perception*, vol. 18, no. 5, pp. 681–687, 1989.

[22] X. D. Pang, H. Z. Tan, and N. I. Durlach, "Manual discrimination of force using active finger motion," *Perception & Psychophysics*, vol. 49, no. 6, pp. 531–540, 1991.

[23] S. Feyzabadi, S. Straube, M. Folgheraiter, E. A. Kirchner, S. K. Kim, and J. C. Albiez, "Human force discrimination during active arm motion for force feedback design," *IEEE Trans. on Haptics*, vol. 6, no. 3, pp. 309–319, 2013.

5

THRESHOLD FOR CHANGES IN PERCEPTION OF SYSTEM DYNAMICS

Chapter 4 has investigated the coupling of the JNDs in stiffness and mass, as well as the effects of stiffness and mass on the JND in damping. In this chapter, we further explore the interaction among the JNDs in the three mechanical properties, focusing on how changes in damping affect the threshold in perceiving changes in stiffness and mass. More importantly, we aim to bridge the gap between JNDs in mechanical properties of a system and the JND in the dynamics of that system. Based on the findings of the previous two chapters, we link the perception thresholds for mass, stiffness, and damping properties to thresholds for the frequency response of the system they belong to. This allows us to represent the threshold for perceiving changes in the dynamics of a system with two dimensions: the real and imaginary axes in the complex plane. Furthermore, the models developed in Chapter 4 are extended based on observations from two experiments, permitting us to propose a unified model for the JND in system dynamics.

This chapter is based on the following publications: (1) W. Fu, M. M. van Paassen and M. Mulder, "Modeling the Coupled Difference Threshold of Perceiving Mass and Stiffness from Force," *IEEE International Conference on Systems, Man, and Cybernetics (SMC)*, Miyazaki, Japan, Oct 2018, pp. 1427-1432; (2) W. Fu, M. M. van Paassen and M. Mulder, "Unified Human Threshold Model for Perceiving Changes in System Dynamics from Force," *IEEE Transactions on Human-Machine Systems*, under review.

5.1. INTRODUCTION

At present, haptic displays are becoming increasingly indispensable in many manual control tasks. A control manipulator acts as the haptic interface between a human operator and the system being controlled. It allows the operator to perceive the dynamics of the system through the relation between the applied input (the manipulator movement) and the perceived output (the presented force feedback). More importantly, haptic presentation enables one to physically act upon what one feels, making a task more intuitive [1–6].

Depicting the desired system dynamics correctly is important to ensure that professionals can rely on their skills to accomplish tasks efficiently and proficiently. However, the information that the force feedback conveys about the system dynamics one intends to present is inevitably distorted. This is due to limitations of control systems and actuators [7], time delays in communication [8], and compromises needed to resolve stability issues [9–14].

Aiming for perfect transparency can place excessive, and even unnecessary demands on haptic devices, as *some distortions may not even be perceived* by the human operator. We propose that a human-centric assessment is more useful to determine whether a particular haptic device performs in a satisfactory way, allowing for more efficient trade-offs between transparency and stability. Knowledge about how large a distortion of the system dynamics must be to alter the human perception of that dynamics is crucial. Thresholds for human perception are typically known as *just-noticeable difference* (JND) [15, 16]. Attempts to directly measure the JND in perceiving system dynamics are scarce, however. It is challenging to select representative control variables, and a systematic approach to generalize results from a limited number of studies is currently lacking.

As mass-spring-damper mechanical systems account for the majority of systems we come across in daily life, most previous studies focus on the JNDs in perceiving changes in *stiffness*, *mass*, and *damping* [17–24]. In general, it appears that Weber's law, which states that the JND is proportional to the reference stimulus amplitude, applies when humans sense each of the three properties *in isolation*. For example, the human JND in spring stiffness, in the case of a system with negligible mass and damping, is indeed proportional to the selected stiffness [22]. However, the *interactions* between perceiving any of the three properties are very difficult to predict from the isolated measurements. The JND in each property of a mass-spring-damper system seems to be affected by variations in the other two properties. For example, our ability to discern a change in a system's damping *varies* with that system's mass and stiffness properties (see Chapter 4). This fact, violating Weber's law, limits the generalization of previous findings and the formulation of a general concept.

This chapter aims at extending the current state-of-the-art in modelling human difference thresholds in perceiving system dynamics from force feedback. We continue on the previous chapter, explore in depth the characteristics of all JNDs in perceiving mechanical properties, and focus in particular on *understanding the interactions* between these. Furthermore, we will bridge the existing gap between JNDs in isolated mechanical properties and the JND in the *total* dynamics of a system. This connection is established based on the fact that humans lack dedicated sensors to perceive

mass, stiffness and damping, and therefore must *estimate* these properties based on the relation between movement and force (see Chapter 3). The JND in *each of* the three mechanical properties in fact represents the JND in the total system dynamics considered (that determines the full relation) *in one* particular direction. Section 5.2 explains this important finding in greater detail by addressing the problem using the complex-valued system dynamics' frequency response function (FRF), which provides a detailed *and complete* insight about how a JND change in one direction should be interpreted. This allows us to systematically investigate *any* threshold in perceiving *any* change in system dynamics, leading to a unified human threshold model for *all* force-feedback based haptic displays.

The remainder of this chapter is organized as follows. The next section elaborates on our previous findings, and lays the foundations for the transition from the JNDs in mechanical properties of a mass-spring damper system to the JNDs in the real- and imaginary-part frequency response of that system. Section 5.3 discusses a first experiment which extends our previously proposed JND rule to systematically describe the interaction between the JNDs in the two complex components. Section 5.4 validates the unified threshold model and shows that the JND in both parts have the same value. Section 5.5 generalizes the unified model for the JNDs in the two complex parts, and extends our findings to systems with arbitrary dynamic orders. Section 5.6 discusses the findings, and puts forward challenges for future research. Section 5.7 summarizes our contributions.

5.2. PRELIMINARIES

Assume that the dynamics presented by a haptic control manipulator reflect a mass-spring-damper system. Define $H(\omega j)$ as the frequency response function that describes the relation between the device displacement (or deflection angle) $X(\omega j)$ and the force (or torque) $F(\omega j)$ feedback:

$$H(\omega j) = \frac{F(\omega j)}{X(\omega j)} = \underbrace{k - m \cdot \omega^2}_{\Re H(\omega j)} + \underbrace{b \cdot \omega \cdot j}_{\Im H(\omega j)}, \tag{5.1}$$

where $\Re H(\omega j)$ and $\Im H(\omega j)$ denote the real and imaginary parts of the complex-valued FRF. These two parts, respectively, determine the in-phase and the out-of-phase force response to the displacement. Please note that the imaginary number j means that the force response generated by the system's damping has a 90° phase difference with respect to an input displacement.

The real part $\Re H(\omega j)$ is the *combined* frequency response of stiffness k and mass m, and the imaginary part $\Im H(\omega j)$ is the frequency response of the damping property b. For any given excitation movement, the harmonic force response of the system is determined by the system's FRF. Due to this, when the system's FRF changes, the force feedback that conveys the information about the mechanical properties changes as well. Consequently, the mechanical properties perceived by a human operator may be different. In other words, changes in a mechanical property that an operator experiences from the force feedback can be characterized as changes in the system's frequency response. One can directly see that whereas changes in the real part could

cause the perceived stiffness and mass to change, changes in the imaginary part can lead to variations in the perceived damping.

Hence, we can link the JNDs in the three mechanical properties (m, k, b) to JNDs in the real and imaginary parts of the system's FRF. This makes it possible to directly study the JND in the dynamics of a system. Our previous studies showed that an interaction exists between human perceptions of stiffness and mass, due to the fact that these properties *together* define the real part of the system's frequency responses (see Chapters 3 and 4).

In the previous chapter, it was found that the JNDs in these two mechanical properties are *coupled in the same way*, and can be integrated into the JND in the real-part dynamics:

$$\Delta\Re H(\omega j)_{jnd} = \Delta k_{jnd} - \Delta m_{jnd} \cdot \omega^2 \,, \tag{5.2}$$

with Δk_{jnd} and Δm_{jnd} the 'stiffness JND' and 'mass JND', respectively.

Along similar lines, from Eq. (5.1) one can see that the 'damping JND' Δb_{jnd} can be represented by the JND in the imaginary part:

$$\Delta\Im H(\omega j)_{jnd} = \Delta b_{jnd} \cdot \omega \cdot j \tag{5.3}$$

Now, whereas a time-domain variable is a function of time, a frequency-domain variable is a function of *frequency*. Hence, to understand the characteristics of the JNDs in the frequency response (those given by Eqs. (5.2) and (5.3)), we need to collect the measurements at different frequencies.

A convenient approach is to confine haptic interactions to *each individual frequency*. Investigations were carried out at a single frequency of 6 rad/s in the previous chapter. There we found that the joint JND in stiffness and mass – the JND in the real part – can be expressed with Weber's law when the system's damping is negligible ($b \approx 0$):

$$\left| \frac{\Delta\Re H(\omega j)_{jnd}}{\Re H(\omega j)} \right| = \text{constant} \tag{5.4}$$

Furthermore, in the previous chapter, it was found that the human JND in a system's damping is affected by the system's stiffness and mass. That is, the JND in the imaginary part is affected by the real-part dynamics. Our investigation into this effect demonstrated that this JND is proportional to the magnitude of the system's total frequency response:

$$\left| \frac{\Delta\Im H(\omega j)_{jnd}}{H(\omega j)} \right| = \text{constant} \tag{5.5}$$

This equation can be seen as an *extension* of Weber's law. The effect of $\Re H(\omega j)$ is implicitly shown by this model: when the real part $\Re H(\omega j)$ increases, the magnitude of $H(\omega j)$ increases as well, and as a result the JND in the imaginary part (or damping) becomes *higher*.

Now we have shown that the JND in the imaginary part is affected by the real-part dynamics. An important question that arises, is whether the same holds for the JND in the real part. Based on the fact that these two complex components reflect orthogonal dimensions in the complex plane, one can expect that *both* dimensions will indeed affect each other. It could be that Eq. (5.4) is in fact a simplification of this universal

property, a simplification that excludes the effect of the imaginary component. As can be seen from Eq. (5.1), when a system's damping is negligible, the real component equals the system's frequency response (i.e., $\Re H(\omega j) = H(\omega j)$ when $b = 0$). In this case, Eqs. (5.4) and (5.5) are in fact in the same form. We therefore hypothesize that the effect of the imaginary part on the JND in the real part (i.e., the effect of a system's damping on the JND in that system's stiffness and mass), can *also* be described by the system's total frequency response magnitude, in the same way as in Eq. (5.5). The next two sections present two experiments performed to investigate this hypothesis, and others, to obtain a unified model for *all* human thresholds in perceiving dynamics with haptic force feedback manipulators.

5.3. EXPERIMENT 1: REVISITING THE JND IN REAL-PART DYNAMICS

5.3.1. METHOD

DEPENDENT AND INDEPENDENT VARIABLES

The first experiment will study the effect of $\Im H(\omega j)$ on $\Delta\Re H(\omega j)_{jnd}$, and in particular, to examine whether this effect can also be expressed using the model given in Eq. (5.5). To this end, mass-spring-damper systems that differ in the imaginary part dynamics will be used to measure $\Delta\Re H(\omega j)_{jnd}$. To extend the model, investigations will be conducted at different manipulator movement frequencies ω.

In addition, the model needs to be validated under different *signs* of the real part dynamics. As can be seen from Eq. (5.1), the sign of $\Re H(\omega j)$ depends on the stiffness and mass properties, as well as on the current input frequency. This FRF component acts as a gain, and the force response it generates can be expressed as:

$$F_{si}(\omega j) = X(\omega j) \cdot \left|\Re H(\omega j)\right| \cdot e^{j \angle \Re H(\omega j)},$$
$$\text{where } \angle \Re H(\omega j) = \begin{cases} 0° & \text{if } \Re H(\omega j) > 0 \\ 180° & \text{if } \Re H(\omega j) < 0 \end{cases} \tag{5.6}$$

As can be seen, a spring force that resists the manipulator displacement is produced when $\Re H(\omega j) > 0$; an inertia force that is proportional to the acceleration is produced when $\Re H(\omega j) < 0$. These two force responses have opposite directions. To ensure that the model can describe the JND in the real part of a system's frequency response over the entire complex plane, evaluation of different directions of the force feedback that conveys the system dynamics must be conducted.

EXPERIMENTAL CONDITIONS

The experiment has nine conditions. Whereas Table 5.1 lists the exact system parameters and independent variables, Fig. 5.1 shows the system dynamics defined by the nine conditions in the complex plane. Please note that the system dynamics are expressed in a rotational coordinate system. As can be seen, the JND for each condition will be measured at a single frequency of excitation ω_i (the input displacement frequency). This is achieved by asking subjects to apply (an approximately) sinusoidal

Table 5.1: Conditions of Experiment 1

Condition	$\Re H(\omega_i j)$	$\Im H(\omega_i j)$	ω_i [rad/s]	$r=\left\lvert\frac{\Im H(\omega_i j)}{\Re H(\omega_i j)}\right\rvert$
C1	1.26	0.00	6	0.0
C2	1.26	0.63	6	0.5
C3	1.26	1.26	6	1.0
C4	1.26	1.89	6	1.5
C5	1.26	2.52	6	2.0
C6	1.26	0.00	8	0.0
C7	1.26	2.52	8	2.0
C8	−1.26	0.00	6	0.0
C9	−1.26	2.52	6	2.0

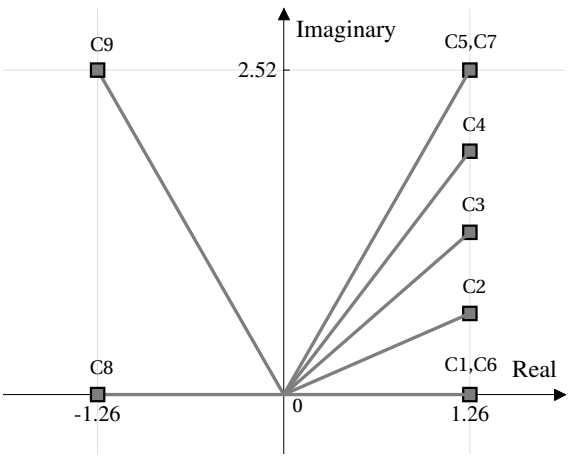

Figure 5.1: Experimental conditions shown on the complex plane.

movement to the manipulator during the experiment. More details about this prescribed movement will be given in Section 5.3.1.

Conditions C1-5 measure the JND in a positive $\Re H(\omega_i)$, which generates a spring force, at an input frequency of 6 rad/s. In addition, they define five levels of $\Im H(\omega_i)$, the ratio of which to $\Re H(\omega_i)$, r, ranges from 0 to 2. Measurements for these five conditions will demonstrate how $\Im H(\omega_i)$ affects $\Delta\Re H(\omega_i j)_{jnd}$. To test the effect of the input frequency, conditions C6-7 define a movement frequency of 8 rad/s. The effect will be evaluated at two different ratios between the two complex parts. Conditions C8-9 define a negative $\Re H(\omega_i)$, which generates an inertia force, to study the effect of the system's response direction (the sign of $\Re H(\omega_i j)$) on the JND. These two conditions differ in the ratio between the two complex components.

The system dynamics defined in Table 5.1 are realized using mass-spring-damper systems. In order to obtain the desired values of $\Re H(\omega_i)$ and $\Im H(\omega_i)$, the three param-

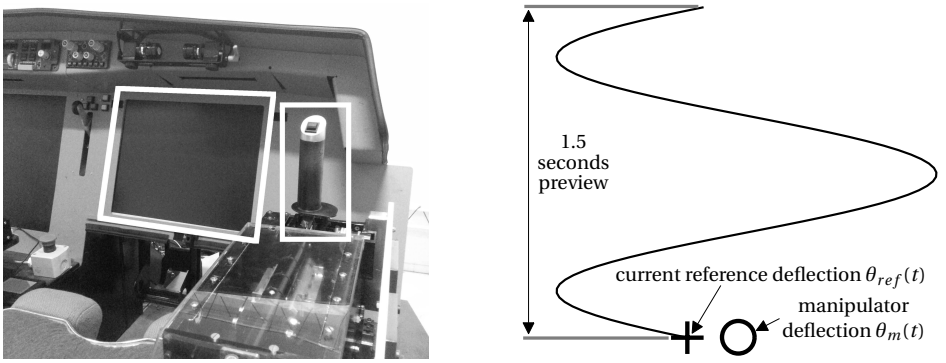

(a) (b)

Figure 5.2: (a): The devices used in the experiments. The side-stick manipulator and the LCD screen are marked by white rectangles; (b): The tracking task shown on the screen. To reduce the manipulator deflection tracking error, here the subject must push the manipulator towards the left.

eters k, m and b (see Eq. (5.1)) are set in the following way:

$$
\begin{aligned}
k &= \begin{cases} \Re H(\omega_i j) + 0.01{\omega_i}^2 & \text{if } \Re H(\omega_i j) > 0 \\ 0 & \text{if } \Re H(\omega_i j) < 0 \end{cases} \\
m &= \begin{cases} 0.01 & \text{if } \Re H(\omega_i j) > 0 \\ \dfrac{-\Re H(\omega_i j)}{\omega_i^2} & \text{if } \Re H(\omega_i j) < 0 \end{cases} \\
b &= \frac{\Im H(\omega_i j)}{\omega_i j}
\end{aligned}
\tag{5.7}
$$

5

In this chapter, these three parameters are also expressed in the rotational coordinate system, their corresponding units are: Nm/rad for k, Nms/rad for b, and kgm^2 for m.

As can be seen from Eq. (5.1), at a single frequency the combination of k and m that yields a particular $\Re H(\omega_i j)$ is not unique. By using the settings defined by Eq. (5.7), $\Delta\Re H(\omega_i j)_{jnd}$ can be simply obtained through measuring the stiffness JND (when $\Re H(\omega j) > 0$) and the mass JND (when $\Re H(\omega_i j) < 0$). Ideally, the mass should be set to zero for $\Re H(\omega_i j) > 0$. However, to maintain stability of the haptic interaction, a minimal mass of 0.01 kgm^2 is maintained. The stiffness k is therefore adjusted accordingly to obtain the desired value of $\Re H(\omega_i j)$, as can be seen from Eq. (5.7).

APPARATUS

The experiment was performed in TU Delft's Human-Machine Interaction Laboratory, with Fig. 5.2a illustrating the used devices. An admittance-type side-stick manipulator driven by an electro-hydraulic motor was used to simulate the mass-spring-damper systems defined by the experimental conditions. This device allows for accurate realization of those dynamics at the desired input frequencies. Position of the manipulator and moment on the manipulator are led through pre-sample filters (bandwidth =

200 Hz) before being digitized and read into the laboratory computer at the execution frequency of the manipulator's control system (2500 Hz). The effective position following bandwidth of the manipulator's control system is around 40 Hz. The manipulator is supplied with a handle, diameter 35 mm, with grooves for placement of the fingers. When a hand is correctly placed on the handle, the center of the hand lies 90 mm above the manipulator rotation axis. The manipulator can rotate in the left/right direction (lateral), and its motion in fore/aft direction is fixed at the neutral position. An LCD screen, placed in front of the subject, was used to help subjects follow the prescribed sinusoidal manipulator movement (see Section 5.3.1).

PARTICIPANTS

Nine subjects, all right-handed and without a history of impairments in moving their arms or hands, participated in the experiment. The experiment was approved by the Human Research Ethics Committee of TU Delft, and informed consent was obtained. Sufficient training was performed by all subjects before the measurements started.

PROCEDURE

In this study, only the upper JNDs were investigated. The JND for each condition was measured by a one-up/two-down staircase procedure [25]. In general, the procedure needed approximately $20-30$ runs to converge. Each run consisted of two 6.3-second simulations. In one simulation the manipulator realized the reference system dynamics defined by the experimental condition being tested (see Table 5.1 and Eq. (5.7)). In the other simulation the subject experienced a controlled system, which only differed from the reference system in the mechanical property being tested (stiffness in the case of conditions C1-7 where $\Re H(\omega_i j) > 0$, mass in the case of conditions C8-9 where $\Re H(\omega_i j) < 0$). The sequence of the two simulations in each run was randomly based on a prior probability of 0.5.

The difference in the corresponding mechanical property between the two systems was an adjusted increment. Therefore the controlled system had higher stiffness or mass than the reference system. In each simulation, the subject was asked to perceive the manipulator dynamics while moving the manipulator with the prescribed sinusoidal movement. After each experimental run, the subject was asked to report in which of the two simulations he/she experienced the stronger manipulator stiffness (conditions C1-7) or the higher manipulator mass (conditions C8-9). The increment for the next run was then adjusted according to the correctness of the subject's answer, and would gradually converge to the upper JND. More details about this staircase procedure can be found in Chapter 4.

PRESCRIBED MANIPULATOR MOVEMENT

To ensure that our subjects would interact with the manipulator at the desired frequencies, they performed a preview tracking task [26] in each simulation, see Fig. 5.2b. The reference deflection angle of the manipulator is calculated according to:

$$\theta_{ref}(t) = 0.37 \cdot \sin(\omega_i t) \tag{5.8}$$

Here ω_i denotes the desired frequency of movement (6 or 8 rad/s, see Table 5.1). In this chapter, the manipulator deflection is given in radians. In addition, the first and last

full cycle of this prescribed movement are used as fade-in and fade-out phases. The movement amplitude gradually increases from 0 to 0.37 during the fade-in phase, and decreases from 0.37 to 0 during the fade-out phase. To perform the tracking task, the subject needs to reduce the tracking error between the current manipulator deflection $\theta_m(t)$ (shown by "∘" in Fig. 5.2b) and the current reference deflection $\theta_{ref}(t)$ (shown by "+"). The two symbols only move horizontally. The visual preview, shown as a winding curve, contains 1.5-second future information about the reference deflection θ_{ref}. It moves downwards as time progresses.

5.3.2. RESULTS

All participants were able to adequately perform the tracking task. The actual movement frequencies in all experimental runs were evaluated. The average only deviates from 6 rad/s by less than 0.1 rad/s. Therefore the experimental observations accurately reflect the effects of the independent variables under the desired conditions.

Table 5.2 and Fig. 5.3 show the JND measurements, expressed with subjects' means and 95% confidence intervals corrected for between-subject variability. When examining the JNDs measured under conditions C1-5 (systems with the same stiffness and mass, but different damping), a clear increase can be seen as the ratio between the two complex components (r) increases. A one-way repeated measures ANOVA performed for these five conditions reveals that the effect of r is significant ($F(4,32) = 8.1$, $p < .01$).

Two one-way repeated measures ANOVAs are performed to investigate: (1) the differences among conditions C1, C6, and C8; (2) the differences among conditions C5, C7, and C9. Results show that when the damping presented to our subjects is negligible (i.e., $r = 0.0$, conditions C1,6,8) the variations in the input movement frequency (ω_i) and the response direction (the sign of $\Re H(\omega_i)$) both fail to cause any significant change in the JNDs ($F(2,16) = .21$, $p > .05$). The same conclusion can be drawn when the presented damping is high (i.e., $r = 2.0$, conditions C5,7,9) ($F(2,16) = .74$, $p > .05$).

These results confirm our hypothesis that the imaginary part of the system's dynamics affects the JND in the real part (i.e., $\Im H(\omega j)$ affects $\Delta\Re H(\omega j)_{jnd}$). The JND in the information conveyed by force feedback about a system's stiffness and mass violates Weber's law when the system's damping varies (since Weber's law expects no

Table 5.2: JND measurements (mean ± 95%CI)

Conditions	$\Delta\Re H_{jnd}(\omega_i j)$ (how it is obtained)	ratio $r=\left\lvert\frac{\Im H(\omega_i j)}{\Re H(\omega_i j)}\right\rvert$				
		0.0	0.5	1.0	1.5	2.0
C1-5	$\Delta\Re H_{jnd}(\omega_i j)$ $(=\Delta k_{jnd})$	$.15 \pm .07$	$.15 \pm .05$	$.22 \pm .05$	$.27 \pm .06$	$.34 \pm .05$
C6-7	$\Delta\Re H_{jnd}(\omega_i j)$ $(=\Delta k_{jnd})$	$.14 \pm .04$	-	-	-	$.29 \pm .06$
C8-9	$\Delta\Re H_{jnd}(\omega_i j)$ $(=\Delta m_{jnd} \cdot \omega_i^2)$	$.16 \pm .05$	-	-	-	$.30 \pm .08$

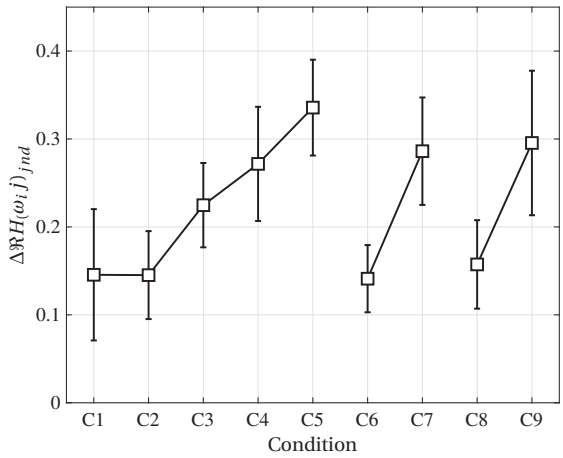

Figure 5.3: Measurements of $|\Delta\Re H(\omega_i j)_{jnd}|$ shown with the subjects' means and 95% confidence intervals corrected for between-subject variability.

differences among conditions C1-5, between conditions C6-7, or between conditions C8-9). In addition, the JND in the real-part dynamics, as well as the effect of the imaginary part on it, are *independent* of the sign of the real part and the input movement frequency. In other words, humans have *similar* JNDs in the spring and inertia forces, and these JNDs remain approximately constant over a relatively low frequency range. When a system possesses higher damping, mass and stiffness changes must be larger before humans are able to notice these differences.

5.3.3. MODEL VALIDATION

To examine whether the JND in the real part can also be described by the model given in Eq. (5.5), the measured JND for each condition is normalized to the magnitude of the frequency response of the corresponding system, according to:

$$\Delta_{real,jnd} = \left| \frac{\Delta\Re H(\omega_i j)_{jnd}}{H(\omega_i j)} \right| \tag{5.9}$$

Fig. 5.4 shows $\Delta_{real,jnd}$ for all conditions. The normalized JNDs remain approximately constant over the nine conditions, with an average of 12.2%. A one-way repeated measures ANOVA shows no significant differences among conditions ($F(8,64) = .59$, $p > .05$). This, therefore, confirms the validity of the model, and indicates that the magnitude of $\Delta\Re H(\omega j)_{jnd}$ is proportional to the magnitude of $H(\omega j)$.

An extension of Weber's law for the joint JND in stiffness and mass is now available. When considering the frequency response of the system to be the reference stimulus, the relative change in its real part dynamics, which alters the perception, is constant:

$$\left| \frac{\Delta\Re H(\omega j)_{jnd}}{H(\omega j)} \right| = \left| \frac{\Delta k_{jnd} - \Delta m_{jnd} \cdot \omega^2}{k - m \cdot \omega^2 + b \cdot \omega \cdot j} \right| = \text{constant} \tag{5.10}$$

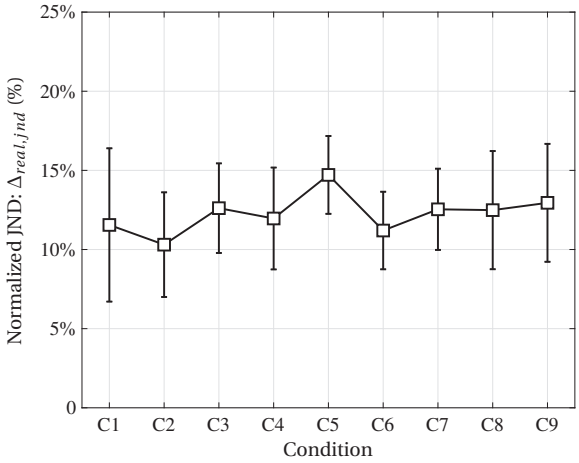

Figure 5.4: The ratio of the measured $|\Delta\Re H(\omega_i)_{jnd}|$ to $|H(\omega_i j)|$. The normalized JNDs are shown with the sample means and 95% confidence intervals corrected for between-subject variability.

5.3.4. DISCUSSION

Experiment 1 demonstrates the effect of a system's damping on human perception of the system's stiffness and mass. Due to the variation in the damping, Weber's law, which is commonly used to estimate the JNDs in mechanical properties, cannot properly describe the experimental observations. As expected, the joint JND in stiffness and mass increases as the system's damping increases.

The results provide a number of insights into the transparency evaluation of haptic interfaces, in terms of the displayed stiffness and mass. On the one hand, higher system damping allows for larger distortions of the information conveyed by the force feedback about stiffness and mass. The high demands put on the control system and hardware, when simulating small mass and high stiffness, can therefore be alleviated, which in turn benefits the system stability. On the other hand, the increase in damping also reduces the human ability to discern changes in stiffness and mass. When additional damping is introduced into the system dynamics presented to human operators, e.g., to increase the stability margin of the haptic interaction [14, 27, 28], its effect must be taken into account for cases where discriminating between different levels of stiffness or mass is important.

The previous two chapters allow us to relate human perception of the three mechanical properties of a mass-spring-damper system to the real and imaginary parts of the system's dynamics. The current study reveals an effect of the imaginary part on the JND in the real part. This effect is similar to that shown in Chapter 4 between the real part and the JND in the imaginary part. Results show that these mutual interactions can be described by a unified rule, which suggests that the JND in each complex part is proportional to the total system's frequency response magnitude $|H(\omega j)|$.

The results also demonstrate the validity of the model for different input frequencies. Although the manipulated variation in the frequency is relatively small, our finding reliably applies to cases where the movement during haptic interaction is mainly

Table 5.3: Conditions of experiment two

Condition	Measured JND	$\Re H(\omega_i j)$	$\Im H(\omega_i j)$	ω_i [rad/s]
C1	$\Delta\Re H(\omega_i j)_{jnd}$	1.50	1.50	5.0
C2	$\Delta\Im H(\omega_i j)_{jnd}$	1.50	1.50	5.0
C3	$\Delta\Re H(\omega_i j)_{jnd}$	1.50	1.50	6.5
C4	$\Delta\Im H(\omega_i j)_{jnd}$	1.50	1.50	6.5
C5	$\Delta\Re H(\omega_i j)_{jnd}$	1.50	1.50	8.0
C6	$\Delta\Im H(\omega_i j)_{jnd}$	1.50	1.50	8.0

generated by the human arm. This scenario covers a wide range of manual control tasks, such as car driving and aircraft flying, in which the main energy of the power spectrum of human control inputs is limited by the neuromuscular system and usually lies below 2 Hz [29].

5.4. EXPERIMENT 2: GENERALIZING THE JND IN SYSTEM DYNAMICS

Experiment 1 showed that the JNDs in the real and imaginary parts are governed by the same rule, see Eqs. (5.5) and (5.10). In this section we discuss the results of a second experiment, which was set up to investigate whether or not the two JNDs can be described by the same ratio. That is, whether the *same constant* applies to both Eqs. (5.5) and (5.10).

5.4.1. METHOD

DEPENDENT AND INDEPENDENT VARIABLES

The experiment draws comparisons between the JND in the real-part dynamics and the JND in the imaginary-part dynamics. Three input frequencies ω were tested. At each frequency, the two JNDs were obtained from only one system. This is because the JND rules (i.e., the proportional relation) stated by Eqs. (5.5) and (5.10) are independent of the system dynamics (i.e., no matter how the denominator changes, the proportional relation will not change). Thus the finding obtained from a single system is representative and applies to all other systems.

A factorial design results in six conditions, listed in Table 5.3. For simplicity, the real and imaginary parts of the system dynamics tested in the experiment are the same (i.e., $\Re H(\omega_i j) = \Im H(\omega_i j)$). In addition, the magnitude of these two parts are kept the same for all the three frequencies. One can imagine that $H(\omega_i j)$ is always a same vector in the complex plane, with equal projections on the two axes.

PROCEDURE

The desired system dynamics were realized using mass-spring-damper systems. Eq. (5.7) was used to obtain the corresponding stiffness, mass, and damping coefficients

(k, m, and b in Eq. (5.1)). These parameters were simulated using the same side-stick manipulator that is described in Section 5.3.1. The JNDs were measured by the same adaptive staircase procedure described in Section 5.3.1. When measuring the JND in the real part (conditions C1, C3, and C5), the subject was asked to identify the simulation with the stronger manipulator stiffness. When measuring the JND in the imaginary part (conditions C2, C4, and C6), the subject was asked to identify the simulation with the higher manipulator damping. The same tracking task described in 5.3.1 was performed by subjects to ensure that the haptic interaction would occur at the desired frequencies.

PARTICIPANTS

Six subjects participated, all right-handed and with no history of impairments in moving their arms or hands. This experiment was approved by the Human Research Ethics Committee of TU Delft. Informed consent was obtained from all participants. All subjects received sufficient training before the formal experiment.

5.4.2. RESULTS

All participants were able to adequately perform the tracking task. The averages of the actual movement frequencies over all experimental runs only deviate from the corresponding desired frequencies by less than 2%. This indicates that the intended effects of the independent variables are indeed accurately reflected by the results.

Fig. 5.5 shows the JND measurements. Here, the JNDs in the two complex parts are normalized to the frequency-response magnitude of the corresponding systems (similar as in Fig. 5.4, see Eq. (5.9)). As can be seen from the figure, the JNDs under the six conditions are approximately the same, with an average of 7.5%. A one-way repeated measures ANOVA showed no significant difference among conditions ($F(5,25) = .57$, $p > .05$). Therefore, the JNDs in both parts of a system's dynamics can be expressed with our extended Weber's law *using the same constant*, which is (for the frequencies analyzed) *independent of the movement frequency*:

$$\left| \frac{\Delta \Re H(\omega j)_{jnd}}{H(\omega j)} \right| \approx \left| \frac{\Delta \Im H(\omega j)_{jnd}}{H(\omega j)} \right| = \text{constant} \tag{5.11}$$

This finding allows us to describe the JNDs in stiffness, mass, and damping with one, *unified* model, which clearly shows how the JNDs in three mechanical properties of a mass-spring-damper system can be related to the JND in perceiving changes in system dynamics.

5.5. UNIFIED JND MODEL FOR SYSTEM DYNAMICS

The information conveyed by the force feedback about a system is determined by the dynamics of that system, its frequency response function. In fact, any change in the system dynamics can always be represented by changes in the real and imaginary parts of the system's frequency response. For example, define a change in the FRF of a mass-spring-damper system as $\Delta H(\omega j)$, which is caused by changes in the three mechanical

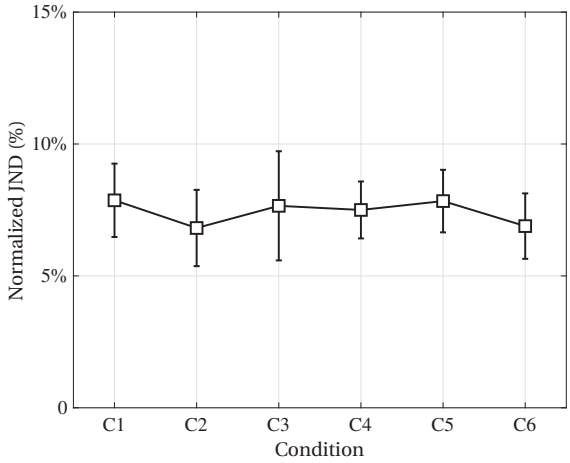

Figure 5.5: Normalized JNDs in the real and imaginary parts, shown with the subjects' means and 95% confidence intervals corrected for between-subject variability.

properties. The complex-valued $\Delta H(\omega j)$ can be expressed by its two components:

$$\Delta H(\omega j) = \underbrace{\Delta k - \Delta m \cdot \omega^2}_{\Delta \Re H(\omega j)} + \underbrace{\Delta b \cdot \omega \cdot j}_{\Delta \Im H(\omega j)} \tag{5.12}$$

Here Δk, Δm, and Δb denote changes in stiffness, mass, and damping, respectively.

This means that $\Delta H(\omega j)$, independent of the parameters that cause it, will alter the human perception of the system once the threshold for perceiving changes in either of the two components is exceeded. In other words, JNDs in these two parts, as defined by Eq. (5.11), in fact represent the JND in $H(\omega j)$.

At the movement frequencies where the haptic interaction takes place, *any* dynamics change that exceeds such a JND will lead humans to perceive the system differently. At each individual frequency, Eq. (5.11) defines the intervals for imperceptible changes in the system's projections on the two axes of the complex plane.

For a straightforward illustration, Fig. 5.6 gives an example which shows the dynamics of an arbitrary system at a single frequency. In the complex plane, the system's FRF – $H(\omega j)$ – at a single frequency is represented by a vector (the black line). The real- and imaginary-part dynamics determine the projections on the two axes, respectively. A change in the system dynamics will result in a different vector which has at least one different projection, as shown by the red and blue vectors. The JNDs in the two complex parts become intervals on the two axes. Therefore, changes in each projection within the corresponding interval cannot be perceived by humans. These two intervals form a threshold region (the gray square), and *any* change in dynamics that lies within this region does *not alter* how humans perceive that system. A change in system dynamics will *only* lead humans to have a different perception when that change exceeds the threshold region.

Fig. 5.7 illustrates the difference thresholds corresponding to a system, at multiple frequencies. We show a second-order system with typical stiffness, mass, and damp-

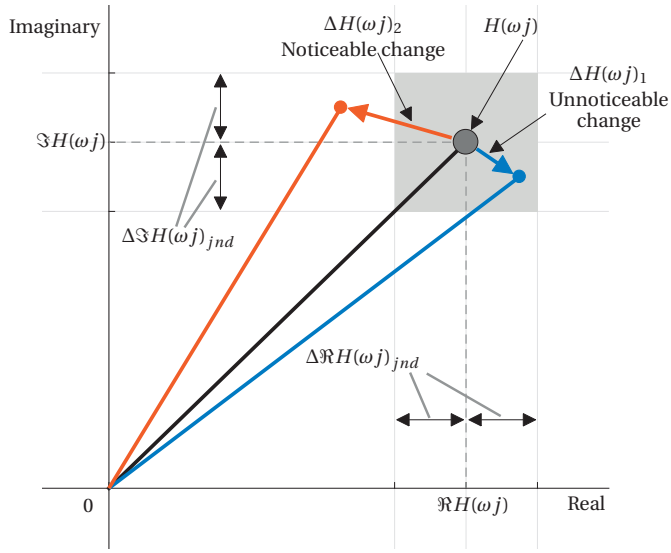

Figure 5.6: An illustration of the threshold for altered perception of the system dynamics (i.e., the gray square). This square is formed by the JNDs in the real and imaginary parts. The two JNDs are the same, and are proportional to the system's frequency-response magnitude which is the length of the black vector. Dynamics changes within the threshold are not perceptible (e.g., the blue vector), whereas those exceeding the threshold alter the perception of the system (e.g., the red vector).

ing properties (i.e, $k = 2.5$ Nm/rad, $m = 0.022$ kgm^2, $b = 0.3$ Nms/rad). The dynamics of the system, $H(\omega j)$, are shown as the black curve; the arrow of the curve indicates an increase in the input frequency ω. As can bee seen, the thresholds at different frequencies (represented by gray squares) are different in size. As the JNDs in the two complex components are proportional to the magnitude of the system's frequency response (see Eq. (5.11)), the threshold region becomes larger as the system's magnitude increases. For example, to alter what humans feel about the system, a larger change in the system's dynamics will be needed at the movement frequency of 14 rad/s than at the frequency of 6 rad/s.

Furthermore, the threshold model proposed in this study is not limited to only mass-spring-damper systems, systems that have second-order dynamics. As already discussed above, humans cannot directly sense stiffness, mass, and damping, instead, they estimate these three mechanical properties through the system's behavior which is determined by the FRF of the system (more specifically, the real and imaginary parts of the FRF since the FRF of any system is comprised of these two parts). One can imagine that this process is similar to a *black-box* estimation problem (i.e., the system appears to humans to be a black-box system with unknown order of dynamics). When estimating these mechanical properties, humans are actually interpreting the responses generated by the real and imaginary parts of the FRF of a black-box system which can in fact process a dynamics order different than two. Therefore, the model given in Eq. (5.11) is *independent* of the system dynamics order, representing human resolution of estimating the magnitudes of the two complex elements of the FRF of all systems.

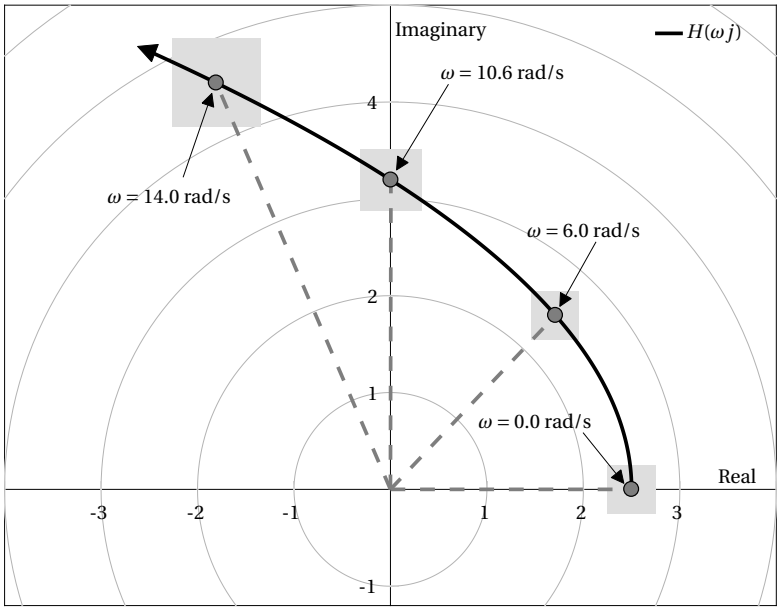

Figure 5.7: An example of the threshold for changes in human perception of a typical mass-spring-damper system. The FRF of the system is shown as the black curve, with its arrow indicating the increase in the frequency of excitation. The threshold regions at four different frequencies are given, to illustrate the correlation between the threshold size and the magnitude of the system's frequency response.

As already mentioned, any change in a system's dynamics can be always represented by (independent of the dynamics order) changes in the two (real, imaginary) components of the system's FRF. Whether or not a dynamics change can initiate a different human perception of the system will depend on whether or not the changes in the two complex components exceed the corresponding threshold for a difference perception. Thus, a different perception will occur if any of the two thresholds given by Eq. (5.11) is exceeded. Therefore, these two threshold also adequately represent the JND in the dynamics of a system with a dynamics order different than two. This frequency-domain model can be used to evaluate the transparency of haptic interfaces. The evaluation can be done in the frequency domain by examining the differences between the desired dynamics and the presented dynamics over the frequency range where the haptic interaction occurs. A haptic interface can potentially lead the operator to have a different perception, if there exists a frequency where the difference is higher than the threshold. This allows for understanding *whether and when* an operator's haptic experience is affected by limiting factors behind a particular application, such as the bandwidth of the control system, inherent actuator dynamics, transmission time delays, and the performance sacrifice made for stability issues.

5.6. DISCUSSION

Through a second experiment, we find that the JNDs in perceiving the two complex components of system dynamics are approximately the same, and are both proportional to the system's frequency-response magnitude. The findings are also generalized to systems with arbitrary orders. This allows us to further extend Weber's law for the JND in system dynamics. When considering the frequency response $H(\omega j)$ to be the stimulus, the JNDs in its real and imaginary part are proportional to its magnitude, $|H(\omega j)|$.

However, possibly due to differences between subjects and the fact that the experiments were carried out at a different time, the measured Weber Fractions – the values of the constants in Eqs. (5.10) and (5.11), as well as those collected in Chapter 4 – are not exactly the same. A larger number of subjects will be necessary to obtain a more representative value.

Eq. (5.11) expresses the JND in system dynamics with two thresholds, one of which corresponds to the real-part changes and the other corresponds to the imaginary-part changes. In fact, this rule can be further simplified without losing generality, into a formula based on a lumped difference in system dynamics:

$$\left| \frac{\Delta H(\omega j)_{jnd}}{H(\omega j)} \right| = \text{constant} \tag{5.13}$$

This simplification describes the change in the frequency response of a system as a whole, rather than going into the corresponding detailed changes in the two complex parts. Such an expression is better in line with Weber's law, describing a relation between a reference stimulus and a direct change in it that causes a different perception. One can imagine that at each individual frequency, the square-shape threshold region (see Fig. 5.6) can be now simplified into a circle, the radius of which is proportional to the length of the vector (i.e., the magnitude of the system's frequency response at this frequency).

This simplification facilitates the development of control solutions that aim at creating a perceptual transparent haptic presentation. A constant ratio can be now directly used as the requirements for any arbitrary change in a system's dynamics without considering the specific changes in the two complex parts. However, determining whether Eq. (5.13) is only a simplified or a more appropriate rule for the JND in system dynamics, is non-trivial. A circle would indicate the existence of an interaction between the JNDs in the two complex parts.

Measuring the thresholds for changes in different directions in the complex plane (e.g., by introducing changes into both real and imaginary components) will be needed for this. It requires a methodology different from that adopted in this chapter. The current methodology required subjects to identify the change in a single mechanical property (i.e., identify the heavier/stiffer or better damped system). This is not appropriate for a system dynamics change in an *arbitrary* direction which may be associated with changes in the perception of more than one property. Devising a new method is therefore necessary for future relevant research.

As already discussed in Section 5.3.4, our findings are currently limited to a relatively low frequency range. In addition, this study is restricted to *linear* systems, and

continuous haptic interaction. The model has not yet been verified for systems that have a considerable nonlinearity (such as strong friction), and does not account for the effects of transient responses that may occur when sudden changes in system dynamics occur, e.g., the changes upon contact with a stiff wall. Despite these limitations, the proposed JND model already covers a wide range of applications, such as [30–36]. Extensions of the model to include nonlinearities and transient responses are topics for future work.

5.7. CONCLUSION

Extending previous work on just-notable-differences in haptic perception, the results of two experiments are described. We conclude that, first, the human perception of the real and imaginary parts of the system dynamics frequency response *are governed by the same rule*. Our unified model states that JNDs in the two components of the FRF are *both proportional to the magnitude of the system frequency response*. Second, results show that these two JNDs have *the same ratio*. Third, the proposed unified JND model applies to systems with arbitrary orders of dynamics. The main result is an extension of Weber's law, and states that a *single ratio* describes the thresholds for perceiving changes in the two dimensions (real, imaginary) of the complex-valued frequency response function defining haptic force feedback of system dynamics.

REFERENCES

[1] J. Rebelo, T. Sednaoui, E. B. den Exter, T. Krueger, and A. Schiele, "Bilateral robot teleoperation: A wearable arm exoskeleton featuring an intuitive user interface," *IEEE Robotics Automation Magazine*, vol. 21, no. 4, pp. 62–69, 2014.

[2] J. G. W. Wildenbeest, D. A. Abbink, and J. F. Schorsch, "Haptic transparency increases the generalizability of motor learning during telemanipulation," in *World Haptics Conf. (WHC)*, Daejeon, South Korea, April 2013, pp. 707–712.

[3] A. M. Okamura, "Haptic feedback in robot-assisted minimally invasive surgery," *Current Opinion in Urology*, vol. 19, no. 1, pp. 102–7, 2009.

[4] R. J. Stone, "Haptic feedback: A brief history from telepresence to virtual reality," in *Int. Workshop on Haptic Human-Computer Interaction*, Glasgow, United Kingdom, Aug 2001, pp. 1–16.

[5] X. Hou, R. Mahony, and F. Schill, "Comparative study of haptic interfaces for bilateral teleoperation of VTOL aerial robots," *IEEE Trans. on Systems, Man, and Cybernetics: Systems*, vol. 46, no. 10, pp. 1352–1363, 2016.

[6] P. F. Hokayem and M. W. Spong, "Bilateral teleoperation: An historical survey," *Automatica*, vol. 42, no. 12, pp. 2035–2057, 2006.

[7] N. Colonnese and A. M. Okamura, "M-width: Stability, noise characterization, and accuracy of rendering virtual mass," *The Int. J. of Robotics Research*, vol. 34, no. 6, pp. 781–798, 2015.

[8] S. Hirche and M. Buss, "Human perceived transparency with time delay," in *Advances in Telerobotics*, M. Ferre, M. Buss, R. Aracil, C. Melchiorri, and C. Balaguer, Eds. Berlin, Germany: Springer, 2007, pp. 191–209.

[9] B. Hannaford, "Stability and performance tradeoffs in bi-lateral telemanipulation," in *Int. Conf. on Robotics and Automation*, vol. 3, Scottsdale, USA, May 1989, pp. 1764–1767.

[10] D. A. Lawrence, "Stability and transparency in bilateral teleoperation," *IEEE Trans. on Robotics and Automation*, vol. 9, no. 5, pp. 624–637, 1993.

[11] R. J. Adams and B. Hannaford, "Stable haptic interaction with virtual environments," *IEEE Trans. Robotics and Automation*, vol. 15, no. 3, pp. 465–474, 1999.

[12] R. Daniel and P. McAree, "Fundamental limits of performance for force reflecting teleoperation," *The Int. J. of Robotics Research*, vol. 17, no. 8, pp. 811–830, 1998.

[13] G. Niemeyer and J. J. E. Slotine, "Stable adaptive teleoperation," *IEEE J. of Oceanic Engineering*, vol. 16, no. 1, pp. 152–162, 1991.

[14] B. Hannaford and J. H. Ryu, "Time-domain passivity control of haptic interfaces," *IEEE Trans. on Robotics and Automation*, vol. 18, no. 1, pp. 1–10, 2002.

[15] S. Feyzabadi, S. Straube, M. Folgheraiter, E. A. Kirchner, S. K. Kim, and J. C. Albiez, "Human force discrimination during active arm motion for force feedback design," *IEEE Trans. on Haptics*, vol. 6, no. 3, pp. 309–319, 2013.

[16] X. D. Pang, H. Z. Tan, and N. I. Durlach, "Manual discrimination of force using active finger motion," *Perception & Psychophysics*, vol. 49, no. 6, pp. 531–540, 1991.

[17] L. A. Jones, "Kinesthetic sensing," in *Workshop on Human and Machine Haptics*, Pacific Grove, USA, Dec 1997, pp. 1–10.

[18] L. A. Jones and I. W. Hunter, "A perceptual analysis of stiffness," *Experimental Brain Research*, vol. 79, no. 1, pp. 150–156, 1990.

[19] ——, "A perceptual analysis of viscosity," *Experimental Brain Research*, vol. 94, no. 2, pp. 343–351, 1993.

[20] H. Z. Tan, N. I. Durlach, G. L. Beauregard, and M. A. Srinivasan, "Manual discrimination of compliance using active pinch grasp: The roles of force and work cues," *Perception & Psychophysics*, vol. 57, no. 4, pp. 495–510, 1995.

[21] G. L. Beauregard, M. A. Srinivasan, and N. I. Durlach, "The manual resolution of viscosity and mass," in *ASME Dynamic Systems and Control Division*, vol. 1, 1995, pp. 657–662.

[22] W. Fu, M. M. van Paassen, and M. Mulder, "On the relationship between the force JND and the stiffness JND in haptic perception," in *ACM Symp. on Applied Perception*, no. 11, Cottbus, Germany, Sept 2017.

[23] M. Kühner, J. Wild, H. Bubb, K. Bengler, and J. Schneider, "Haptic perception of viscous friction of rotary switches," in *IEEE World Haptics Conf.*, Istanbul, Turkey, Jun 2011, pp. 587–591.

[24] J. Schmidtler and M. Körber, "Human perception of inertial mass for joint human-robot object manipulation," *ACM Trans. on Applied Perception (TAP)*, vol. 15, no. 3, 2018.

[25] F. A. A. Kingdom and N. Prins, *Psychophysics: a Practical Introduction*. Academic Press, 2016.

[26] K. van der El, D. M. Pool, H. J. Damveld, M. M. van Paassen, and M. Mulder, "An empirical human controller model for preview tracking tasks," *IEEE Trans. on Cybernetics*, vol. 46, no. 11, pp. 2609–2621, 2016.

[27] J. H. Ryu, J. Artigas, and C. Preusche, "A passive bilateral control scheme for a teleoperator with time-varying communication delay," *Mechatronics*, vol. 20, no. 7, pp. 812–823, 2010.

[28] P. Arcara and C. Melchiorri, "Control schemes for teleoperation with time delay: A comparative study," *Robotics and Autonomous systems*, vol. 38, no. 1, pp. 49–64, 2002.

[29] M. M. van Paassen, "Biophysics in aircraft control: A model of the neuromuscular system of the pilot's arm," Ph.D. dissertation, TU Delft, Delft University of Technology, 1994.

[30] D. Van Baelen, J. Ellerbroek, M. M. van Paassen, and M. Mulder, "Design of a haptic feedback system for flight envelope protection," in *AIAA Modeling and Simulation Tech. Conf.*, no. AIAA-2018-0117, Kissimmee, USA, Jan 2018.

[31] S. de Stigter, M. Mulder, and M. M. van Paassen, "Design and evaluation of a haptic flight director," *J. of Guidance, Control, and Dynamics*, vol. 30, no. 1, pp. 35–46, 2007.

[32] R. J. A. W. Hosman, B. Benard, and H. Fourquet, "Active and passive side stick controllers in manual aircraft control," in *IEEE Int. Conf. on Systems, Man and Cybernetics (SMC)*, Los Angeles, USA, Nov 1990, pp. 527–529.

[33] T. M. Lam, M. Mulder, and M. M. van Paassen, "Haptic feedback in uninhabited aerial vehicle teleoperation with time delay," *J. of Guidance, Control, and Dynamics*, vol. 31, no. 6, pp. 1728–1739, 2008.

[34] M. Mulder, D. A. Abbink, M. M. van Paassen, and M. Mulder, "Design of a haptic gas pedal for active car-following support," *IEEE Trans. on Intelligent Transportation Systems*, vol. 12, no. 1, pp. 268–279, 2011.

[35] J. Venrooij, M. Mulder, M. Mulder, D. A. Abbink, M. M. van Paassen, F. C. T. van der Helm, and H. H. Bülthoff, "Admittance-adaptive model-based approach to mitigate biodynamic feedthrough," *IEEE Trans. on Cybernetics*, vol. 47, no. 12, pp. 4169–4181, 2017.

[36] J. Smisek, E. Sunil, M. M. van Paassen, D. A. Abbink, and M. Mulder, "Neuromuscular-system-based tuning of a haptic shared control interface for UAV teleoperation," *IEEE Trans. on Human-Machine Systems*, vol. 47, no. 4, pp. 449–461, 2017.

Part III

Performing a perception-oriented evaluation of haptic presentation

6

APPLYING PERCEPTION CHARACTERISTICS TO THE EVALUATION OF HAPTIC INTERFACES

As discussed in the Introduction of the thesis, attempts to evaluate haptic interfaces on the basis of what dynamics humans actually perceive are scarce. Previous chapters have established understanding of the most relevant characteristics of human haptic perception. This chapter demonstrates how these advances can be incorporated into the evaluation of haptic interfaces. First, a two-step approach to evaluating the display fidelity is proposed, accompanied by a numeral example. These two steps, respectively, allow us to know when and how a particular haptic device alters what the operator perceives. Second, the active manipulator developed in Chapter 2 is evaluated in terms of the control feel associated with the feedback about the aircraft rotational velocity. Analysis shows that pilots will experience approximately constant stiffness, mass, and damping, which is a control feel the same as that from a conventional passive manipulator.

This chapter is based on the following publications: (1) W. Fu, M. M. van Paassen, and M. Mulder, "Framework for a Two-Step Evaluation of Haptic Displays," *to appear in the proceedings of IFAC HMS 2019*; (2) W. Fu, M. M. van Paassen and M. Mulder, "Revisiting Active Manipulators in Aircraft Flight Control," *AIAA Scitech 2019 Forum*, no. AIAA-2019-1231, San Diego, USA, Jan 2019.

6.1. INTRODUCTION

Haptic interfaces can facilitate manual control by establishing bilateral communication between human operators and machines ([1, 2]). In most cases, a haptic interface is a control manipulator through which the human operator can sense the force feedback while performing a control task. It allows the operator to directly feel the dynamics of the environment in which the task is performed, or the dynamics of the system which is being controlled, such as a vehicle or a slave robot (for example, the active manipulator discussed in Chapter 2, or the applications that are discussed in [3–7]).

The feedback fidelity is one crucial factor for a successful application of haptic communication. Poor fidelity may lead the operator to perceive the system dynamics differently, deteriorating the interface effectiveness. Ideally, the dynamics as portrayed by a haptic device should appear to be exactly the same as the dynamics that one intends to communicate. Such perfect transparency is considered to be the objective by many studies (i.e., [4, 8–10]). However, this may not be possible in many cases, or prohibitively expensive. Inevitable distortions of the haptic display, such as those caused by limitations from the control systems and actuators, and transmission time delays in tele-operation, can distort this communication.

Most studies, however, do not consider the human element in their evaluations. This is caused by the fact that our understanding of the limitations of human haptic perception is rather limited. We claim that an evaluation should always be centered around what the human operator *perceives* from the haptic device. Some changes in the displayed dynamics caused by the haptic interface design may not be perceived at all by the operator, because of for instance a threshold for perceivable changes. Working towards a perfect transparency can place excessive, and even unnecessary (because small changes are no longer perceived), demands on the haptic device. In addition, some crucial elements regarding *how* the dynamic changes which *are* perceived can affect the operator in characterizing the system's response are usually overlooked. This considerably hampers a further optimization of the haptic display.

Apart from issues concerning the display fidelity, in the design phase it is also important to understand how humans interpret the system dynamics presented to them. As discussed in Chapter 1, digital control systems allow for various possibilities for generating artificial haptic feedback. Knowing how humans characterize a particular signal fed back to them is a crucial parameter in optimizing the control feel. For example, Chapter 2 demonstrated that a large portion of the aircraft's dynamics is absorbed by the control device when the device's movement reflects the angular velocity of the aircraft. While moving such a control device (the active manipulator), what a pilot feels is determined by the absorbed dynamics, as those dynamics determine the manipulator's response. An issue that has not been explored is how a pilot characterizes these dynamics. One can imagine that the pilot's perception of the active manipulator is different from the conventional passive control device. In addition to the improvement in task performance, it must be guaranteed that implementing such an active control device will not lead to any unpleasant control feel. Understanding how pilots characterize the behavior of the active manipulator can certainly facilitate further improvement on this concept.

This chapter demonstrates how the advances made in previous chapters in under-

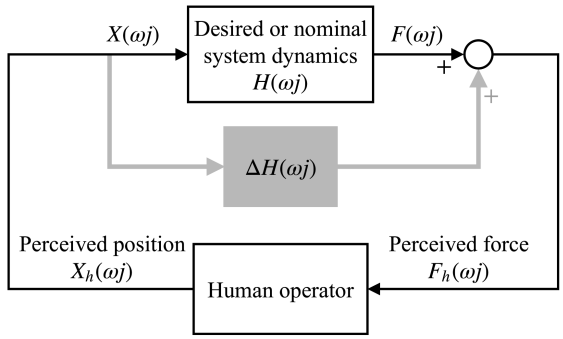

Figure 6.1: Haptic interaction between a human operator and an arbitrary system.

standing human haptic perception allow us to integrate perception characteristics into the design and evaluation of haptic interfaces. The next section will recapitulate the theoretical foundations established in previous chapters. Section 6.3 proposes a two-step approach to evaluation of haptic display fidelity. Based on the model of human haptic difference threshold (proposed in Chapter 5), the first step allows us to know the frequency bandwidth of "perceptual transparency". The second step, based on results from Chapter 3, allows us to understand *how* the changes in dynamics which *are* perceived, are characterized by the human operator as changes in the mechanical characteristics. A numerical example is given to illustrate how the two steps of the evaluation can be performed. On the basis of the findings from Chapters 3, 4, and 5, Section 6.4 reveals the characteristics that pilots would perceive from the active manipulator through drawing an analogy with basic mechanical properties. Section 6.5 summarizes the contributions of this chapter.

6.2. CHARACTERISTICS OF HAPTIC PERCEPTION

6.2.1. PRELIMINARIES

As also discussed in Chapter 1, restrictions must be placed in order to make the problem more tractable. Firstly, this chapter is restricted to *linear* systems, as the majority of relevant studies concern. Such a restriction allows for the development of powerful analytic tools. Due to the fact that many nonlinear systems at/around the equilibrium conditions possess strong linearity, this study covers a broad class of systems. Secondly, this study only concerns the *continuous* haptic interaction with *soft* objects. Although these restrictions exclude the cases of hard environments (such as stiff walls), and the effects of transient responses (such as the moment of contact), this chapter is still relevant to a large number of applications, such as [2, 11–16].

Imagine that the human operator is directly interacting with an arbitrary system, as shown in Fig. 6.1. Define $H(\omega j)$ as the frequency response function (FRF) of the desired or nominal system dynamics, which describe the force $F(\omega j)$ that is generated in response to the displacement $X(\omega j)$:

$$H(\omega j) = \frac{F(\omega j)}{X(\omega j)} \tag{6.1}$$

The FRF is a complex-valued function which can be divided into two parts:

$$H(\omega j) = \Re H(\omega j) + \Im H(\omega j) \tag{6.2}$$

Here, $\Re H(\omega j)$ and $\Im H(\omega j)$ denote the real and imaginary parts of the system's frequency response, respectively.

The dynamics actually presented to a human operator may be different from the desired or nominal dynamics. Here we define the difference in system dynamics as $\Delta H(\omega j)$ (see Fig. 6.1). It can also be expressed with the real and imaginary parts:

$$\Delta H(\omega j) = \Re \Delta H(\omega j) + \Im \Delta H(\omega j) \tag{6.3}$$

As can be seen from Fig. 6.1, the dynamics the human operator perceives are affected by both $H(\omega j)$ and $\Delta H(\omega j)$. Two important issues now arise. The first concerns *when* $\Delta H(\omega j)$ causes what the operator perceives to be different from that he/she would experience when directly interacting with $H(\omega j)$. The second concerns *how* a perceived change caused by $\Delta H(\omega j)$ is characterized by the human operator.

6.2.2. MODEL OF HAPTIC DIFFERENCE THRESHOLD

Although the system presented to the operator is different from $H(\omega j)$, it is not necessarily perceived differently due to the limitation of human sensory system. The change in the system dynamics must exceed a certain level to become noticeable. The threshold for causing a different perception is usually referred to as *just-noticeable difference* (JND).

Knowledge about the JND in the system dynamics is necessary to address the first aforementioned issue. As can be seen from Eq. (6.3), any change in a linear system's dynamics can be represented by changes in the real and imaginary components of the system's FRF. Whether or not the human perception of the system is altered will in fact depend on whether or not the changes in the two complex components can be noticed. Through Chapters 4 and 5, we have found that the JNDs in the two complex parts of a system's frequency response, i.e., the minimum changes in $\Re H(\omega j)$ and $\Im H(\omega j)$ that are likely to alter human perception of the system, can be described as a function of the system's FRF:

$$\left| \frac{\Delta \Re H(\omega j)_{jnd}}{H(\omega j)} \right| \approx \left| \frac{\Delta \Im H(\omega j)_{jnd}}{H(\omega j)} \right| = \text{constant} \tag{6.4}$$

The magnitudes of the JNDs are proportional to the magnitude of the system's frequency response. As can be seen from previous chapters, for the general impedance range used in typical manual control tasks, such an uncertainty in the perception can be roughly approximated to by a ratio of 10% (i.e., the constant in Eq. (6.4) will be approximately equal to 0.1).

This model defines a threshold region in which a change in the system's dynamics does not alter the perception of the operator. To better illustrate this, Fig. 6.2 shows an example which considers the dynamics of an arbitrary system at a single frequency. In the complex plane, the FRF at a single frequency is represented by a vector (the black line). The real and imaginary parts define the projections on the two axes, respectively.

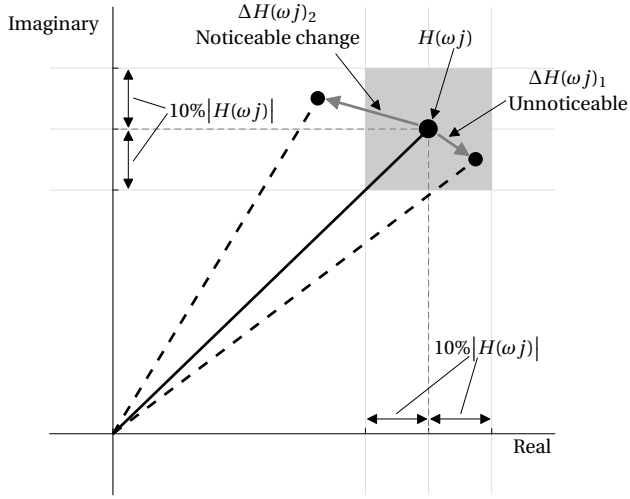

Figure 6.2: An illustration of the threshold for perceiving a change in the dynamics of a system, considered at a single frequency. For the haptic interaction occurring at this particular frequency, dynamic changes within the threshold are not perceptible (e.g., $\Delta H(\omega j)_1$), whereas those exceeding the threshold do change the perception of the system (e.g., $\Delta H(\omega j)_2$).

A change in the system dynamics will result in a different vector which has at least one different projection, as shown by two dashed lines. The two JNDs given by Eq. (6.4) defines the intervals for imperceptible changes in the projections on the two axes of the complex plane. These two intervals form a square region within which humans perceive different systems as being the same. One can imagine that when the haptic interaction occurs at this particular frequency, for example using a sinusoidal manipulator movement, ΔH will only lead the human operator to have a different perception if it exceeds the threshold region at this frequency, see Eq. (6.4).

6.2.3. CHANGE IN PERCEIVED CHARACTERISTICS OF THE SYSTEM

Studies suggest that humans characterize the behavior of a system according to the relation between the movement and force perceived during the interaction (See Chapter 3). Humans are inclined to compare the system behavior to that of mechanical systems, particularly when one needs to assess the mechanical properties (i.e., mass, damping, and stiffness), as demonstrated by Chapter 3. In general, the force against a displacement (spring force) is usually perceived as the behavior of a spring; the force resisting the movement velocity (viscous damping force) is considered to be the effect of damping; and the effort to change the movement direction (inertia force) is related to inertia.

What mechanical behavior a system exhibits is determined by the FRF (i.e., $H(\omega j)$ in Eq. (6.1)), in particular, the real and imaginary parts. Firstly, the real part $\Re H(\omega j)$ affects the stiffness and mass properties that humans perceive from the system (see Chapter 3). Depending on the frequency of excitation, this part generates a spring or

inertia force:

$$F_{si}(\omega j) = X(\omega j)\left|\Re H(\omega j)\right| e^{j\angle \Re H(\omega j)},$$
$$\text{where } \angle \Re H(\omega j) = \begin{cases} 0° & \text{if } \Re H(\omega j) > 0 \\ 180° & \text{if } \Re H(\omega j) < 0 \end{cases} \tag{6.5}$$

When the haptic interaction occurs at a frequency where $\Re H$ is positive, the system feels like a mechanical spring. This is because the system generates a spring force which is directly proportional to the displacement (with a ratio of $\Re H$). When $\Re H$ is negative, the system exhibits an inertia-like behavior. It generates a force which is 180-degrees out of phase with the displacement, thus directly proportional to the acceleration. Therefore, the *sign* of $\Re H$ determines which of these two mechanical behaviors the system exhibits, and the *magnitude* of $\Re H$ determines the amount of the corresponding force that an operator perceives.

Secondly, a positive imaginary part (i.e., when $\Im H > 0$) generates a force which has a 90-degrees phase shift from the displacement:

$$F_d(\omega j) = X(\omega j)\left|\Im H(\omega j)\right| e^{j\angle \Im H(\omega j)},$$
$$\text{where } \angle \Im H(\omega j) = 90° \tag{6.6}$$

Such a phase shift makes this force proportional to (and normally resist) the movement velocity. The magnitude $|\Im H|$ determines the amount of this force. One can imagine that this part affects the damping property humans perceive from the system. Please note that a negative imaginary part leads to non-passive behavior, and how humans characterize this is beyond the scope of this chapter.

When a change in the dynamics of a system, $\Delta H(\omega j)$, is sufficient to alter what humans feel, its effect on the perception of mechanical properties can be understood by means of changes in the two parts of the system dynamics. Fig. 6.3 shows an example which considers the dynamics of an arbitrary system at a single frequency. As can be seen, a change in the real part, $\Delta \Re H$, alters the perception of stiffness (see Fig. 6.3a) or mass (see Fig. 6.3b). And a change in the imaginary part, $\Delta \Im H$, leads to a different perception of the damping property.

6.3. A TWO-STEP APPROACH TO EVALUATING THE FIDELITY OF HAPTIC DISPLAYS

This section explains how the characteristics of human haptic perception can be used to evaluate the display fidelity of haptic interfaces. Starting from the perspective that what the operator *perceives* is what matters most, we consider the two following questions to be crucial:

1. At what point, or, *when* does a haptic device start to cause what the human perceives to be different from that is desired?

2. When the perception changes, *how* does this change affect the operator's characterization of the system's properties?

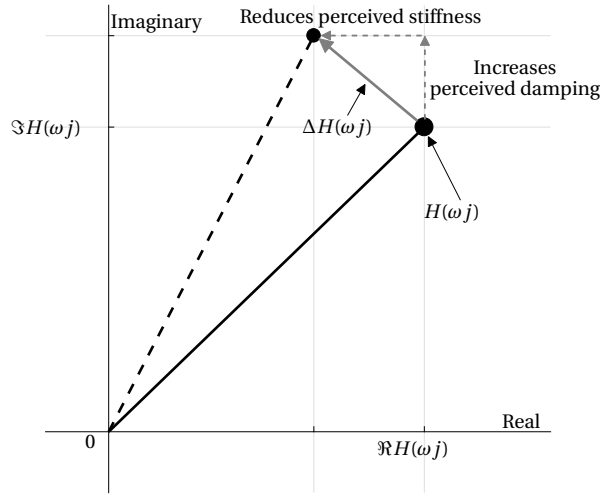

(a)

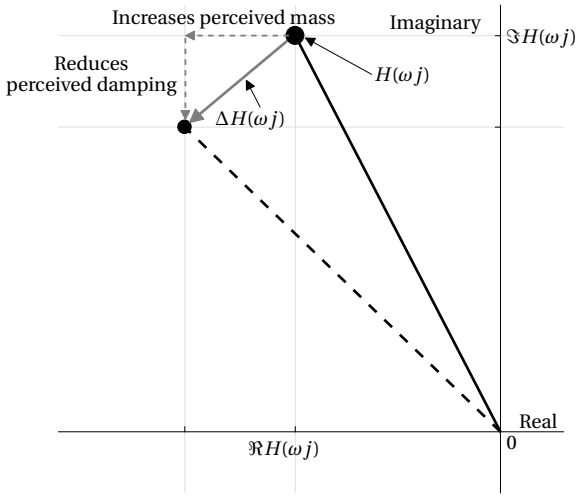

(b)

Figure 6.3: An illustration of the changes in the mechanical characteristics perceived by humans, associated with a change in the system dynamics, (a): when $\Re H(\omega j)$ is positive; (b): when $\Re H(\omega j)$ is negative.

Two address these two questions, this section presents a two-step evaluation approach. The first step is based on the frequency-domain JND model described in the previous section. It evaluates a haptic device in terms of the frequency range within which the desired system dynamics are presented with "perceptual transparency". In other words, up to what frequency are changes in the dynamics *not perceived*? The second step, which is based primarily on the framework given by Section 6.2.3, allows us to understand *how* the changes in dynamics which *are* perceived, are characterized by

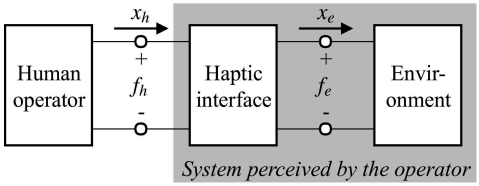

Figure 6.4: Two-port representation of the interaction between the operator and the environment through the haptic interface. Here we consider the *flow* to be the position x instead of the commonly used velocity $\dot{x}$. Such a modification is made to keep the expressions consistent with those given in Section 6.2.3.

the human operator as changes in the mechanical characteristics of the system.

The evaluation approach will be given in a numerical example, which also shows how such an approach can be implemented. Although for the sake of a straightforward illustration the problem considered here is simple, the evaluation routine suits much more complicated cases in practice as well.

Consider a manual control task in which a human operator interacts with a virtual environment through a haptic interface, as shown by a modified two-port representation in Fig. 6.4. In this example, we consider the environment to be a typical mass-spring-damper system:

$$H_{env}(\omega j) = \frac{F_e(\omega j)}{X_e(\omega j)} = m \cdot (\omega j)^2 + b \cdot (\omega j) + k, \tag{6.7}$$

where m, b, and k denote the mass, damping and stiffness, respectively. Table 6.1 gives the settings of these three parameters.

In this example, the environment dynamics $H_{env}(\omega j)$ can be considered to be the nominal system dynamics $H(\omega j)$ shown in Fig. 6.1. The dynamics perceived by the human operator are those that exist between the perceived movement x_h and force f_h (as can be seen from Fig. 6.1, the perceived dynamics are the sum of $H(\omega j)$ and $\Delta H(\omega j)$). For simplicity, the effects of the haptic device's dynamics are modelled through using a second-order low-pass filter. The dynamics rendered by the haptic interface (those perceived by the operator) are defined as:

$$\begin{aligned} H_p(\omega j) &= \frac{F_h(\omega j)}{X_h(\omega j)} \\ &= H_{env}(\omega j) \cdot \frac{6400}{(\omega j)^2 + 80(\omega j) + 6400} \end{aligned} \tag{6.8}$$

Here $H_p(\omega j)$ represents the dynamics presented by the haptic interface.

Table 6.1: Parameters of the environment

Stiffness k [N/m]	Mass m [kg]	Damping b [Ns/m]
100	1.8	15

Therefore, the difference in dynamics between the environment and the haptic display can be expressed as:

$$\Delta H(\omega j) = H_p(\omega j) - H_{env}(\omega j) \tag{6.9}$$

The frequency range for the evaluation is set to 0-15 rad/s. The higher end of this range is slightly higher than the bandwidth of the neuromuscular system [17]. Frequencies beyond this range are of no interest because humans seldom generate voluntary actions beyond the capacity of their neuromuscular system in manual control tasks.

The first step is to examine whether or not the haptic interface alters the operator's perception of the environment. That is, if the haptic perception associated with $H_p(\omega j)$ is different from $H_{env}(\omega j)$. Comparisons between the JND thresholds and the changes caused by the haptic device in the system dynamics can be carried out over the selected frequency range. To this end, the following two ratios are calculated:

$$r_r(\omega) = \left| \frac{\Re \Delta H(\omega j)}{H_{env}(\omega j)} \right|, \; r_i(\omega) = \left| \frac{\Im \Delta H(\omega j)}{H_{env}(\omega j)} \right| \tag{6.10}$$

According to Eq. (6.4), the rendered dynamics will be perceived to be the same as the environment dynamics only if both r_r and r_i are below 10%.

Fig. 6.5 shows the two ratios corresponding to the dynamics given by Eq. (6.8). As can be seen, the difference in the real and imaginary parts exceed the threshold at 8 and 12 rad/s, respectively. As a result, this haptic device can only display the environment dynamics without altering the operator's perception at frequencies below 8 rad/s. This frequency range can be interpreted as the bandwidth of perceptual transparency for this particular device.

In addition, this also implies that the frequency content of the haptic interaction must be limited to ensure an unaffected perception of the environment. What an op-

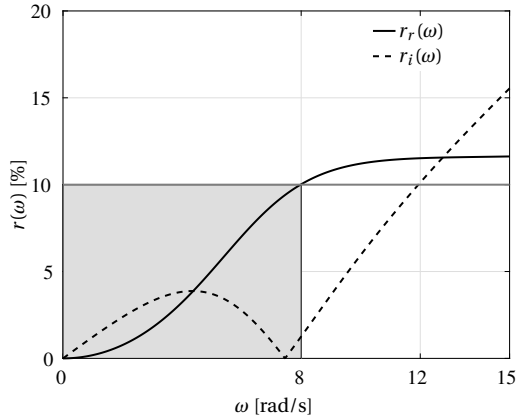

Figure 6.5: The normalized dynamic difference caused by the haptic device in the real and imaginary parts. The gray area represents the frequency range within which the haptic display will be perceived to be the same as the environment.

erator perceives will be the same as that he/she would experience when directly interacting with the environment, only if the human operator uses relatively slow movements (predominantly with the frequency content below 8 rad/s) to interact with the haptic interface. Any movement with substantial energy beyond this frequency range may cause a difference in perception.

The second step is to assess how the distortion of the environment dynamics is reflected in the mechanical properties perceived by the human operator. Fig. 6.6 shows the Nyquist plots of the dynamics of the environment and those presented by the haptic device. The arrows of the curves indicate an increase in frequency. Each point on a curve corresponds to the frequency response of the system at a particular frequency. As can be seen, the characteristics of the two curves are similar, indicating that the behavior of the presented system is similar to that of the environment. However, the rendered dynamics (shown as the red curve) deviate more from the environment dynamics (shown as the blue curve) as frequency increases.

The Nyquist plot shows a clear image of the mechanical characteristics of the two systems. Firstly, as can be seen from the real projection, the two systems both exhibit spring behaviors at relatively low frequencies and exhibit inertia behavior at higher frequencies. The environment's changeover frequency at which the sign of the real projection changes is the undamped eigen frequency: $\omega = \sqrt{k/m} = 7.45$ rad/s. As can be seen from Fig. 6.5, the frequency from which the difference in the real part starts to exceed the threshold is higher than the changeover frequency of the environment. This means that the stiffness of the environment is preserved no matter what movements the human operator uses to interact with the environment, whereas the per-

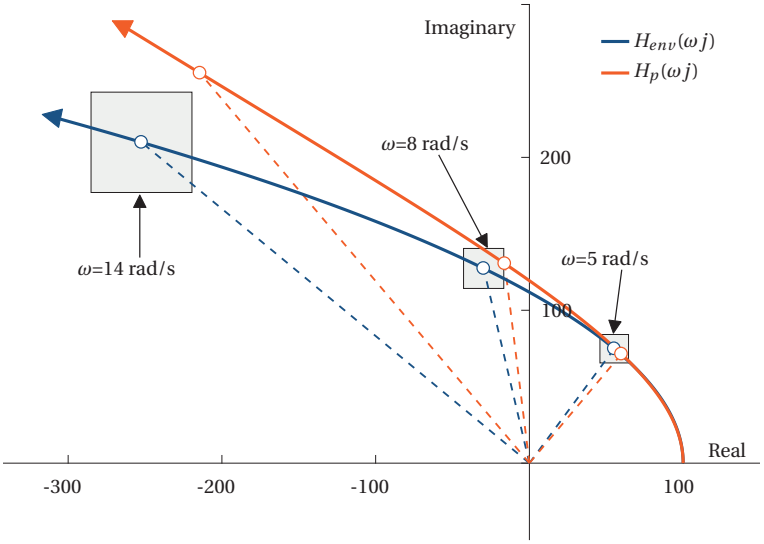

Figure 6.6: Nyquist plots of the environment dynamics and those rendered by the haptic interface. The frequency range for the Nyquist plot is 0-15 rad/s. To facilitate the comparison between the two systems, their frequency responses at three different frequencies are also shown. The gray squares represent the haptic difference thresholds at these frequencies.

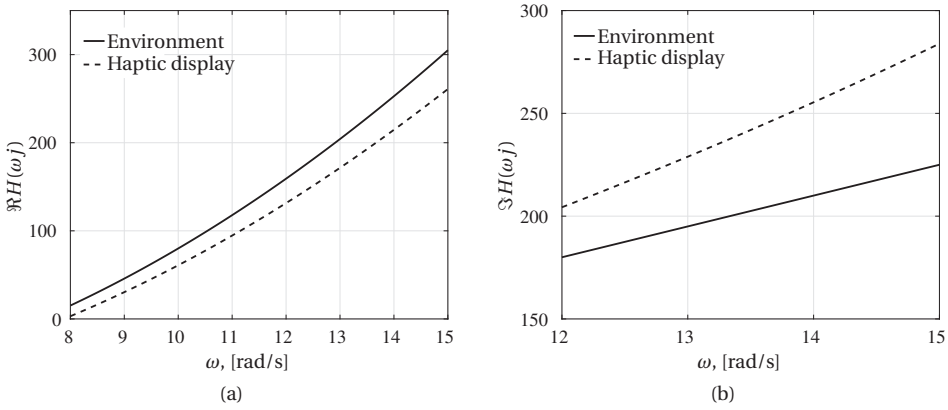

Figure 6.7: The real and imaginary parts of the dynamics of the environment and the haptic display, at frequencies where the corresponding distortions exceed the thresholds.

ceived mass will be different from the mass of the environment for most of the time.

To facilitate the understanding of how the perceived mass is affected, Fig. 6.7a shows the absolute value of the real projections at frequencies above 8 rad/s. As can be seen, the haptic interface will lead the operator to always perceive the environment mass as smaller since the rendered dynamics have a smaller negative projection value.

Secondly, the haptic interface also alters the operator's perception of the environment damping if the interaction occurs at frequencies higher than 12 rad/s, the frequency where the difference in the imaginary part starts to exceed the threshold (see Fig. 6.5). Fig. 6.7b shows the imaginary projections of the two systems beyong this threshold frequency. As can be seen, the rendered dynamics always have larger projections on the imaginary axis. This indicates that a haptic interaction that occurs at these higher frequencies may lead the operator to perceive the environment as having higher damping.

In many previous studies, the difference between the presented and the desired system dynamics is used as an indication of the performance of haptic devices (e.g., [10, 18]). However, it is not always known when these deviations can even be felt by a human, and how these then affect the perception of the display. With this numerical example, we have demonstrated how the characteristics of human haptic perception can be incorporated into the evaluation of haptic displays. Focused on what the operator perceives, our approach consists of two steps which can provide designers aiming at enhancing the effectiveness of their haptic devices with important insights. The first step can be used to determine with what settings a haptic device starts to change the operator's perception of the desired dynamics. This indicates the allowable bandwidth of the haptic interaction with a particular device if a perceptually transparent haptic display is required. Furthermore, the threshold model used in this step can be considered an alternative to existing criteria for haptic devices, such as the EASA qualification standards for control loading systems in vehicle simulators [19]. The second step assesses the changes caused by a haptic device in the perception of mechanical proper-

ties. This provides insights into how stability and transparency can be more effectively balanced. It allows us to know that the rendering of which mechanical property still has room to be compromised to improve stability, and that of which must be maintained or improved.

6.4. PERCEIVED MECHANICAL CHARACTERISTICS OF THE ACTIVE MANIPULATOR

As discussed in Section 6.1, the control feel associated with a particular setting of haptic feedback is a crucial parameter for making a proper design choice. Knowledge established in previous chapters will facilitate such an evaluation. This section presents an approach to evaluate how humans characterize the system dynamics presented by haptic interfaces. We use the active manipulator developed in Chapter 2 as an example, because a good control "feel" is particularly important during manual flight control.

The findings described in Section 6.2 will be used to assess the haptic perception of aircraft dynamics presented by the active manipulator. This requires us to obtain the FRF of the deflection-to-force dynamics of such a control device. The aircraft dynamics used in Chapter 2 are taken for the assessment, see Eq. (2.3). Again, we assume that the force sampling and position servo systems have negligible effects on the frequency content of human control behavior. In addition, the disturbance signal is excluded from the investigation, as it does not change the apparent manipulator dynamics. Thus, the manipulator dynamics perceived by the pilot can be expressed as:

$$H_p(\omega j) = \frac{F_m(\omega j)}{X_m(\omega j)} = \frac{u(\omega j)}{K_f K_m \Phi(\omega j) \cdot \omega j} = \frac{1}{K_f K_m} \cdot \frac{1}{H_c(\omega j) \cdot \omega j} \tag{6.11}$$

Please refer to Fig. 2.14 for definitions of the variables in this equation. The gains, K_f and K_m, equal 1 and 1/3.5, respectively (the same as the values used in the first experiment of Chapter 2). To focus on the perceived characteristics of the aircraft dynamics conveyed by the feedback about aircraft rotational velocity, the lead-lag filter designed in Section 2.6 is excluded from the investigation. The effect of such a filter can be evaluated under the same procedure presented in this section.

Fig. 6.8 shows the Nyquist plot of the apparent dynamics of the active manipulator, $H_p(\omega j)$. The frequency range for this plot is 0 to 15 rad/s. Frequencies beyond this range are of no interest to the current investigation, as humans seldom intentionally generate such high-frequency movements in manual control tasks. As can be seen, the active manipulator in general possesses mass-spring-damper characteristics, despite the fact that it exhibits some negative damping behavior at frequencies below 0.8 rad/s. This is due to the partial cancellation of the two second-order polynomials in the numerator and the denominator of the aircraft dynamics (see Eq. (2.3)). Be that as it may, this non-passive behavior only exists in a narrow range of fairly low frequencies, and its magnitude is fairly small. None of our subjects noticed this unstable behavior during the experiment described in Chapter 2.

The pilot will perceive the manipulator as having spring and damping properties in the frequency range between 0.8 to 5.3 rad/s, and inertia and damping properties at higher frequencies. Moreover, the characteristics of the curve closely resemble that of a mass-spring-damper system. This allows us to quantify the mechanical properties

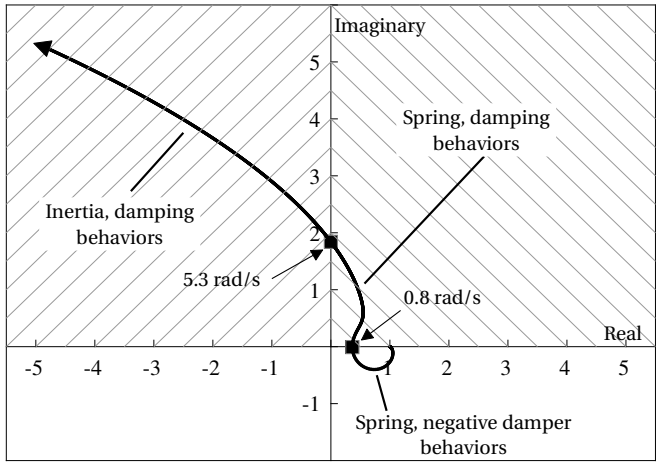

Figure 6.8: Nyquist plot of the system dynamics presented by the active manipulator, for the frequency range of 0 to 15 rad/s.

which a pilot would perceive, using a second-order system which processes constant stiffness, mass, and damping. The quantification involves minimizing the difference in the FRF between the dynamics of a mass-spring-damper system and the apparent dynamics of the manipulator in the frequency range of interest:

$$J = \int_{\omega_0}^{\omega_1} \left| H_{msd}(\omega j) - H_p(\omega j) \right|^2 d\omega \tag{6.12}$$

As stated earlier, the frequency range is chosen as ω_0=0 to ω_1=15 rad/s. Table 6.2 lists the approximate mechanical properties that would be perceived. Please note that the mechanical properties are defined in the rotational coordinate system, since control devices of aircraft are controlled by means of the deflection angle. The FRF of this mass-spring-damper system is shown in Fig. 6.9, along with the FRF of the manipulator. As can be seen, except for the minor difference in a narrow range of low frequencies, these two systems are nearly identical over the chosen frequency range. The JND model given in Eq. (6.4) can be used to establish a better understanding of *when* this difference leads the active manipulator to be perceived as different from the approxi-

Table 6.2: Estimates of the mechanical properties perceived from the active manipulator

m [kgm^2]	b [Nms/rad]	k [Nm/rad]
0.0243	0.3489	0.6738

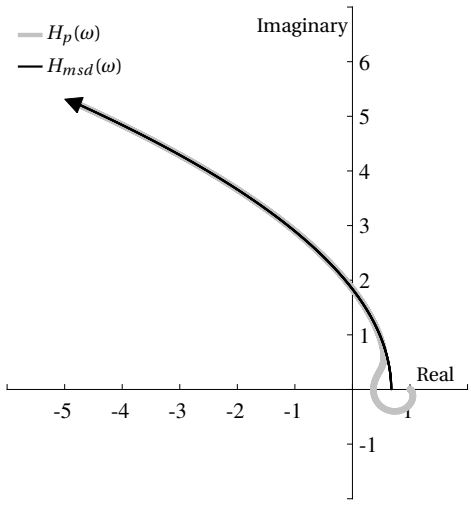

Figure 6.9: Nyquist plot of the apparent dynamics of the active manipulator (H_p) and the dynamics of the approximate system (H_{msd}).

mate system. Similar to the previous section, the following two ratios are calculated:

$$r_r(\omega) = \left| \frac{\Re \Delta H(\omega j)}{H_{msd}(\omega j)} \right|, \; r_i(\omega) = \left| \frac{\Im \Delta H(\omega j)}{H_{msd}(\omega j)} \right|, \tag{6.13}$$
$$\text{where } \Delta H(\omega j) = H_p(\omega j) - H_{msd}(\omega j)$$

According to Eq. (6.4), the active manipulator will be perceived to be the same as the approximate system if both ratios r_r and r_i are below 10%.

Fig. 6.10a compares these ratios with the threshold ratio of 10%. As can be seen, the differences in the real and imaginary parts exceed the threshold at the frequency ranges of 0-1.5 and 0-1.1 rad/s, respectively. As a result, the active manipulator will be perceived as exactly the same as the approximate system if one moves the manipulator at frequencies beyond 1.5 rad/s. This frequency is much lower than the active manipulator's changeover frequency (5.3 rad/s, where the response of the system changes from a spring force to a inertia force, see Fig. 6.8). This indicates that a pilot will always experience constant manipulator mass of 0.0243 kgm^2 (see Table 6.2). For most of the time, the perceived stiffness and damping properties will also remain at the constant levels given in Table 6.2, although they slightly deviate from the approximation in the case of nearly static haptic interaction, as can be seen from Fig. 6.10b.

This implies that a pilot will consider the active manipulator to be similar to a conventional passive manipulator, in terms of the perceived mechanical properties. The aircraft dynamics employed in Chapter 2 result in fairly good mass-spring-damper characteristics. In practice, although the aircraft dynamics are nonlinear, in many cases the behavior of an aircraft can still be approximated by, or is at least similar to, the linear model derived from the equilibrium condition. Therefore, the pilot's perception of the active manipulator will still be associated with mass-spring-damper character-

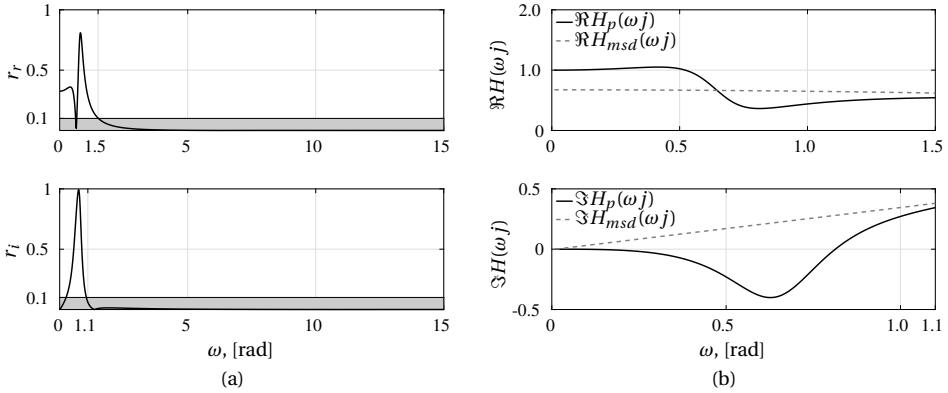

Figure 6.10: (a): The normalized dynamic difference in the system dynamics between the active manipulator and the approximate system. The gray area represents the threshold within which the two systems are perceived as the same. (b) The real and imaginary parts of the frequency responses of the two systems, at frequencies where the differences between the two systems exceed the haptic difference threshold. As can be seen, the apparent stiffness of the active manipulator will be changing around the approximate stiffness while the apparent damping will be always lower than that approximated.

istics. In addition, different flight conditions may lead to different model parameters. This indicates that the perceived mechanical properties of the active manipulator also vary with the condition of the flight, which can inform the pilot about the current flight condition, possibly enhancing situation awareness.

6.5. CONCLUSION

Based on findings from previous chapters, this chapter explains how we can incorporate the characteristics of human haptic perception into evaluation of haptic interfaces.

First, a two-step fidelity-evaluation approach is proposed. The first step allows us to know the frequency spectrum in which a haptic device causes a noticeable distortion of the desired system dynamics. The second step is then to understand how this distortion affects the operator in characterizing the system's behavior.

Second, to provide more insights into the active manipulator developed in Chapter 2, this chapter evaluates the control feel associated with the aircraft dynamics conveyed by feedback of the aircraft rotational velocity. Similar to a conventional passive manipulator, it is found that the apparent dynamics of the active manipulator can be described by approximately constant stiffness, mass, and damping properties. One should note, however, that these apparent mechanical properties may slightly vary with flight conditions).

REFERENCES

[1] D. A. Abbink and M. Mulder, "Exploring the dimensions of haptic feedback support in manual control," *J. of Computing and Information Science in Engineering*, vol. 9, no. 1, pp. 011 006–011 006(9), 2009.

[2] J. Smisek, E. Sunil, M. M. van Paassen, D. A. Abbink, and M. Mulder, "Neuromuscular-system-based tuning of a haptic shared control interface for UAV teleoperation," *IEEE Trans. on Human-Machine Systems*, vol. 47, no. 4, pp. 449–461, 2017.

[3] M. C. Cavusoglu, F. Tendick, M. Cohn, and S. S. Sastry, "A laparoscopic telesurgical workstation," *IEEE Trans. on Robotics and Automation*, vol. 15, no. 4, pp. 728–739, 1999.

[4] Y. Yokokohji and T. Yoshikawa, "Bilateral control of master-slave manipulators for ideal kinesthetic coupling-formulation and experiment," *IEEE Trans. on Robotics and Automation*, vol. 10, no. 5, pp. 605–620, 1994.

[5] X. Hou, R. Mahony, and F. Schill, "Comparative study of haptic interfaces for bilateral teleoperation of VTOL aerial robots," *IEEE Trans. on Systems, Man, and Cybernetics: Systems*, vol. 46, no. 10, pp. 1352–1363, 2016.

[6] J. G. W. Wildenbeest, R. J. Kuiper, F. C. T. van der Helm, and D. A. Abbink, "Position control for slow dynamic systems: Haptic feedback makes system constraints tangible," in *IEEE Int. Conf. on Systems, Man, and Cybernetics (SMC)*, San Diego, USA, Oct 2014, pp. 3990–3995.

[7] D. Reintsema, K. Landzettel, and G. Hirzinger, *DLR's Advanced Telerobotic Concepts and Experiments for On-Orbit Servicing.* Berlin, Germany: Springer Berlin Heidelberg, 2007, pp. 323–345.

[8] K. H. Zaad and S. E. Salcudean, "Adaptive transparent impedance reflecting teleoperation," in *IEEE Int. Conf. on Robotics and Automation*, vol. 2, Minneapolis, USA, Apr 1996, pp. 1369–1374.

[9] J. Kim, P. H. Chang, and H. Park, "Two-channel transparency-optimized control architectures in bilateral teleoperation with time delay," *IEEE Trans. on Control Systems Technology*, vol. 21, no. 1, pp. 40–51, 2013.

[10] P. H. Chang and J. Kim, "Telepresence index for bilateral teleoperations," *IEEE Trans. on Systems, Man, and Cybernetics, Part B (Cybernetics)*, vol. 42, no. 1, pp. 81–92, 2012.

[11] D. Van Baelen, J. Ellerbroek, M. M. van Paassen, and M. Mulder, "Design of a haptic feedback system for flight envelope protection," in *AIAA Modeling and Simulation Tech. Conf.*, no. AIAA-2018-0117, Kissimmee, USA, Jan 2018.

[12] S. de Stigter, M. Mulder, and M. M. van Paassen, "Design and evaluation of a haptic flight director," *J. of Guidance, Control, and Dynamics*, vol. 30, no. 1, pp. 35–46, 2007.

[13] R. J. A. W. Hosman, B. Benard, and H. Fourquet, "Active and passive side stick controllers in manual aircraft control," in *IEEE Int. Conf. on Systems, Man and Cybernetics (SMC)*, Los Angeles, USA, Nov 1990, pp. 527–529.

[14] T. M. Lam, M. Mulder, and M. M. van Paassen, "Haptic feedback in uninhabited aerial vehicle teleoperation with time delay," *J. of Guidance, Control, and Dynamics*, vol. 31, no. 6, pp. 1728–1739, 2008.

[15] M. Mulder, D. A. Abbink, M. M. van Paassen, and M. Mulder, "Design of a haptic gas pedal for active car-following support," *IEEE Trans. on Intelligent Transportation Systems*, vol. 12, no. 1, pp. 268–279, 2011.

[16] J. Venrooij, M. Mulder, M. Mulder, D. A. Abbink, M. M. van Paassen, F. C. T. van der Helm, and H. H. Bülthoff, "Admittance-adaptive model-based approach to mitigate biodynamic feedthrough," *IEEE Trans. on Cybernetics*, vol. 47, no. 12, pp. 4169–4181, 2017.

[17] M. M. van Paassen, "Biophysics in aircraft control: A model of the neuromuscular system of the pilot's arm," Ph.D. dissertation, TU Delft, Delft University of Technology, 1994.

[18] W. Iida and K. Ohnishi, "Reproducibility and operationality in bilateral teleoperation," in *The 8th IEEE International Workshop on Advanced Motion Control*, Kawasaki, Japan, Mar 2004, pp. 217–222.

[19] EASA, "CS-FSTD(A): Certification specifications for aeroplane flight simulation," Initial Issue, 2012.

7

Conclusions & Recommendations

The journey is the thing.

Homer

This chapter first highlights the major findings of the previous four chapters. To this end, the research objectives along with the corresponding key research questions will be recapitulated and addressed, in the light of the results that have been obtained. Next comes a discussion of the findings, their impacts and implications, ending with recommendations for future research.

7.1. MAIN FINDINGS

7.1.1. EXPLOITING THE POTENTIAL OF HUMAN CONTROLLERS

The focus of this thesis, with regard to the design philosophy of haptic interfaces, is narrowed down to applications in aircraft. As a passive control device fails to establish a haptic connection between a pilot and the aircraft being controlled, the control performance of a pilot is limited. The first objective of this thesis is creating haptic feedback on control devices to involve the neuromuscular system in regulating the aircraft states.

Research objective I

Develop a haptic interface that establishes a full haptic connection, particularly one that more effectively exploits the potential of human controllers.

To attain this objective, this thesis revisits the active manipulator [1, 2], a design concept that is different from, but complementary to, existing haptic interfaces. A research question is put forward for further improvement on this concept.

Key Question I-1

How does the active manipulator improve the flight control performance, and can we use this knowledge to further improve on this concept?

Chapter 2 addresses this research question. It presents an evaluation of the effect of the active manipulator on human control behavior using the cybernetic approach. An experiment corroborated the previous findings, showing that the haptic feedback about the rotational velocity of the controlled element greatly facilitates target following and disturbance rejection in compensatory tracking tasks. In addition, we found that larger improvements in task performance were associated with higher forcing-function bandwidths. These findings are explained by the fact that the active manipulator reduces the effective controlled-element dynamics into integrator-like dynamics. At the same time, controlling the aircraft dynamics absorbed by the active manipulator, as well as rejecting the disturbance acting on the aircraft, are performed by the neuromuscular system. The two independent forcing functions allowed us to estimate the impedance of the neuromuscular system. This provided clear evidence of the role that the muscle co-contraction played in suppressing the disturbance.

Furthermore, the observations from the experiment were used to improve the effectiveness of the active manipulator. It was observed that the high-frequency disturbances acting on the aircraft, conveyed by the feedback about the aircraft state, caused involuntary arm movements. To mitigate this effect without affecting the task perfor-

mance, we designed a lag-lead filter which was tuned base on the passivity theory and the crossover characteristics observed in the experiment. A second experiment confirmed the effectiveness of this filter.

7.1.2. CHARACTERISTICS OF HUMAN HAPTIC PERCEPTION

As discussed in Chapter 1, a human-centric treatment will facilitate the optimization of haptic presentation, and allow for a more effective balance between transparency and stability of a haptic device. The second objective of this thesis is to establish the understanding that is necessary for this purpose.

Research objective II

Identify, model and understand the characteristics of human haptic perception, to facilitate the development and evaluation of haptic devices, and to guide optimization of haptic presentation according to what humans perceive.

To achieve this objective, this thesis puts forward two key research questions. These two questions respectively concern how a change in the dynamics of a system is characterized by humans, and how large this change has to be for this effect to occur. Key Question II-1 particularly focuses on the effect of time delays on human perception of mass, damping and stiffness, as perceptions of these three properties are the most relevant to the majority of applications and our understanding of the perception change associated with delayed feedback is the most limited, with seemingly contradicting results reported in literature. Recall the first key research question:

Key Question II-1

How does delayed haptic feedback affect humans in estimating the mass, damping, and stiffness characteristics of the original system?

Chapter 3 addresses this research question. It proposes a unified framework that allows for estimating the effect of delayed force feedback on the mechanical properties perceived by humans. Two psychophysical experiments, which measured our subjects' perception associated with different time delays and interaction frequencies, were conducted. A first experiment showed that the delayed force feedback led subjects to underestimate all the three mechanical properties. In addition, subjects perceived additional mechanical properties that were different from those simulated. These perceptual changes were explained by the fact that our subjects estimated the three properties using the relation between movement and force, a process that resembles a *black-box* estimation problem. Due to this, they could not distinguish the effect of time delays on the system's phase characteristics from the phase changes caused by variations in mechanical properties. This principle lays the foundation of the proposed framework.

In a second experiment, participants could explore a mass-damper environment with freely-selected movement patterns. The framework successfully predicted the underestimation of the mass and the overestimation of the damping associated with the delayed force feedback. In addition, the framework also explained the observed effect

of the individual difference in the frequency of interaction movement, and enabled prediction of the quantitative variations in the perceived mechanical properties.

Key Question II-2 concerns the conditions when the perception changes discussed in Chapter 3 occur. This requires knowledge about the human haptic threshold (or JND) for perceiving changes in the three mechanical properties. Moreover, this research question also calls for an extension of the conventional JND rule, one that can bridge the gap between JNDs in mechanical properties and the JND in the dynamics of a system.

Key Question II-2

How can we build a threshold model that describes the perceptual interactions among mechanical properties, and would allow for a generalization from JNDs in a system's mechanical properties to the JND in the dynamics of the system?

Chapters 4 and 5 address this research question. In Chapter 4, we extended the rule governing the JND in mechanical properties that humans would perceive from force feedback. The extension was obtained through mapping psychophysical findings to formulations based on frequency response functions. The two most relevant cases were studied: 1) the JND in the stiffness of systems with varying mass; 2) the JND in the damping of systems with different stiffness and mass. To this end, two experiments were conducted. It was found that, without deeper consideration, the measured JNDs violated Weber's law in both cases. Due to the increase in mass, the Weber fraction for stiffness decreases as the system's stiffness increases. The damping JND increases when the system possesses higher stiffness and mass.

These observations can be all accounted for by our extended JND rule, which states that: 1) the JNDs in a system's stiffness and mass are *coupled*, they form a joint JND that is proportional to the combined frequency response of stiffness and mass; 2) the frequency response magnitude of a system's damping JND is proportional to the frequency response magnitude of the system. Furthermore, the joint JND in stiffness and mass, and the JND in damping, can be described by the JNDs in the real and imaginary parts of the system's frequency response, respectively. This establishes a link between the JNDs in the three mechanical properties of a mass-spring-damper system and the JNDs in the dynamics of the system.

Continuing on Chapter 4, Chapter 5 establishes a further understanding of the JNDs in the two complex components, and in particular, the interaction between them. Results of the first experiment in this chapter showed that a same rule governed the variation of these two JNDs, i.e., the JNDs in these two parts are *both* proportional to the magnitude of the system's frequency response. A second experiment further completed this rule, demonstrating that these two JNDs could be described with the same ratio. Furthermore, the findings were then generalized to systems with arbitrary orders. This allows for a unified model that describes the threshold for changes in human perception of any system dynamics with two dimensions: the real and imaginary axes in the complex plane, representing, respectively, the in-phase and the out-of-phase force response to movement.

7.1.3. APPLYING PERCEPTION CHARACTERISTICS TO THE EVALUATION OF HAPTIC INTERFACES

Previous chapters establish the knowledge necessary for a human-centric evaluation of haptic interfaces. Based on the findings, Chapter 6 shows how the characteristics of human haptic perception can be applied to the evaluation of haptic interfaces.

First, a two-step fidelity-evaluation approach is proposed with a numerical example. As discussed in Chapter 1, it is usually possible to describe the degree of haptic display fidelity in technical terms, but it is not always known when the distortion of display can even be felt by an operator, and how the operator's perception of the presented system dynamics is then affected. The first step of the proposed approach allows us to know the frequency spectrum in which a haptic device causes a noticeable distortion of the desired system dynamics. The second step is then to understand how this distortion affects the operator in characterizing the system's behavior.

Second, the active manipulator developed in Chapter 2 is evaluated in terms of the control feel associated with the feedback about the aircraft rotational velocity. In addition to issues concerning the display fidelity, in the design phase it is also important to understand how humans interpret the dynamics conveyed by a particular piece of haptic feedback. Based on the findings from previous chapters, we found that the active manipulator could maintain not only the conventional means of aircraft control (the aircraft is controlled through the deflection angle of the manipulator), but also the conventional control feel. The analysis showed that the apparent dynamics of the active manipulator could be described by approximately constant stiffness, mass, and damping properties, a characteristic similar to a conventional passive manipulator.

7.2. DISCUSSION AND RECOMMENDATIONS

Chapter 2 demonstrates that making the control device active can significantly reduce the order of the controlled-element dynamics, into a single integrator. This is because the rest of the vehicle dynamics are absorbed by the control device. In fact, the dynamics presented to the pilot are those of the entire system that lies in-between the pilot force input and the aircraft rotational velocity output. Thus, when the active manipulator is implemented in an aircraft, its dynamics will be the *lumped* dynamics of the digital control system (including the stability or control augmentation system), the actuators, and the aircraft. The action of the autopilot will also be reflected by the movement of the control device. This will completely integrate the pilot into the aircraft automation system, considerably enhancing his or her engagement in the control loop. In addition, the active manipulator is complementary to existing haptic interfaces. It can directly merge with support systems that provide additional forces on the control device, such as flight envelope protection systems [3] and haptic shared control systems [4–6].

The combination with the haptic shared control system makes an additional approach available for optimizing the apparent mechanical properties of the active manipulator. One can imagine that what a pilot feels on the control device is the combination of the dynamics of the haptic shared control system and the dynamics conveyed by the feedback about the aircraft rotational velocity. How the pilot interprets such lumped dynamics can be understood by using the approach provided by Chapter 6.

The apparent mechanical properties can be considered to be an additional parameter for tuning the gains of the haptic shared control system.

In Chapter 2, a lag-lead filter is designed to reduce the involuntary arm movement caused by the disturbances possessing substantial energy at frequencies beyond the capacity of the neuromuscular system. The filter's passband is adjusted according to our subjects' disturbance rejection bandwidth collected from the experiment. A more effective approach would require one to also take into account the correlation between the degree of spinal reflex responses and the perturbation bandwidth. The reflexive activity is hypothesized to be suppressed when the limb is excited at frequencies higher than a certain threshold [7, 8]. The frequency range that guarantees an optimal neuromuscular admittance without affecting the target-following response is therefore a key parameter to be determined in future research.

Chapter 3 focuses on how humans perceive mass, stiffness, and damping from delayed force feedback. When the delay was relatively large, the mechanical properties perceived by our subjects varied with the frequency of the movement that they used to interact with the system. This is in fact due to the increased number of poles of the system dynamics. As the time delay introduces an infinite number of poles, the system's behavior cannot be approximated by a second order system that possesses constant mass, stiffness, and damping. This is particularly true for larger time delays. In this case the additional poles lie closer to the origin of the complex plane, having a larger impact on the system behavior in the low-frequency range where the interaction between humans and machines usually occurs.

As discussed in Chapter 1, the time delay is not the only factor that limits the degree of fidelity of haptic presentation. The findings of Chapter 3 can be directly applied to assessing the effect of other factors on human perception of the three mechanical properties. The proposed framework can be used to understand the effects of low-pass filters and the inherent actuator dynamics, as well as the virtual coupling [9] and the wave-variable transformation [10, 11]. This is because the associated perception changes, in the context of linear dynamics, are only determined by the changes in the magnitude and phase characteristics of the system's frequency response, but independent of the physical or mathematical form of the element that actually causes these changes.

The findings of Chapters 4 and 5 provide a number of insights into the balance between performance and stability. Chapter 4 demonstrates that a system with higher stiffness and mass leads humans to have a higher JND in the system's damping. In most cases, a haptic system with higher damping possesses a greater stability margin. Our findings indicate that more room is allowed for improving stability without affecting the perceived system dynamics. From the results of Chapter 5, a similar suggestion can be made to the presentation of stiffness and mass. Systems possessing higher damping will allow for larger distortions of the depicted stiffness and mass. For admittance haptic displays, simulating small mass is challenging since this requires a considerable reduction of the inherent impedance of the actuator, which can cause severe contact instability. Stability is also a critical issue for impedance haptic devices when high apparent stiffness is needed. Our findings indicate that increasing the system's damping can reduce the high demand on control systems and hardware for simulating small mass and high stiffness, at the same time still maintaining a high degree of fidelity in

the presentation of these two properties.

In addition, Chapters 4 and 5 present a model of human haptic threshold in perceiving changes in system dynamics. The model expresses the threshold with JNDs in the two complex components of the system's frequency response. The dynamics used for the investigation are selected from the general impedance range of control devices that are available in manual control tasks. In this case, it is demonstrated that the two JNDs are both proportional to the system's frequency-response magnitude, allowing us to propose a rule that is similar to Weber's law. However, we hypothesize that the Weber fraction of our JND rule is only constant over a certain impedance range, a characteristic similar to the case of the force JND. For systems with very low impedance, the fraction is expected to rise as the impedance decreases, because in this case the external impedance can be masked by the impedance of our arm.

The findings of Chapters 3, 4, and 5 form a two-step approach to evaluate the quality of haptic displays, as given in Chapter 6. The first step focuses on when a haptic device starts to change the operator's perception of the desired dynamics. It will provide the allowable frequency content of the haptic interaction with a particular device if a perceptually transparent haptic display is required. The second step assesses the changes caused by a haptic device in the perception of mechanical properties. This provides insights into how stability and transparency can be more effectively balanced. It allows us to know that the presentation of which mechanical property still has room to be compromised (e.g., to improve stability), and that of which must be maintained or improved. Furthermore, this approach can be considered an alternative to existing criteria for haptic devices, such as the EASA qualification standards [12] for control loading systems in vehicle simulators.

As already discussed in previous chapters, findings of the second part of this thesis are limited to the continuous haptic interaction with linear systems. Future work is suggested to focus on an extension that removes these limiting factors, such that the effect of transient responses (such as crossing the boundary of a force field [13]) on human perception, and the difference threshold for nonlinear dynamics (such as friction [14, 15]), can be understood and explained.

REFERENCES

[1] R. J. A. W. Hosman and J. C. van der Vaart, "Active and passive side stick controllers: Tracking task performance and pilot control behavior," in *AGARD Conf. on the Man-Machine Interface in Tactical Aircraft Design and Combat Automation*, no. 425, Stuttgart, Germany, Sept 1988.

[2] R. J. A. W. Hosman, B. Benard, and H. Fourquet, "Active and passive side stick controllers in manual aircraft control," in *IEEE Int. Conf. on Systems, Man and Cybernetics (SMC)*, Los Angeles, USA, Nov 1990, pp. 527–529.

[3] D. Van Baelen, J. Ellerbroek, M. M. van Paassen, and M. Mulder, "Design of a haptic feedback system for flight envelope protection," in *AIAA Modeling and Simulation Tech. Conf.*, no. AIAA-2018-0117, Kissimmee, USA, Jan 2018.

[4] D. A. Abbink, M. Mulder, and E. R. Boer, "Haptic shared control: Smoothly shifting control authority?" *Cognition, Tech. & Work*, vol. 14, no. 1, pp. 19–28, 2012.

[5] M. Mulder, D. A. Abbink, and E. R. Boer, "Sharing control with haptics: Seamless driver support from manual to automatic control," *Human Factors*, vol. 54, no. 5, pp. 786–798, 2012.

[6] S. M. Petermeijer, D. A. Abbink, M. Mulder, and J. C. F. de Winter, "The effect of haptic support systems on driver performance: A literature survey," *IEEE Trans. on Haptics*, vol. 8, no. 4, pp. 467–479, 2015.

[7] F. C. T. van der Helm, A. C. Schouten, E. de Vlugt, and G. G. Brouwn, "Identification of intrinsic and reflexive components of human arm dynamics during postural control," *J. of Neuroscience Methods*, vol. 119, no. 1, pp. 1–14, 2002.

[8] W. Mugge, D. A. Abbink, and F. C. T. van der Helm, "Reduced power method: How to evoke low-bandwidth behaviour while estimating full-bandwidth dynamics," in *IEEE 10th Int. Conf. on Rehabilitation Robotics*, Noordwijk, Netherlands, Jun 2007, pp. 575–581.

[9] R. J. Adams and B. Hannaford, "Stable haptic interaction with virtual environments," *IEEE Trans. Robotics and Automation*, vol. 15, no. 3, pp. 465–474, 1999.

[10] G. Niemeyer and J. J. E. Slotine, "Stable adaptive teleoperation," *IEEE J. of Oceanic Engineering*, vol. 16, no. 1, pp. 152–162, 1991.

[11] W. Fu, M. M. van Paassen, and M. Mulder, "Perception centered transparency evaluation of wave-variable based bilateral teleoperation," in *IEEE Int. Conf. on Systems, Man and Cybernetics (SMC)*, Miyazaki, Japan, Oct 2018, pp. 4279–4284.

[12] EASA, "CS-FSTD(A): Certification specifications for aeroplane flight simulation," Initial Issue, 2012.

[13] I. Nisky, F. A. Mussa Ivaldi, and A. Karniel, "A regression and boundary-crossing-based model for the perception of delayed stiffness," *IEEE Trans. on Haptics*, vol. 1, no. 2, pp. 73–82, 2008.

[14] D. Gueorguiev, E. Vezzoli, A. Mouraux, B. Lemaire-Semail, and J.-L. Thonnard, "The tactile perception of transient changes in friction," *J. of The Royal Society Interface*, vol. 14, no. 137, 2017.

[15] D. A. Lawrence, L. Y. Pao, A. M. Dougherty, Y. Pavlou, S. W. Brown, and S. A. Wallace, "Human perception of friction in haptic interfaces," in *ASME Int. Mechanical Engineering Cong. and Expo.*, Anaheim, USA, Jan 1998, pp. 287–294.

A

THE RELATIONSHIP BETWEEN THE FORCE AND STIFFNESS JNDS

A large variation of the haptic just-noticeable difference (JND) in stiffness is found in literature. But no underlying model that explains this variation can be found. Two experiments are conducted to investigate the cause of this variation from humans' strategy for stiffness discrimination. We demonstrate that for stiffness discrimination, subjects attempt to reproduce the same amount of manipulator deflection and use the difference in the terminal forces as the indication of the stiffness difference. In addition, we show that the differences between the stiffness Weber fraction and the force Weber fraction could be explained from the systematic bias in the deflection reproduction, which is caused by the difference in the manipulator stiffness. This suggests that the accuracy of reproducing the manipulator position for stiffness discrimination, which may be susceptible to experimental setting, can be used to explain the variation of stiffness JND in literature.

This appendix is based on the following publication: W. Fu, M. M. van Paassen and M. Mulder, "On the Relationship Between the Force JND and the Stiffness JND in Haptic Perception," *The ACM Symposium on Applied Perception*, no. 11, Cottbus, Germany, Sept 2017.

A.1. INTRODUCTION

Nowadays, pilots conduct a major part of their flight training in ground-based simulators (Fig. A.1a). A real-world manipulator (such a an aircraft sidestick, or a control column) is simulated in a simulator by a control inceptor (see Fig. A.1b for an example) attached to a control loading system (CLS). By replicating the physical appearance of a manipulator and reproducing the corresponding feel of control, the control inceptor provides pilots trainees with realism of a flight.

In general cases, the basic dynamics (the feel of control) of a manipulator are defined by mechanical properties such as stiffness, damping and mass. Thus moving an aircraft manipulator resembles moving a mass that is connected with a stiff wall by a spring and a damper. Of these, stiffness, generating force proportionally to the position, contributes an important part to the control feel since most flight control inputs only have energy in the low frequency range. Inevitable problems such as the limitations from the digital control system and actuator, as well as the modeling inaccuracy of the aerodynamic forces, induce differences in stiffness between the simulator's inceptor and the aircraft manipulator. Standard evaluation procedures are required by certifying authorities, e.g., the sweep test required by the European Aviation Safety Agency (EASA) [1]. The ultimate goal of such evaluation tests is to ensure that the inceptor stiffness is not distinguishable from the stiffness of the desired aircraft manipulator. However, this goal is not necessarily guaranteed since the evaluation is not based on the haptic perception of humans.

We intend to propose an alternative evaluation standard based on the limitation of humans' continuous haptic perception, i.e., the Just Noticeable Difference (JND) [2–5]. By comparing the change in stiffness with the JND in the perception of stiffness, the inceptor's fidelity can be known. The JND in stiffness in most cases follows Weber's law [6–9], i.e., the JND is a invariant fraction of the stiffness level. However, this fraction, usually being referred to as Weber fraction, seems to be susceptible to experimental

(a)

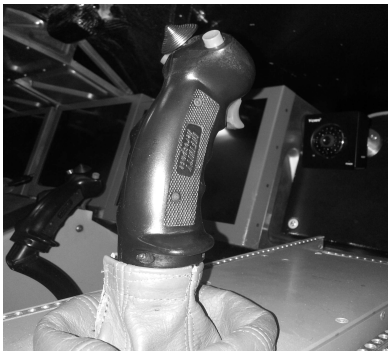

(b)

Figure A.1: (a): Example of a modern flight simulator: the SIMONA Research Simulator (SRS) at the faculty of Aerospace Engineering, Delft University of Technology. (b): the control inceptor in SRS which simulates a typical aircraft side-stick manipulator.

Table A.1: Spring Stiffness JND in literature

appendix	Experimental Conditions	Weber Fraction
[6]	Bilateral Matching	23%
[8]	Fixed Displacement	8%
	Roving Displacement	22%
[10]	Visual Information	14.2%
	No Visual Information	17.2%

settings since a large variation can be found among results. Several representative results are shown in Table A.1.

Due to this, individual measurements of the stiffness JND lack application value. An appropriate value and an underlying model that explains the variation, are essential for our practical application, but have yet to be found. In our view, addressing this problem will not only give better guidelines for simulator certification, but also be beneficial to the design of haptic support systems for vehicle control and the evaluation of transparency of tele-operation systems. To this end, we investigated the stiffness JND and the strategy that humans use for stiffness discrimination in two experiments performed by human subjects. The main tasks in the two experiments were both discriminating between different levels of manipulator stiffness, but were conducted for different reference levels of stiffness or different instructions for manipulator motion. More details will be given in Section A.2. Based on the observed strategy for stiffness discrimination during self exploration, we demonstrated that the stiffness JND can be related to the force JND, by a systematic bias in the reproduced manipulator deflection in the discrimination task. This bias, caused by the stiffness differences that was to be identified in the discrimination tasks, can be used to explain the variation of stiffness JND measurements in literature.

This appendix is organized as follows. The experiment setup and procedure, as well as the method for measuring the JNDs, are elaborated in Section A.2. Section A.3 describes the conditions and results of the first experiment, as well as subjects' strategy for stiffness discrimination. The stiffness JND was then formulated as a function of the force JND and the accuracy of displacement control. In Section A.4 the conditions and results of the second experiment are given. The formulation obtained from the first experiment is validated by the measurements. We discuss the results, conclusion on the strategy and causes of variations of the stiffness JND in Section A.5. Conclusions on the contribution of this work are given in Section A.6.

A.2. EXPERIMENTAL SETUP AND METHODOLOGY

A.2.1. APPARATUS

Experiments were conducted in the Human-Machine Interaction Laboratory at the faculty of Aerospace Engineering, TU Delft. An illustration of the devices can be seen in Fig. A.2a. A hydraulic side-stick manipulator was used in the experiment. It could be moved around the roll axis (left/right) like a joystick. The deflection of the manipulator in the pitch axis (forth/back) was fixed in the neutral point. The manipulator

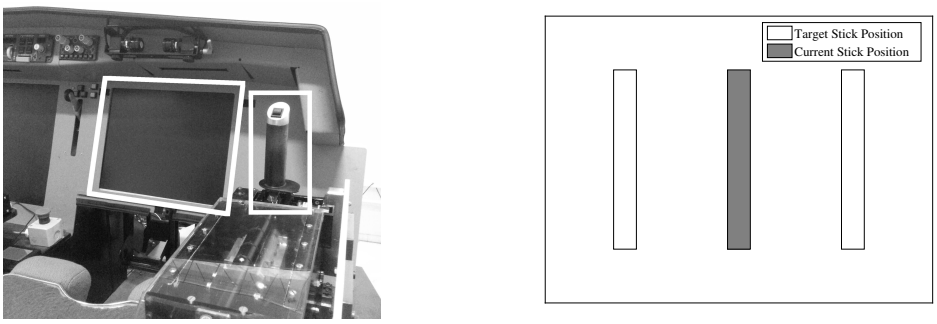

(a) (b)

Figure A.2: (a): The devices used in the JND experiment. The side-stick manipulator and the LCD screen are marked by white rectangles. The manipulator could be moved about the roll axis (left/right) like a joystick. The headphone used in the experiment is not shown in this figure. (b): The visual presentation of the angle of manipulator deflection shown on the LCD screen in the second experiment. Two target deflections of the manipulator on the two sides represent different directions (left/right) of motion.

was configured to use minimum mass and damping settings. The stiffness setting K of the manipulator was configured according to different experimental conditions. So the manipulator resembled a spring generating torque ($\tau(t)$) to its deflection (angular displacement, $x(t)$):

$$\tau(t) = K \cdot x(t) \tag{A.1}$$

The center of the grip point on the manipulator was 0.09 m above the rotation origin, which can be used to calculate the corresponding force. An LCD screen (marked by the rectangle in Fig. A.2a) was placed in front of the subject, to show the timing of experimental simulations for both experiments, and the visual presentation of the manipulator deflection (shown in Fig. A.2b) for the second experiment only. Subjects were asked to wear an active noise suppression headphone (David Clark H10-66XL), to cancel possible auditory cues.

A.2.2. SUBJECTS

Eight subjects participated in the first experiment, and 11 subjects participated in the second. All were PhD students or academic staff from Delft University of Technology. They were all right handed and reported no abnormality of the neuromuscular system or hand/arm impairment. An informed consent was signed by subjects before experiments.

A.2.3. PROCEDURE

The upper JND in stiffness accounting for the difference threshold for stiffness increments was investigated in this study. We used an one up/two down weighted adaptive staircase procedure (the same as those used in Chapters 4 and 5) to measure the stiffness JND for all the conditions in both experiments. This procedure converges to a JND level corresponding to 80.35% correct performance.

For each condition, a complete staircase procedure, which generally contained

Table A.2: Stiffness Settings in the First Experiment

	C1	C2	C3
K_r [N m/rad]	2.0	3.5	5.0

about 20 trials, was performed by the subject. Each trial consisted of two 5-second simulations. In one of the two simulations, a fixed reference stiffness setting (K_r) was simulated by the manipulator, and in the other simulation an adjustable controlled setting, a stiffer manipulator ($K_c = K_r + \delta K, \delta k > 0$) was simulated. The order in which the two settings were simulated in each trial was random. In this appendix, we define the simulation simulating the reference stiffness setting as the reference simulation and the other simulation as the controlled simulation.

During each trial, we asked the subject to identify in which simulation the manipulator was felt to be stiffer to move. The controlled stiffness was adjusted according to a subject's response. δK was reduced in the following trial when the subject correctly identified the controlled simulation in two consecutive trials, and was increased by a wrong identification. We define a reversal as a point where the staircase curve changes its direction (please refer to Fig. 4.3 for more information). A staircase procedure ended when the 7th reversal occurs, or when the total trial number reached 40. The JND measurement was taken as the average of δK in the last four reversals.

Sufficient training was performed preceding the formal experiment to familiarize our subjects with the procedure and requirements. Note that we define the stiffness by a rotational convention (Nm/rad), which can be transformed to the linear convention (N/m) by the rotational radius (0.09 m) given in Section A.2.1.

A.3. THE FIRST EXPERIMENT

The aim of the first experiment is to investigate how humans estimate differences in manipulator stiffness during self exploration. The stiffness JND was measured on three reference stiffness levels, as shown in Table. A.2.

The stiffness JND is found to follow Weber's law in literature, these three conditions are sufficient to verify such characteristics. We expect to obtain an invariant Weber fraction from the result (define ΔK_{jnd} as the stiffness JND, $\Delta K_{jnd}/K_r$ is constant).

During the experiment, subjects were encouraged to develop their own strategies to identify the stiffness difference between the two simulations in each trial. They were also suggested to apply any motion to the manipulator as they would like to (however, extremely fast movement making the system respond at the eigenfrequency was not allowed). The visual display (the LCD screen shown in Fig. A.2a) only indicates the time of the starting and ending of each simulation. So subjects had no additional visual feedback on the manipulator motion from the LCD screen. Such experimental instruction allowed subjects to distinguish between different manipulator stiffness during self exploration, and allowed us to investigate subject's strategies for stiffness discrimination in a more general way.

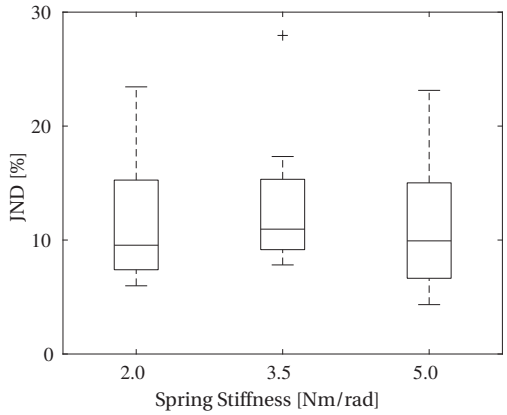

Figure A.3: Boxplots of the stiffness JND (plotted as the Weber fraction: $\frac{\Delta K_{jnd}}{K_r}$) for three stiffness settings; the "+" symbol represents the outliers.

A.3.1. RESULT

Measurements of the stiffness JND for the three conditions are shown as Weber fractions in Fig. A.3. As expected, different stiffness levels have no significant effects on Weber fraction for stiffness (one-way ANOVA, $F(2,21 = 0.23), p = 0.7969$). Thus Weber's law is indeed observed for the stiffness JND. The average of the Weber fractions is $12.13\% \pm 1.06\%$. The remaining questions is how humans estimate a stiffness change.

A.3.2. STRATEGY

After the experiment, we verbally questioned subjects on strategies they used for the assessment of stiffness differences. We found that all subjects used the terminal (maximum) force as an indication of a change in manipulator stiffness. This finding is in line with the conclusion given by [8], in which the author also suggested the contribution of the terminal force.

With more detailed verbal survey we found that the two variables: the manipulator deflection and force, played different roles for stiffness discrimination. During each trial, the subject reproduced a same angular displacement (deflection) in the two simulations, then reported the decision on the stiffer manipulator in response to the stronger terminal force. In each simulation, all subjects generally resampled the force maximums (the terminal forces) for several times through several individual motions, in order to confirm their perceptions of the terminal force. An example of the manipulator deflection data obtained in one trial is given in Fig. A.4. In this case, an angular displacement was reproduced in the two simulations, and each terminal force (the forces at the displacement peaks) was sampled twice.

We use a diagram to illustrate the stiffness discrimination procedure in each trial, as shown in Fig. A.5a. In each trial, a desired angular displacement of the manipulator (X_d) is reproduced for several times in both simulations. We define X_r and X_c as the averages of realizations of the angular displacement in the corresponding simulations (subscripts r and c correspond to the reference and controlled simulations re-

spectively), an example is shown in Fig. A.4, in which X_r and X_c are represented by the two horizontal lines respectively. F_r and F_c denote the terminal forces corresponding to these displacements. These two force maximums are compared as the indication of stiffness changes. The actual force discrimination procedure undertaken in the central nervous system is assumed to be probability based. We assume a fixed value to account for the converged threshold effect, as shown by a deadband in Fig. A.5b. Since the force difference threshold can be formulated by the Weber's law, in addition it was found that threshold sizes for elastic forces and constant forces are roughly the same [8]. We quantify the deadband's threshold size as a constant fraction W_f of the terminal force in the reference simulation F_r. The output of this deadband ΔS accounts for the perceived force change. Subjects identify the stiffer manipulator according to a criterion based on ΔS:

$$\Delta S \begin{cases} > 0, \text{select } K_c \text{ as the stiffer simulation} \\ = 0, \text{a random selection (guess)} \\ < 0, \text{select } K_r \text{ as the stiffer simulation} \end{cases} \tag{A.2}$$

A decision regarding to the stiffer manipulator is made in response to the larger force. When no force difference is perceived, e.g., the force difference is smaller than the force JND, a subject has to guess.

Normalizing ΔF to F_r, we get:

$$r = \frac{\Delta F}{F_r} = \frac{X_c \cdot K_c - X_r \cdot K_r}{X_r \cdot K_r} \tag{A.3}$$

In each trial, if the absolute value of r is larger than the Weber fraction for the force W_f, a decision will be made accordingly. A guess answer occurs when r falls into the range

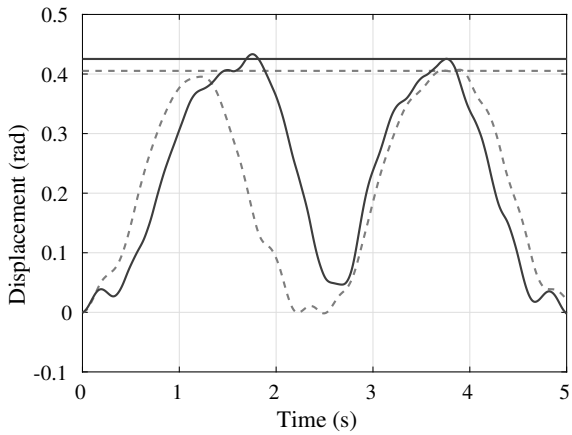

Figure A.4: An example of the side-stick motion trajectories in one trial. The black solid curve represents the manipulator deflection in the reference simulation, and the dashed one is for the controlled simulation. The horizontal lines show the average amounts of terminal displacements (peaks of the deflection) applied in the two simulations (solid and dashed ones for the reference and controlled simulations, respectively).

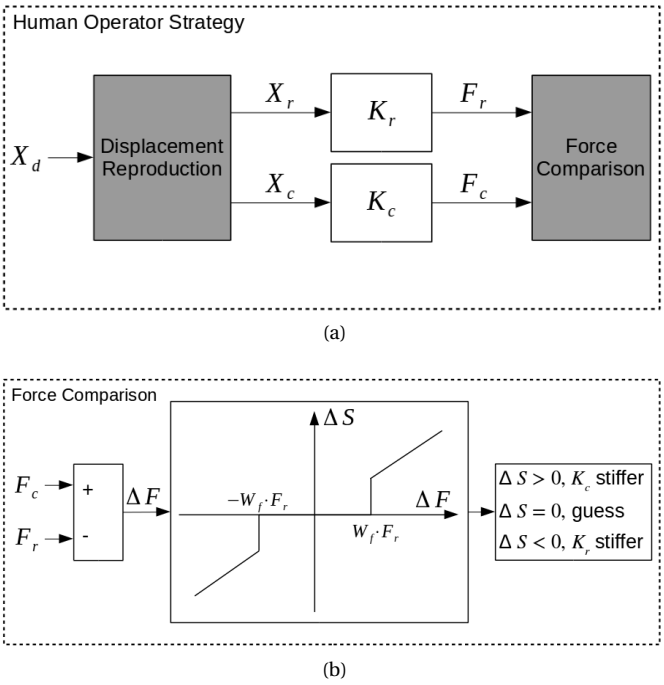

Figure A.5: (a): spring stiffness comparison procedure in each trial (b) and details of the force comparison process.

of $[-W_f, W_f]$. Simplifying this equation by defining α as the ratio between X_c and X_r:

$$\begin{aligned} r &= (\alpha - 1) + \alpha \cdot \frac{\delta K}{K} \\ \text{where} \quad \alpha &= \frac{X_c}{X_r} \quad , \quad K_c = K_r + \delta K \end{aligned} \tag{A.4}$$

As shown by the example in Fig. A.4, subjects seldom made identical deflections in the two simulations in each trial ($\alpha \neq 1$). The variation of α could result a fluctuation in the level of detectable stiffness difference from trial to trial. For a staircase procedure, the converged level of δK, i.e., the stiffness JND measurement ΔK_{jnd}, is determined by the average of α. By equating r to W_f, the Weber fraction for stiffness can be formulated:

$$\begin{aligned} W_k &= \frac{\Delta K_{jnd}}{K_r} \\ &= \frac{W_f - (E(\alpha) - 1)}{E(\alpha)} \end{aligned} \tag{A.5}$$

Here $E(\alpha)$ denotes the average of α.

If the variation of α is only caused by random errors, i.e., $E(\alpha) = 1$, the staircase would converge to a stiffness Weber fraction identical to the force Weber fraction ($W_k =$

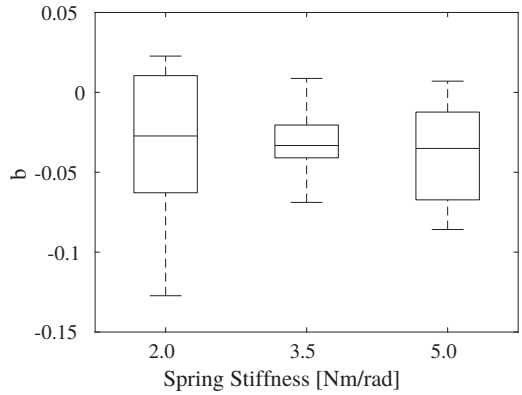

Figure A.6: The bias ratios $b = E(\alpha) - 1$ of subjects for the three conditions.

W_f). Whereas if the errors also contain systematic components (bias), differences between the two fractions would be observed. $E(\alpha) < 1$ indicates a stiffness Weber fraction larger than the force Weber fraction. For $E(\alpha) > 1$ the opposite happens.

A.3.3. EFFECTS OF THE DEFLECTION REPRODUCTION

In order to investigate whether a systematic bias exists, we examined the ratio of bias (b) of each subject's data obtained in trials after the third reversal, according to:

$$b = E(\alpha) - 1 = \frac{1}{N} \sum_{i=1}^{N} \frac{X_{c,i} - X_{r,i}}{X_{r,i}} \quad , \tag{A.6}$$

in which N denotes the total number of trials after the third reversal of a staircase, $i = 1$ denotes the first trial after the third reversal.

The distribution of the bias (b) of subjects is shown by a boxplot in Fig. A.6. No significant difference is found among different conditions (one-way ANOVA, $F(2,21) = 0.08, p = 0.9204$). The average of b is -0.032, the result from T-test shows this average differs from zero with significance. This implies that a systematic bias indeed exists in the angular displacement reproduction, and the angular displacements of the stiffer manipulator are 3.2% smaller on average for all three stiffness levels, $E(\alpha) = 0.968$.

Taking the averages of both b and the stiffness Weber fraction measurement W_k into Eq. (A.5), we get 8.2% for the force Weber fraction W_f. This value is in line with the literature results (5% - 10%,[3, 4]), indicating that the force JND and the stiffness JND can indeed be related by Eq. (A.5).

From this, it seems that the level of humans' haptic JND in stiffness is determined by two factors, i.e., the accuracy of the position reproduction and the force JND. The model in Eq. (A.5) states that humans' sensitivity to stiffness variations can be improved by increasing their accuracy in the position reproduction. When the bias is removed, the stiffness Weber fraction is equal to the force Weber fraction. To verify this, a second experiment was designed.

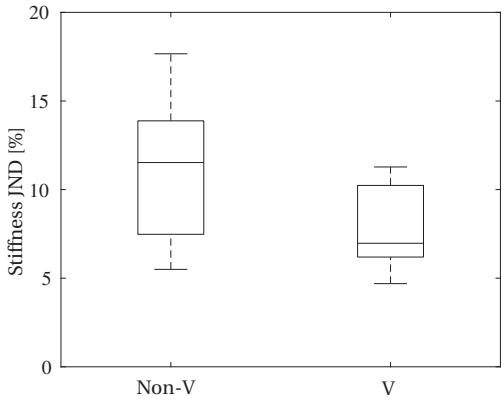

Figure A.7: The Weber fractions for stiffness ($\Delta K_{jnd}/K_r$) obtained from the two conditions.

A.4. THE SECOND EXPERIMENT

A.4.1. EXPERIMENT SETTINGS

In the second experiment, we measured the stiffness JND for a reference stiffness of 3.5 Nm/rad with two conditions. In one condition, on the LCD screen (marked by the rectangle in Fig. A.2a) a presentation of the manipulator angular displacement (see Fig. A.2b) was shown. As can be seen, the presentation provides the target and the current manipulator defections. The current manipulator deflection is shown by the solid bar. The targets are shown by the empty bars on the two sides, they are both 0.37 rad but denote different directions. Deflecting the manipulator to the right by an angle of 0.37 rad will reach the target on the right side, and a deflection to the left will reach the left target.

During each trial of the staircase procedure, in addition to the stiffness discrimination task, we asked our subjects to move the manipulator to either of the targets for two or three times in each simulation. Since in this way no errors should exist in the displacement reproduction, this condition would give a stiffness JND that is only determined by the force JND. In the remainder of this appendix, we refer to this condition as the visual condition. The other condition was performed without this displacement presentation, subjects were asked to discriminate between different stiffness settings in a way similar to the first experiment. In order to minimize the uncertainty resulting from different manipulator movement frequencies, we suggested subjects to apply a manipulator motion with a similar pattern (two or three moves) as for the visual condition. We refer to this condition as the non-visual condition. Results of the two conditions should be related by Eq. (A.5), if their difference is mainly determined by the displacement reduction for the stiffer-manipulator simulation.

A.4.2. RESULT

The obtained Weber fractions for the two conditions are shown in Fig. A.7. An improvement in the stiffness JND induced by the visual presentation was found to be significant (T-test). The average Weber fraction was 11.08% for the non-visual condition,

and this fraction reduced to 7.79% for the visual condition.

A.4.3. ANALYSIS OF RESULTS

As expected, lower stiffness JND was found when subjects were helped in the visual condition to perform two almost identical manipulator deflections. The resulting Weber fraction, 7.79%, as discussed earlier in Section A.4.1 is also the force Weber fraction of our subjects. The JND measurement for the non-visual condition (11.08%) is similar to that obtained in the first experiment (12.13%). Moreover, for the non-visual condition a reduction in deflection of the stiffer manipulator is again observed. The average of the bias ratio b is 3.22%, significantly differs from zero (T-test). Thus $E(\alpha)$ for the non-visual condition is 0.9678. By taking this value and the JND measurement (11.08%) into Eq. (A.5), we get 7.50% for the force Weber fraction W_f. This value is almost identical to the measurement for the visual condition, the model obtained from the first experiment is therefore validated.

A.5. DISCUSSION

We can conclude that in our experiment the estimate of stiffness a change is dominated by the perceived force difference, and therefore can be affected by a systematic biases existing in the position reproduction. Subjects appear to use a strategy in which they compare the force at its maximum, and in the cases where there is a position bias, a stiffness difference is no longer fully reflected by the force difference. The smaller deflection of a stiffer manipulator would make the force difference less evident, and a larger stiffness difference is thus required to provide a detectable quantity.

In [11], it was shown that humans detect the time delay in elastic force by interpreting the change in the perceived stiffness. There it was suggested that humans use the ratio between maximum force and perceived (not actual) amount of spring deflection as the indication of the amount of stiffness. In our work the perceived manipulator deflections during each discrimination task should be the same, since subjects intended to reproduce this variable. Hence comparing the maximum force is basically in line with this previous finding, implying that this strategy is the intuitive choice for stiffness discrimination.

The second experiment validated the conclusion obtained from the first experiment. The measurements obtained for the two conditions, i.e., the force Weber fraction obtained in the visual condition and the stiffness Weber fraction obtained in the non-visual condition, can be related by the formulation in Eq. (A.5). The accurate estimate of the force Weber fraction excludes the significance of other possible causes for the differences between stiffness and force Weber fractions, allowing us to formulate the stiffness JND as a function of the force JND and position reproduction accuracy.

The systematic bias in the position reproduction caused by the stiffness variation reflects the effect of motion in the stiffness JND, and could be used to explain the variation of the stiffness JND measurements in the past research. Different experimental settings and procedures may affect the accuracy of position reproduction, hence inconsistency of stiffness JND measurement is expected. The large Weber fraction given by [6] may indicate that the accuracy is lower when one tries to reproduce the position of one arm by the other arm. The force threshold may also be affected by bi-

lateral comparison, so that both a smaller α and a higher W_f result a larger stiffness JND. Similar to our work, in [8], when a fixed displacement was imposed the force and stiffness Weber fractions were found to be equal. The involvement of other sensory cues such as visual presentation may, on the upside, provide improvement in motion perceiving accuracy, on the downside, introduce bias or even suppress proprioceptive position cues and induce illusions. Without a fixed visual target as introduced in our work [10], the stiffness JND was still improved from 17% to 14% when vision cues were provided. Because of the visual contribution, the bias in perception of stiffness caused by different spatial locations of the object was eliminated, and the JND was also improved from 10% to 5% [12]. Visual cues are also found to suppress the proprioceptive position sense, which could largely vary the perception of stiffness so that even an obviously detectable stiffness increment may not be perceived or misperceived as a decrement [13]. We conjecture that these changes are due to the effect of vision on the perceiving and reproducing of the arm motion, which results in a different force for comparison. Hence, with different visual cues or other causes affecting the position reproduction process, the stiffness JND measurements in previous research are bound to show variation. In some other cases due to some imposed constraints subjects had to choose different strategies rather than the intuitive one obtained in this work. When the amounts of spring deflection during discrimination were artificially varied, such as by providing roving displacements [8], subjects couldn't compare the maximum force leading to a significant increase in the stiffness JND. In addition to the above, the variations in the devices should also be considered. For different devices, the dynamics of actuators in moderate and high frequency range, which could be effectively perceived as mechanical properties such as the mass and damping, are different. If the stiffness discrimination is conducted during non-static motion, for example using a sinusoidal motion profile, the stiffness JND could also be altered by the effective mass and damping perceptions due to the masking effect among mechanical properties [14].

Typical situations in flight control are similar to a tracking process with a compensatory task [15, 16]. This leads to a high accuracy of the manipulator position control. The stiffness Weber fraction would in these cases approach the force Weber fraction, indicating that the force Weber fraction is more appropriate to evaluate the stiffness of the simulator inceptor.

The result obtained in this study is from a manipulator that has minimal achievable mass and damping settings, so that the perception of manipulator stiffness is in isolation. The results can be used to examine that whether the stiffness difference between the aircraft manipulator and simulator inceptor cause a changed perception when the pilot maintains a static inceptor motion. The current results will need to be extended for cases where the control input contains energy in higher frequency range. This is because the mass and damping of a real-world manipulator are usually much higher than the settings used in this study. So that the force caused by manipulator mass and damping can not be ignored, which will probably affect the stiffness JND since the perceptions of these three mechanical properties are found to be coupled [14].

Nevertheless, the cause of the observed position bias should be addressed. It may be a result of the involvement of the force in humans' haptic position estimates. Evidence [17, 18] has shown that when a correlation exists between the force and motion, e.g., a spring loaded manipulator, the perception of the position is affected by the force.

An unnoticeable stiffness increment causes the blindly reproduced displacement to be overestimated (a negative bias) [18], which is in line with our observation. This phenomenon still needs detailed research, and will be addressed in our future work.

A.6. CONCLUSION

In this study with two experiments we formulated the stiffness JND as a function of the force JND and position reproduction accuracy. In the first experiment, the stiffness JND was measured at three stiffness settings. Consistent with results in literature, the results followed Weber's law. Subjects used a maximum force strategy based on position reproduction for stiffness discrimination. A negative bias was observed in the reproduced deflection of the stiffer manipulator. The stiffness JND was then formulated as a function of this bias and the force JND. In order to validate this formulation, we used an experiment condition in which a visual presentation eliminated the bias in the deflection reproduction during stiffness discrimination, which resulted a stiffness Weber fraction equal to the force Weber fraction. The result was compared to the stiffness JND obtained without visual cues from the same group of subject. A negative bias along with the stiffer manipulator was again observed when the visual cues were turned off. With this bias, the force JND and stiffness JND measured in the two conditions could be related. The formulation obtained from the first experiment was validated.

Future work includes investigation into the cause of the systematic error observed in this work. Since other mechanical properties such as the manipulator damping and mass also produce force responses to the motion in ways similar to the stiffness, we expect to characterize the JNDs for these two properties by similar models. These models will probably be based on the control of arm velocity, and the control of arm acceleration (through controlling the arm velocity and accelerating time).

REFERENCES

[1] EASA, "CS-FSTD(A): Certification specifications for aeroplane flight simulation," Initial Issue, 2012.

[2] L. A. Jones, "Kinesthetic sensing," in *Workshop on Human and Machine Haptics*, Pacific Grove, USA, Dec 1997, pp. 1–10.

[3] ——, "Matching forces: Constant errors and differential thresholds," *Perception*, vol. 18, no. 5, pp. 681–687, 1989.

[4] X. D. Pang, H. Z. Tan, and N. I. Durlach, "Manual discrimination of force using active finger motion," *Perception & Psychophysics*, vol. 49, no. 6, pp. 531–540, 1991.

[5] S. Feyzabadi, S. Straube, M. Folgheraiter, E. A. Kirchner, S. K. Kim, and J. C. Albiez, "Human force discrimination during active arm motion for force feedback design," *IEEE Trans. on Haptics*, vol. 6, no. 3, pp. 309–319, 2013.

[6] L. A. Jones and I. W. Hunter, "A perceptual analysis of stiffness," *Experimental Brain Research*, vol. 79, no. 1, pp. 150–156, 1990.

[7] ——, "A perceptual analysis of viscosity," *Experimental Brain Research*, vol. 94, no. 2, pp. 343–351, 1993.

[8] H. Z. Tan, N. I. Durlach, G. L. Beauregard, and M. A. Srinivasan, "Manual discrimination of compliance using active pinch grasp: The roles of force and work cues," *Perception & Psychophysics*, vol. 57, no. 4, pp. 495–510, 1995.

[9] G. L. Beauregard, M. A. Srinivasan, and N. I. Durlach, "The manual resolution of viscosity and mass," in *ASME Dynamic Systems and Control Division*, vol. 1, 1995, pp. 657–662.

[10] V. Varadharajan, R. Klatzky, B. Unger, R. Swendsen, and R. Hollis, "Haptic rendering and psychophysical evaluation of a virtual three-dimensional helical spring," in *Symp. on Haptic Interfaces for Virtual Environment and Teleoperator Systems*, Mar 2008, pp. 57–64.

[11] A. Pressman, L. J. Welty, A. Karniel, and F. A. Mussa Ivaldi, "Perception of delayed stiffness," *The Int. J. of Robotics Research*, vol. 26, no. 11-12, pp. 1191–1203, 2007.

[12] W. Wu, C. Basdogan, and M. A. Srinivasan, "Visual, haptic, and bimodal perception of size and stiffness in virtual environments," in *ASME Dynamic Systems Control Division*, vol. 67, Nashville, USA, Nov 1999, pp. 19–26.

[13] M. A. Srinivasan, G. L. Beauregard, and D. L. Brock, "The impact of visual information on the haptic perception of stiffness in virtual environments," in *ASME Winter Annual Meeting*, vol. 58. New York, NY, 1996, pp. 555–559.

[14] M. Rank, T. Schauß, A. Peer, S. Hirche, and R. L. Klatzky, "Masking effects for damping JND," in *Int. Conf. on Human Haptic Sensing and Touch Enabled Computer Applications*, Tampere, Finland, Jun 2012, pp. 145–150.

[15] D. T. McRuer and H. R. Jex, "A review of quasi-linear pilot models," *IEEE Trans. on Human Factors in Electronics*, vol. HFE-8, no. 3, pp. 231–249, 1967.

[16] M. M. van Paassen, J. C. van der Vaart, and J. A. Mulder, "Model of the neuromuscular dynamics of the human pilot's arm," *J. of Aircraft*, vol. 41, no. 6, pp. 1482–1490, 2004.

[17] P. Wydoodt, E. Gentaz, and A. Streri, "Role of force cues in the haptic estimations of a virtual length," *Experimental Brain Research*, vol. 171, no. 4, pp. 481–489, 2006.

[18] W. Mugge, J. Schuurmans, A. C. Schouten, and F. C. T. van der Helm, "Sensory weighting of force and position feedback in human motor control tasks," *The Journal of Neuroscience*, vol. 29, no. 17, pp. 5476–5482, 2009.

B

EFFECT OF DISCRIMINATION STRATEGY ON THE JND IN STIFFNESS

To assess changes in a mechanical property of a control manipulator, humans must infer the change through changes in perceived contact force and/or manipulator displacement. To study the roles of these two signals, we measure the stiffness JND under three conditions which are referred to as the force, displacement and free conditions. In the force condition, the manipulator displacement is fixed and subjects can only base their stiffness discrimination on changes in the contact force, and likewise in the displacement condition, discrimination is on the basis of changes in the manipulator displacement while the contact force is fixed. In the free condition both force and displacement cues are available. The lowest stiffness JND is observed under the force condition, followed by a similar results from the free condition. The highest JND and a poor consistency among individuals are obtained under the displacement condition. We use two models, one assumes force differences as a criterion for detection and the other assumes the displacement, to estimate the experimental results. Results indicate that subjects' stiffness discrimination is largely based on detection of force differences.

This appendix is based on the following publication: W. Fu, M. M. van Paassen and M. Mulder, "The Influence of Discrimination Strategy on the JND in Human Haptic Perception of Manipulator Stiffness," *AIAA Modeling and Simulation Technologies Conference*, no. AIAA-2017-3668, Denver, USA, Jun 2017.

B.1. INTRODUCTION

The Control Loading System (CLS) is of importance to a flight simulator, as it aims to provide pilots with the right "control feel" on the manipulator during simulation. The similarity between dynamics of the simulated manipulator and dynamics of the manipulator in a real aircraft is generally referred to as fidelity. In order to present the pilot with the proper feel, such that the pilot trainee obtains the right skills that they can correctly transfer to the real aircraft, the fidelity is a key factor for a simulator's feel system design.

In general, the CLS realize the manipulator dynamics by an admittance architecture [1], as shown in Fig. B.1. With this control protocol, the CLS moves the inceptor (the manipulator) in response to the measured force. The desired inceptor motion is calculated in real-time in the control loading computer, according to the dynamic model of the desired manipulator.

Differences exist in the presented control dynamics, for instance due to time delays in the digital system, and magnitude changes and phase lags in the response of the servo system. As all sorts of thresholds are known to exist in humans' haptic perception, questions on whether humans are capable to feel the difference between real and simulated manipulator dynamics have yet to be answered, which could provide better guidelines to the CLS design. The linear dynamics of a manipulator are generally determined by mechanical properties such as the spring stiffness, damping and mass. Answering the above questions requires knowledge on humans' haptic just noticeable difference (JND) in perceiving these properties.

In the current work, we will investigate the JND in perceiving stiffness, as this property relates to a manipulator's static response and bandwidth, hence contributes an important part to the feel of control. Humans could only estimate the stiffness, since no known receptors in haptic system measure this quantity directly. During the interaction with a spring loaded device, receptors in muscles provide the human central nervous system (CNS) with information about motion and force. The CNS can relate both cues to estimate the spring stiffness, and use a change in perception of either or both of these two quantities as an indication of a stiffness change. Strategies relating the stiffness difference to the force difference and to the motion difference are both

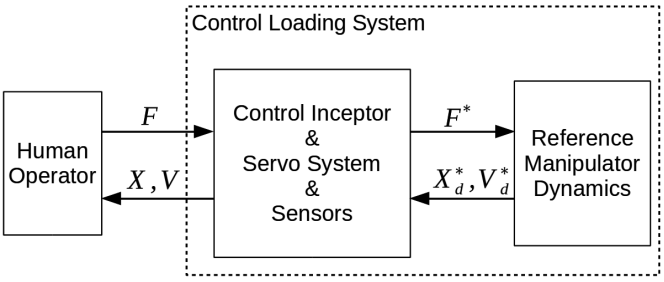

Figure B.1: General structure of the control loading system with an admittance causality. Here, F denotes the force that a pilot applies on the control inceptor, X and V are the angular displacement and velocity of the inceptor. Superscript "*" denotes the discrete signals.

found in previous research (see Appendix A and [2, 3]).

Different strategies could affect the level of noticeable stiffness difference, as the haptic force and motion difference thresholds of a human may not be the same. In the current work, we will investigate two strategies that humans could use for stiffness discrimination, namely the force strategy and the displacement strategy. The former definition means that humans discriminate between different stiffness levels on the basis of changes in the contact force when pushing the manipulator to the same amount of displacement. The later one consider the reverse, i.e., basing the stiffness discrimination on changes of manipulator displacement while trying to push the manipulator with the same amount of force.

To find which of the two strategies yields a higher sensitivity to stiffness variations, we measured their resultant stiffness JNDs in two conditions independently. The stiffness JND was measured through a staircase stiffness discrimination procedure, during which our human subjects had to conduct a series of discrimination between different stiffness settings of a spring-loaded manipulator. The stiffness JND resulting from the force strategy was measured in the force condition, in which our subjects were instructed to match a fixed manipulator angular displacement and discriminate between different stiffness settings from differences in the contact force. Likewise in the displacement condition the displacement strategy was imposed, where subjects were asked to match a fixed contact force and compare different manipulator displacements.

In addition to these two conditions, in another condition, which we referred to as the free condition, the stiffness JND were measured when no instructions on controlling either the contact force or manipulator displacement were given. Subjects were free to choose between the force strategy and the displacement strategy, or develop one involving both force and displacement changes. The JND measurement obtained from this condition was used as the reference to be compared with the results of the other two conditions. We also investigated the use of strategy in this condition by questioning subjects on the strategies they used for stiffness discrimination. To validate the conclusion of the investigation, we used two models respectively based on the force and displacement strategies to estimate the results of the free condition. Comparison between model estimates and experimental results were made to find the actual used strategy.

This appendix is organized as follows: In the following section, the experiment procedure and conditions are described. In Section B.3 the two models are elaborated. The results, analysis, and comparison of models are given in Section B.4. We discuss the results and future work in Section B.5. Section B.6 concludes the contribution of this work.

B.2. EXPERIMENT SETUP AND METHODOLOGY

B.2.1. APPARATUS

The experiment were performed in the Human-Machine Interaction Laboratory at the faculty of Aerospace Engineering, TU Delft. To simulate the desired stiffness setting, a side-stick manipulator with minimum mass and damper properties was used to generate an elastic force in response to its angular displacement. The manipulator could

Figure B.2: An illustration of experimental devices. The side-stick and the LCD screen are marked by rectangles. The side-stick could be moved around the roll axis (left/right). The headphone used in the experiment is not shown in this figure.

be only moved around the roll axis and was fixed in the pitch axis. An LCD screen was positioned in front of the subject, to indicate the timing of experimental simulations, and also to provide the visual reference to assist our subjects to achieve the proper manipulator control. Subjects were asked to wear an active noise suppression headphone (David Clark H10-66XL), to cancel any possible auditory cue. An illustration of the devices can be seen in Fig. B.2.

B.2.2. SUBJECTS

Seven subjects participated in the experiment. All were PhD students or academic staff from Delft University of Technology. They were all right-handed and reported no abnormality of the neuromuscular system or hand/arm impairment. An informed consent form was signed by subjects before the experiment.

B.2.3. PROCEDURE

The difference threshold of a quantity is usually symmetric, which means the upper JND and the lower JND respectively defining the just noticeable increment and decrement of the quantity are roughly identical. Hence in this study we only measured the upper JND in stiffness. The measurement was obtained through the same adaptive staircase procedure used in previous chapters, except that the duration of each simulation was 5 second. Readers are referred to Chapter 4 for more information.

B.2.4. EXPERIMENTAL CONDITIONS

Three conditions, which differed by the strategies used for stiffness discrimination, are defined respectively as the force, displacement and free conditions.

- The force condition (discriminate between forces).

  In this condition, the manipulator displacement was controlled. Subjects were instructed to apply a fixed stick displacement (0.37 rad) in the two simulations in each trial, and were then asked to identify the simulation in which they perceived a higher force at this displacement. In this case, a stronger force reflects a stiffer spring (the controlled stiffness setting), and the stiffness difference in the

Table B.1: Conditions of the Experiment

Conditions	Reference Stiffness K_r [Nm/rad]	Fixed Variable	Compared Variable (Strategy)
Force	3.5	Displacement (0.37 rad)	Force
Displacement	3.5	Torque (1.295 Nm)	Displacement
Free	3.5	-	Stiffness

following trial is adjusted according to the correctness of identification as discussed above. The stiffness JND measurements for this condition would indicate humans' best stiffness discrimination ability, if a force strategy is used.

- The displacement condition (discriminate between displacements).

  In this condition, we asked our subjects to apply the same amount of force (corresponds to a torque of 1.295 $N \cdot m$) in each simulation, and identify the simulation with a smaller stick displacement. With the same force applied, the smaller spring deflection indicates the stiffer spring. Thus identifying a smaller displacement in the controlled simulation contributes a correct answer. Similarly, the observed stiffness JND would suggest the best performance of the displacement strategy.

- The free condition (free comparison).

  In this condition, no variables were controlled. Subjects were required to report the simulation in which they experienced a stiffer spring. We asked our subjects to develop their own strategy for stiffness discrimination, and afterwards report the strategies they used.

All the conditions were performed on a reference stiffness setting of 0.35 Nm/rad. A summary of conditions is shown in Table B.1.

B.2.5. MANIPULATOR CONTROL AND VISUAL DISPLAY

In order to assist subjects to control the manipulator in the desired way (reproduce the right final displacement in the force condition and reproduce the right force in the displacement condition), we designed a tracking task during each simulation. In the force condition, the current and target stick displacement (fixed at 0.37 rad) were shown on a visual display, as shown in Fig. B.3. We asked our subjects to track the target in each simulation in order to achieve the displacement reproduction.

A 1.5-second preview of the target stick displacement was shown on the display (Fig. B.3a). The previewed target shown as a curve moved downward vertically across the display. The current target (+) is where the curve ends at the bottom. The current stick displacement was shown by an open circle. Participants were asked to reduce the tracking error $e(t)$ as possible as they could. The reference side-stick displacement in

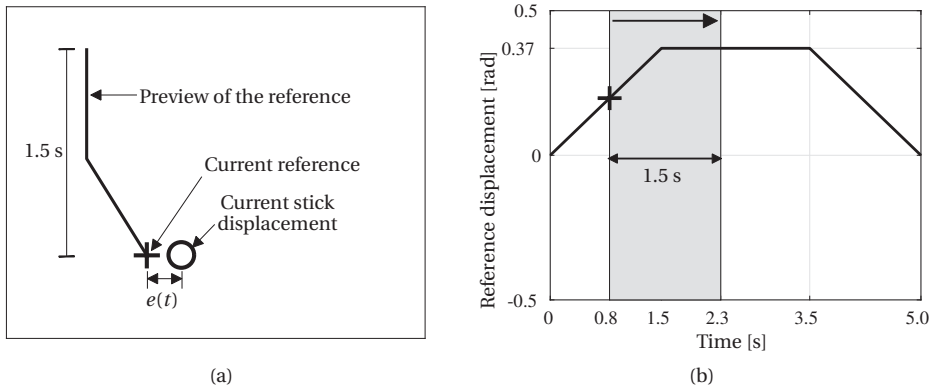

(a) (b)

Figure B.3: (a) The visual display and (b) the trajectory of the target side-stick displacement in the force-condition experiment.

each simulation is 0.37 rad as shown in Fig. B.3b. The slow ramps in the first and last 1.5 seconds are used to reduce the force caused by the inertia and damping properties of the manipulator, which could affect the JND measurement. The reference displacement signal shown on the visual display is illustrated using the gray rectangle. It moves to the right when time progresses, in the same way as the reference curve shown on the visual display moves downwards.

In the displacement condition, a force tracking task was performed. This would guarantee that subjects apply a same amount of torque on the stick (1.295 Nm) in each simulation. The display had exactly the same pattern as for the force condition, but with displacement cues replaced by force cues.

In the free condition, no reference was provided. We suggested our subjects to apply a similar motion pattern to the side stick (like a single push), to keep the perceptions in the three conditions being stimulated in the same frequency range.

B.3. MODELS

To models, namely the force model and the displacement model, are compared in their capability to characterize the behavior of subjects in the free-condition experiment. The force model estimates subjects' response by implementing the force strategy. Model estimates were based on the force data collected in the experiment. In each trial, this model identifies the simulation in which a larger force is observed as the controlled simulation. The displacement model estimates subject's behavior based on the displacement strategy. The simulation with a smaller stick displacement is considered as the controlled simulation, since this is the simulation simulating the stiffer spring.

In the experiment, we measured the torque instead of the contact force. Using this variable in the force model does not affect the estimates since subjects did not change their grip point on the manipulator. We define $\{F_{1,i}, P_{1,i}\}$ and $\{F_{2,i}, P_{2,i}\}$ as the torque-displacement pairs for the two simulations in the ith trial. An example is shown in Fig.

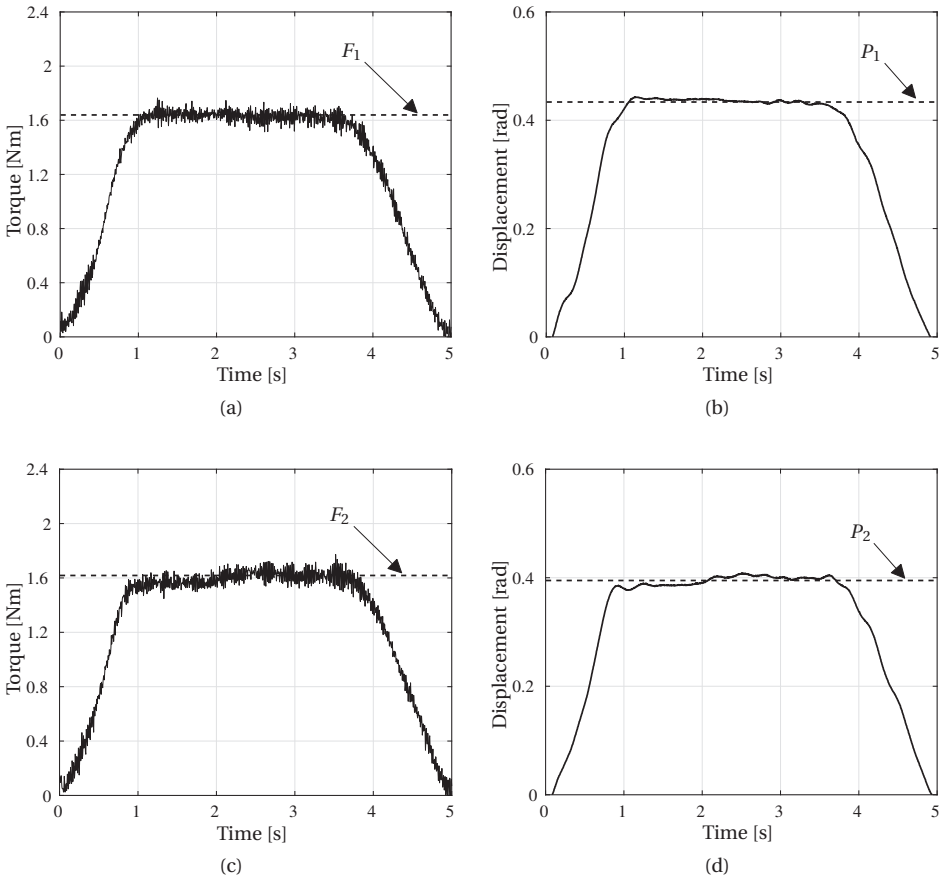

Figure B.4: Side-stick forces and displacements applied by a subject in one trial in the free condition. F and P are obtained as the average of the stationary region, as shown by the red dashed lines.

B.4.

Define ΔI_i as the criterion for models to select the controlled simulation, thus the force strategy can be formulated as:

$$\Delta I_i = F_{1,i} - F_{2,i} \quad , \quad \Delta I_i \begin{cases} \geq 0, \text{ select } R_{1,i} \\ < 0, \text{ select } R_{2,i} \end{cases} , \tag{B.1}$$

in which $R_{1,i}$ and $R_{2,i}$ denote the first and second simulation respectively. Similarly, the displacement strategy can be expressed as:

$$\Delta I_i = P_{1,i} - P_{2,i} \quad , \quad \Delta I_i \begin{cases} \leq 0, \text{ select } R_{1,i} \\ > 0, \text{ select } R_{2,i} \end{cases} \tag{B.2}$$

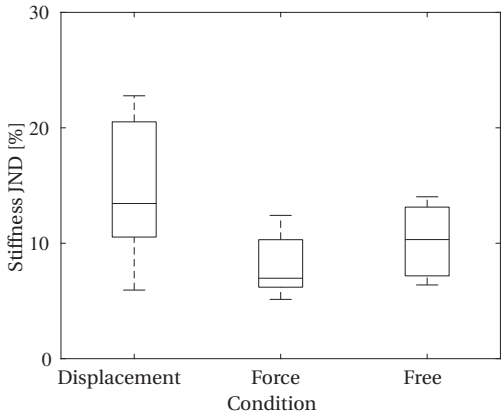

Figure B.5: Boxplot of the JND measurements.

Thus, given the force and displacement data, the two models could estimate a subject's response in each trial. The correspondence between the two model estimates and our subjects' actual responses would then indicate the plausibility of each model.

B.4. RESULTS

B.4.1. RESULT

The JND measurements for the three conditions are shown in Fig. B.5. Here we express the stiffness JND as a fraction of the reference stiffness level (the Weber fraction). The stiffness JND observed for the displacement condition was 14.64%±6.16%, for the force condition it was 8.01%±2.72%, and for the free condition 10.28%±3.12%. A significant effect of different strategies was observed, one-way ANOVA: $F(2,18)$=4.31, $p = 0.0295$. Posthoc t-tests revealed significance between the force and displacement conditions, $p = 0.0233$.

Apparently our subjects were less sensitive to stiffness variations when they were instructed to estimate stiffness differences from discriminating between different manipulator displacements. When they were instructed to compare forces for a fixed displacement, the lowest level of the stiffness JND were found. The observations in the free condition were in-between the results of the other two conditions. This implies that the choice of the strategy may not have been consistent among subjects, or that a different strategy was used. This will be investigated in more detail by questioning subjects on their strategies and using the model analysis.

B.4.2. STRATEGY INVESTIGATION

After the experiment, we interviewed subjects on the strategy for identifying the stiffer spring under the free condition. We found that all subjects based their selection on a force strategy. That is, to discriminate between two different stiffness levels subjects attempted to reproduce the same amount of manipulator displacement in the two simulations, and use the force difference as the indication of the stiffness difference. An

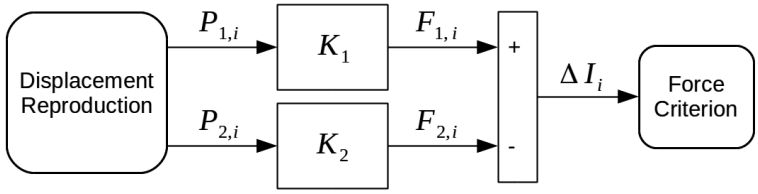

Figure B.6: Stiffness discrimination process in the free-condition experiment.

illustration of this process can be seen in Fig. B.6.

The process of stiffness discrimination in the free condition was the same as what was imposed in the force condition. The reason for the slight difference between results could be an inaccurate use of the force strategy (see Appendix A). That is, although our subjects intended to reproduce the side-stick displacement, without the visual presentation their accuracy was degraded. Define b_i as the displacement difference ratio for individual trials:

$$\Delta P_i = P_{c,i} - P_{r,i} \quad , \quad b_i = \frac{\Delta P_i}{P_{r,i}} \tag{B.3}$$

Here subscripts c and r denote the control simulation and reference simulation, i denotes the trial number. Define $N_b(E,\sigma)$ as the overall-subject distribution of b_i for trials after the third reversal. A good displacement control would result in zero mean and small variance of N, for example in the force condition these two quantities were -0.0005 and 0.03. For the free condition, the stick displacement in the control simulation (P_c) was smaller than that in the reference simulation (P_r) by 2% on average. A large variation $\sigma = 0.11$ was also observed.

This finding is consistent with the conclusion from Appendix A. The bias in displacement reproduction explains the difference in JND measurements found between these two conditions. A smaller deflection of the stiffer spring would generate a lower force difference, this makes the force comparison harder and a larger stiffness difference is thus required to provide a detectable force difference. This bias could be the result of a systematic error due to involving a force cue in human position estimates [4, 5] used for a position reproduction.

B.4.3. MODEL VALIDATION

In order to validate the use of the force strategy in the free condition, we examined the correspondence of the model estimates to subjects' responses in a way similar to the work done in the perception of delayed stiffness [6].

Define A_i as the response that a subject gives in the ith trial, and $\hat{A}_i$ is the response estimated by a model. We further define the proportion of trials in which a model's estimate agrees with the response of a subject ($A_i = \hat{A}_i$) as the agreement rate of the

model:

$$C_i = \begin{cases} 1, \text{ if } \hat{A}_i = A_i \\ 0, \text{ if } \hat{A}_i \neq A_i \end{cases} \quad , \quad G = \frac{\sum_{i=1}^{i=N} C_i}{N} \tag{B.4}$$

Here G denotes the agreement rate of a model. N denotes the number of trials. The agreement rates of the force and displacement models are calculated for trials after the third reversal, as can be seen in Fig. B.7.

The agreement rates of the force model for the force condition and of the displacement model for the displacement condition are also calculated. This allows us to know the best correspondence between model estimates and experiment observations. As can be seen in Fig. B.7, both rates indicate a non-perfect agreement and distribute around the level of 0.75. This is due to the wrong guess answers that resulted from unperceivable force or displacement differences.

The force model provides a similar agreement rate for the free condition. The average among subjects is 0.7338. The displacement model fails to provide an acceptable agreement. This indicates the plausibility of the force strategy over the displacement strategy, and is consistent with subjects' reported strategy.

B.5. DISCUSSION

In the current work, we investigated two strategies that could provide humans with the information of stiffness differences, namely the force strategy and displacement strategy. There are also many other possible strategies that we have not included in

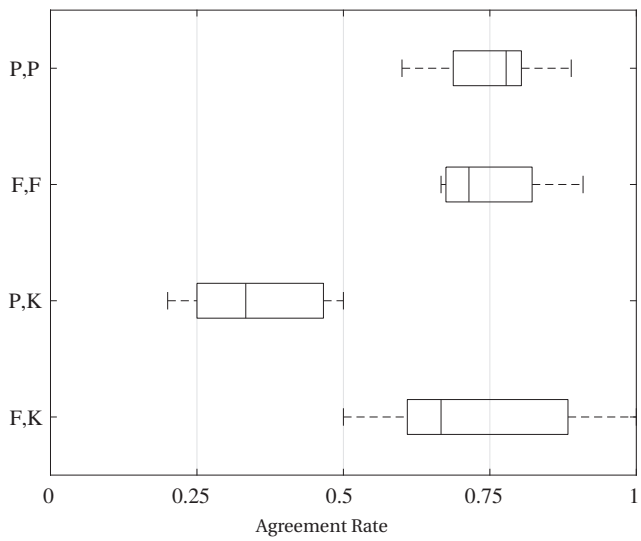

Figure B.7: Agreement rate of each model. Boxplots represent the distribution of model agreement rates of subjects. The first terms in the labels of the vertical axis represent the strategy, with P for displacement and F for force. The second terms represent the condition, P, F and K are substitutions of displacement, force and free conditions respectively.

the current work. For example an admittance strategy (comparing the manipulator velocity), which is difficult to be evaluated by the current experimental setting, and worth to be investigated in future work.

When subjects were forced to use a displacement strategy, the obtained stiffness JND was higher then that resulted from a force strategy. The large variation of the stiffness JND for this case also indicates a poor consistency among individuals. This indicates that this strategy could not result in an optimal and stable difference threshold for the perception of stiffness.

Subjects indicated that they used force differences for discriminating between different stiffness settings. The JND in the free condition was slightly larger than the JND found in the force condition, corresponding to the findings from Appendix A. In the force condition, with the help of the visual presentation, subjects reached their lowest stiffness JND. The 8% Weber fraction reflects our subjects' limits to discriminate between different elastic forces. It is known that humans exhibit a similar difference threshold for elastic force and constant force [2]. This fraction (8%) is indeed in accordance to the force JND in literature [7]. With the current results, we would propose that the force JND indicates the humans' highest haptic resolution on stiffness. When evaluating the performance of CLS, one should therefore consider the force JND as the tolerance for the static response of the system.

B.6. CONCLUSION

In the current work, two stiffness discrimination strategies, namely the force strategy and displacement strategy, and their resultant stiffness JNDs were investigated. We invited seven human subjects to participate in a stiffness JND experiment with three conditions. We related the stiffness JND to subjects' force difference threshold in the force condition, and in the displacement condition the stiffness JND was measured from subjects' displacement difference threshold. In the free condition, the stiffness JND were measured when no constraints were imposed on the choice of the strategy, which means both force and displacement changes could be used for the stiffness discrimination. Subjects were most sensitive to stiffness variations when the force strategy was imposed (the force condition). In the free condition, subjects indicated the use of the force strategy for stiffness discrimination. But the JND measurements were slightly higher due to the reduction of accuracy in their displacement reproduction. The displacement strategy resulted in the highest level of the stiffness JND and a poor consistency among subjects. Two models based on the two strategies estimated the behaviors of subjects in the free condition. One assumed the force-strategy based discrimination, the other assumed the basis as the displacement strategy. Comparison between model estimates and experimental results validated the conclusion on the strategy used in the free condition, and indicates that when free to apply their own strategy, subjects largely based their stiffness discrimination on the detection of force differences.

REFERENCES

[1] R. J. Adams and B. Hannaford, "Stable haptic interaction with virtual environments," *IEEE Trans. Robotics and Automation*, vol. 15, no. 3, pp. 465–474, 1999.

[2] H. Z. Tan, N. I. Durlach, G. L. Beauregard, and M. A. Srinivasan, "Manual discrimination of compliance using active pinch grasp: The roles of force and work cues," *Perception & Psychophysics*, vol. 57, no. 4, pp. 495–510, 1995.

[3] M. Rank, "Dynamic models of human perception and action and their application in telepresence," Ph.D. dissertation, Universitätsbibliothek der TU München, 2012.

[4] P. Wydoodt, E. Gentaz, and A. Streri, "Role of force cues in the haptic estimations of a virtual length," *Experimental Brain Research*, vol. 171, no. 4, pp. 481–489, 2006.

[5] W. Mugge, J. Schuurmans, A. C. Schouten, and F. C. T. van der Helm, "Sensory weighting of force and position feedback in human motor control tasks," *The Journal of Neuroscience*, vol. 29, no. 17, pp. 5476–5482, 2009.

[6] A. Pressman, L. J. Welty, A. Karniel, and F. A. Mussa Ivaldi, "Perception of delayed stiffness," *The Int. J. of Robotics Research*, vol. 26, no. 11-12, pp. 1191–1203, 2007.

[7] L. A. Jones, "Kinesthetic sensing," in *Workshop on Human and Machine Haptics*, Pacific Grove, USA, Dec 1997, pp. 1–10.

ACKNOWLEDGEMENTS

Pursuing my PhD at TU Delft, a world class university, over the last four years has been the most fulfilling period in my life. I have had the privilege of conducting my research with resources that many people dream about, working with and learning from scientists who are among the best in the world, and in particular, receiving incredible support from those to whom I would like to express my genuine appreciation in this final chapter.

First and foremost, I would like to show my deepest gratitude towards my daily supervisor and promotor, Dr. ir. M. M. (René) van Paassen. While being an excellent scientist of great wisdom, René is also a distinguished engineer with invaluable practical experience. Over the past years, he has been the person whom I could always consult, no matter what question I had. René is not only my mentor giving me incredible support and enlightenment, but also an amazing teammate with whom I have had so many inspiring discussions (although a "mere mortal" like me usually needs a certain amount of time to digest many of his brilliant ideas). Being your student is one of the luckiest things in my life, and it was a great pleasure to work with you, René. No words are sufficient to express my feeling of gratitude, thank you very much!

Second, I would like to convey my heartfelt appreciation to my promotor, Prof. dr. ir. Max Mulder. In addition to Max's incredible support and highly constructive feedback for which I am deeply indebted, I have also learnt how to be a rigorous scientist from him, which is the true scientific characteristic one should possess. Max is also an excellent professor whose lectures are always very interesting and clear. I never thought that I could love Fourier theory until I attended his lecture on Stochastic Systems. Moreover, Max also has a wonderful sense of humor (of course, his iconic laugh is an integral part of it), and I enjoyed every conversation with him. It was an enormous privilege to be your student, Max, you are the best professor that all students wish to have!

I would not complete this challenging journey as smooth as it was without the invaluable help from a number of people. Dr. ir. Qi. P. Chu, I would like to extend my profound gratitude to you. I am grateful for all the conversations we had and the excellent advice you gave me on control theory, especially those on INDI. Prof. dr. ir. David A. Abbink, I am genuinely grateful for your guidance on my research and the brainstorms we had. I was so lucky to listen to some of your presentations which were extremely inspiring and full of insights. Ir. Olaf Stroosma, I appreciate all your support over the past four years. I would like to particularly thank you for taking me on the excursions to a number of flight simulator companies, which played a pivotal role in shaping my future career. Dr. ir. Daan M. Pool, sincere thanks for you letting me participate in many teaching activities. Teaching students is the most rewarding thing during my PhD. In addition, you are one of the few Dutch people who use their natural talent for basketball (height)!

Furthermore, I want to thank my office mates in room 3.21: Emmanuel, Junzi, and Sherry. I appreciate all the good moments we had, particularly the heated debates surrounding the concept of "universal basic income". I would like to thank Emmanuel for the barbecues and his excellent Indian dishes. Moreover, my warm thanks go to all the Chinese fellows in C&S. Particularly, I am greatly indebted to Junzi, who is like my elder brother and always willing to help. Also thank you for organizing the regular Chinese New Year parties. In addition, I am deeply grateful to Yingzhi and short Ye, as well as Sihao and Sherry, who are the two dynamic duos that are joys to have around, thank you for our unforgettable trips to Austria and Iceland.

Also many thanks go to all my three-month office mates in Sim 0.11: Kimberly (my nice neighbour), Sihao, Ezgi, Yingfu, Paolo, Mario, Jelmer, Federico, and Diana; as well as Daniel, who is the “most regular participant” in the coffee breaks. I would like to particularly thank Dirk for participating in almost all my experiments, you have my highest regard! My profound gratitude also goes to Sarah, Kasper, Jerom, Tom, Annemarie, Isabel, Ivan, Julia, Kirk, Bo, Tommaso, Sophie, Shuo, tall Ye, Hann Woei, Marta, Malik, Shushuai, Ying, Dyah, Matej, and Stephan, as well as all other PhD colleagues and MSc students in C&S who are not mentioned above. Of course, I also wish to thank Bertine, for all your help over the past years, as well as Clark, Joost, Erik-Jan, Coen, Andries, Harold, Alwin, and all other C&S staff members for creating the nice C&S atmosphere.

Last but not least, to my beloved wife and parents: thank you for your unconditional support all the way along this incredible journey. I couldn’t think of attaining even any achievement without your love, which is my infinite source of motivation. My particular heartfelt gratitude goes to my dear wife, Gehua. This dissertation is to you, as I also indicated in the beginning of this book. Thank you for being the most loyal subject of my experiments, I owe half of my PhD to you! More importantly, I am indebted so much to you for cheering me with your love, your support, and of course your natural sense of humor, which have carried me through the most difficult part of my PhD and always make my day.

CURRICULUM VITÆ

Wei FU

15-04-1990 Born in Xi'an, China.

EDUCATION

2008.09–2012.07 BSc in Automation
Northwestern Polytechnical University, Xi'an, China

2012.09–2015.04 MSc in Control Theory and Control Engineering
Northwestern Polytechnical University, Xi'an, China

2015.07–2019.06 PhD in Aerospace Engineering
Delft University of Technology, Delft, the Netherlands
Thesis: Evidence-based development and evaluation of haptic interfaces for manual control
Promotors: Dr. ir. M. M. van Paassen and Prof. dr. ir. M. Mulder

PROFESSIONAL ACTIVITIES

- Reviewer for the IEEE Transactions on Human-Machine Systems
- Reviewer for the IEEE Transactions on Haptics
- Reviewer for the IEEE Haptics Symposium
- Reviewer for the IEEE World Haptics Conference
- Reviewer for the IFAC Conference on Cyber-Physical & Human-Systems
- Reviewer for the IEEE/RSJ International Conference on Intelligent Robots and Systems

LIST OF PUBLICATIONS

JOURNAL ARTICLES

4. **W. Fu**, A. Landman, M. M. van Paassen and M. Mulder, "Modeling Human Difference Threshold in Perceiving Mechanical Properties From Force," *IEEE Transactions on Human-Machine Systems*, vol. 48, no. 4, pp. 359-368, 2018.

3. **W. Fu**, M. M. van Paassen, D. A. Abbink and M. Mulder, "Framework for Human Haptic Perception with Delayed Force Feedback," *IEEE Transactions on Human-Machine Systems*, vol. 49, no. 2, pp. 171-182, 2019.

2. **W. Fu**, M. M. van Paassen and M. Mulder, "Developing Active Manipulators in Aircraft Flight Control," *Journal of Guidance, Control, and Dynamics*, published online, pp. 1-13, 2019.

1. **W. Fu**, M. M. van Paassen and M. Mulder, "Unified human threshold model for perceiving changes in system dynamics from force," *IEEE Transactions on Human-Machine Systems*, under review.

CONFERENCE ARTICLES

7. **W. Fu**, M. M. van Paassen, O. Stroosma and M. Mulder, "Objective inceptor cueing test for control loading systems: Principle and initial design," *AIAA Modeling and Simulation Technologies Conference*, no. AIAA-2017-3668, Denver, USA, Jun 2017.

6. **W. Fu**, M. M. van Paassen and M. Mulder, "The Influence of Discrimination Strategy on the JND in Human Haptic Perception of Manipulator Stiffness," *AIAA Modeling and Simulation Technologies Conference*, no. AIAA-2017-3668, Denver, USA, Jun 2017.

5. **W. Fu**, M. M. van Paassen and M. Mulder, "On the Relationship Between the Force JND and the Stiffness JND in Haptic Perception," *The ACM Symposium on Applied Perception*, no. 11, Cottbus, Germany, Sept 2017.

4. **W. Fu**, M. M. van Paassen and M. Mulder, "Modeling the Coupled Difference Threshold of Perceiving Mass and Stiffness from Force," *IEEE International Conference on Systems, Man, and Cybernetics (SMC)*, Miyazaki, Japan, Oct 2018, pp. 1427-1432;

3. **W. Fu**, M. M. van Paassen and M. Mulder, "Perception Centered Transparency Evaluation of Wave-Variable Based Bilateral Teleoperation," *IEEE International Conference on Systems, Man, and Cybernetics (SMC)*, Miyazaki, Japan, Oct 2018, pp. 4279-4284;

2. **W. Fu**, M. M. van Paassen and M. Mulder, "Revisiting Active Manipulators in Aircraft Flight Control," *AIAA Scitech 2019 Forum*, no. AIAA-2019-1231, San Diego, USA, Jan 2019.

1. **W. Fu** M. M. van Paassen, and M. Mulder, "Framework for a Two-Step Evaluation of Haptic Displays," *to appear in the proceedings of IFAC HMS 2019*